

**Novel silver containing antimicrobial coatings  
for implant materials: new applications of  
Ag(I) coordination networks**

**Inaugural dissertation**

zur

Erlangung der Würde eines Doktors der Philosophie

vorgelegt der

Philosophisch-Naturwissenschaftlichen Fakultät

Der Universität Basel

von

Tünde Vig Slenters

aus Eger (Ungarn)

Basel, 2009

Genehmigt von der Philosophisch-Naturwissenschaftlichen Fakultät  
auf Antrag von:

Prof. Dr. Katharina M. Fromm

Prof. Bernd Giese

Basel, den 28.04.2009

Prof. Dr. Eberhard Parlow  
Dekan

Originaldokument gespeichert auf dem Dokumentenserver der Universität Basel  
**edoc.unibas.ch**



Dieses Werk ist unter dem Vertrag „Creative Commons Namensnennung-Keine kommerzielle Nutzung-Keine Bearbeitung 2.5 Schweiz“ lizenziert. Die vollständige Lizenz kann unter  
**[creativecommons.org/licences/by-nc-nd/2.5/ch](http://creativecommons.org/licences/by-nc-nd/2.5/ch)**  
eingesehen werden.

*« Dans la vie, rien n'est à craindre, tout est à comprendre. »*

*Marie Curie*

TO ALEX, ERIC  
AND MY FAMILY

Some of these results have been reported in these publications [1,2]

[1] T.Vig Slenters, I.Hauser-Gerspach, A.U. Daniels, K.M.Fromm: Silver coordination compounds as light-stable, nano-structured and anti-bacterial coatings for dental implant and restorative materials; *J.Mater.Chem.*, **2008**, *18*, 5359

[2] K.Belser, T.Vig Slenters, C.Pfumbiadzai, G.Upert, L.Mirolo, K.M.Fromm, H.Wennemers: Silver nanoparticle formation in different sizes induced by peptides identified within split-and-mix libraries, *Angew.Chem.Int Ed.*, **2009**, *48*, accepted

Tünde Vig Slenters, Oliver Gordon, Priscilla S. Brunetto, Reto Luginbühl, Michael Otto, Laurent Mirolo, Regine Landmann and Katharina M. Fromm:  
Biochemical action of silver coordination polymers for the prevention of implant infection: interaction with iron-sulfur clusters and hydroxyl radical induction, *in preparation*



## ACKNOWLEDGEMENT

The work presented in this thesis could not have been achieved without the continued support of people around me.

First I would like to thank very much Prof. Dr. Katharina M. Fromm for giving me the chance to be part of her group and to work on this interesting interdisciplinary subject. Her support during all these years and her trust in me were very much appreciated. Moreover, she was always available for discussions, in which she gave me invaluable help and advice.

I thank to Prof. Bernd Giese for giving me a place in his group which allowed me to continue to work in Basel. I very much appreciated that he accepted the role of external examiner at my thesis defence. Of course, I also like to thank all the members of the my group in Fribourg: first to Priscilla Brunetto for all her help, Antoine Fleury, Aurélien Crochet, Dr. Adeline Robin, Fabienne Gschwind, Dr. Jorge Sague Doimeadios, Dr. William Maudez, Dr. Rémi Bergougnant, Inès Chevier, Dr. Jing Chen, Jérôme Girard, as well as all my lab-mates in Basel: Natasa and Vladimir Cmiljanovic, Dr. Olivier Jacques, Dr. Min Wang. Special thanks to Laurent Mirolo for his help in solving crystallographic problems and for the nice moments shared.

Many thanks to Prof. Dr. Helma Wennemers for fruitful discussions in realizing an extraordinary publication as well as for accepting to be chairwoman for my doctoral exam. I also would like to thank to Dr. Kirsten Belser for introducing me in the peptide chemistry and to Dr. Gregory Upert and Conelious Pfumbidzai to continue the work on the AgNPs project . I would like to thank to Dr. Irmgard Hauser-Gerspach for her precious collaboration in the dental implant project and her friendship.

Many thanks to Prof. Dr. Alma U. “Dan” Daniels and his group (Dr. Ueli von Ah and Dr. Olivier Braissant) for the IMC measurements.

Many thanks as well to Prof. Dr. Regine Landmann for sharing her broad knowledge and Oliver Gordon to help me in any theoretical and technical questions concerning the microbiological experiments. I thank to Dr. Reto Luginbühl and the RMS for the implant materials.

I thank all the scientific and technical staff who help me to use different techniques and analysis methods: to Dr. Olivier Casse and Nicholas Cotteyen for the AFM measurements, to Dr. Theresa de Los Arcos for the XPS measurements and the analysis of the results, to all co-workers of the ZMB Basel: Daniel Mathys, Evi Bieler, Marcel Düggelein, Gianni Morson, UniFR: Profs. B. Grobety, C. Bernhard for the hundreds of SEM measurements, to Prof. Dr. Rudolf Gschwind for the light measurements.

Naturally, my family as well as my good friends in Switzerland and in Hungary played a central role in making this thesis possible, providing constant encouragement and unconditional support.

My deepest love goes to Eric for his patience and support and to Alex.

Finally, I acknowledge funding from NCCR-NANO the University of Basel and Fribourg.

## Abstract

Modern medicine continuously develops new artificial short-term or permanent devices to assist in the performance of physiological functions. Implantation of medical devices represents one of the most important risk factors of all nosocomial infections, when implant materials become infected due to bacterial adhesion and subsequent formation of bio films. The latter are impossible to treat with antibiotics and represent a dramatic complication for the patient, leading to implant replacement, in the worst case to death. Therefore, prevention of bacterial adhesion and bio film formation is important.

We have developed new coordination compounds with silver ions and specially designed ligands. This way, one can tune the structure, the light stability and, most importantly for the biological application, the solubility. With an appropriate chemical linker, one is able to connect such compounds to metallic surfaces forming a nano-structured coating. We analyzed the coated surfaces and present the nano-structured surface topography. The chemical composition of the coating on Au(111) as a model surface, the antimicrobial properties of the coated implants, and, on a molecular level, the interaction of silver ions with peptide sequences and subsequent silver nanoparticle formation are presented in this thesis.

We have investigated this coating using several methods, namely powder X-ray, XPS, AFM, SEM, micro- and nano-calorimetry and antimicrobial studies with different bacteria. XPS and powder x-ray analyses have shown that the deposited compound is  $[\text{Ag}(\text{L})\text{NO}_3]$ , described previously. The AFM revealed peak-like nano-structures and the SEM measurements the bigger sized crystalline structures 0.5-1000  $\mu\text{m}$ . AAS method have been used to determine the silver loading on the surface in function the crystallisation time and the concentration. The results show that we are able to control the silver loading on the surface choosing the appropriate treating conditions. Our silver coordination compound was shown to form regular material coatings on different metal substrates.

Several anti-microbial tests were carried out. Flow-chamber experiments with *S. sanguinis* have been done to test the coating on dental implant material. The vitality of adhered bacteria was evaluated by applying a dual fluorescent staining, with the result that 99% of bacteria were killed. Plating of coated samples (Au(111) and titanium and steel restorative implant materials) in agar in presence of *S. epidermis* or *S. aureus* for 24h showed the formation of large inhibition zones of the order of  $>2$  cm. *In vivo* microbiological assays show a high efficiency of the silver coating against *S. epidermis*. The antimicrobial properties were confirmed by microcalorimetry, measuring the bacterial cell multiplication heat. Furthermore the antimicrobial properties are proven for dental as well as general implant materials.

To study the working mechanism of the silver inside of the bacteria and determining the silver affinity of some amino acids and short amino acid sequences, on-bead screening of split-and-mix libraries have been used. It is a powerful tool for the identification of peptides that attach the silver and induce the formation of silver nanoparticles (AgNPs) when using either light or a chemical reducing agent. It allowed identifying simple tripeptides that would have been difficult to predict rationally. In addition, the study revealed peptide motives that generate AgNPs with distinctly different sizes. Some microbiological assays have been done using isothermal microcalorimetry method to test the antimicrobial effect of the generated AgNPs.

We have thus developed a new coating which is able to stop bacterial adhesion and multiplication, while being biocompatible with fibroblasts.

# Index

<b>1</b>	<b>INTRODUCTION .....</b>	<b>3</b>
<b>2</b>	<b>SUBJECT OF THE THESIS.....</b>	<b>19</b>
<b>3</b>	<b>RESULTS AND DISCUSSION.....</b>	<b>21</b>
3.1	AG COMPOUNDS .....	21
3.1.1	<i>Introduction and description.....</i>	<i>21</i>
3.1.2	<i>Synthesis and characterisation.....</i>	<i>25</i>
3.2	COATINGS.....	33
3.2.1	<i>Materials.....</i>	<i>33</i>
3.2.1.1	Chemical fixation by anchor molecules.....	33
3.2.1.2	Substrates .....	36
3.2.2	<i>Coating methods.....</i>	<i>37</i>
3.2.3	<i>Coatings on Au(111) surface.....</i>	<i>39</i>
3.2.3.1	Crystallisation and nanotopography .....	40
3.2.3.2	Influence factors of the coating formation.....	43
3.2.3.2.1	Time dependence .....	45
3.2.3.2.2	Concentration dependence .....	47
3.2.3.3	Stability of Adl7 coating: dissolution test in two biological media .....	48
3.2.3.3.1	Silver release during the dissolution test .....	50
3.2.3.3.2	Conclusions.....	51
3.2.3.4	Chemical analysis of the coated surface: XPS measurements .....	51
3.2.4	<i>Coatings on gold and titanium dental implant materials.....</i>	<i>56</i>
3.2.5	<i>Coatings on titanium and steel restorative implant materials.....</i>	<i>61</i>
3.2.5.1	Titanium rough and smooth restorative implant materials .....	61
3.2.5.2	Smooth and rough stainless steel restorative implant materials.....	68
3.2.6	<i>Coating on other surfaces.....</i>	<i>71</i>
3.2.7	<i>Conclusions.....</i>	<i>74</i>
3.3	MICROBIOLOGICAL <i>IN VITRO</i> AND <i>IN VIVO</i> ASSAYS .....	78
3.3.1	<i>In vitro experiments.....</i>	<i>80</i>
3.3.1.1	Isothermal microcalorimetry (IMC) experiments.....	80
3.3.1.1.1	IMC measurements on silver coordination polymers.....	82
3.3.1.1.2	IMC measurements on AgNPs generated on solid surface by peptides.....	88
3.3.1.1.3	Conclusion of the IMC measurements .....	92
3.3.1.2	<i>In vitro</i> microbiological assays: inhibition zone experiments.....	93
3.3.1.2.1	General description .....	93
3.3.1.2.2	Preliminary AgNO <sub>3</sub> assays.....	97
3.3.1.2.3	Microbiological assays on Au(111) substrate .....	98
3.3.1.2.4	Microbiological assays on coated titanium and stainless steel implant material .....	103
3.3.1.2.5	Conclusions on <i>in vitro</i> inhibition zone experiments .....	106
3.3.1.3	Flow chamber experiments.....	107
3.3.1.4	Conclusions.....	112
3.3.2	<i>In vivo experiments.....</i>	<i>113</i>
3.3.3	<i>Conclusions.....</i>	<i>115</i>
3.4	MOLECULAR MECHANISM OF Ag <sup>+</sup> .....	117
3.4.1	<i>Preliminary experiments with isonicotinate grafted T-Gel resin.....</i>	<i>119</i>
3.4.1.1	XPS measurements.....	121
3.4.1.2	Conclusions.....	125
3.4.2	<i>Combinatorial experiments.....</i>	<i>126</i>
3.4.2.1	Solid phase peptide synthesis and combinatorial chemistry.....	126
3.4.2.2	Combinatorial experiments .....	128
3.4.3	<i>Silver affinity and AgNP generation of tripeptides on solid support.....</i>	<i>133</i>
3.4.3.1	Light reduction .....	134
3.4.3.2	Chemical reduction.....	137
3.4.3.3	Other complementary experiments with the solid phase tripeptide sequences .....	140
3.4.4	<i>Complementary experiments in solution.....</i>	<i>141</i>
3.4.5	<i>Conclusions.....</i>	<i>143</i>
<b>4</b>	<b>CONCLUSIONS.....</b>	<b>145</b>

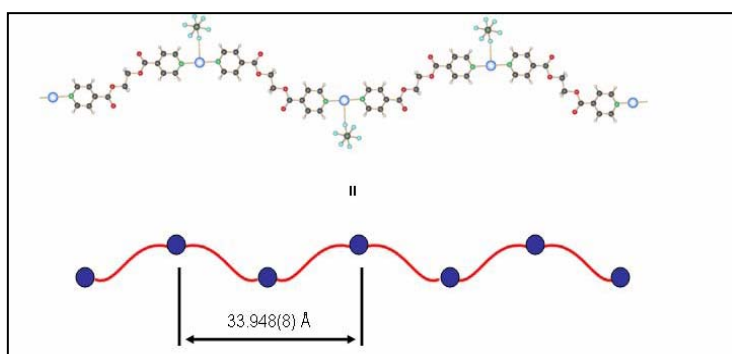
<b>5</b>	<b>EXPERIMENTAL PART.....</b>	<b>151</b>
5.1	EQUIPMENTS AND MATERIALS .....	153
5.1.1	<i>Analytical equipments</i> .....	153
5.1.2	<i>Solvents and chemicals</i> .....	155
5.2	SYNTHESIS AND CHEMICAL CHARACTERISATION .....	156
5.2.1	<i>Ligand</i> .....	156
5.2.2	<i>Bis 2-((4-pyridinylcarbonyl)oxy)ethyl disulfide</i> .....	156
5.2.3	<i>Ag coordination networks</i> .....	160
5.2.4	<i>Peptide synthesis</i> .....	163
5.2.4.1	General procedures of the peptide synthesis.....	163
5.2.4.1.1	Manual peptide synthesis on solid support.....	163
5.2.4.1.2	Peptide synthesis on solid support with automatic synthesizer .....	164
5.2.4.2	Peptide synthesis for Nanoparticle generation.....	166
5.3	COATINGS.....	180
5.3.1	<i>Au(111) plates</i> .....	180
5.3.1.1	In situ crystallisation .....	180
5.3.1.2	Layer-by-layer method .....	184
5.3.2	<i>Ti and Au dental implant materials</i> .....	184
5.3.3	<i>Titanium and steel implant materials</i> .....	186
5.3.4	<i>Coating on T-Gel resin</i> .....	188
5.4	MOLECULAR MECHANISM OF $Ag^+$ .....	189
5.4.1	<i>General method descriptions</i> .....	189
5.4.2	<i>Preliminary experiments with isonicotinate T-Gel beads</i> .....	192
5.4.3	<i>Peptide <math>Ag^+</math> interactions</i> .....	192
5.4.3.1	Combinatorial assay .....	192
5.4.3.2	Silver nanoparticle generation on a surface .....	197
5.4.3.3	Complementary experiments of the solution phase tripeptides .....	199
5.5	BIOLOGICAL ASSAYS .....	200
5.5.1	<i>Isothermal microcalorimetry experiments</i> .....	200
5.5.2	<i>Flow chamber experiments</i> .....	201
5.5.3	<i>In vitro biological assays</i> .....	202
5.5.3.1	<i>In vitro</i> bacterial growth inhibition tests.....	202
5.5.3.2	<i>In vivo</i> assays.....	205
<b>6</b>	<b>BIBLIOGRAPHY.....</b>	<b>207</b>

# 1 Introduction

The title of the thesis: “**Novel silver containing antimicrobial coatings for implant materials: new applications of Ag(I) coordination networks**” suggests a complex interdisciplinary work based on chemistry using knowledge of materials and surface sciences, the analytical methods and the understanding of microbiology to finally give a useful solution to medicine. Prior to the report of our results, some main topics should be discussed.

## Coordination chemistry and polymer networks

At the beginning of the 20<sup>th</sup> century, coordination chemistry became an individual discipline of the chemistry thanks to Werner’s theory. In a complex molecule, the central metal atom binds, via coordination bonds, ligand molecules in a determined geometry. The crystal field theory completed Werner’s model. Since 1950, the scientists use these theories to explain the coordination bond. The molecular orbitals of the central metal atom determine the geometry e.g. as octahedral, tetrahedral and square planar of the complex. Since these coordination compounds have in general a determined geometry, this facilitates the special arrangements in the solid state, and thus the crystallisation. Hence, the principal analytical method for solid state coordination compounds is X-ray crystallography. The huge variety of the possible coordinating ligands, which can be mono-, bi-, tri-, tetra-, polydentate (depending on how many coordination sites are present in the molecule) or open chain or cyclic ligands results in a large number of a possible compounds. If the metal atom is coordinating to more than one ligand and the ligand is able to bond to at least two different metal atoms, the possibility to build an infinite network via coordination bonds exists. Compounds formed in such a way are called coordination networks or coordination polymers referring to the organic polymers. The number of structures of coordination networks can be infinite due to the large variety of the



ligand molecules and metal ions. The motif of the ligand-metal network can vary from linear one dimensional (1D) chains to complicated 3D motifs.

**Figure 1-1:** 1D linear chain motif

of  $\{[Ag(L1)PF_6]\}_n$  coordination polymer. [207]

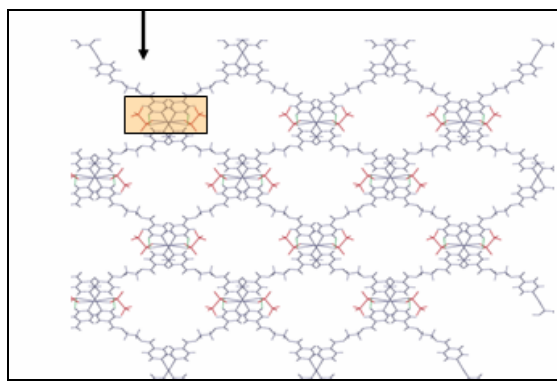
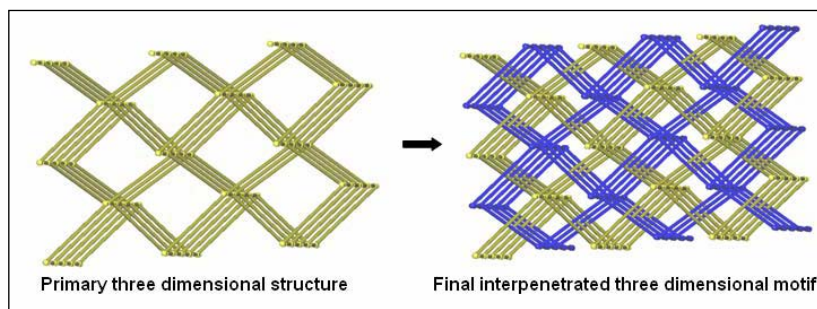


**Figure 1-2,** Polycatenane 3D motif of  $\{[Ag(L1)SO_3CF_3]\}_n$  coordination polymer [207]



Transition metal ions are generally used to build up coordination compounds. For these special coordination compounds (coordination networks), the  $d^{10}$  metals (Ag, Cu) are widely used because their flexible coordination sphere allows building up various structures with N, O and/or S donor atom containing ligands. Silver may have the oxidation states Ag(I), Ag(II), and Ag(III) [208]. Ag(II) complexes are less stable than those of Ag(I) and Ag(III), which not very stable either [209]. The most stable and used one is Ag(I). Ag(I) has a very flexible coordination sphere: it can adopt coordination number from 2 to 6 (from linear geometry [210,211] to octahedral [203] respectively), and it prefers to form simple linear chain motifs. Ag(I) being a soft Lewis acid, it has a coordination preference with donor atoms in the order  $S > N > O$ . Silver ions bind to ligands and organic molecules not only in glassware in the chemistry laboratory, but it binds readily to proteins in the human body (including albumins and metallothioneins) and interacts with trace metals in metabolic pathways [197].

### Silver in the past

For thousands of years, silver was used as a noble metal: as money or as tableware. In parallel to the common wear of the metal, the silver chemistry also developed fast. Hippocrates, who described the virtues of silver in healing, mentions the biological effect. The Phoenicians also used to store water, wine, and vinegar in silver bottles to prevent spoiling. In the early 1800s, doctors used silver sutures in surgical wounds with very successful results. Silver compounds were applied successfully to prevent infections in World War I. Prior to the discovery of

antibiotics silver leaf was used to combat infection in wounds sustained by troops during the war. By 1940, there were approximately four dozen different silver compounds on the market. They were used to treat every known infectious disease. The widespread use of silver went out of fashion with the development of modern antibiotics. Recently, however, there has been renewed interest in silver as a broad-spectrum antibiotic. These are designed to prevent infections as part of wound management procedures, in particular applicable to burn victims [79].

In the 18<sup>th</sup> century, another important invention drew attention to the silver compounds. Johann Heinrich Schulze made the first «pictures» of an image using light, in 1727. Schulze found that silver nitrate solution would darken in response to light, forming a transient image, but these images darkened with the time. In 1839, however, Louis J. M Daguerre patented a new procedure based on silver halide photochemistry and included a process for making the image permanent. At the end of the nineteenth century, William Henry Fox Talbot improved the process for coating silver halides directly on paper in combination with a hyposulfite fixative. Although technologically more advanced, the basic procedures developed by Fox Talbot are used in all silver-based photography. In the era of the numeric photography, the light sensitivity of the silver salts and other silver compounds gets another meaning: The silver nanoparticle formation by photochemical induction or the preparation of light stable silver compounds comes into the focus of interest.

### Silver today

The main interest turned again to the well-known antimicrobial effect of silver. In everyday life numerous products can be found containing silver:

In a medical use: *Elastoplast® Silver Healing™ bandages*: The pads in these bandages contain silver ions. *Silver Sulfadiazine*: is an antibacterial and antifungal agent. It is used as a topical cream to prevent and treat skin infections on areas of burned skin. *Silver Chloride* has the ability to eliminate or flush out mercury from the body and it is used as a thin coating on the surface of medical electrodes for ECG machines.

In other fields of life: *Washing machines* introduced by **Samsung** inject silver ions into the wash and rinse cycles to kill 99.9% of bacteria causing undesirable odours. Silver atoms, electrolytically removed of an electron, are injected during the wash and rinse cycles, allowing over  $10^{17}$  silver ions to penetrate deep into the fabric to “sterilize” clothing without the need for hot water or bleach. These machines can wash about 3,100 loads using 31.1 grams of silver metal. This new invention seems to be very practical in the household, but

nothing is known about the environmental consequences. Several kinds of silver containing (mainly as nanoparticles) underwear are sold on the market. One thing is common to all these products: they exploit the antimicrobial effect of silver.

### Silver in the body

With the spreading use of silver, the question of the toxicity becomes an issue. As silver is part of the group of heavy metals, this question should be clarified. Silver is much better tolerated by the body than most heavy metals [3]. The concentration level where silver is efficient against bacteria but not harmful for the human organism is very important. We are not living in a “silver free” environment. Silver is the sixty-third most abundant metal in the Earth's crust; the average concentration of silver in water is 0.5 ppb, in soil it is 10 ppb. To illustrate the toxicity of the silver compounds some examples are given. For silver oxide the LD<sub>50</sub> for rats at oral intake is 2820 mg/kg [188], and for silver nitrate the LD<sub>50</sub> for mice at oral intake is 50 mg/kg [159]. (Silver metal) Oral LD<sub>50</sub> (rat): >5000 mg/kg [4]. Studies concerning silver coated medical technologies report that silver ion concentrations higher than 10 mg/L may be toxic to certain human cells [141] other studies shows higher limits 18 mg/L for AgNO<sub>3</sub> [138]. The body of an adult contains approximately 2 mg of silver. Our daily intake of silver is 0.02-0.08 mg, of which approximately 10% is absorbed. The drinking water guideline for silver is 0.05 mg/L, if a guideline is fixed at all. At higher silver salt intake, the body may protect itself by converting it to insoluble silver chloride [5]. The toxicity of the insoluble salts is high, but silver ions are only present in low concentration, which it is not active against the micro organisms. Since the early part of the 20th century, doctors have known that silver or silver compounds can cause some areas of the skin and other body tissues to turn gray or blue-gray. The argyria occurs in people who eat or breathe in silver over a long period (several months to many years e.g. in silver mines). A single exposure to a silver compound may also cause silver to be deposited in the skin and in other parts of the body; however, this is not known to be harmful. It is likely that many exposures to silver are necessary to develop argyria. Once the disease develops, it generally remains permanent. The condition is not simply a "cosmetic problem". Discoloration of the skin seen in argyria is however not the most serious health effect of silver. In extreme cases it has been observed to cause brain damage [6], seizures [7], and death or a persistent vegetative state [8].



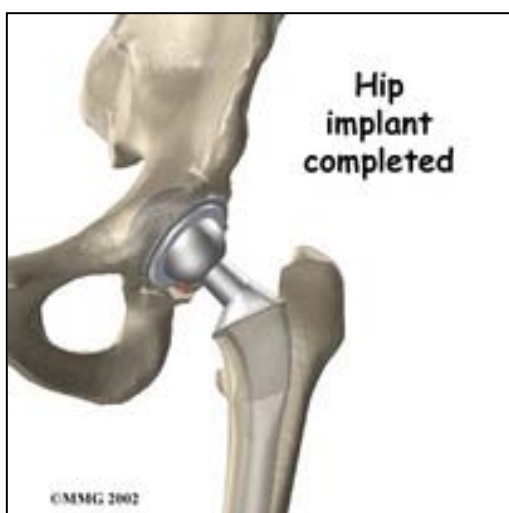
### Silver in medicine

While silver is commonly used in every day life, silver compounds are also present in the medical use. Different silver complexes are already subjects in research. It might be possible to design chemotherapeutic agents that employ silver complexes [9]. It has also been shown that silver chelates are more effective than silver salts as therapeutical agents. It was found that the chelated silver efficiency is much larger (ca.30 times) than the efficiency of the “free” silver [10]. Numerous silver compounds are studied for their antimicrobial activity. The antimicrobial silver compound and products can be divided into two main groups regarding the oxidation state of silver. The first group summarizes the compounds of silver salts and complexes containing silver ions. Several studies have been done on these compounds. Silver complexes can be prepared using amino acids or other biologically active molecules as ligand [11] or sulphur donor atom containing ligands [12,13]. Complexes have been successfully tested regarding their antimicrobial activity prepared from phosphates [14] cyanides [15] and carbenes [16] Naturally, silver salts are also present in the list of the antimicrobial agent [17-19]. The “packing” of the silver complex is also important since it determines the stability and usability. Some silver complex containing composite [20,19], hydrogels [22], films [23,21] and oils [25] are known and used. The compounds/products based on silver nanoparticles belong to the second group. Several hundreds of silver nanoparticle containing compounds/products are known. The size of the nanoparticles, their production and stabilisation methods and their form in the substrates containing nanoparticles can be various. Nowadays, the use of these particles is trendy [26-28]; yet, their toxicity is also in the current societal discussion.

### Biomaterials and implants

Biomaterials are materials and/or devices developed essentially for medical applications. Biomaterials must fulfil the mechanical and biological requirements for their use. They have to be sterilizable, solid, not degradable and easily manufactured. The most important requirement remains the biocompatibility. Biocompatibility of the implanted material is determined by the host response. This means that the implant material must not generate undesirable effects such as biofilm formation or infections, but should help the bio integration, e.g. Osseo integration. Therefore, the implant material should at best behave in the same way as the original body part that is supposed to be replaced by the implant. This is a huge challenge for the medical technical industry. There is an impressive diversity of implants and materials on the market, which facilitates finding the required implant for a

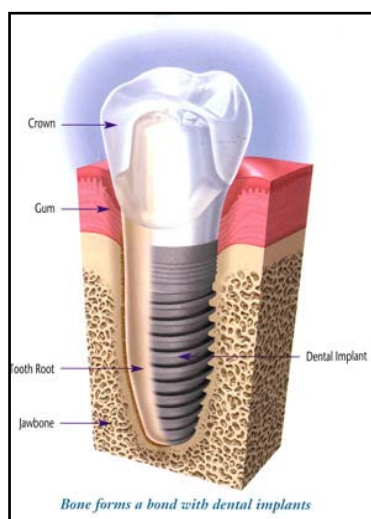
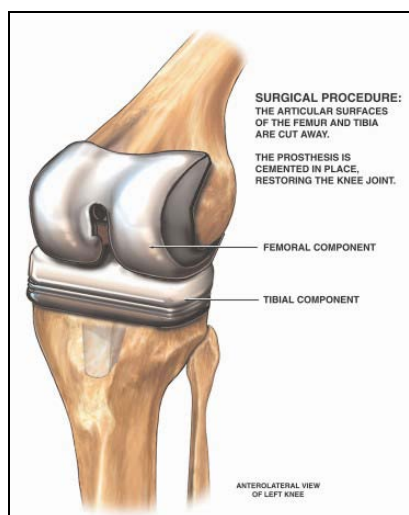
patient. The most commonly used hip implants may have different forms: the metal neck, placed into the femur during the implantation, is made generally from titanium and has various forms and lengths to increase the stability. The surface roughness of this part of the implant can also vary to help the Osseo integration. The diversity of the materials used for the head and the cup is also large: The metal and polymer implants are the most commonly used hip replacement implants.



**Figure 1-3:** Scheme of a modern hip implant [29]

Metal-on-metal implants do not wear out as quickly as the metal and plastic materials. The metal and plastic implants wear out at a rate of about 0.1 millimetres each year. The metal-on-metal implants lose only about 0.01 millimetres each year. The metal wear metal ions are however released into the blood, which might cause serious medical problems. Ceramic-on-ceramic implants are designed to be the most resistant in wear but some cases are known where implants broke inside the body. The newest group of the hip implants, using metal and highly cross linked polyethylene is designed to be most resistant against the wear. This diversity in material and geometry offers the patient individual treatment. The various choices, however might create confusion.

Other implants: knee implants and dental implants have also a huge market.

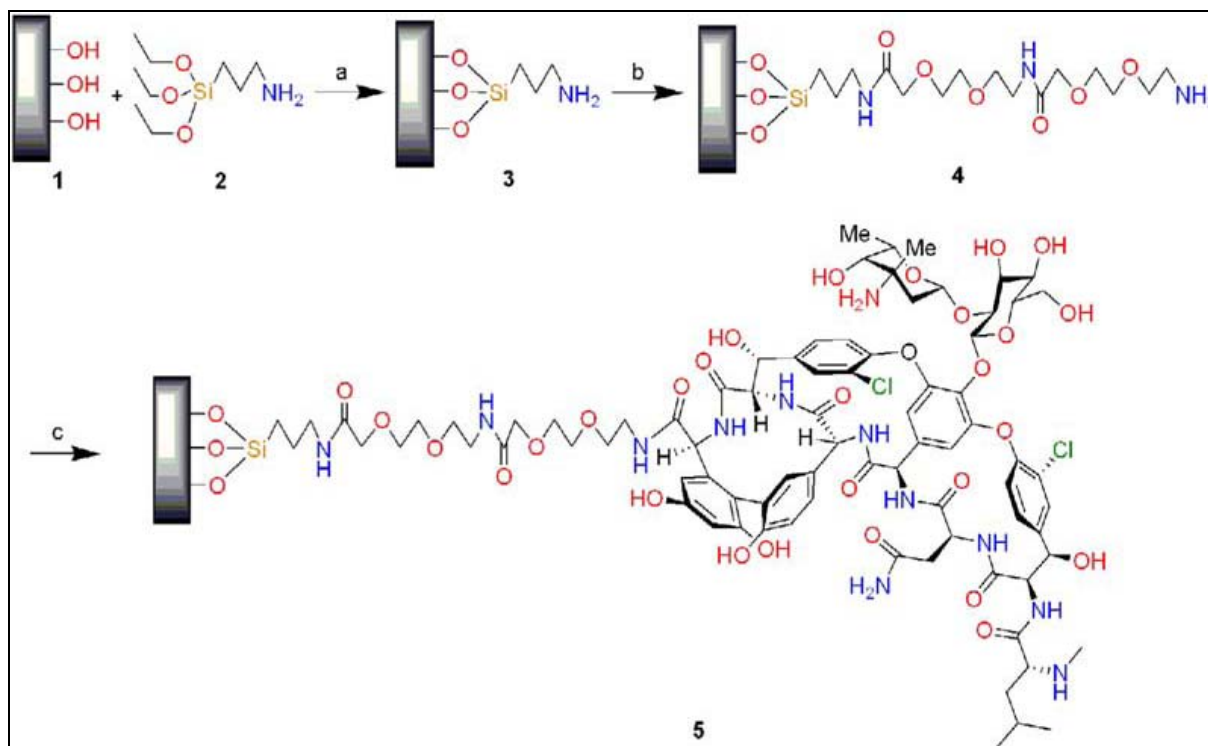


**Figure 1-4:** Scheme of a knee implant and a dental implant [30] and [31]

The diversity in the materials is also present for the knee and dental implants, but titanium metal remains one of the most used materials. Its mechanical characteristics are very good and easy to manufacture. The oxide surface is chemically stable and inert in the body. However, its Osseo integration is not as good as it should be. During the wear, small particles are removed from the surface, causing inflammation around the implant. The infection caused by the micro particles of titanium is just one of the series of problems. Bacterial biofilm formation and infection are most frequently the origin of an implant loosening. If an implant should be removed due to infection and/or inflammation another temporary implant is used to help the healing of the surrounding parts of the body. This temporary implant is generally mechanically not as stable as the definitive one, needing to be treated with antibiotics on the surface to help the healing process. Besides, complementary oral antibiotic treatment is also needed. At the end of the treatment, the temporary implant is replaced by a definite one. This whole process requires 3 operations, a long healing time and high medical costs. Prevention of the infection and biofilm formation, or using a material having an antimicrobial coating as replacement implant may thus decrease the healing time and the medical costs.

### Implant coatings:

The purpose of such coated implant materials is to prevent the biofilm formation followed by infections. Out of 2.6 million orthopaedic implants inserted annually into humans in the United States, approximately 112,000 (4.3%) become infected. The annual infection rate for cardiovascular implants is even higher (7.4%). When considering all implanted devices, the number of implant-associated infections approaches approximately 1 million per year [32]. To avoid these undesirable side effects several coatings for implants have been developed. Coatings have been developed to reduce bacterial adhesion, which is the initial step of the biofilm formation (described later), by altering the physicochemical characteristics of the substrate. Thus, these coatings do not favour the bacteria-substrate interactions. These coatings are referred to as “passive” or anti-adhesive and include surfaces modified with e.g. poly(ethylene glycol) [33], poly(ethylene oxide) brushes [34], and hydrophilic polyurethanes [35]. Unfortunately, the activity of passive coatings reducing the bacterial adhesion is limited and varies depending on bacterial species. Other coatings have antimicrobial characteristics to prevent biofilm formation. One part of these coatings contains antibiotics on the surface [36] [37]. Vancomycin has been successfully attached on titanium surfaces and shows a good anti-microbial activity against *S.aureus* [38].

**Figure 1-5:** Vancomycin attached on a titanium implant surface [38]

Another approach modifies the surface using for example peptides [40-42] or flavonoids [43] to render it antibacterial. The acquired bacterial resistance against antibiotics makes these solutions vulnerable. A major part of the surface modification of the implant materials is realized with silver containing compounds. The most current method to have an antimicrobial silver coating is to use silver nanoparticles in the coating. These nanoparticles can be “packed” [39] for example in hydroxyapatite [44-45] or use silver metal as a deposit on the surface [46,141]. Also silver complexes are used as coating of the implant materials: [47,48]. Sheehan et al reported that silver coatings applied to model orthopaedic implants did not result in decreased *S.epidermidis* and *S.aureus* adhesion [49]. An explanation for the limited antibacterial efficiency of silver coatings is that they do not actively release silver ions. Notably, the antibacterial properties of silver have been attributed to its oxidized form (i.e.,  $\text{Ag}^+$ ), a form of silver that is not necessarily present at a surface coated with metallic silver. Polymers that actively release silver in the oxidized state, however, have exhibited strong antibacterial activity [50]. Such coatings act as reservoirs of silver and are capable of releasing bactericidal levels of  $\text{Ag}^+$  for extended periods (>3 months) [51]. These materials can release silver ions from the polymer reservoir [52] or small silver nanoparticles [53] but the key issue in the antimicrobial activity of these silver containing coatings is the concentration of the released  $\text{Ag}^+$ .

### Bacterial adhesion and biofilm formation

Infection remains a major problem of the long-term use of many implanted devices like joint prostheses, catheters or dentures [54]. Frequently, failure of such devices comes from bacteria biofilm built up on a surface of the device. This biofilm is extremely resistant to host defence mechanisms [55] and antibiotic treatment [56]. Often, the only solution is the surgical removal of the infected device. Bacterial adhesion on a surface of the biomaterial is the essential cause of the infection, however, the mechanism of this process has not been understood in detail. It has been shown that *Coagulase Negative Staphylococci* are the most commonly reported pathogens. These bacteria, most commonly *S.epidermidis*, are normal inhabitants of human skin. The most important characteristic of these bacteria is the ability to colonize by forming a thick, multilayered biofilm on a surface of the foreign-body [57]. *S.epidermidis* does not produce as many toxins as *S.aureus* but adheres fast to the surface and remains there under a protective layer of extra cellular material. The adhered mass of bacteria and its extra cellular polymeric material (slime) on a solid surface are called biofilm. The following figure (Fig.1-6) [58] shows a model of *S.epidermidis* biofilm formation and bacterial factors that play a role in this process.

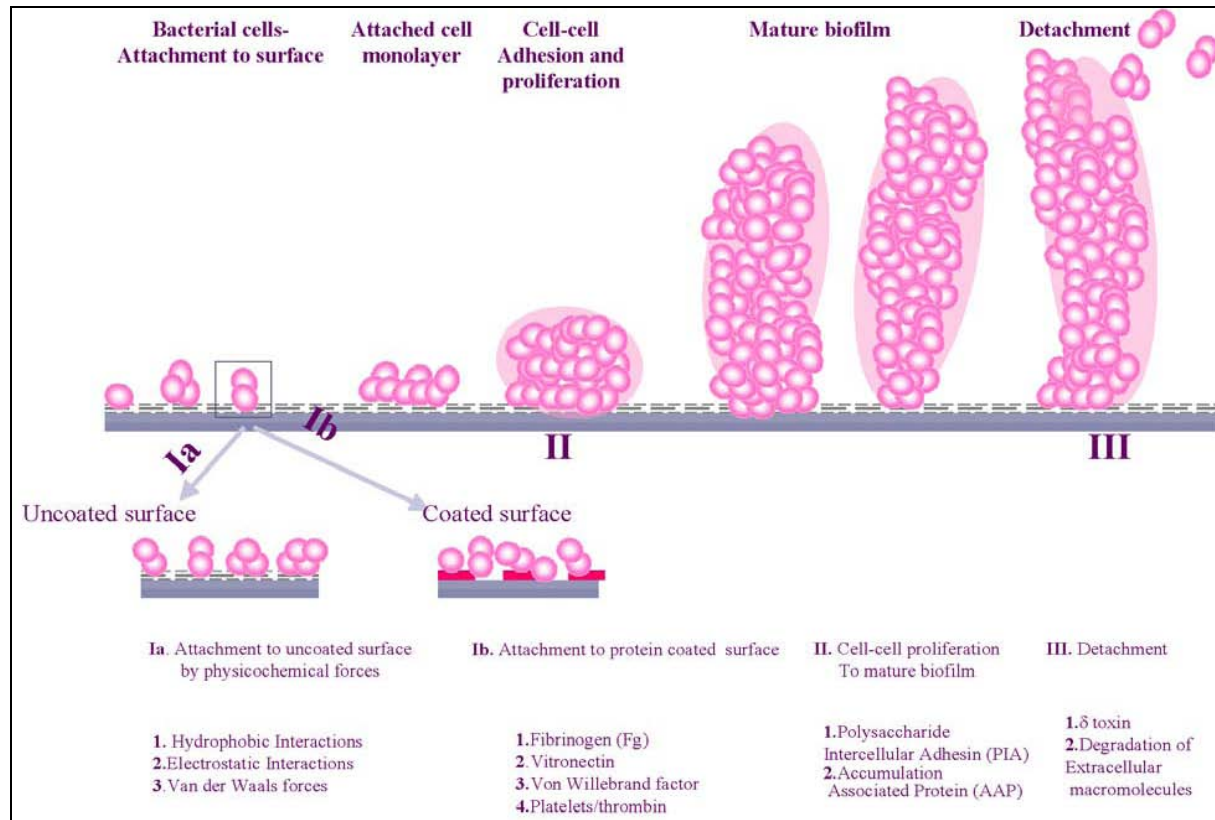


**Figure 1-6:** Scheme of the process of biofilm formation

Bacterial strains that do not produce slime are less adherent and less pathogenic. Bacteria that do not adhere quickly on a surface are rapidly killed by the cleaning mechanism of the body. Slime-forming bacteria are less susceptible to antibiotics (ex. Vancomycin) when they are on a surface.

In a first phase of the biofilm formation, the bacterial adhesion is initiated by an attraction between the cell and a surface. The initial attraction is followed by an adsorption and attachment. From a physicochemical point of view, we can distinguish two types of interactions: long-range interactions (distances  $> 50\text{nm}$ ) take place during the free movement of the bacteria described by mutual forces. The bacteria are transported to the surface by these forces. The short-range interactions (distances  $\leq 5\text{nm}$ ) become more important when the cell and the surface come into close contact. This can be a chemical bond or ionic and dipole interactions. In phase two, the molecular and cellular interaction between the bacteria and a surface become predominant. These kinds of molecular interactions reinforce the adhesion and act like a bridge between the surface and the cell wall. *S.epidermidis* has several polysaccharide adhesins that mediate the adhesion of this bacterium to various material surfaces. [58].

There are several factors influencing the bacterial adhesion. Here, some of these important influencing factors are described, focused on the general environmental and the surface characteristics. These environmental characteristics, e.g. time, temperature, bacterial concentration and flow condition or presence of an antibiotic, do affect the bacterial adhesion. Among others, the flow conditions are considered as one of the most important factors. Numerous works have been made studying this during the last decades. The flow conditions strongly influence the number of the surface attached bacteria [59] as well as the biofilm structure [60]. It was generally shown that higher shear rates generate a decrease in bacterial attachment and make the biofilm denser and thinner. After the bacterium reaches the surface, it is able to interact with the surface. The number of bonds joining the bacterium to the surface can vary. There is a balance between the force of the bonds and the force of the flow. If the shear stress is higher than the bonding force, the bond breaks up. If the number of the bonds decreases under a certain level, the bacterium begins to detach. There is an optimum flow rate regarding the biofilm formation where the delivery of bacteria by the flow is high enough and the shear stress low enough to make the best conditions [61]. As the number of bonds attaching the bacterium to the surface is variable, in a case of higher flow rates, the elevated shear stress on the attached bacteria forces them to increase the number of the bonds [62].

Among the environmental factors, one has to take into account: the effect of the electrolyte concentration and the pH [63]. Generally, the presence of an antibiotic decreases the biofilm formation [64]. However, the adhered *S.epidermidis* was less susceptible to antibiotic treatment than free cells [65]. This can be explained by the slowdown of bacterial metabolism inside of the biofilm, or the changed metabolism and selectivity of the bacteria on the surface, e.g. the multiplication of the antibiotics resistant mutants on the surface. For these strains, the conditions on the surface are then more favourable. This and the fact that only a small range of antibiotics is efficient against biofilm producing bacteria make the work of researchers in this field more demanding.

The surface characteristics of the material are also a determinant factors in the biofilm formation. Surface chemistry influences the bacterial adhesion and proliferation. Different functional groups determine the surface charge and hydrophobicity that affect the behaviour of bacteria versus the surface. It was shown that on a negatively charged surface, the bacterial adhesion decreased, while a positively charged surface facilitated biofilm formation [66]. If the surface chemistry is modified, such as, with silver, plasma coatings or organic molecules like peptides or drugs, the bacterial adhesion is handicapped. These kinds of coatings have been described previously. Several surface modifying methods disadvantage the biofilm formation. The surface roughness also plays a key role in the process of biofilm formation. It has been found that irregularities on a smooth surface increase the bacterial adhesion [67]. In a case of PMMA, modified with silicon carbide paper, it has been shown that the bacterial adhesion increases with roughness, but a too rough surface has no significant influence on a biofilm deposit [68]. The initial distribution of the bacteria is random on a smooth surface, but follows some preferential direction on microrough surfaces. There is a relationship between the size of roughness and bacterial size, which affects the initial step of the bacterial adhesion, and the extra cellular polymer material production. If the parameters of the topography are in the same order as the bacterial dimension, it was shown that the bacteria attach easily and less extra cellular matrix is produced. Bacteria can thus act in response to the nano topography, can choose the most favourable direction of the attachment, the morphology and the extra cellular matrix production under the given nano environment [69].

In biofilm formation the first step of bacterial adhesion is a reversible one. This is the time when the coating of the implant can effectively act. Hence, a 6 h post-implantation “decisive period” has been identified during which prevention of bacterial adhesion is critical to the long-term success of an implant [70]. After this period, an implant is particularly susceptible to surface colonization. It is very important to avoid the biofilm formation during this period,

and both, passive and active coatings, should be reliable. An active coating only could be effective if appropriate release of the active substance is realized [71].

### Silver as antimicrobial agent and silver resistance

It has been previously described that the key step in the antimicrobial activity of the silver containing coatings depends on the concentration of the released  $\text{Ag}^+$ . This means that in the action mechanism, the  $\text{Ag}^+$  plays a determining role; the silver metal is rather an inactive form. However, how does silver act inside the cell?

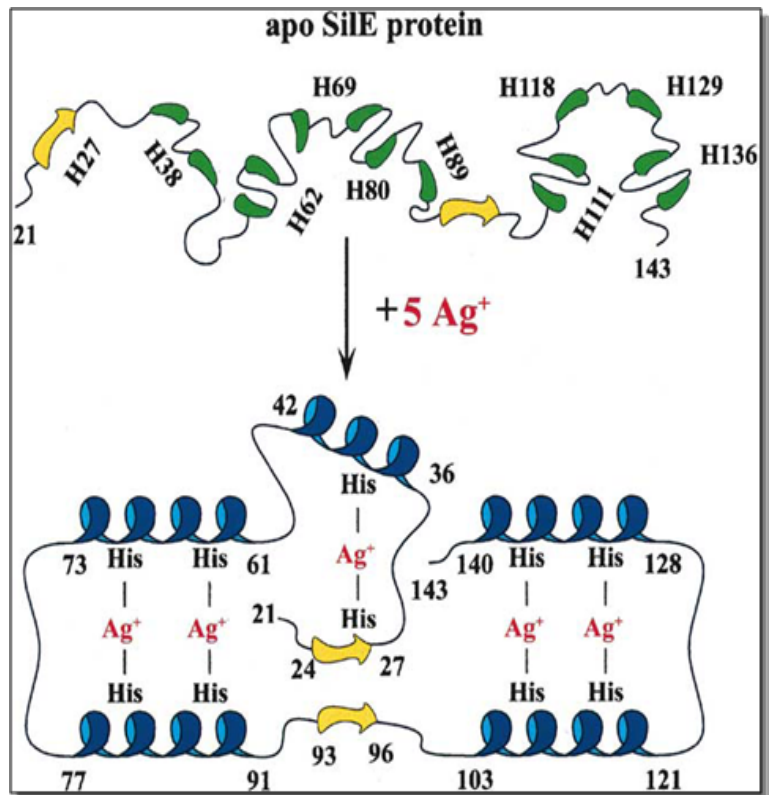
Silver products have been used for their beneficial effects in medicine and in general hygiene. For more than a thousand years, silver has been used to heal and prevent diseases without knowledge of the working mechanism. In the last decades, silver has had a renaissance in clinical applications using its antibacterial properties, for treatment of burns [72,152] and in wound care. This renaissance and modern methods allow the scientists to complete this lack of knowledge.

Since 1929, when Alexander Fleming observed the antibacterial effect of the penicillin, numerous different new molecules and antibiotics were developed. As long as antibiotics have been applied, bacteria have developed resistance against them. Resistance to an antimicrobial agent can occur either by “intrinsic” or acquired mechanism. Therefore, intrinsic resistance would involve natural resistance via the structure of the cell surface and its chemical composition. [73]. Acquired resistance to a wide range of antibiotics has been observed in a variety of micro-organisms [74]. One of the biggest challenges is to introduce compounds that prevent the development of bacterial resistance against them. Contrary to the antibiotics, it is also generally accepted that the antibacterial mechanisms of  $\text{Ag}^+$  are such that bacteria will not develop resistance [75]. Biocides (such as silver) and antibiotics have different modes of action. Biocides tend to target multiple sites on or within bacterial cells and have broad-spectrum activity. Antibiotics tend to target specific sites on or within bacterial cells and have a narrower spectrum of activity. It seems that the majority of the biocides acts on cell surface components of the bacteria and/or the cytoplasmic membrane [76]. Silver resistance is also postulated in the literature, but the number of resistant bacteria is largely inferior to the number of known bacterial resistances against antibiotics. The proteins and genes involved in bacterial resistance to  $\text{Ag}^+$  have been studied in recent years. These studies help to understand the working mechanism of silver, how silver ions react causing the antimicrobial effect. The works of *S.Silver* [77] are focused on the understanding of the process: how silver is eliminated from the interior of the cell, which genes and pumps



are responsible for this process. The described model proposes a key role for histidine as binding compound in the silver elimination process [78].

**Figure 1-7:** Scheme of the SilE protein [79]



SilE is a small periplasmic Ag(I)-binding protein that binds Ag(I) ions specifically at the cell surface,

presenting the first line of resistance against Ag(I) toxicity. Studies with purified SilE protein using atomic absorption spectroscopy (AAS) and inductive-coupled plasma analysis showed very high specificity for Ag(I) binding. The SilE protein contains 10 histidine residues that are able to bind up to five Ag(I) cations, (**Fig.1-7**). [79] This mechanism does not correspond to a classical way of a resistance process known in the case of antibiotics, but to an efflux pump eliminating the silver ions from the cells and storing the harmful metal in a safe way.

There are also studies done to find out how silver acts in the interior of the cells and which molecular biological steps are blocked or disturbed by it. The mechanism of the antibacterial action of the silver ions is discussed to be closely related to their interaction with thiol groups [80,81] although other target sites are also proposed [82]. Studies on *Pseudomonas aeruginosa* PAOI bacteria, this bacterial strain had been found to be very sensitive to silver compound [83], have shown that sulphur containing amino acids, as cysteine and reduced glutathione are an effective neutralizer of silver nitrate. Other tested amino acids, not containing thiol groups, as cystine, methionine, glycine, glutamic acid, are coordinating silver ions via their N atoms, resulting in a coordination ratio 0.28-0.4 silver ions per nitrogen atoms. This value is much lower than the 3.1 coordination ratio measured by the thiol group

containing amino acids, which proposes an important role of the thiol groups in action of silver ions [84]. To gain insight into the inhibition mechanism of silver ions in a living cell, bacterial strains: a Gram- negative *Escherichia Coli* and Gram-positive *Staphylococcus aureus* and *Staphylococcus Epidermidis* were treated with silver nitrate and studied by electron microscopy and X-ray microanalysis, focusing on the morphological changes of the cells [85]. This work showed that the free state of DNA after the silver treatment changed to a condensed form. In this form, the DNA lost its replication ability and inactivates the bacteria. The condensed DNA is present in the centre of the electron light region of the cells. This electron light region is supposed to protect the DNA against harmful processes and the composition of this region is unknown, except the DNA being situated normally randomly inside. The X-ray microanalysis demonstrates the presence of silver in the cytoplasm, in the DNA and in the electron dense granules, which should correspond to silver, as well as the depositions of proteins surrounding the cell wall and the electron light region. Since the EDAX spectrum shows also the presence of *S.epidermidis*, they proposed that the silver ions interact with the thiol groups in proteins resulting in their inactivation. The gram-positive *S.aureus* is suffering a less important morphological change, thanks to the thicker cell wall protecting the cell against the penetration of the silver into the cytoplasm.

Other works study the silver acting mechanism against bacteria focusing on the effect of silver on the respiratory chain of the bacteria [86]. The addition of around 10  $\mu\text{M}$   $\text{AgNO}_3$  to suspended or immobilized *E. coli* results in stimulated respiration before death, signifying uncoupling of respiratory control from ATP synthesis. This is a typical sign of the interaction of  $\text{Ag}^+$  with enzymes of the respiratory chain. Experiments using an alternative electron acceptor than oxygen, suggests that  $\text{Ag}^+$  inhibits at a low potential point of the chain, possibly the NADH dehydrogenase stage. Surface-enhanced Raman spectroscopy of bacteria treated with  $\text{AgNO}_3$  and sodium borohydride suggests that  $\text{Ag}^+$  binds preferentially to sites associated with flavin groups [87]. These are proposed as the major site of inhibition, and represent a NADH binding site. *E. coli* possesses only two different NADH dehydrogenases: the proton pumping NDH-I, containing FMN (flavin mononucleotide) and up to nine FeS clusters, and the noncoupled NDH-II, which contains FAD (flavin adenine dinucleotide) [92]. Both dehydrogenases appear as possible sites for  $\text{Ag}^+$  binding, containing cysteine residues that have a high affinity for  $\text{Ag}^+$  [84].

Different theories exist on how silver can affect the respiratory chain, e.g. that it disturbs the citric acid cycle. This is one of the metabolic pathways of the cellular respiration, inside of the mitochondria. We call cellular respiration the complex processes taking place in the cells to

convert nutrients into adenosine triphosphate (ATP), which is the main form of energy in the cell, and release waste products. [88].

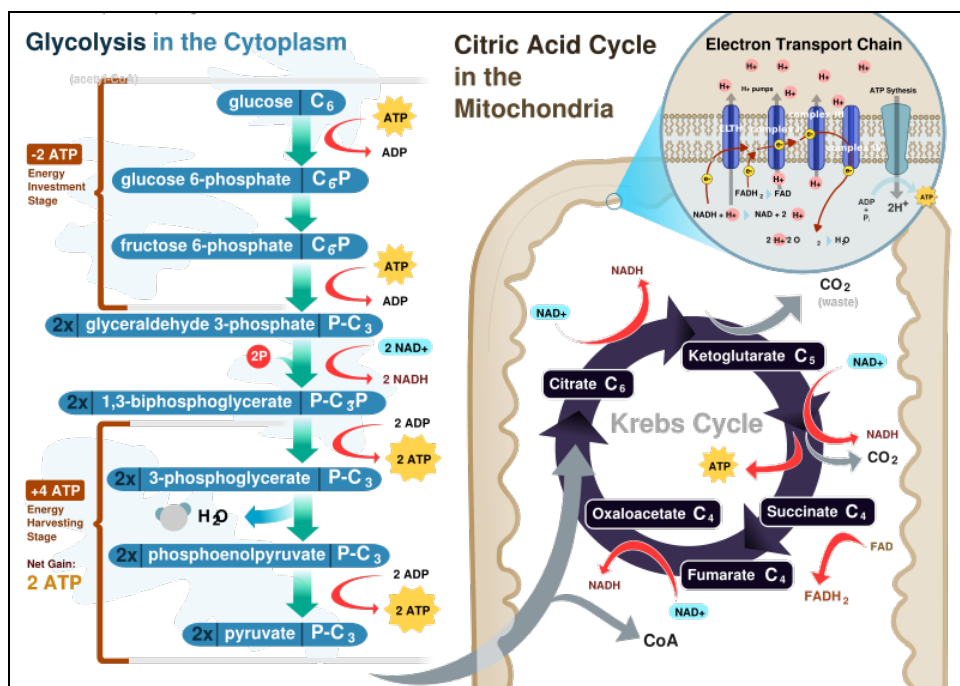


**Figure 1-8:** Cellular respiration in a typical eukaryotic cell. [89]

The citric acid cycle is the third step in the breakdown of sugars (carbohydrate catabolism). Glycolysis breaks glucose (a six-carbon-molecule) down into pyruvate (a three-carbon molecule). In eukaryotes, pyruvate moves into the mitochondria. It is converted into acetyl-CoA by decarboxylation and enters the citric acid cycle inside the mitochondrial matrix. Here, it gets oxidized to CO<sub>2</sub> while at the same time reducing NAD to NADH which can be used by the electron transport chain to produce further energy (ATP). To fully oxidize the equivalent of one glucose molecule, two acetyl-CoA must be metabolized by the citric acid cycle. Two waste products, H<sub>2</sub>O and CO<sub>2</sub>, are created during this cycle. The citric acid cycle is an 8-step process involving 8 different enzymes. Throughout the entire cycle, Acetyl CoA changes into Citrate, Isocitrate, α-ketoglutarate, succinyl-CoA, succinate, fumarate, malate, and finally, oxaloacetate.

One of these enzymes is aconitase (aconitate hydratase) which catalyses the stereo-specific isomerization of citrate to isocitrate via *cis*-aconitate. The heart of the enzyme is an iron-sulfur cluster which reacts directly with an enzyme substrate. This active [Fe<sub>4</sub>S<sub>4</sub>]<sup>2+</sup> cluster may convert to an inactive [Fe<sub>3</sub>S<sub>4</sub>]<sup>+</sup> form. Three cysteine (Cys) residues have been shown to be ligands of the [Fe<sub>4</sub>S<sub>4</sub>] centre.

**Figure 1-9:** Aconitase in complex with iron-sulfur cluster and isocitrate, [90]



In the active state, the labile iron ion of the  $[\text{Fe}_4\text{S}_4]$  cluster is not coordinated by Cys but by water molecules. In this enzyme, the cysteine molecules which are very good complexing agents of silver, have a main role. Because of the cysteine molecules and the sulphur itself, the iron sulphur cluster might be also sensitive to silver ions. If silver ions disturb the function of this enzyme, e.g. by exchanging the iron or other interaction with the cluster, the metal can appear as antibacterial or toxic as it damages the cell. If the silver exchanges the iron from the cluster, the free iron behaves as a radical that can cause the death of the cell. Since the aconitase is directly involved in mtDNA stability and organization [91], it may enhance the activity of the silver.

The following question remains open after the review of the literature concerning the working mechanism of the antimicrobial silver: which processes or enzymes are disturbed or/and blocked by the silver that manifests in the antimicrobial behaviour of this metal?

## 2 Subject of the thesis

There is a high demand by the orthopaedic medical community for implant materials that are not susceptible to bacterial adhesion, biofilm formation and thus infection. The previously described examples do not offer a perfect solution. Hence, the aim of this work is to propose a new coating method for implant materials that prevent the biofilm formation and resulting infections in medical applications.

Preparing antimicrobial silver containing coatings on implant surfaces is a complex challenge. It is an interdisciplinary activity combining chemistry, surface physics, material sciences, microbiology and medicine. The target coating should fulfil many requirements, as it is generally the case for materials used in human medicine. These requirements are:

- chemically defined
- light stable coating
- mechanical stability
- long-term activity
- reproducibility
- non-toxicity
- bio integration
- antimicrobial activity of the coated surface.

The first step is to find the silver compound having the appropriate stability, solubility, and chemical characteristics. Working with silver coordination polymers has been one of the principle activities in our group. Several of these coordination networks have been synthesized and described by former group members: Dr. Adeline Y. Robin and Dr. Jorge Sagué Doimeadios. These descriptions are focused on the crystalline structure and the complexation behaviour of the compounds. However, these compounds haven't been tested for their chemical stability and microbiological effect. Thus, a suitable Ag-coordination compound has to be identified with regard to solubility and stability. Then the compound should be attached on a surface in a way that it resists against chemical and mechanical impacts. The characterization of the coating has to be complete with respect to chemical composition and topography. The behaviour of the coating in biological media and its silver release needs to be analysed in detail. The silver ion release determines the antimicrobial and/or toxic effects, therefore the properties of the coatings have to be studied and optimized. Different implant substrates such as metal and polymers will be taken into account. The application of the silver as antimicrobial agent, and the understanding of the

action mechanism of the silver ions against bacterial cells are also part of this study. Therefore, the interaction of silver ions with short peptide sequences is studied. In this context, silver nanoparticles (AgNPs) formation became an issue.

Finally, after the extensive chemical, topographical analysis and effectiveness of the coating - both silver coordination polymers and nanoparticles - against bacteria are tested. For this purpose from a number of existing microbiological methods several will be used. These microbiological experiments are outside our chemical knowledge and material possibilities, and are thus made in collaboration with Dr. I. Hauser-Gerspach of the Oral Microbiology Laboratory of the University of Basle, Prof A.U.Daniels of the Orthopaedics Biomechanics Laboratory of the University of Basle and Prof. R.Landmann of the University Hospital of Basle.

The aim of this work is to describe the chemical and topographical analysis of an antimicrobial silver coating from silver coordination polymer and silver nanoparticles. A flexible coating method is developed to control the silver release and the antimicrobial effect. Different short peptide sequences will be tested regarding their affinity to silver ions, giving some important information about the action mechanism of the silver ions as antimicrobial agents. Finally, the study is completed with *in vitro* and *in vivo* antimicrobial experiments.

## 3 Results and discussion

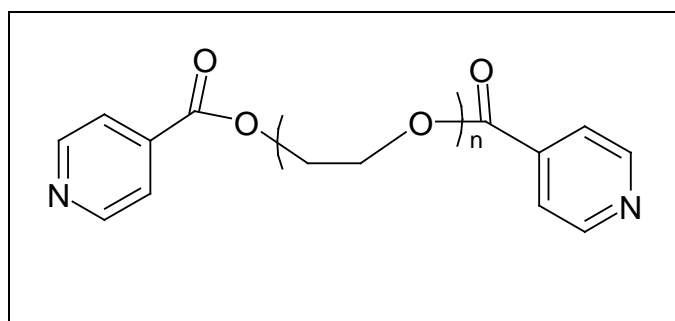
### 3.1 Ag compounds

#### 3.1.1 *Introduction and description*

Working with silver coordination polymer networks is one of the main profiles of our group. In our previous works, these compounds were fully described [207,93,94] concerning their synthesis, crystallographic characterisation, IR and UV studies. Here, the previous results are briefly presented and completed with other data such as dissolution and light stability tests.

**Figure 3.1-1:** General structure of the bidentate bipyridil ligands:

**L<sub>n</sub>:** where (n:1, 2,3,...)



This work focused on the first generation of the bidentate bipyridyl ligands: the ethanediyl bis(isonicotinate) ligand synthesized and studied in our group. This ligand, containing two N and two O donor atoms and a flexible linker is capable of building up various structures by coordinating two or more metal ions. The L1 ethanediyl bis(isonicotinate) can adopt two conformations, anti and gauche resulting of the free rotation around the ethyl group C-C bond.

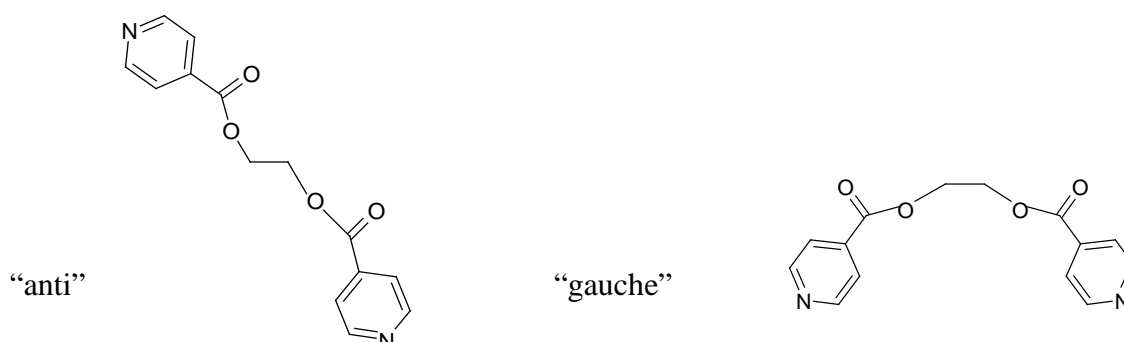










**Figure 3.1-2:** Anti and gauche conformation of the L1

The different conformations of the ligand in a coordination polymer can completely change their structure. Therefore, their chemical and physical characteristics could be dissimilar while the chemical composition of the compounds can be the same (polymorphism, isomerism).

[95] As the Ag metal ion has a flexible coordination sphere, the coordination number can vary between two and six, and the geometry from the simplest linear to octahedral. Silver ions with the ethanediyl bis(isonicotinate) ligand (L1) build up at least eight different coordination networks, [96] as shown in the following table (**Table 3.1-1**) :

**Table 3.1-1:** Structural diversity of the polymer networks build up from Ag(I) and L1

Name	Cristallisation conditions: Ag salt; solvent	Molecular formula	Chain motif
Adl3	AgNO <sub>3</sub> ; THF/H <sub>2</sub> O	{[Ag(L1)]NO <sub>3</sub> } <sub>n</sub>	
Adl4	AgNO <sub>3</sub> ; THF/H <sub>2</sub> O	{[Ag(L1)]NO <sub>3</sub> .H <sub>2</sub> O} <sub>n</sub>	
Adl5	AgNO <sub>3</sub> ; THF/H <sub>2</sub> O	{[Ag(L1)]NO <sub>3</sub> .2H <sub>2</sub> O } <sub>n</sub>	
Adl6	AgNO <sub>3</sub> ; EtOH	{[Ag <sub>2</sub> (L1)(NO <sub>3</sub> ) <sub>2</sub> ]} <sub>n</sub>	
Adl7	AgNO <sub>3</sub> ; CH <sub>3</sub> CN	{[Ag(L1)]NO <sub>3</sub> } <sub>n</sub>	
Adl8	AgCF <sub>3</sub> SO <sub>3</sub> ; THF/H <sub>2</sub> O	{[Ag(L1)] CF <sub>3</sub> SO <sub>3</sub> } <sub>n</sub>	
Adl9	AgClO <sub>4</sub> ; THF/H <sub>2</sub> O	{[Ag(L1)] ClO <sub>4</sub> } <sub>n</sub>	
Adl10	AgPF <sub>6</sub> ; THF/H <sub>2</sub> O	{[Ag(L1)] PF <sub>6</sub> } <sub>n</sub>	

● : silver ion  : ligand

Besides these polymer networks, the longer ligand (L2) readily forms ring structures with two silver ions and two ligands in a complex. [207]

For the purpose of antimicrobial coatings, we would like to focus on the following three compounds: Adl3, Adl6 and Adl7 for further discussion. The compounds other than nitrate-containing are excluded from the planned biological assays due to their toxic counter ions for the living species. The two compounds containing water molecules in the crystalline structure, Adl4, Adl5 have no long-term stability. The co-crystallizing water molecules can be released, which results in an instability of the structure.

Even though the building blocs of the three compounds Adl3, Adl6 and Adl7 are the same, their crystalline structures are significantly different. Adl3 crystallizes in a monoclinic space group P<sub>2</sub><sub>1</sub>/n. The pyridine N-atoms coordinate to the silver ions creating a one-dimensional chain motif: the silver atoms are coordinating to two N atoms of two different ligands (L1). The conformation of the ligand is “anti” and the direction of the ligand between the silver atoms is alternating: going down to up then up to down as shown in **Fig.3.1-3**.



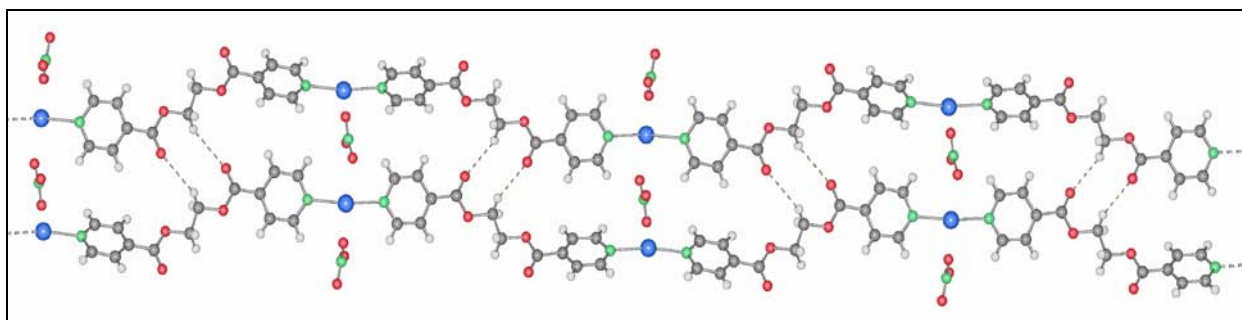


**Figure 3.1-3:** Crystalline structure of Adl3

In Adl3, the nitrate anion acts as tridentate ligand towards two silver atoms. The nitrate acts as a linker between two silver atoms: each nitrate atoms are connected to two different silver ions and each cation is connected to two different nitrate anions. The most important bond lengths are the following:

Bond	Lengths Å		
	<b>Adl3</b>	<b>Adl6</b>	<b>Adl7</b>
Ag—N	2.232(2), 2.239(2)	2.226(7)	2.183(4), 2.189(4)
Ag—O(O2N)	2.669(2), 2.724(2), bidentate 2.800 (3), monodentate	2.354(5), 2.390(7) 2.72(1)	2.599(5), 2.703(7), bidentate 3.044(4), 3.122(4), bidentate
Ag—Ag	8.02 (3)	5.210	4.017(2)

**Table 3.1-2:** Most important bond length of Adl3, Adl6 and Adl7

Other additional interactions coexist between two chains. Some H-bonds were found between close ligand molecules, between the nitrate anions and pyridine hydrogen atoms or ethyl hydrogen atoms. A  $\pi$ - $\pi$  interaction of rings at a distance of 3.62 Å is also observed. Although the Ag—Ag distance is too long to have a contact, the closest distance between two silver ions is mentioned in **Table 3.1-2**, because it will be important during the comparison of the different compounds.

Adl7 crystallizes in the triclinic space group P-1 (no.2). In this case, similar as the previous one, the silver atoms are coordinated by two different ligands through their nitrogen atoms. The ligand molecules act thus as connectors between the silver atoms, the final motif being a charged one-dimensional chain. This compound is a polymorph to Adl3 showing the same arrangement of one-dimensional chains with bringing nitrate anions. Even so, many differences appear. The conformation of the ligand is “anti” as in Adl3 but here the direction of the ligands differs compared to Adl3: the direction is constantly up-to-down. Here, as shown before, the nitrate anions function as a linker between two chains. Each nitrate is connected to two different silver ions in neighbouring chains.

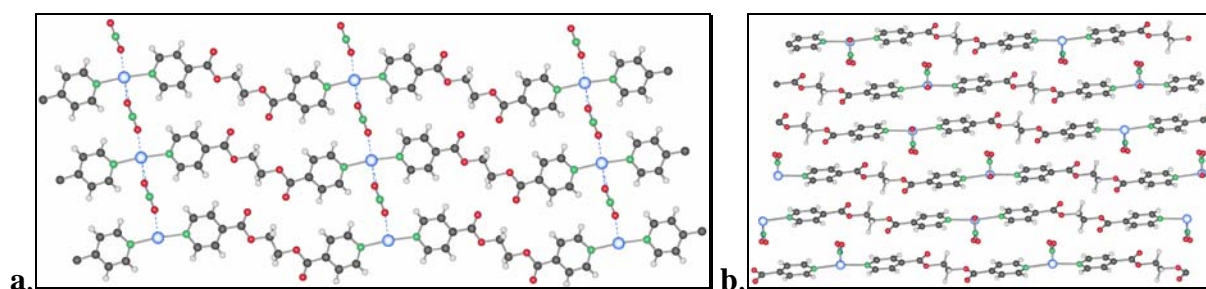


**Figure 3.1-4 a,b:** Crystalline structure of Adl7

Some comments about the inter-chain and layer interactions. These interactions are very different from the previously discussed Adl3 compound. The layers stack parallel in alternating their orientations.

Comparing the bond lengths of Adl7 to the bonds of the Adl3 (**Table 3.1-2**), two data attract attention. First, that the Ag—N bond lengths are slightly shorter in the case of Adl7, and the Ag—Ag contact existing in the case of Adl7 but not in Adl3. These two characteristics point to the possible higher stability of the Adl7 compound. Further investigation should prove this hypothesis.

Adl6 crystallizes in the monoclinic space group  $C2/c$  (no.15). There are eight asymmetric units (one silver atom, one nitrate molecule and one half ligand) in each unit cell, which means there are two silver atoms for one ligand molecule. Ligand molecules, silver atoms, and nitrate counter anions are organized so that a neutral two-dimensional motif appears. This motif is called a “fishbone”-like layer, **Fig.:3.1-5**.

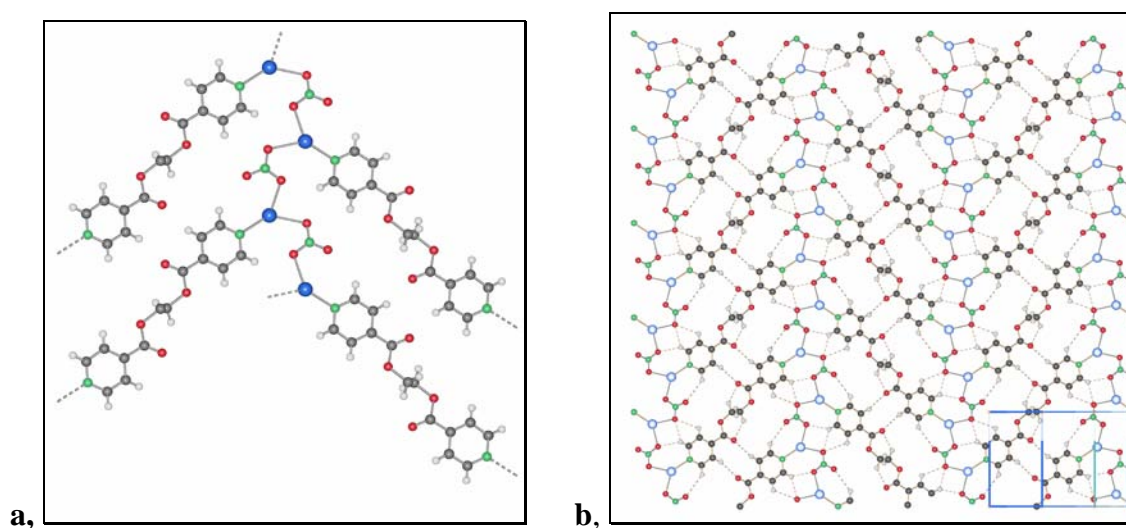


**Figure 3.1-5a,b:** Crystalline structure of Adl6

The main difference of this structure and the previous ones is that the main one-dimensional chains are silver nitrate chains, linked together via the ligands. The bond lengths, shown in **Table 3.1-2**, confirm this major difference.

Each silver atom is coordinated with one ligand L1 molecule and with two different nitrate counter anions. The bond lengths Ag—O(O<sub>2</sub>N) 2.354, 2.390 Å correspond to short silver nitrate distances showing a strong coordination bond. The silver-oxygen distances belong to the shortest ones known from the literature [97, 98, 99]. The conformation of the ligand is *anti* as in the two previous examples. Regarding the Ag-Ag interactions, the distance between the two silver ions is too long for any interaction (same situation as described for Adl3).

Concerning the interactions between the layers and chains, just some weak interactions can be found. The layers are stacked parallel to each other to form an overall three-dimensional structure. Hydrogen bonds between two parallel ligand molecules have been observed. Furthermore, the nitrate anions are involved in hydrogen bonding to the surrounding pyridyl hydrogen atoms. The silver ion has, besides of the three short contacts within a plane, a fourth weak bond with a nitrate anion O, perpendicularly to the plane connecting to the other layer. On the other side of the silver atom, there is a metal-ring interaction to stack the layers together. No other interactions were found between two layers except these interactions involving silver atoms.

Adl6 is expected to be very soluble, while the higher content of ligand in compounds Adl7 and Adl3 makes them less soluble in aqueous media and thus more interesting for our study. This hypothesis demands some further investigations to prove the suitability of these compounds for the *in vitro* and *in vivo* biological assays. Based on this hypothesis, further investigations are focused on Adl7 in comparison with Adl3.

#### **3.1.2 Synthesis and characterisation**

Here, an easy way is described to synthesize and identify the compounds Adl7 and Adl3, and to study their dissolution in different media generally used in biological assays. Their light stability was measured to make sure that the silver is stable enough in the complex to avoid a fast reduction through light. Such colour change due to reduction of the compound is unfavourable regarding the medical use.

Since the chemical composition of compounds Adl3 and Adl7 is the same, but their crystalline structure is different, the easiest and fastest way to identify them is to measure the powder X-ray spectra and compare them to their crystallographic data [93,94].

The powder X-ray spectra of Adl3, Adl6 and Adl7 are shown in **Fig.3.1-6**.

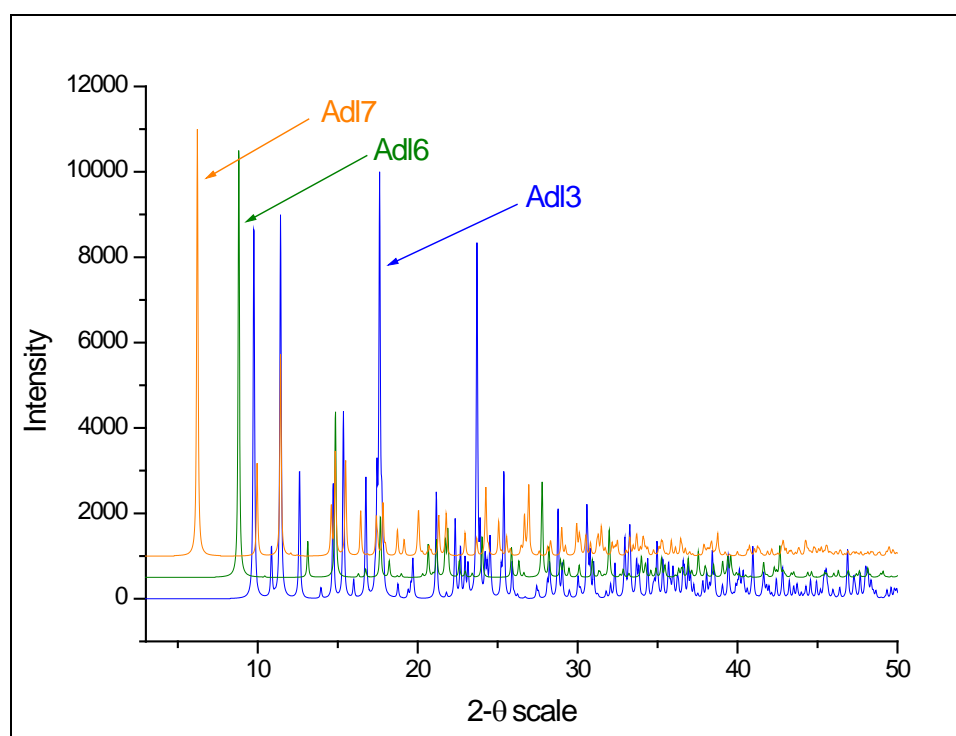


**Figure 3.1-6:** Powder X-ray spectra of Adl3, Adl6 and Adl7

To obtain information on the solubility of the different Ag-compounds, important for biological assays, dissolution tests were performed. The solubility of the compound is crucial. If the silver leaking were too high, the effect of the silver would be so strong that it kills not only the bacterial cells but also damages the healthy eucaryotic cells. If the silver leaking is too low, we cannot observe the antibacterial effect. There is an antibacterial effect when silver ions can be released from the implant, which then penetrate the cell wall and enter into the cell, subsequently turning DNA into an inactive form and at the same time reacting with proteins [100,141]. For this test, two different biological media were used: the synthetic medium, prepared artificially (composition described in the experimental part) and the Müller-Hinton medium. The synthetic medium is composed of an important quantity of sodium and other chlorides and phosphates, a mixture of several amino acids and vitamins, and trace elements. The exact composition of the Müller-Hinton medium is unknown, being a natural product from meat infusion. Some milligrams of compound were weighed into a glass vessel and a given volume of medium was added. The flask was closed and shaken. At stated time intervals, the solution was removed, filtered and the silver concentration was determined. The precipitate was washed with ethanol, dried and a powder X-ray spectrum was made of the solid (**Fig.3.1-11**). The filtered solutions were analyzed for their  $\text{Ag}^+$ -content using AAS (atomic absorption spectroscopy), comparing to a standardized  $\text{AgNO}_3$ -solution. The measured silver concentrations are represented as a function of time in **Fig.3.1-7a,b**.

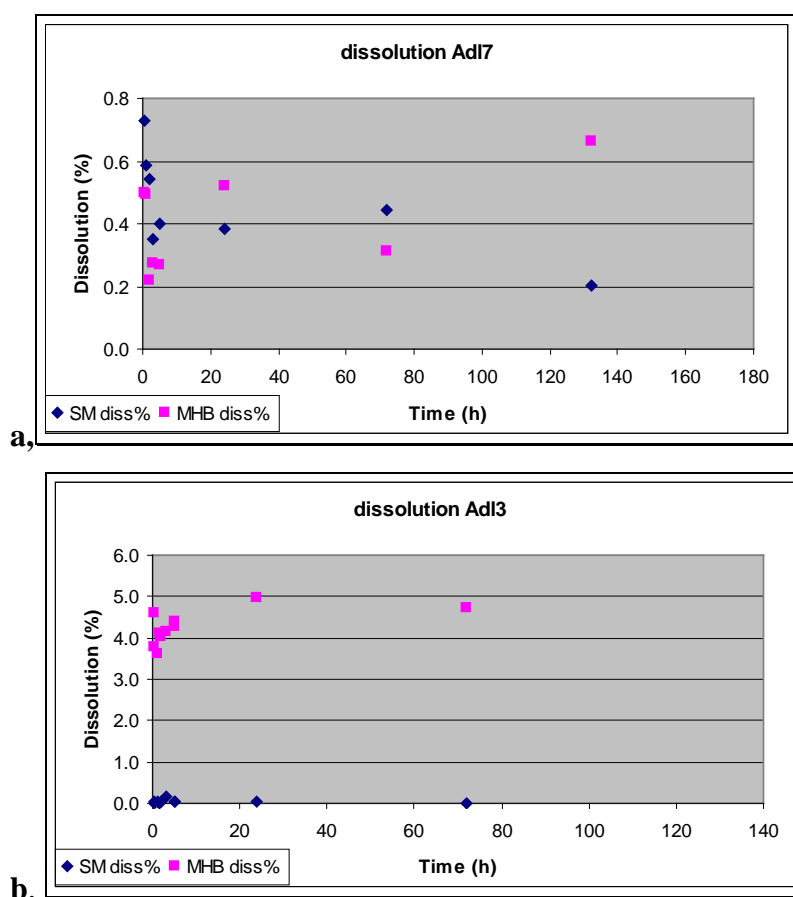


**Figure 3.1-7a,b:** Dissolution tests of Adl7 and Adl3 in MHB and SM medium

Comparing the solubility of the two compounds in percentage, it is an order of magnitude higher for Adl3 in the case of the Müller-Hinton medium. The ten times lower solubility of Adl7 can be explained by the structure of its polymer network. As previously discussed, the ligand-Ag contacts are shorter and stabilize the structure by Ag—Ag contacts. During the dissolution of the silver compounds, the polymer network is cut into pieces and several different composition complexes can be found in solution [93]. Regarding the structures of these complexes, for example  $[\text{Ag}(\text{L}1)_2]^+$  they are different for the Adl3 and Adl7 (**Fig.3.1-8**).

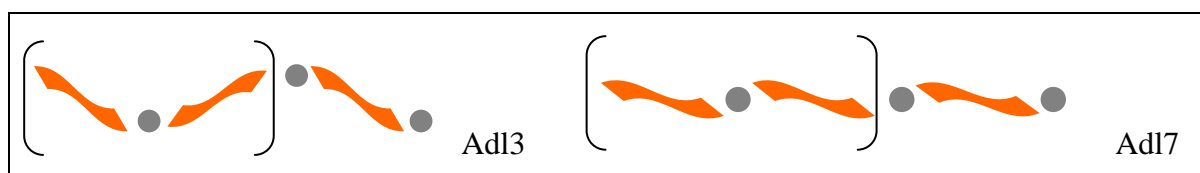


**Figure 3.1-8:** Conformation of the  $[\text{Ag}(\text{L}1)_2]^+$  of Adl3 and Adl7

The resulting form of the complex of Adl3, has a dipole moment in contrast to Adl7 where the same complex is apolar. Thus, Adl3 should be more soluble in polar solvents as water and thus in aqueous biological media.

Concerning Adl3, the difference of the solubility in the two media is more than remarkable. The major part of the synthetic medium is a NaCl isotonic solution, and if the Ag leakage is high and fast, a precipitation formation of AgCl is probably immediate. On the other hand, more peptide, protein and other bio molecules can be found in the Müller-Hinton medium. These molecules can easily complex the silver ions and act as a masking agent to keep the silver ions in solution.

In comparison, a solubility test for AgCl was carried out (**Fig.3.1-9**). While the solubility of Adl3 is much higher, the solubility of Adl7 and AgCl is comparable in SM. The solubility of AgCl in water is around 0.1mg/l, and this is about the same as in SM, as was measured by AAS. In MHB medium, the AgCl solubility is clearly higher, as shown in **Table 3.1-3**.

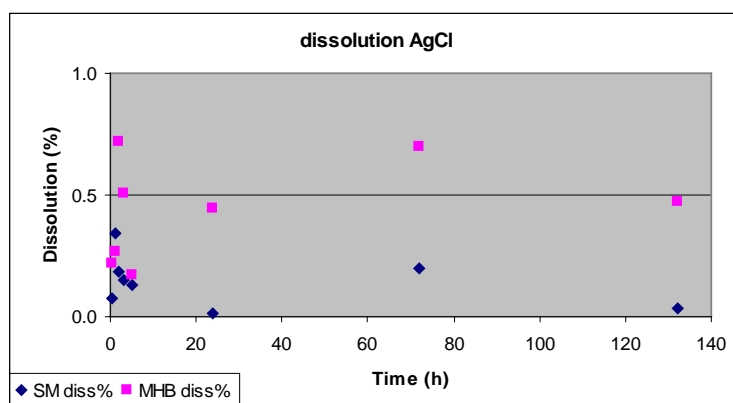


**Figure 3.1-9:** Solubility of AgCl in SM and MHB

Compound	Medium	Silver conc. (ppm)
Adl7	MHB	1,3-4,3
	SM	1,4-5
Adl3	MHB	21-33
	SM	0-0,4
AgCl	MHB	0,1-0,8
	SM	0,4-0

**Table 3.1-3:** Solubility values of AgCl, Adl3 and Adl7 in the two media (SM and MHB)

AgCl being an insoluble compound its LD50 value is high: Acute oral toxicity (LD50): >5000 mg/kg for Guinea pig [206]. A similar value thus expected for Adl3.

The solubility of the AgNO<sub>3</sub> as a very soluble silver compound in water in the two biological media was tested.

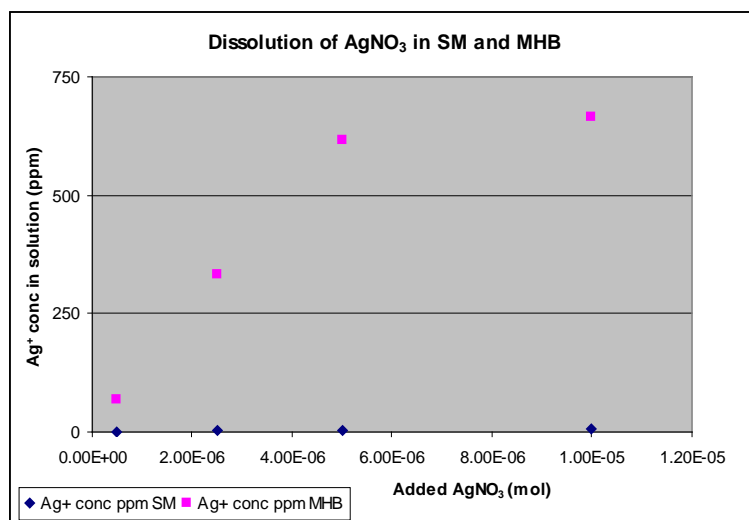


**Figure 3.1-10:** Solubility curve of AgNO<sub>3</sub> in SM and MHB as a function of the concentration

Added AgNO <sub>3</sub> (mol)	solubility in SM (mol <sup>2</sup> /l <sup>2</sup> )	solubility in MHB (mol <sup>2</sup> /l <sup>2</sup> )
5.00E-07	1.27E-10	4.19E-07
2.50E-06	3.31E-10	9.58E-06
5.00E-06	1.18E-09	3.32E-05
1.00E-05	2.28E-09	3.87E-05

**Table 3.1-4:** Solubility values of AgNO<sub>3</sub> in SM and MHB as a function of the concentration

In **Fig.3.1-10**, the dissolution of AgNO<sub>3</sub> is shown and the solubility values are calculated for the silver nitrate in the two media. During the solubility test a white precipitation has been observed in SM after addition of  $5.00 \times 10^{-7}$  mol AgNO<sub>3</sub>, while with the MHB medium, the solution became slightly cloudy after  $5.00 \times 10^{-6}$  mol AgNO<sub>3</sub> was added. While the solubility of the AgNO<sub>3</sub> in SM is in a same range as the solubility of the AgCl in water ( $10^{-10}$  mol<sup>2</sup>/l<sup>2</sup>), the solubility of the AgNO<sub>3</sub> in MHB is a hundred times higher. This measurement confirms the hypothesis that the composition of the MHB medium favours the complexation of the silver ions contrary to the SM medium, which generates immediately a precipitate.

The other main question regarding the behaviour of the compounds in contact with the biological media is: what happens during the dissolution process? Does the compound remain intact and just some Ag ions are released from the surface into the solution, or is there a complete change of the compound? What is the nature of the formed precipitate? Is it the proposed AgCl? If there is a passivation of the surface of the crystals, the surface is covered by the formed AgCl which inhibits the further dissolution, hence the solubility of the AgCl and Adl7 are similar. The powder X-ray spectra, taken before and after the dissolution test, helps to answer a part of the previously asked questions. (**Fig.3.1-11**)



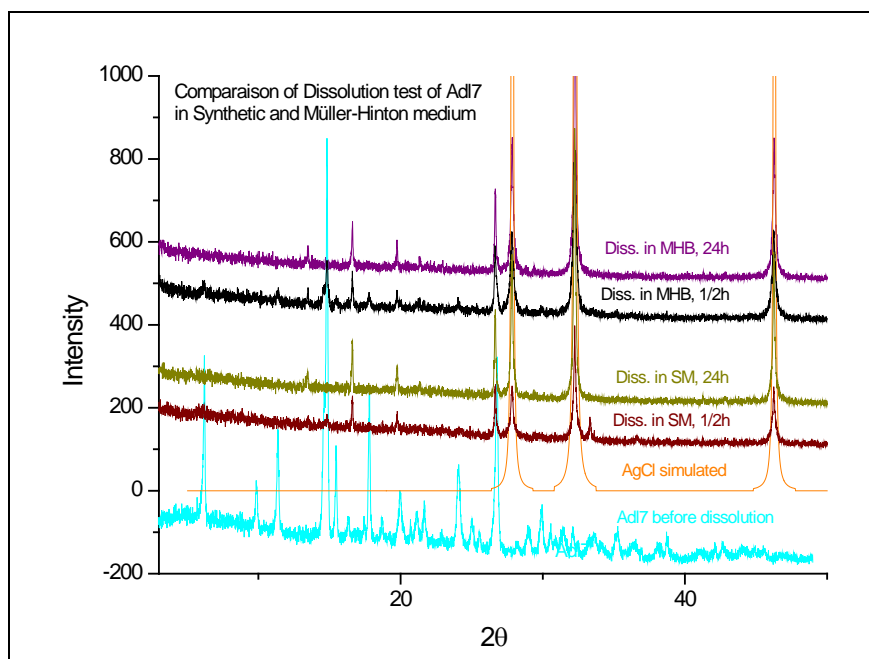


**Figure 3.1-11:** Powder X-ray spectra of the AdI7 before and after the dissolution tests

The spectra show that the main product after the dissolution is AgCl, but there are also some other, non-identified products. To follow the transformation of the product, time dependent spectra (**Fig.3.1-12**) show that the dissolution of AdI7 and AgCl precipitation are almost immediate in MHB. This is even more significant in the case of SM. We can still observe the main peak of the AdI7 after 30 minutes in MHB, which is not perceptible any more in SM. That means that the speed of the dissolution-precipitation is probably higher in SM where we could find less Ag-complexing molecules.

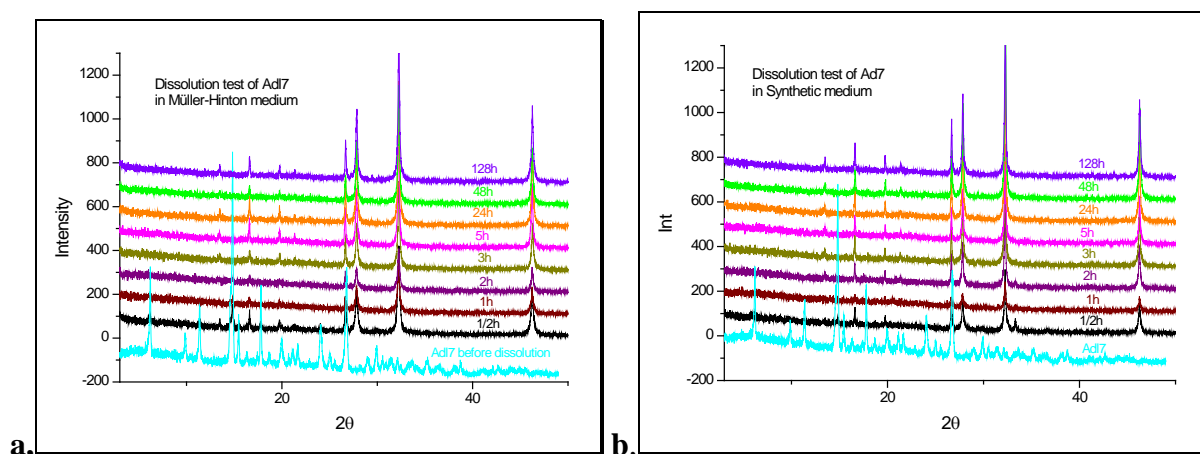


**Figure 3.1-12a,b:** Time dependent powder X-ray spectra of the dissolution of AdI7 in SM and MHB media

This experiment with AdI7 in solution does not answer the question of passivation. Further investigations of the compound as a coating would confirm or stand against the theory of the



passivation. The dissolution tests, confirm the structural analysis, i.e. the most suitable compound seems to be Adl7. The Ag concentration of the Adl7 solution (1,4-4 ppm) is in the range of the non-toxic concentration [141]. Further investigations should be made to confirm the biocompatibility of the compound.

The stability of the compound is another relevant characteristic. The light sensitivity of silver containing materials is well known. Heavy decomposition of materials due to light may hinder their utilisation as coating for implant materials.

To examine the light stability of different compounds, testing them in solution was more favourable since the crystal degradation is so slow that it renders the quantification difficult. For this purpose, solutions of our Ag-compounds in organic solvents were deposited on filter papers, and subsequently exposed to light (Philips 15W, from 10 cm distance) for 3.5 hours, in comparison to simple  $\text{AgNO}_3$ . To test the influence of the crystalline structure and the counter ions effect we have chosen the following compounds: Adl7 [ $\text{Ag}(\text{L}1)\text{NO}_3$ ]<sub>n</sub> (simple chain structure), Adl3: [ $\text{Ag}(\text{L}1)\text{NO}_3$ ]<sub>n</sub> (simple chain structure), Adl8: [ $\text{Ag}(\text{L}1)\text{CF}_3\text{SO}_3$ ]<sub>n</sub> (structure with different counter ions, chain conformation the same as in Adl7, the Ag—N contact is slightly shorter than in Adl7 and no Ag—Ag contact occurs) Adl10: [ $\text{Ag}(\text{L}1)\text{PF}_6$ ]<sub>n</sub> (structure with different counter ions, chain conformation is the same as Adl3 but shorter Ag—N bond lengths) and a new structure the J11: {2[ $\text{Ag}(\text{L}3)\text{NO}_3$ ]}<sub>n</sub> (ring structure) [207]

The photos of the exposed filter papers are shown bellow (**Fig.3.1-13-14**):

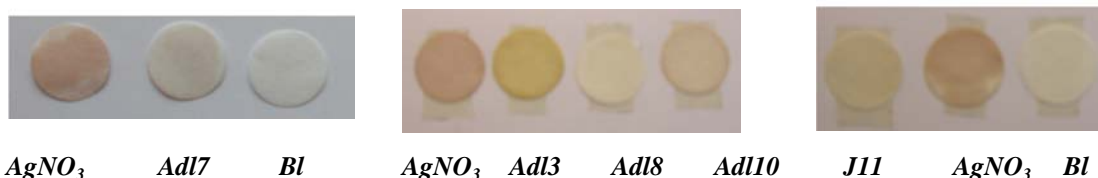


**Figure 3.1-13:** Photos of the filter papers immersed in a solution of the different compounds and exposed to light for 3.5h

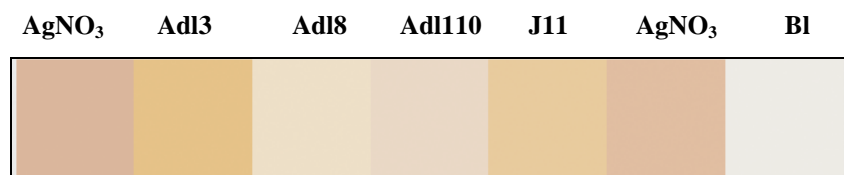


**Figure 3.1-14:** Quantitative colour measurements of the filter papers immersed in a solution of the different compounds and exposed to light for 3.5h

Although the compounds are dissolved in acetonitrile, the silver ions remain coordinated by the ligands (previous MS measurements detected fragments of the silver complexes after

dissolution [93 pp.:94-95]). These fragments are less photodegradable than the silver ions in solution. The structure of the fragment determines the level of the photosensitivity of the silver compound. The chain conformation, the Ag—N bond length (as the longer bonds indicate weaker coordinating effect) and the existent Ag—Ag contacts, solidifying the crystalline structure in a level of inter layer and inter chain contacts, seem to be an influencing factor for the light stability. Comparing Adl7 and Adl3, the first is clearly more stable in light, the shorter Ag—N contacts and the Ag—Ag contact can explain the higher stability.

Regarding the compounds with different counter ion, Adl10 has a similar chain conformation as Adl3 and slightly longer Ag—N bond lengths than Adl8, which has a similar chain conformation as Adl7. It is the same situation as Adl3 versus Adl7 with other counter ions, thus the stability of Adl8 is clearly higher than the one of Adl10. The counter ion effect seems not to influence the light stability. However, the strength of the Ag—N contact, the principal coordination bond, is fundamental. Therefore, the shorter it is, the more light stable is the compound.

The general conclusion of this chapter is that Adl7 is the most suitable compound for the further experiments thanks to its good light stability and poor solubility. This compound has facile synthetic access, forming small and big crystals depending on the starting concentration (see also Chapter 3.2.3), which is also in its favour. The microbiological characterisation of the compound is described in Chapter 3.3.1.1.1.

## 3.2 Coatings

The general concept is to build up a resistant coating of our compound, primarily AdI7, on a surface to render it antimicrobial. In an ideal case, the compound is attaching on a surface via covalent bonds or at least with coordination binds to ensure a strong attachment. Thus, we aim to reach long-term efficiency and a slow leakage of the silver ions. Two methods of coatings will be tested in this chapter: the in-situ crystallization and layer-by-layer method. The coating methods were carried out as a function of time and concentration in order to test their influence on coverage and loading of the substrate with our compounds.

To analyse the surface and describe the topography we have used different surface analytical methods such as AFM, SEM, XPS and powder X-ray. Concerning the substrates, for the basic characterisation of the coating, simple clean gold Au(111) surfaces were used, surface which is frequently used for physical and surface chemistry experiments. This is the most reproducible surface, which guarantees the reliability of our measurements. On Au(111) substrates, where atomically flat islands are generated by flame annealing, the conformation and orientation of the molecules, the attaching forces and the chemical composition of the surface are easy to study. This surface is one of the most used for STM and AFM experiments. The uniform composition of Au(111) makes it also a good substrate for XPS studies or other surface analytical methods. Other substrates used in medical environments were also studied: titanium and gold dental implant materials as well as titanium and steel internal medical implant materials are also used in the following studies.

Some dissolution experiments were performed on a coating, as discussed in the previous chapter for the bulk compound. The aim of these tests is to study the silver leakage and the stability of the coating.

### **3.2.1 Materials**

#### 3.2.1.1 Chemical fixation by anchor molecules

To build a solid coating on a surface, we need to guarantee the firm attachment of the compound on a surface. The best solution is a covalent bond between the substrate and the surface; this is the concept of the chemical fixation on a surface.

For a model surface, Au(111) surface was used. To build up the coating of the silver polymer network on the surface, the compound should be firmly attached. To fix AdI7 on a gold Au (111) or a dental gold implant surface, a sulphur-containing molecule with an isonicotinate tail was synthesized. The sulphur atoms of the molecule form then covalent bonds with the

gold atoms, and then the polymer network can be formed using the isonicotinate end as a starting point. For this purpose, a disulfide molecule was synthesized since these molecules are much less sensitive than the mercaptane type molecules. They show no degradation in air, are easy to handle and to prepare. The carbon chain linking the sulphur and the isonicotinate residue was kept short even though there is no higher arrangement of the molecules on the surface (carbon chains formed from 8-10 carbons, with or without any aromatic groups have the tendency to stick together vertically making nice SAMs (self arranged monolayer) [193]). The synthesis of the bis 2-((4-pyridinylcarbonyl)oxy)ethyl disulfide molecule [101] is described in scheme (Fig.3.2-1).

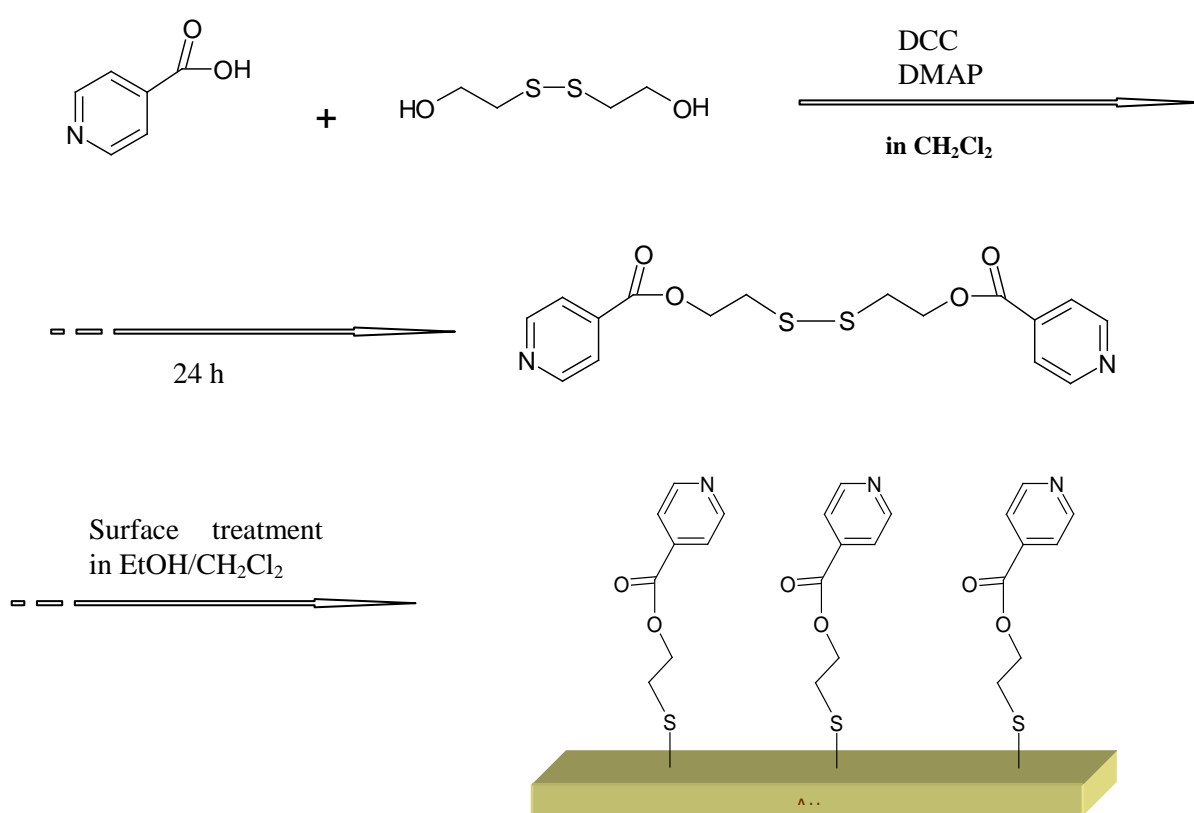


**Figure 3.2-1:** Scheme of the synthesis of the disulfide molecule and the surface treatment with it

During the purification, the last step is a recrystallization. The crystalline structure of the bisulfide is the following:

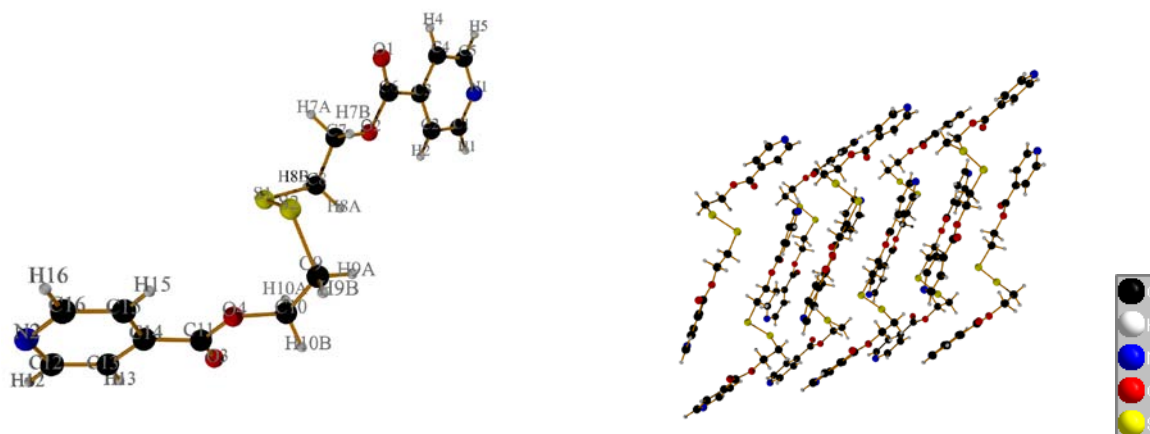


**Figure 3.2-2:** Crystalline structure and packing of the disulfide molecule

*Description of the crystalline structure:*

The crystal shapes of the disulfide are thin plates. The ligand crystallizes in the monoclinic space group  $P2(1)/c$ . There are four ligands per unit cell. The ligands form a Z shape where the two isonicotinate tails are connected by the almost perpendicular disulfide part. The two isonicotinate tails are almost parallel. One pair of the parallel arranged Z shaped ligands (these layers are parallel with the y axis of the unit cell) is crossed by a third Z shaped ligand (situated in the same plane than the first pair) in a way that the isonicotinate acid tails of the ligands belonging to the pair and the crossing ligand are vis-à-vis. The zigzag layer builds up in this way. These zigzag layers stick together having generally around 4 Å distance between the layers. The pyridine rings in the zigzag layer are slightly tilted. The intra layer cohesion between the ligands is maintained by interactions between the isonicotinate carbonyl oxygen atom and the one H atom of the of the nearest pyridine ring of the next ligand the (H·····O) distances are 2.655 and 2.666 Å. The principal inter layer interactions are the hydrogen bonds between the pyridine N and the H atom of the connecting CH chain between the sulphur and the isonicotinate tail with a distance of (H·····N) 2.494 Å. The direction of this contact is parallel with the plane of the pyridine ring. Another weak interaction between carbon and hydrogen solidify the interactions between layers. (**Fig.3.2-3**)

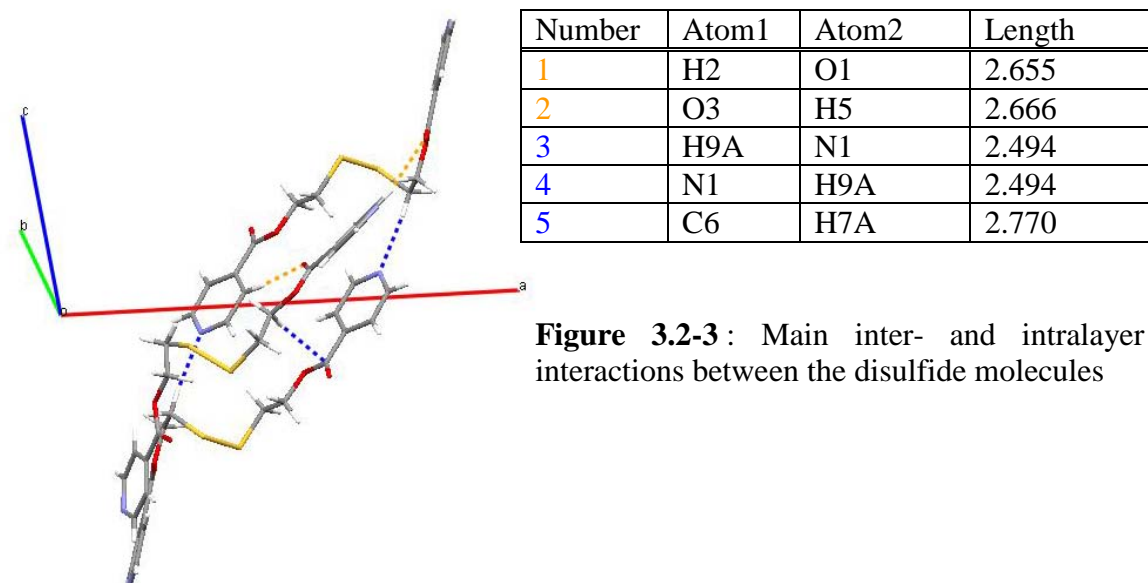


**Figure 3.2-3:** Main inter- and intralayer interactions between the disulfide molecules

Regarding the titanium substrates, another anchor molecule should be used. Since the titanium is a reactive metal, a  $\text{TiO}_2$  layer generates immediately on a surface exposed to air. Bibliographic data show that the isonicotinic acid molecule absorbs on the  $\text{TiO}_2$  surface [102]. Thus, this molecule can serve directly as an anchor molecule for the Ti surfaces.

### 3.2.1.2 Substrates

As model surface, an oriented gold Au(111) surface commercially available from Arrandee™ Germany was used. The basic material, a borosilicate glass is usually 0.7 mm in thickness. These glass substrate is well suited for the flame annealing procedure to obtain Au(111) terraces with a 200-300nm thick final gold layer. With this method, a constant quality of the surface can be reached independently of the plates, and further cleaning procedures or pre-treatment are not needed.

Other substrates have been chosen for the deposition. These are typical metallic dental implant and restorative materials: titanium (99.9% Tritan, RematitanM, Dentaurem, Ispringen, Germany) and gold alloy (Au 71%, Pt 3.7%, Ag 12.7%, Cu 10.8%, Zn 1.1%, Ir 0.1%; Neocast 3, Cendres+Metaux SA, Biel-Bienne, Switzerland). Both were used as polished (roughness  $R_a = 0.24 \mu\text{m}$ ) flat plates of 14x14 mm, the polishing being similar to that used for real dental applications.

More substrates for the *in vitro* and *in vivo* microbiological assays are delivered from the Robert Mathys Stiftung, Bettlach, Switzerland. The titanium and steel materials have two geometries: disk ( $\phi$ :4.90mm; l:1.30mm) and cylinder ( $\phi$ :2.00mm; l:3.30mm) with two different roughnesses. Since the titanium disks have a more suitable form for the *in-situ* crystallization, this substrate was used for most of the microbiological assays. The Ti cages used for the *in vivo* experiments are of the same material as the Ti disks, one-end-open (closed with a silicon cap during the experiment) empty cylinder ( $\phi$ :10.00mm; l:30.0mm) with 135 small  $\phi$ :1.00mm holes to keep the flow of the cell fluid free.

#### 3.2.2 Coating methods

Based on the preliminary analytical characterisations of the different silver polymer networks, the Adl7 compound has been chosen. The next step is to build up a solid crystalline coating of this compound on a surface. The crystallisation process should take place on surfaces of the different substrates. Two main coating methods, the *in-situ* crystallization for a continuous ongrowth and the layer-by-layer method, dip-coating with alternating solutions of  $\text{AgNO}_3$  and L1, were used.

Generally, the coating process consists of three phases, cleaning, pre-treatment, crystallisation. Before deposition, the dental implant substrates, used several times, were treated with a solution of 30%  $\text{ccH}_2\text{O}_2$  and 70%  $\text{ccH}_2\text{SO}_4$  to remove all of the residues, were then rinsed abundantly with EtOH and distilled water, dried and kept under vacuum. All internal medical implant materials were washed with EtOH and water before the treatment. The gold plates were used immediately after flame annealing; additional cleaning procedures are not needed.

The pre-treatment (= binding of the anchor molecule) was always carried out in the same way for the Au(111) surfaces: 5days, 5mM disulfide in EtOH/ $\text{CH}_2\text{Cl}_2$ , 1/1 solvent mixture. The importance of the disulfide in the case of the Au(111) was proven. The coating without any pre-treatment is less stable and can be washed out more easily from the surface. In addition, the structure of the coatings shows more inhomogeneities. This unfavourable situation has not been observed in the case of the gold dental implant substrate since this material contains silver in the alloy. Direct coating can be employed there.

During the *in-situ* crystallisation of our Adl7 compound, we have used the same solvent THF/EtOH, 1/1 mixture, as for the crystallisation of bulk Adl7 to guarantee the same structure on the surface. As described previously, the most reliable method to identify Adl7 is the powder X-ray analysis. A complementary powder X-ray spectrum of the treated Au(111) plates was carried out and it confirms the presence of Adl7 on the surface. (Fig.3.2-4)

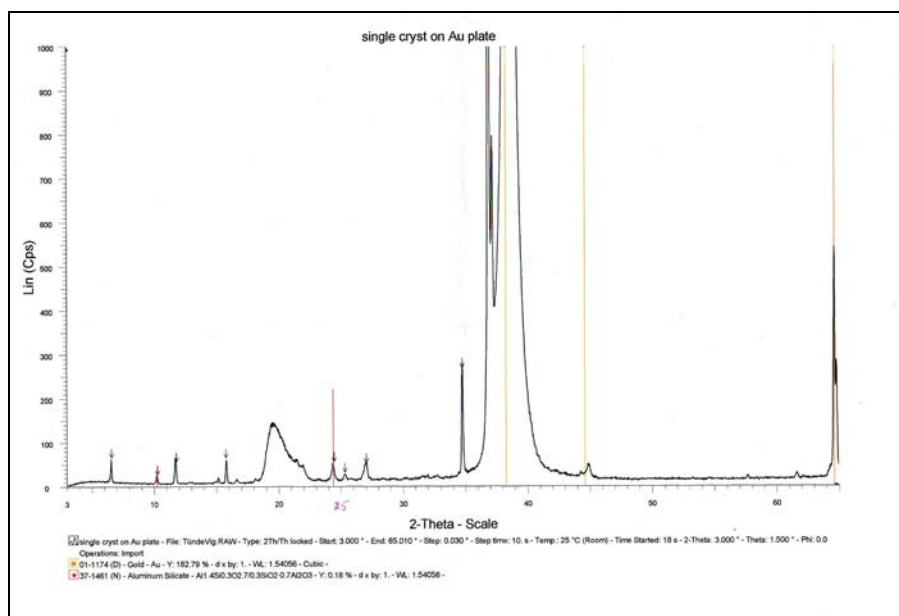


**Figure 3.2-4:** Powder X-ray spectra of the Adl7 coating on Au(111) surface

The concentration of the treating solution and the crystallisation time are varied, to study their influence on the desired loading. In a preliminary test, carried out under similar concentration conditions, both methods, *in-situ* crystallization and layer-by-layer deposition, gave very similar results in SEM analysis (**Fig.3.2-5**), leading to a nanocrystalline structuring of the surface.

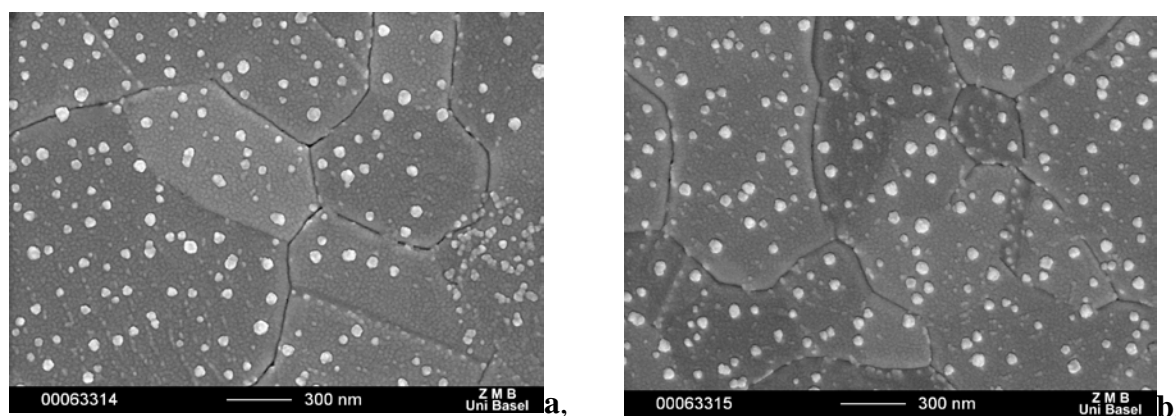


**Figure 3.2-5a,b:** SEM images of the surface coating prepared by multilayer (15x2mM  $\text{AgNO}_3$  15x2mM  $\text{L}_{\text{ad}}$ ) method



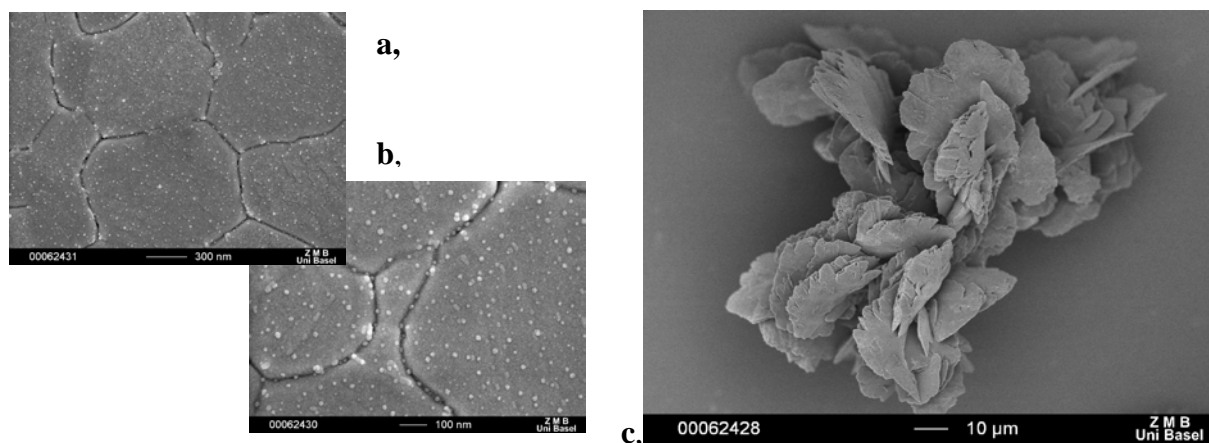


**Figure 3.2-6a,b,c:** SEM images of the surface coating prepared by *in-situ* crystallisation (2mM, 14 days)

The main difference between the achieved coatings is that by *in-situ* crystallisation, big macro structures (50-100μm) form accompanied by smaller nanocrystals covering the whole surface, whereas by layer-by-layer deposition, only nanostructures are present covering the surface. The nanostructure is present in both cases but is completed with bigger crystals during *in situ* crystallisation. This method gives the opportunity to reach a higher loading and less time consuming than the layer-by-layer method. This is not a negligible aspect considering the numerous samples needed for the biological assays.

### 3.2.3 Coatings on Au(111) surface

There are a many questions to be answered regarding the coatings: What kind of structure is present on the surface? How does the topography look? What is the loading of the different substrates? Does the compound stay on the surface or it is washed out easily? To clarify these questions, further investigations were done to understand the mechanism of the crystallisation and study the topography and the stability of the coating. AFM and SEM measurements were carried out on a coated surface of Au(111), allowing the investigation of the topology. XPS, AAS and additional SEM measurements were done to understand how the concentration of the treating solution and time of the crystallisation influence the loading and the topography of the surface. The powder X-ray measurement of the surface always proves the presence of Adl7. Further dissolution tests in biological medium were carried out to get acquainted with the stability of the coating. The following results have always been confirmed with at least three identical samples for statistical reasons.

## 3.2.3.1 Crystallisation and nanotopography

The crystallisation process follows the classical way, described by Ostwald in 1896 [103]. The Ostwald ripening features on the surface are clearly seen with the WET SEM method (high resolution imaging of fully hydrated samples) (**Fig.3.2-7**). For this measurement, an  $\text{AgNO}_3$  solution was mixed with the ligand solution, in a special liquid cell for SEM, then the crystallization process was followed over several minutes up to hours [104]. A complete study will be described by Priscilla Brunetto in her thesis.

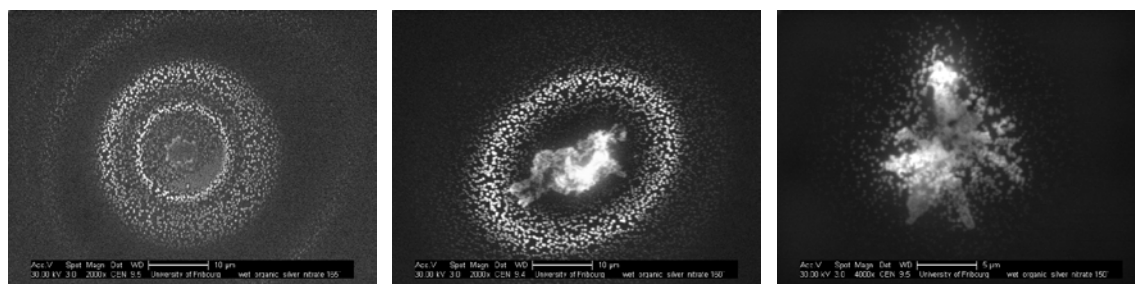


**Figure 3.2-7:** WET SEM images of the crystallisation of Adl7

AFM measurements revealed peak-like structures, which were analyzed with respect to their height and width (**Fig.3.2-8**).

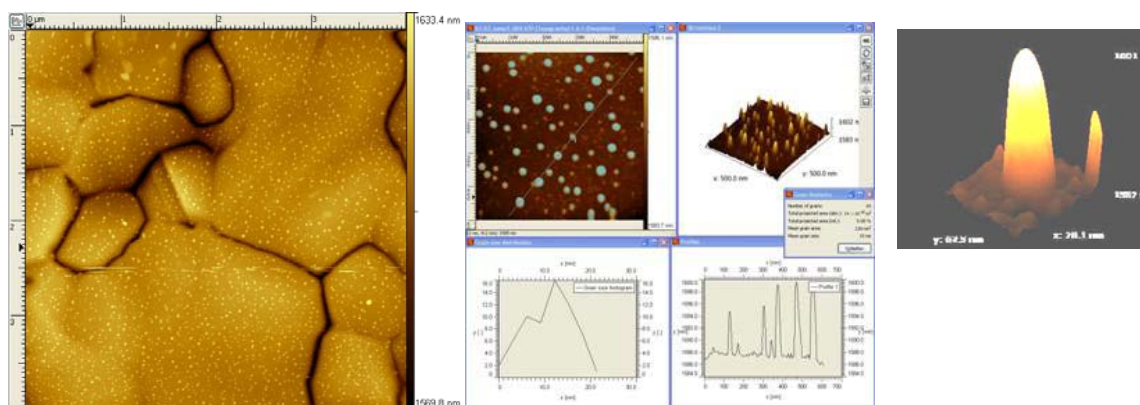


**Figure 3.2-8:** AFM measurements, profile and single peak image of the nanocoating

The surface pattern corresponds to Ostwald ripening motifs on a two-dimensional surface with a main interpeak distance of 20–30 nm, a distance that is known to be ideal for cell ongrowth [105]. From the mean peak height of 11–14 nm, the average polymer chain length, supposed to be standing upright on the surface, could be determined as an octameric chain [Ag8L7]. From the width of the peaks, it can be concluded that more than one chain is attached to the surface to form such a peak. With approximations of the peak width of ca. 10–20 nm, and the unit cell of Adl7, one can conclude that there are ca. 200–400 chains linked together within one peak. From the profile sequence in (**Fig.3.2-8**), it can be seen that the whole surface, also in between the peaks, is covered with product, even though at a lower

thickness. SEM pictures (previously shown) and further AFM measurements (later shown) of several Au(111) samples coated with different methods confirm this analysis as shown in (Fig.3.2-5,6). They also reveal the size distribution of the peaks on the surface. Several pictures were taken at different scales, and the peaks measured. Most, about 80%, of the peaks seen by AFM are ca. 10–20 nm in height and have a mean diameter of 10–20 nm. The unit cell volume of AdI7 being ca.  $777 \text{ \AA}^3$ , this leads to roughly 25000 units of AdI7 within one such peak. About 10% of the surface peaks are 50–80 nm in height and have a mean diameter of 20 nm (roughly 60000 repeat units of AdI7), whereas another 10% of the peaks are >100 nm in height and have a mean diameter of ca. 50 nm (ca. 500000 repeat units of 1a). The coating can thus be estimated to be roughly  $12.5 \text{ mg/m}^2$  compound ( $3.04 \text{ mg/m}^2$  silver) or  $3 \times 10^{-11} \text{ mol/cm}^2$  concerning the nanostructure. This is very important information since the nanostructure should stay constantly on a surface while the macro structures risk leaving from the surface through mechanical and biological impacts. The surface nano-coating was thus impossible to detect with an analytical balance.

Further AFM measurements were performed on different samples. The disulfide treated sample (Fig.3.2-9) shows some nm thick coating on the Au(111) surface. That excludes the presence of the monolayer which should not be thicker than 7-8Å. It shows larger aggregates of the compound and a dense coverage.

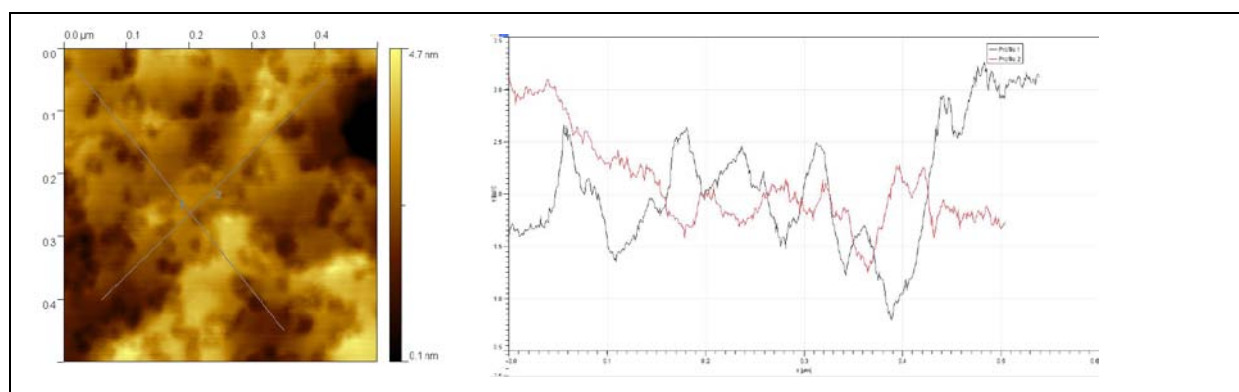


**Figure 3.2-9:** AFM image and profile of the disulfide coated (5mM/ 5d) Au(111) plate

The further AFM measurements on different samples (using low concentrations of the treating solution: 0,25mM AdI7 in THF/EtOH to avoid big macro structure formation, destroying the AFM tip) confirm that longer treating times, 7 days (Fig.3.2-12) versus 3h (Fig.3.2-10), result in a denser and thicker coverage on the surface with aggregate formation. Otherwise, the same nanostructure built up for both treating time. The 3h sample shows the previously described very homogeneous nanostructure, the first step of the crystallisation, and there is no time to build up bigger structures.

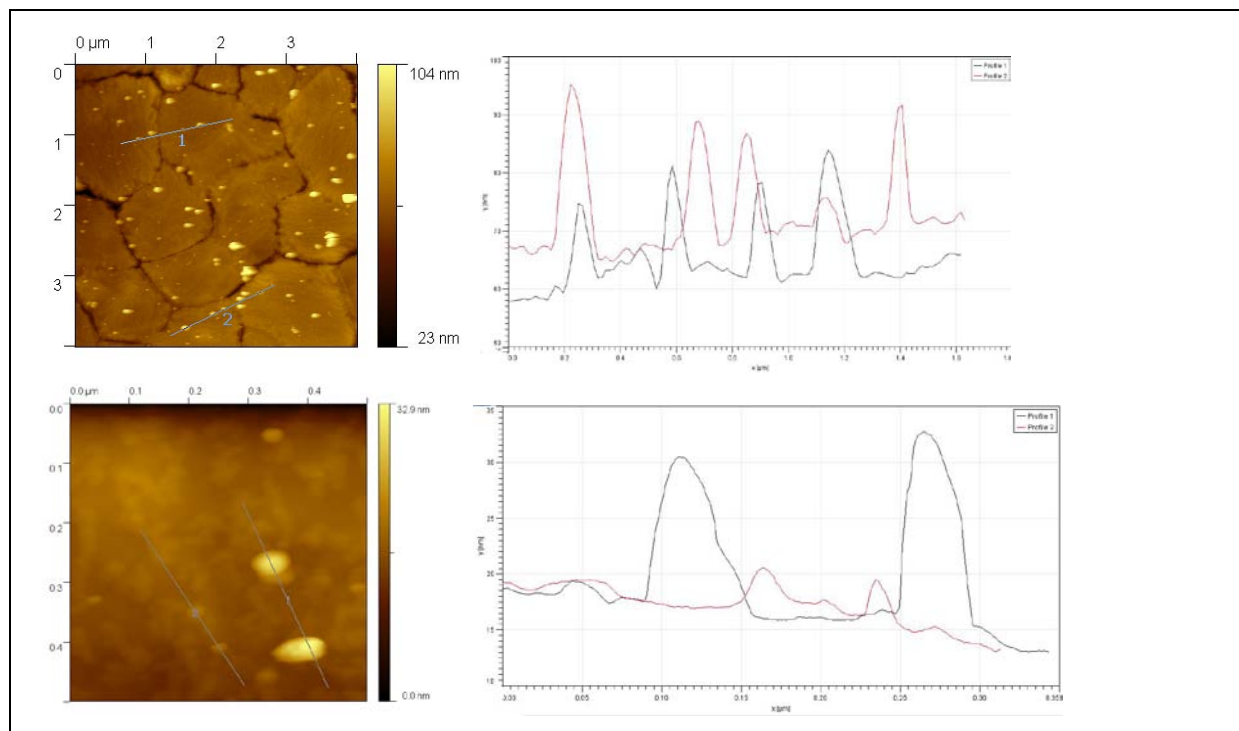


**Figure 3.2-10:** AFM images and profiles of the AdI7 coated (0,25mM/3h) Au(111) plate. Concerning samples treated with higher concentrations, but with the same treating time (0,5mM AdI7 in THF/EtOH; 3h) (fig6), formation of larger structures and flat round structures can be observed with 10nm height and 0,4  $\mu\text{m}$  in diameter (profile2) referring probably to the Ostwald ripening motifs.

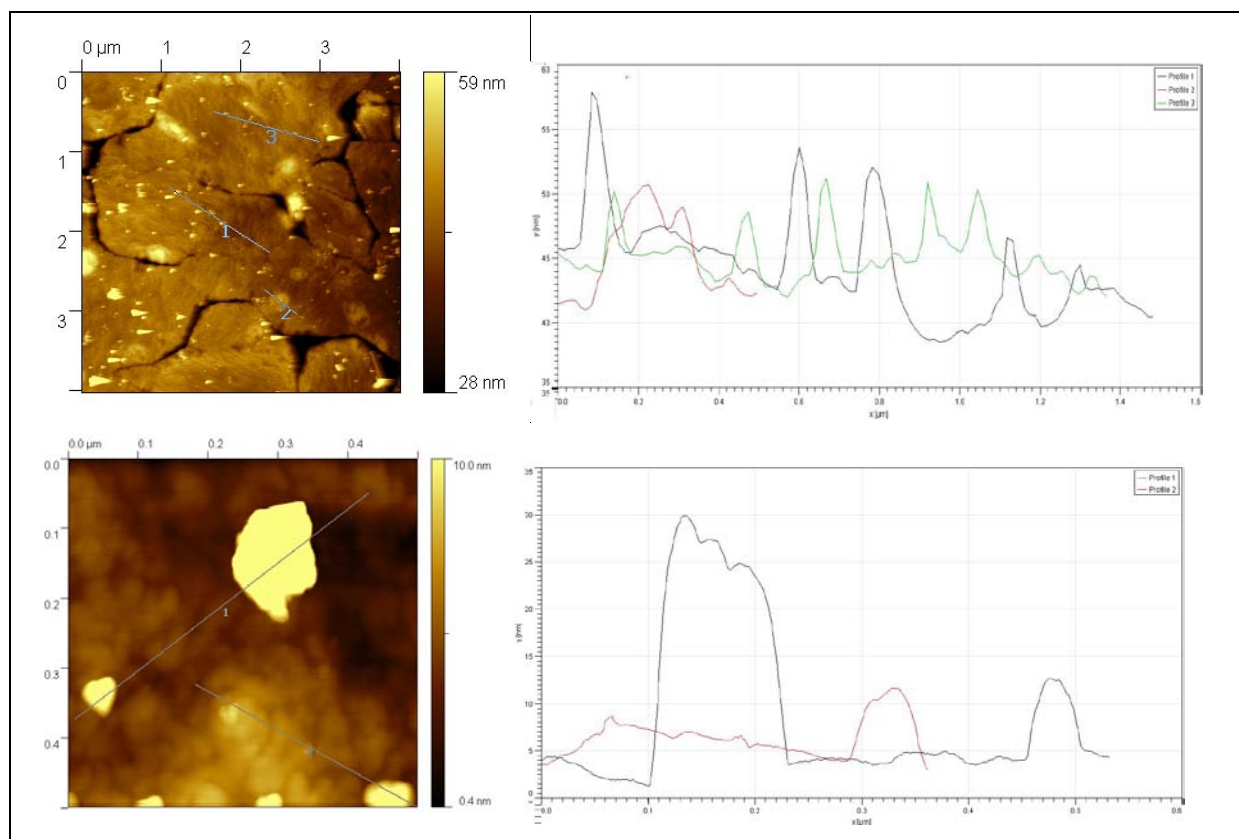


**Figure 3.2-11:** AFM images and profiles of the AdI7 coated (0,5mM/3h) Au(111) plate



### 3 Results and discussion

Higher concentrations facilitate the crystal formation, and the growth of the homogeneous nanostructure is changed by aggregates formation. A thick layer of the compound covering solidly the surface can be found in such cases, as e.g. on a 7days sample (**Fig.3.2-12**). The thick layer formed after 7 days is accompanied by nanocrystals and big aggregates. In addition, macroscopic crystal formation starts to take place.

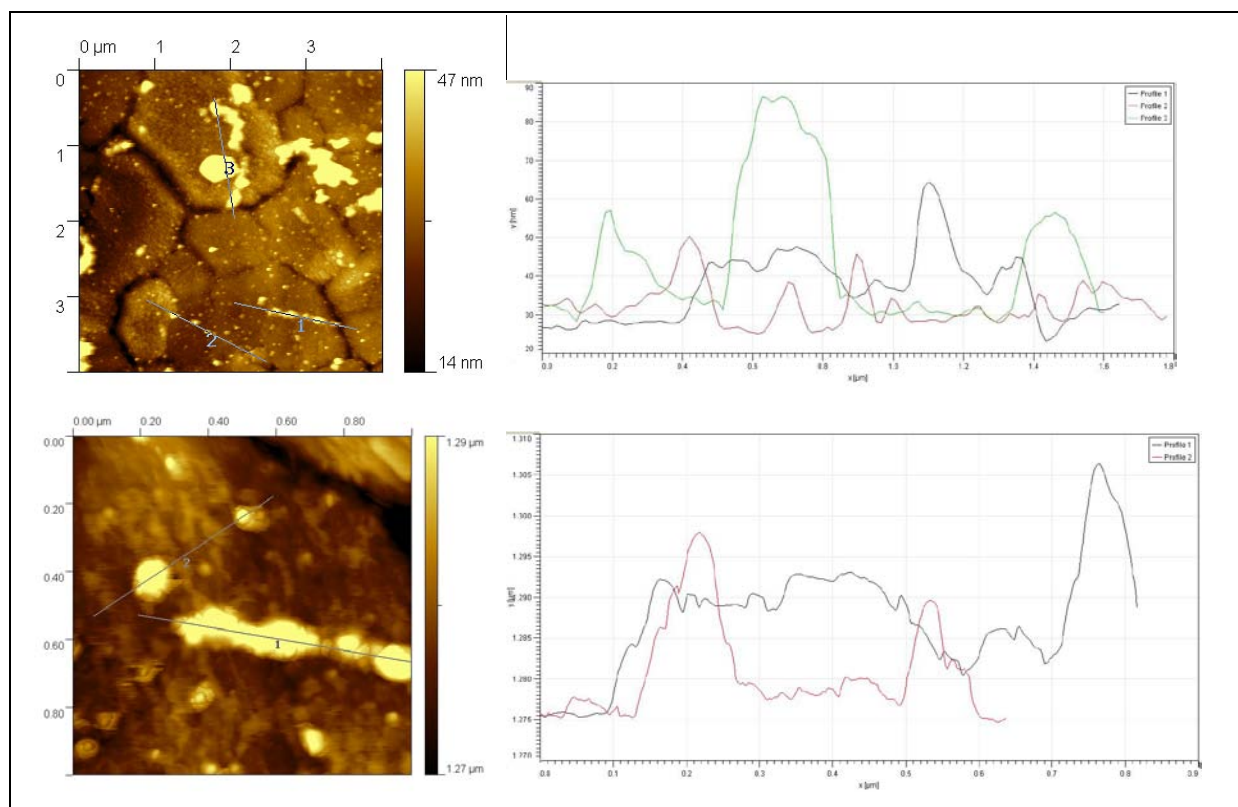


**Figure 3.2-12:** AFM images and profiles of the Adl7 coated (0,25mM/7d) Au(111) plate

From these data, it can be concluded that in each case a well-defined, nanostructured topology is formed on the substrate surface, and that with high probability, similar structural features are obtained on the polished substrates of the titanium and gold alloy. As the dental implant materials were polished prior to deposition of the compound, the surface of these substrates was too rough for AFM, which was therefore carried out for Au(111) samples only.

#### 3.2.3.2 Influence factors of the coating formation

The topography described previously through AFM measurements is confirmed by SEM measurements. This method has been chosen also to follow how the loading is influenced by the concentration of the treating solution and the crystallisation time. Numerous plates are prepared, varying the concentration of the treating solution and the treating time. One part of the plates is incubated in biological media: in synthetic medium (SM) and Müller-Hinton medium (MHB). The prepared plates are analyzed by SEM, some of them also by XPS,

shown later. Their coating is then removed with  $\text{HNO}_3$ , the silver concentration is determined and the loading (Ag on a surface in ng) is calculated. The results are listed in the **Table 3.2-1** and **Fig.3.2-13,14,15**.

Coating: Ag (ng) on a surface

conc (Ad7)	time (h)	orig (0.5)	MHB (0.5)	SM (0.5)
0.5	3	0.432	0.437	0.336
0.5	24	0.985	0.884	0.730
0.5	72	2.754	1.764	1.687
0.5	168	3.778	3.345	2.663
1.0	3	2.176	0.364	0.412
1.0	24	16.800	1.070	0.812
1.0	72	51.323	23.960	17.474
1.0	168	34.714	3.588	2.195
2.0	3	55.800	11.068	19.138
2.0	24	135.150	64.000	30.675
2.0	72	211.475	80.100	39.275
2.0	168	234.175	80.575	68.325

**Table 3.2-1:** Summary of the surface loading giving in Ag (ng) of the different samples 0.5-2.0 mM treating concentration and 3-168h treating time, before and after dissolution (24h incubation in SM and MHB)

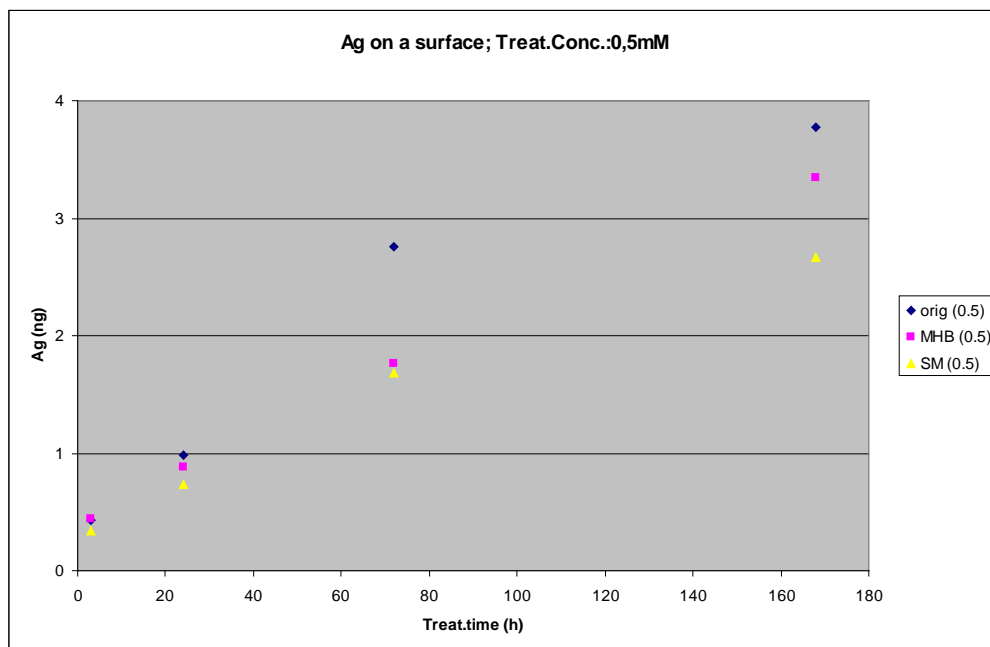


**Figure 3.2-13:** Surface loading of the 0.5mM treated samples before and after dissolution (24h incubation in SM and MHB )in function of the time

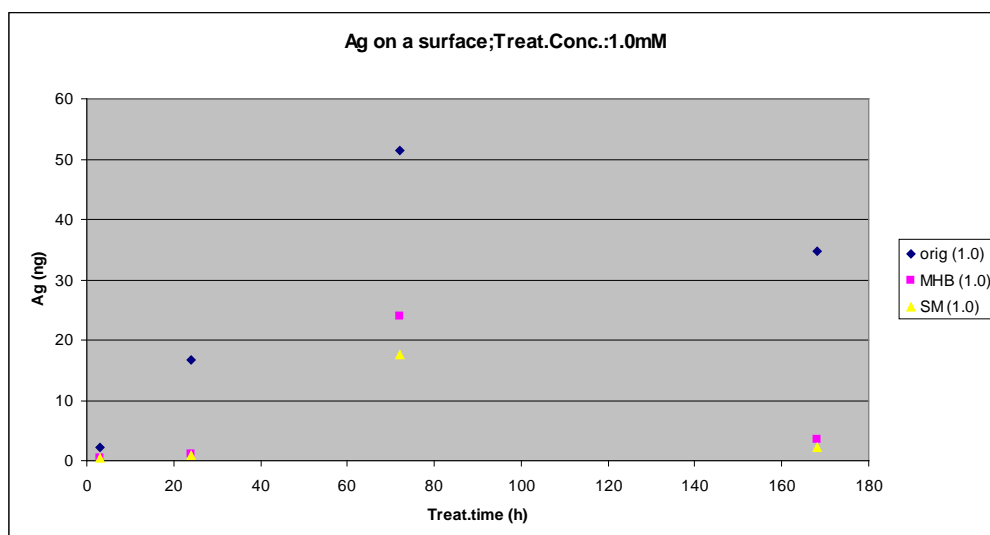


**Figure 3.2-14:** Surface loading of the 1.0mM treated samples before and after dissolution (24h incubation in SM and MHB) in function of the time

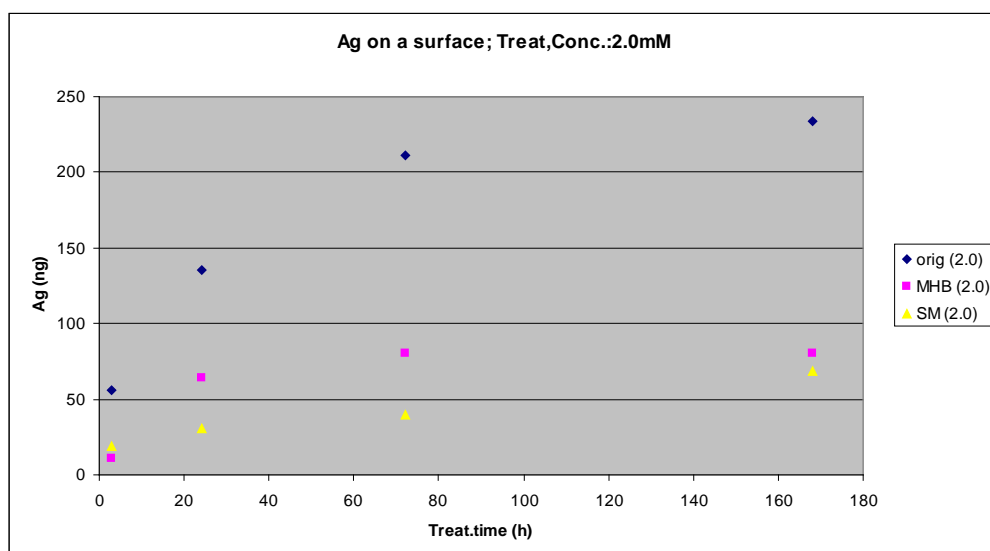


**Figure 3.2-15:** Surface loading of the 2.0mM treated samples before and after dissolution (24h incubation in SM and MHB) in function of the time

### 3.2.3.2.1 Time dependence

The coating was prepared using four different time intervals. The treating concentration was kept fixed, the change of the coating structure was followed by SEM and the loading concentration determined by AAS. The following four SEM images show Au(111) plates treated with 0.5mM Adl7 solution for 3 hours, 1day, 3 days and 7 days. The increase of the polymer network is evident (**Fig.3.2-13**) and comparing the images, the change of the topography manifests.

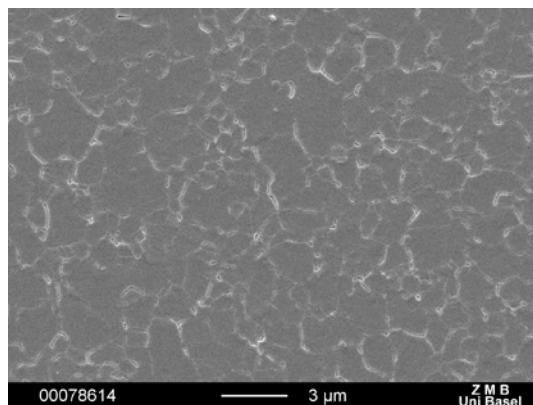


**Figure 3.2-16:** Sample 0.5mM/3h

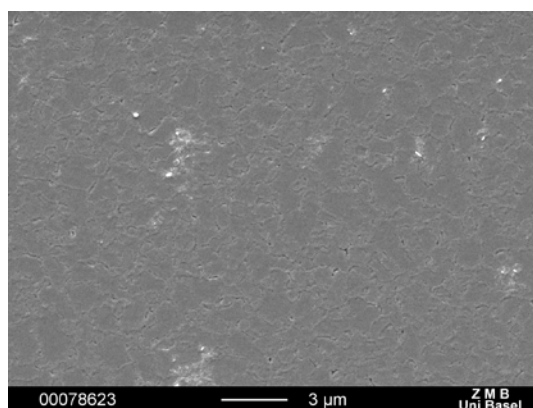


**Figure 3.2-17:** Sample 0.5mM/1d

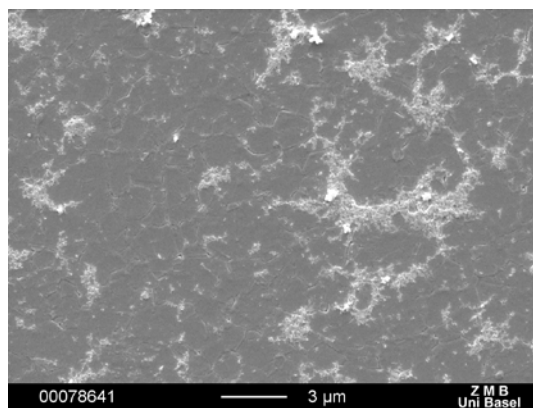


**Figure 3.2-18:** Sample 0.5mM/3d

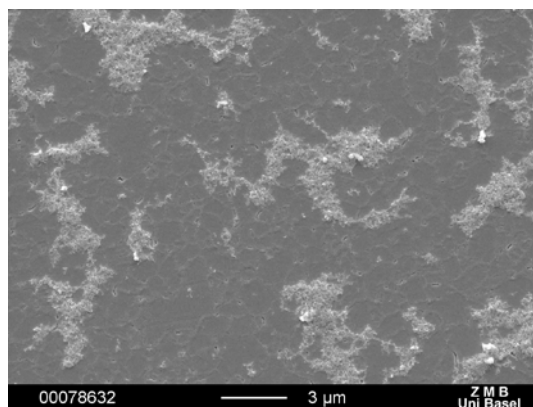


**Figure 3.2-19:** Sample 0.5mM/7d

On the surface of the first sample, we can recognize deposits on the rims of the gold 111 terraces. This is the initial step of the crystallisation; the irregularities initiate the crystal formation. The surface of the second sample is already one step further in a coating formation. There is a thin layer formed on the surface, this layer seems thicker above the boards. Larger crystals of 100-500nm appear on the surface and some  $\mu\text{m}$  aggregates sporadically. The number of these aggregates increase fast with time and on a 3 days sample many more can be observed. Comparing this one with the 7 days sample, the topography change is not as significant as the difference between the 1 and 3 days samples. The loading quantification measurement proves that the crystal formation increases with time. The measurements show that the slope of the saturation curve becomes steeper and steeper with the concentration of the solution and the maximal loading, represented by the plateau of the curve, is reached earlier in the case of higher concentration. Comparing the curve of the 2mM treating concentration (**Fig.3.2-15**), the maximal loading is almost reached after 3 days contrary to the 0.5mM (**Fig.3.2-13**) treating concentration where reaching the maximal loading would need probably several weeks. This observation seems obvious if we take into consideration the fact that the crystallisation is slower in weak concentration. It is also interesting to compare the coating change with the concentration keeping the treating time constant.



If we observe together the three curves of the loading with the three different concentrations, we can set out that there is almost an order of magnitude difference in loading when the treating concentration increases twice. This is discussed in details in the next chapter.

#### 3.2.3.2.2 Concentration dependence

The concentration of the AdI7 solution influences strongly how the coating forms on the surface. To describe the effect of the concentration on the coating, three different concentrations were used to treat the Au(111) plates. The prepared plates were measured by SEM and the loading concentration determined by AAS. The images here presented are the 0.5mM, 1.0mM concentration and the 2.0mM samples after 3 days of treatment. Comparing the two lower concentrations, the size of the crystals is clearly higher in the case of the 1.0mM sample, and the flat structures are not visible any more. Increasing the concentration, larger crystal structures built up on the surface in the same time interval. Moreover, the nanostructure is always present.

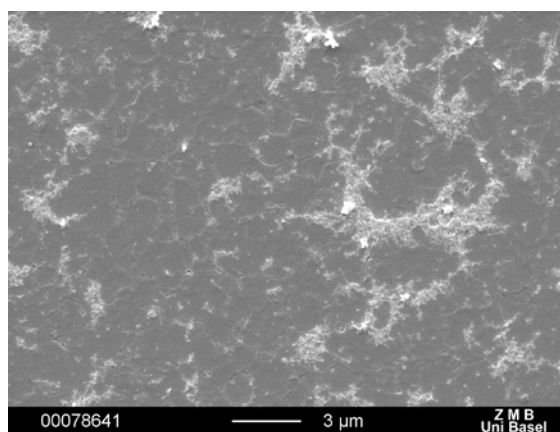


**Figure 3.2-20:** Sample 0.5mM/3days

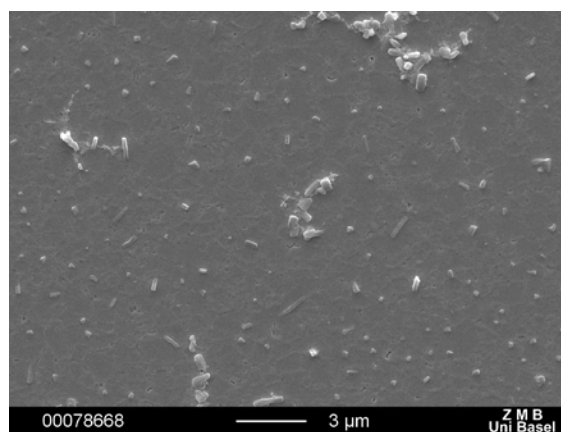


**Figure 3.2-21:** Sample 1.0mM/3days

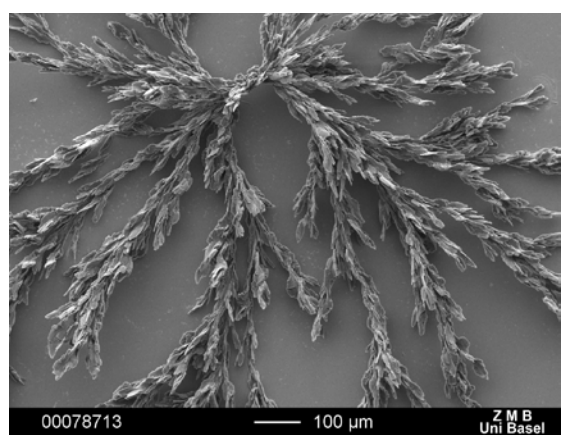
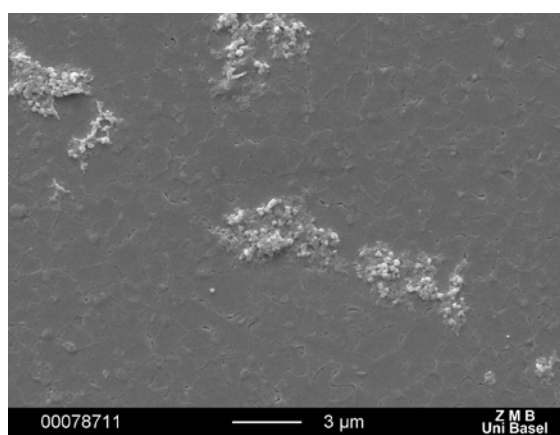


**Figure 3.2-22a,b:** Sample 2.0mM/3days

If the concentration is increased to 2.0mM, big, well designed crystals form on the surface.

### 3.2.3.3 Stability of AdI7 coating: dissolution test in two biological media

The stability of the coating is very important in medical application. The coating should stay on the surface of the implant material after its implantation. Ideally, the treated implant material preserves the antimicrobial effect, thus the silver containing material, to avoid the biofilm formation. The following dissolution tests are intended to study the behaviour of the AdI7 coating in a situation close to an *in vitro* biological assay. The dissolution tests are carried out in two biological media presented previously. The different Au(111) samples, with varying treating times and concentrations, are incubated in the media for 24h, then the plates are removed, washed and dried. The incubated Au(111) samples are analyzed by SEM. The remaining coating is then removed by HNO<sub>3</sub> solution and the silver concentration is measured. The results are listed in **Table 3.2-1**, **Fig.3.2-13,14,15**. The crystalline structures on the surface can be divided into three different size regions: nanocrystals of some 10nms, middle size structures of some 10μms, and big well designed microscopic crystals up to 1-200μm. The structures with different sizes behave differently during the incubation in media. The small structures are mechanically and chemically more stable. They remain on the surface after incubation. This is clearly shown on the **Fig.3.2-13**, and the **Table 3.2-1**. Mainly nanostructures are formed from the treatment with 0.5mM AdI7 solution. The crystal formation at this concentration is so slow, that, after 3h and 24h we can observe only nanostructures on the surface. The dissolution tests show that after 24h incubation in both media, the samples keep the nanostructured coating and no removal can be observed. This observation is confirmed by SEM measurements. In the following two images (**Fig.3.2-23**, **24**), the first one is the 2mM/3h plate incubated in MHB; the second is the same case, incubated in SM with the well known nanostructures present on both.

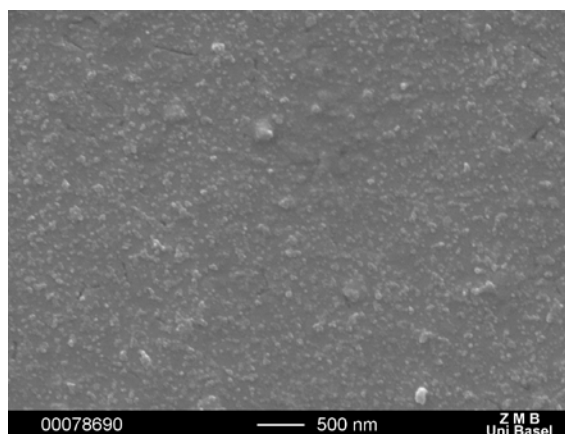


**Figure 3.2-23:** Sample 2mM/3h incubated 24h in MHB

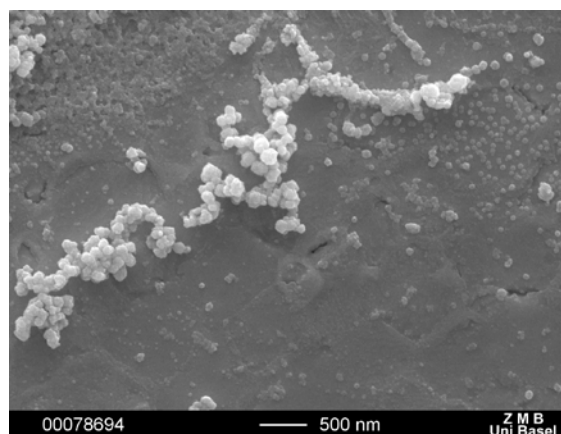


**Figure 3.2-24:** Sample 2mM/3h incubated 24h in SM

This nanostructure is completely built up just after one week if we use a weak concentration (0.5mM), while using the double concentration the nanostructure is built up after 3 hours. Middle size aggregates are then also more present on the surface. The washing out effect becomes more pronounced in the case of the two higher concentrations, hence the middle size and macro size structures seem to have a minor stability against biological media and shear. In cases where principally nanostructures and some middle size structures are present on the surface, the values of the Ag-concentration remained similar after incubation in both media. If higher concentrations and longer treating times are used the macro size crystals dominate the surface. In these cases, more coating remains on the surface after incubation in MHB than in SM. This fact seems to contradict the previous observation that the AdI7 compound is more soluble in MHB than in SM. The possible explanation is that the AgCl formation is more pronounced in the synthetic medium and the formed AgCl is washed off when the plate is removed from the medium and rinsed with ethanol. In any case, the AgCl formation was observed in both media concerning the free compound. Thus, the dissolution and the AgCl formation modify the surface of the crystals (**Fig.3.2-25**).

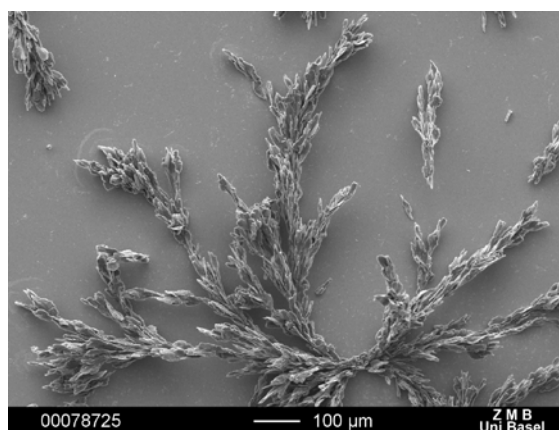


**Figure 3.2-25:** Crystals on sample 2mM/3days no incubation

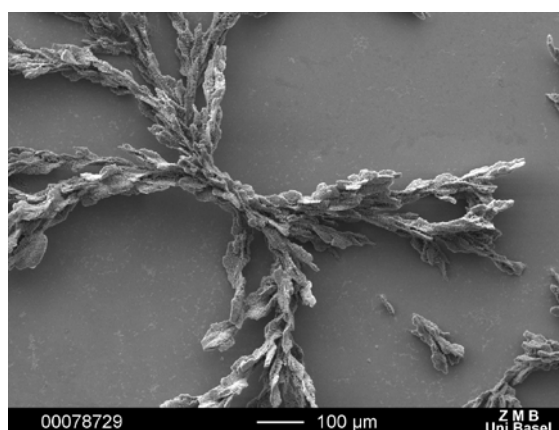


**Figure 3.2-26:** Crystals on sample 2mM/3days, MHB incubated for 24h

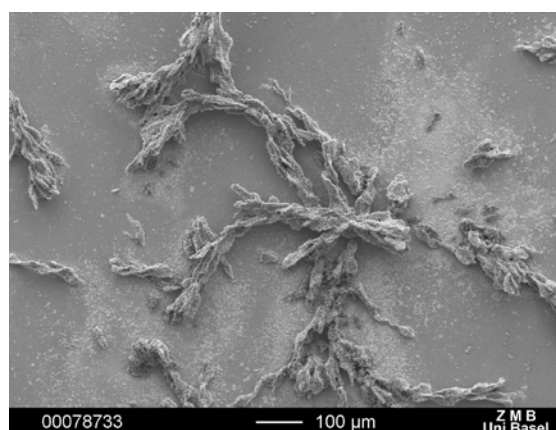
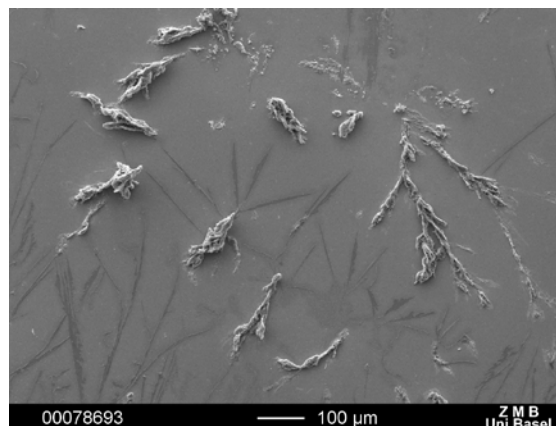


**Figure 3.2-27:** Crystals on sample 2mM/3days, SM incubated for 24h

The AgCl layer formation is more pronounced in the case of SM. The hypothesis of the passivation made after the free AdI7 dissolution tests has been confirmed by the coating dissolution tests. Upon the passivation after the incubation in the medium the surface of the crystal changes, large crystals can break and leave the surface but the subsequent nano-structure remains intact. These large crystals are not as well adhering on the surface as the small structures and remain only partially after the incubation in the medium. (**Figure 3.2-28**)

**Figure 3.2-28:** Crystals washed out sample 2mM/3h incubated in MHB for 24h (The imprint of the original crystals is visible on a surface nevertheless one part remains on the surface.)



### 3.2.3.3.1 Silver release during the dissolution test

The silver concentration of the solution just above the coated substrate is crucial from the biological point of view. The measurements show (Table 3.2-2) that the silver concentration does not reach the 5ppm limit in the solution in both media, which is exactly in the ppm range determined for the free AdI7 compound.

Sample	Ag conc.ppm in MHB	Ag conc.ppm in SM
Samp0.5mM/3h	0.0000	0.0000
Samp0.5mM/1d	0.0000	0.0000
Samp0.5mM/3d	0.0000	0.0000
Samp0.5mM/7d	0.0000	0.5697
Samp1.0mM/3h	0.0000	0.0000
Samp1.0mM/1d	0.0000	1.0291
Samp1.0mM/3d	1.7597	0.8154
Samp1.0mM/7d	1.1412	1.0571
Samp2.0mM/3h	4.7042	1.8134
Samp2.0mM/1d	3.0908	1.7462
Samp2.0mM/3d	4.3457	3.1580
Samp2.0mM/7d	3.0235	1.2756

**Table 3.2-2:** Silver concentration of the solution above the samples after 24h incubation time

As it was expected, the silver concentration is slightly higher in the Müller-Hinton medium and doesn't depend much on the loading of the plates. The concentration of the silver ions present in the solution depends more on the concentration of the other molecules masking the silver ions and keeping it in solution. These kinds of molecules are more frequent in the Müller-Hinton medium. When loading is weak, the major part of the compound is in the nanostructures and no silver can be observed in solution (the concentration is under the detection limit (0.2 ppm taking into consideration the dilution)).

#### 3.2.3.3.2 Conclusions

To conclude the results of the dissolution tests some principal observations should be outlined: Changing the treating time and the concentration of the treating solution, the topography of the substrate coating can be designed. If the well-designed macro structures are frequent on a surface, the Ag release is maximal (the loading exceeds ca. 50ng Ag per plate) and similar for the bulk compound. In contact with biological media, the nanostructures have the tendency to stay on the surface, while the macro structures are washed out. To reach an intermediate release, the medium sized structures e.g. some  $\mu\text{m}$  aggregates and crystals, are preferable. The lower concentration favours the slower crystallisation with a smaller and more compact crystal formation. Further microbiological investigations will decide which are the most suitable coating conditions.

#### 3.2.3.4 Chemical analysis of the coated surface: XPS measurements

While the topography is well described by the two previously mentioned methods AFM and SEM, further XPS measurements help to analyse these surfaces chemically.

The XPS measurements are performed on different substrates. Several coated Au(111) plates as model surface were measured. Since the AFM and SEM measurements underline the importance of the concentration and the treating time, the following substrates were used for the measurements:

Sample name	Treat.concentration	Treat. time	Incubation in medium
<i>sample2:</i>	0,25mM	3h	no
<i>sample3</i>	1mM	3d	no
<i>sample 4</i>	2mM	3h	no
<i>sample5</i>	1mM	3d	MHB/24h
<i>sample6</i>	1mM	3d	SM/24h

**Table 3.2-3:** Samples for XPS measurements

*Samples 5 and 6* will also take part in the previously described dissolution tests in different biological media. Here, the chemical change on the surface resulting from the incubation in these biological media is studied. Thanks to this technique, we can learn more about the atomic state of the elements, on the surface calculate their repartition and evaluate the proportion of these elements in different chemical environments. This technique is shortly presented before the profound evaluation of the results.

Photoelectron spectroscopy utilizes photo-ionization and energy-dispersive analysis of the emitted photoelectrons to study the composition and electronic state of the surface region of a sample. Traditionally, when the technique has been used for surface studies it has been subdivided according to the source of exciting radiation into: X-ray Photoelectron Spectroscopy (XPS) using soft x-ray (200-2000 eV) radiation to examine core-levels and Ultraviolet Photoelectron Spectroscopy (UPS) - using vacuum UV radiation (10-45 eV) to examine valence levels. Photoelectron spectroscopy is based upon a single photon in/electron out process and from many viewpoints, this underlying process is a much simpler phenomenon than the Auger process. In XPS, the photon is absorbed by an atom in a molecule or solid, leading to ionization and the emission of a core (inner shell) electron. The kinetic energy distribution of the emitted photoelectrons (i.e. the number of emitted photoelectrons as a function of their kinetic energy) can be measured using any appropriate electron energy analyser and a photoelectron spectrum can thus be recorded. For each and every element, there will be a characteristic binding energy associated with each core atomic orbital i.e. each element will give rise to a characteristic set of peaks in the photoelectron spectrum at kinetic energies determined by the photon energy and the respective binding energies. The presence of peaks at particular energies therefore indicates the presence of a specific element in the sample under study - furthermore, the intensity of the peaks is related to the concentration of the element within the sampled region. Thus, the technique provides a quantitative analysis of the surface composition and is sometimes known by the alternative acronym, *ESCA* (*Electron Spectroscopy for Chemical Analysis*). The exact binding energy of an electron depends not only upon the level from which photoemission is occurring, but also upon the formal oxidation state of the atom and the local chemical and physical environment. Changes in either one or other give rise to small shifts in the peak positions in the spectrum - so-called *chemical shifts*. Such shifts are readily observable and interpretable in XP spectra because the technique is of high intrinsic resolution (as core levels are discrete and generally of a well-defined energy) and is a one electron process thus simplifying the interpretation. Atoms of a higher positive oxidation state exhibit a higher binding energy due to the extra

electric interaction between the photo-emitted electron and the ion core. This ability to discriminate between different oxidation states and chemical environments is one of the major strengths of the XPS technique. In practice, the ability to resolve between atoms having slightly different chemical shifts is limited by the peak widths that are governed by a combination of the following factors. Especially the intrinsic width of the initial level and the lifetime of the final state, also the line-width of the incident radiation - which for traditional x-ray sources can only be improved by using x-ray monochromators and the resolving power of the electron-energy analyser take part in these factors. In most cases, the second factor is the major contribution to the overall line width.

The sample measurements were carried out with the help of Dr. T. de los Arcos, Dept. of Physics of the University of Basle. The measurements of our samples take place in a high vacuum chamber and several points on the surface are addressed. At the beginning of every measurement, an overview was registered to screen the sample concerning which elements are found on the surface. (**Fig.3.2-29**)

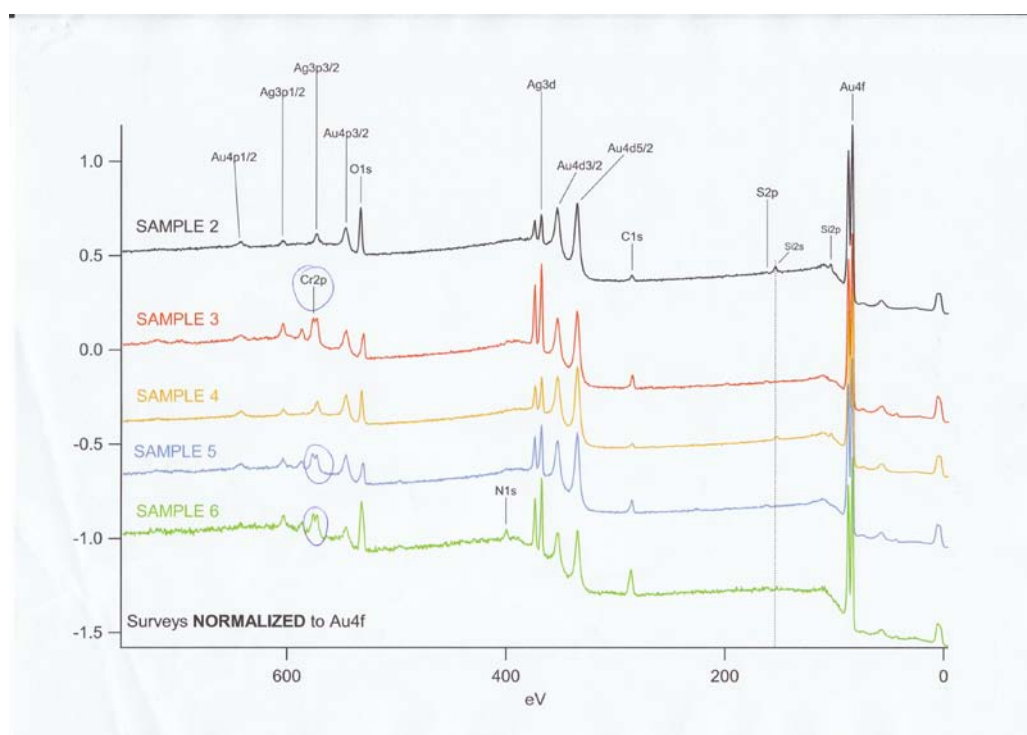


**Figure 3.2-29:** Summary of the survey spectra of the *Samples 2,3,4,5 and 6*

The major elements Ag, O, C were found as well as the S from the disulfide in most of the samples. The S2p peak is not present in the spectrum of *sample4*, possibly because the coverage is so dense that this technique does not allow detecting the disulfide attached directly on the surface. Similar for *sample6* where a big amount of AgCl formed on the

### 3 Results and discussion

surface and hides the disulfide. The Cr as well as the Si signal in some samples is coming from the substrate. The N peak is so weak that it can not be recognized on a survey.

In **Table 3.2-4**, the respective concentrations of the elements are presented. For some elements, more than one component was found. These components signify different chemical environments for the element in question.

		Au4f	Ag3d	O1s			C1s			S2p
Sample 2	BE (eV)	83.87	367.9	533.1			284.9	286.2		161.8
	at%	35.3	5.7	44.3			14.8			-
	Only Au/Ag	86	14							
Sample 3	BE (eV)	83.93	368.1	530.3	531.9		284.6	285.5	288.5	161.9
	at%	30.5	16.3	22.6			30.5			-
	Only Au/Ag	65	35							
Sample 4	BE (eV)	83.85	567.9	530.1	532.5		284.8	286.1		-
	at%	40.9	8.3	37.3			13.5			-
	Only Au/Ag	83	17							
Sample 5	BE (eV)	83.91	368.1	530.7	531.8	535.8	284.9	285.8	288.5	161.8
	at%	34.3	10.3	22.5			22.9			-
	Only Au/Ag	77	23							
Sample 6	BE (eV)	83.81	368.1	530.7	532.0	533.3	285.4	286.7	288.5	
	at%	16.8	8.1	33.5			31.6			-
	Only Au/Ag	68	32							

**Table 3.2-4:** Calculated atom % of the different elements of different binding energies

The main peaks of the elements are measured and analyzed regarding their chemical shift and their components.

The main peak for silver is the **Ag3d**: the BE is 268.1eV, just slightly higher than for Ag3d of bulk, of the silver metal situated in the same region around BE 268eV (<http://srdata.nist.gov/xps/>). This is in good agreement with the literature data [106]. This slight shift may be explained by the increase in the electronic density around the Ag<sup>+</sup> ions due to coordination. The electron draining of the silver ions from the nitrogen atoms of the isonicotinic acid units through their close interactions result in this shift in the direction of the higher binding energies.

The relative concentration of silver comparing to the Au peak is clearly higher in the case of the samples with a longer treating time (*samp3*, 5, 6), meaning that the coverage of the surface with the silver polymer complex compound is higher. The two samples incubated in biological media (SM and MHB) show slightly lower Ag concentrations. During the incubation in the media, one part of the AdI7 compound reacts with the Cl<sup>-</sup> forming an AgCl precipitate, which is washed out during removal from the solution and the cleaning with



EtOH. The loss of Ad17 from the surface is pronounced in the case of SM, which is confirmed by other analytical methods (previously described dissolution tests AAS).

The main oxygen peak, **O1s**, reveals two components: one around 530.3-7eV and one around 532.0eV. In the case of the not incubated samples, this can be assigned to a carbonyl oxygen C=O and an ether oxygen C-O-C respectively. The fitting shows almost a 1:1 distribution between the two types of oxygen, which fits perfectly the ligand molecule: 2 carbonyl oxygen and 2 ether oxygen atoms per molecule. One more peak shows up around 533,1-3eV in the case of the incubated samples. This component can be assigned to H-bonded oxygen: H<sub>2</sub>O or -OH [107].

The **C1s** signal also shows three different peaks, one 284.9eV for C=C/C-C (aromatic/aliphatic carbons), 286.7eV for C-N and 288.5eV C=O. The fitting (**Fig.3.2-32**) shows a good correspondence for the first two peaks: the first one is twice as high and in the molecule L1 we have 8 C=C/C-C carbon and 4 C-N. Although the third carbon peak is a bit smaller than expected, the three different states of the carbon were detected.

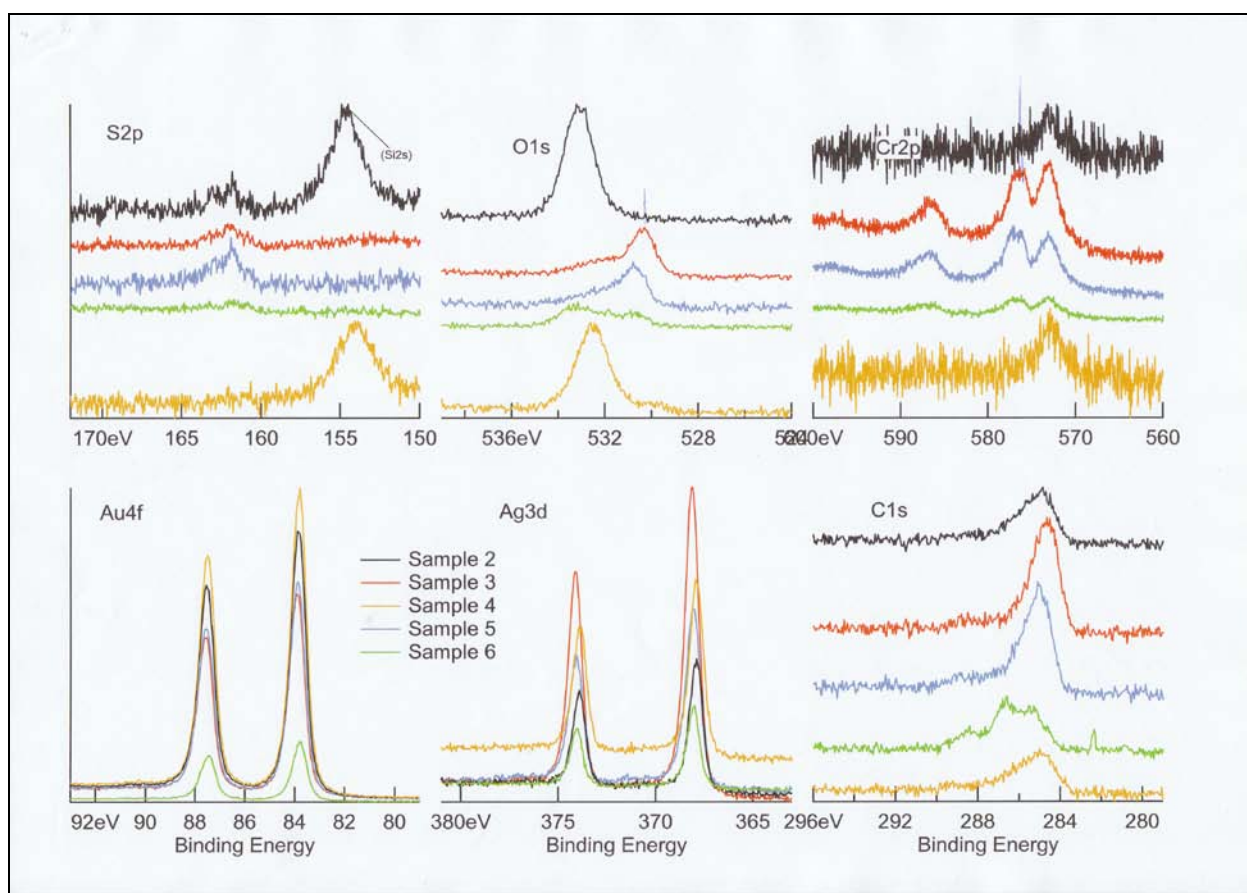


**Figure 3.2-30:** O1s, Au4f, Ag3d, S2p, C1s and Cr2p signals of the different samples

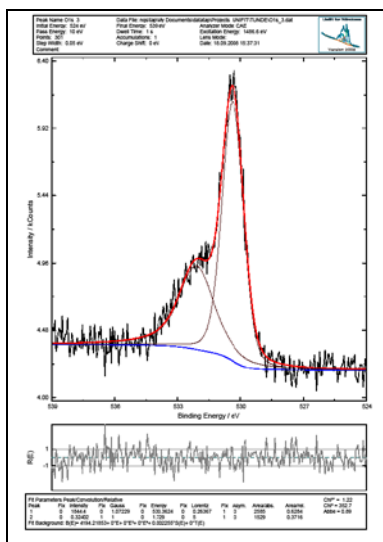


**Figure 3.2-31:** Fitted O1s signal of *sample3*

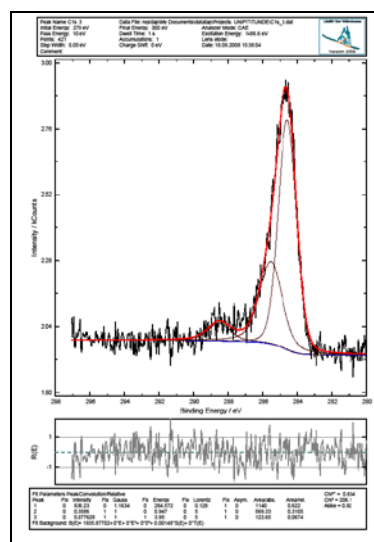


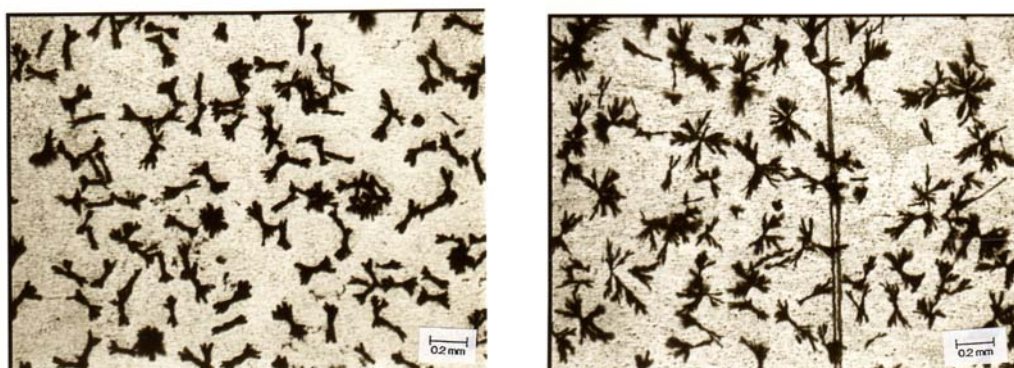
**Figure 3.2-32:** Fitted C1s signal of *sample3*

The XPS results are in a good agreement with the previous experiments, such as the dissolution test and the concentration dependence of the loading. These measurements offer a direct proof for the chemical change of the coating after incubation in a biological media. The significant change of the O and C peak of *sample5* (similar but not as pronounced by the *sample6*) proposed an interaction of the coating with organic molecules.

### 3.2.4 Coatings on gold and titanium dental implant materials

The two substrates described previously as gold alloy and Ti 99% are typically used for dental application. Both surfaces are polished as applied generally in medicine. To coat these samples with Ad17 several conditions were tested for the in-situ crystallisation coating method. The pre-treatment with the disulfide for the gold substrate and the isonicotinic acid pre-treatment for the titanium substrate seemed to be a logical choice to attach our coordination polymer to the surface. Since the gold alloy contains 12,7% of silver, this should help the attachment of the polymer network, with possibly no need for an anchor molecule. In the case of the Ti substrate, the pre-treated samples with isonicotinic acid showed better results. The  $\text{TiO}_2$  is a slightly basic surface, and attaches the carboxylic part of the isonicotinic acid. This way the N-donor atom can coordinate the  $\text{Ag}^+$  and be the starting point of the polymer network. A long treating time has been used, two weeks, with a high concentration: 2mM complex solution in EtOH/THF 1/1 solvent mixture as used previously. The following light microscopic pictures **Fig.3.2-33** show that the loading is very high, the surface is covered by small, some mm-sized crystals.

**Figure 3.2-33a,b:** Light microscopic images of the treated plates

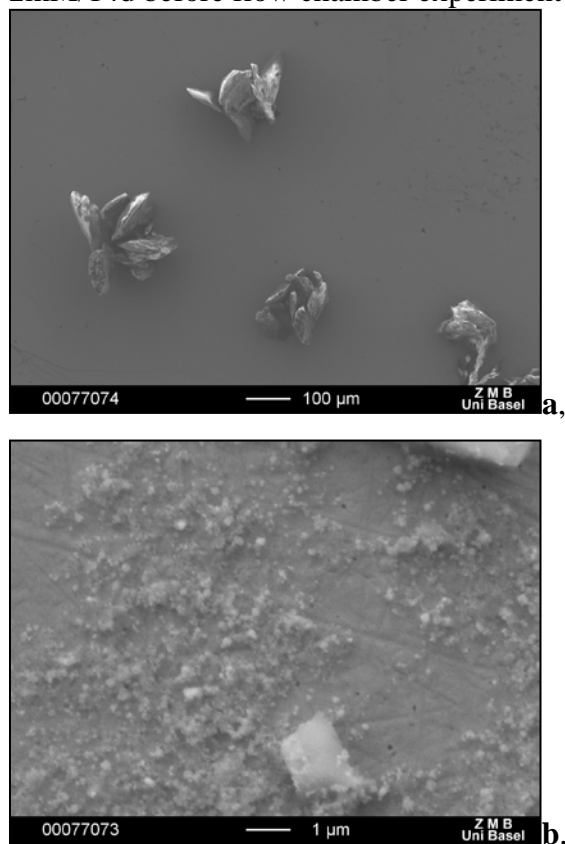
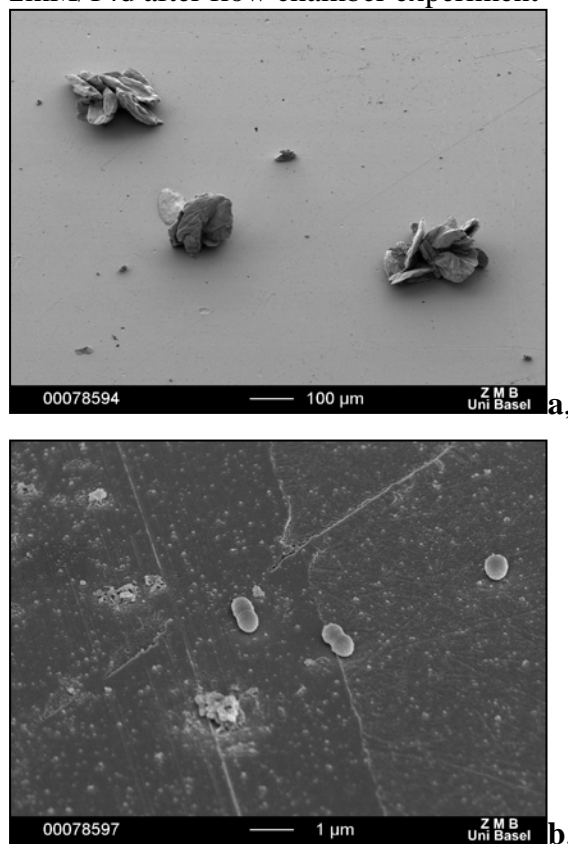


**a,** Gold plate treated 2mM/14d

**b,** Ti plate treated 2mM/14d

The form of the crystals on the gold surface looks slightly different from the titanium, but the loading and the distribution are about the same. To analyse the topography of the surface, SEM measurements were carried out. AFM measurements are not possible because of the high roughness of the samples.

The coated gold and titanium substrates are used for flow chamber experiments is a typical assay in oral microbiology for testing dental materials. In these assays, the test materials are exposed to a bacterial suspension in human saliva for 60min. After the exposure, the bacteria attached on the surface of the test material are counted and the living and dead ones are distinguished. A detailed description of the experiment is found in Chapter 3.3.1.3. The SEM measurements are done on the samples before and after the flow chamber experiment. It gives good information about the solubility of the compounds since no other dissolution tests were carried out. The composition of the previously used biological media is so different to the human saliva used for the flow chamber experiment that it makes no sense to compare. The loading of the plates before the flow chamber experiment is very similar for the gold and the Ti plates:  $\sim 2000 \text{ mg/m}^2$ , which is at the same level as the loading of 2mM/7d treated Au(111) surface. To describe the topography, further SEM measurements were carried out.

**Figure 3.2-34a,b:** Gold substrate treated 2mM/14d before flow chamber experiment**Figure 3.2-35a,b:** Gold substrate treated 2mM/14d after flow chamber experiment

As the images show, part of the macrostructures stay on the surface after the flow chamber experiment. The quantity of these macrostructures is much less than the original loading. Regarding the size of the crystals on the surface, three main groups with the previously described size distribution can be distinguished. The well shaped macro crystals of several 100μm visible to the naked eye, the middle size crystals and flat aggregations with some μm in size, and the nanostructure 50-100 nm. These three main groups behave differently in the flow chamber. While the nanostructure remains on the surface, the middle size aggregates seem all to be leaving from the surface. One part of the macro crystals remains on the surface, another part is removed and remains in pieces in the liquid of the flow chamber. The silver concentration measurement of the chamber liquid shows a big difference between the filtered and unfiltered solutions. The sample without any filtration gives around **1.5 ppm** concentration for Ag (the mistake of the measurement is unusual high due to the inhomogeneity of the samples). The concentration of the filtered sample (0.22μm filter was used) was **0.17 ppm**. This one order of magnitude difference between the filtered and unfiltered samples can have two possible explanations. The silver coordination polymer

network removed from the surface remains in larger pieces than  $0.22\mu\text{m}$ . Since the employed filter removes the bacteria from the solution, it also removes the silver attached to the bacteria. Probably, these two effects combined result in this difference of the silver concentration of the filtered and not filtered solution.

In the case of the Ti treated substrates the same behaviour of the crystals can be observed. The SEM images of the treated Ti plates before and after the flow chamber experiment are shown below:

**Figure 3.2-36a,b:** Ti substrate treated 2mM/14d before flow chamber experiment

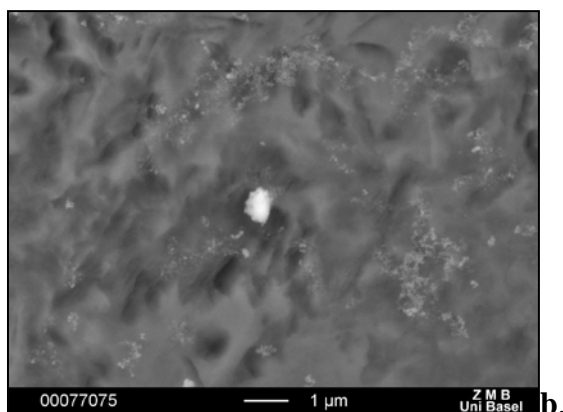
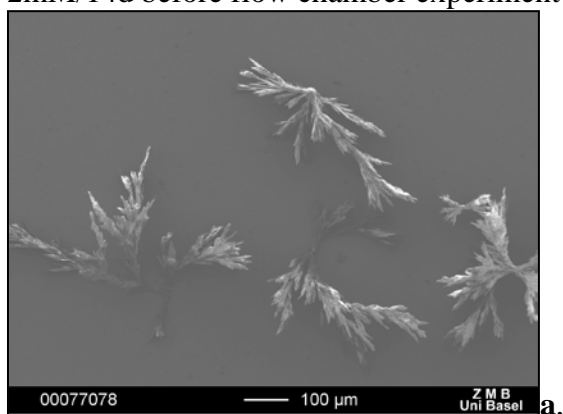
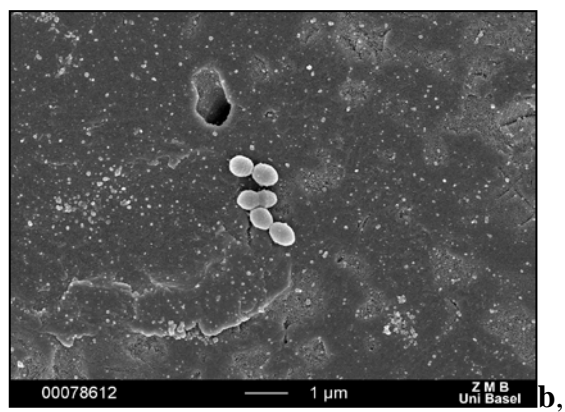
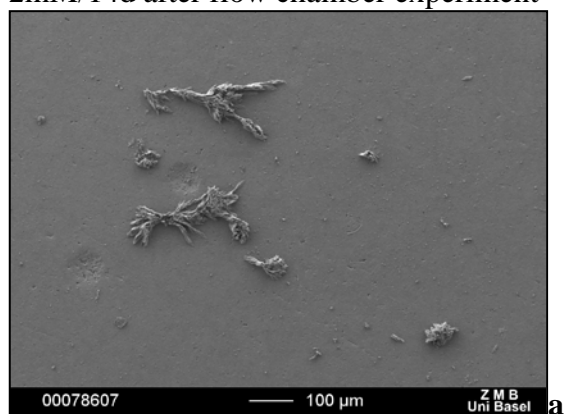


**Figure 3.2-37a,b:** Ti substrate treated 2mM/14d after flow chamber experiment

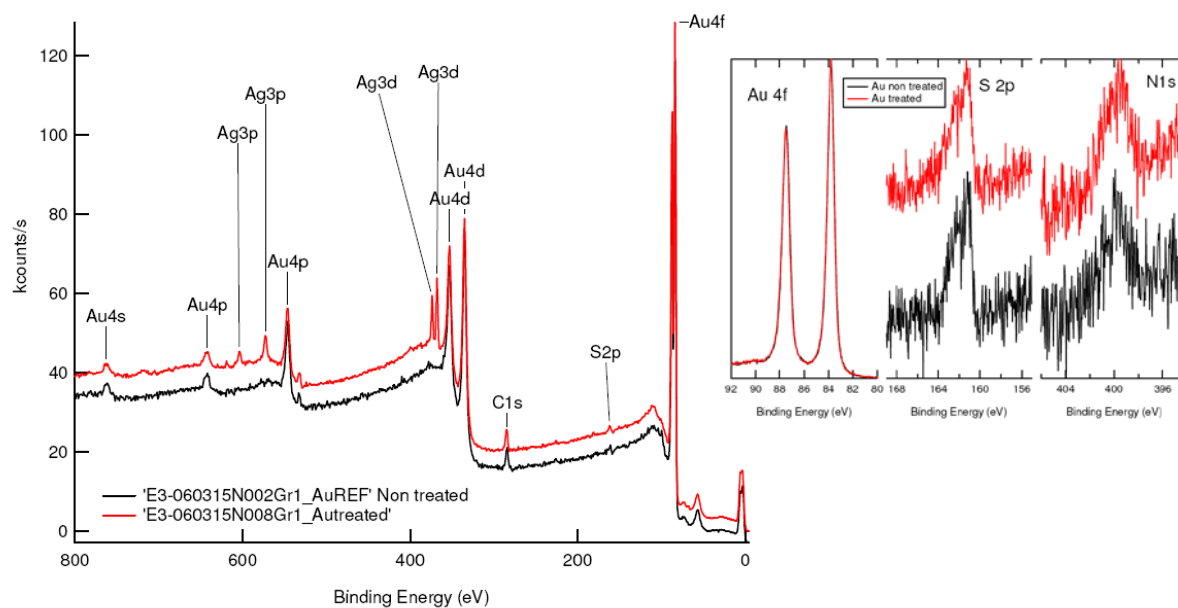


The nanostructures stay on the surface as well as on portions of the damaged macrocrystals. The middle size structures are washed out from the surface. Here, almost the complete absence of these aggregates is observable. The SEM measurements after the flow-chamber experiment show that bacteria are present on the surface. With this technique, it is impossible to distinguish between killed or living bacteria. For this purpose another method is described during the presentation of the microbiological assays in Chapter 3.3.1.3

### 3 Results and discussion

The complementary XPS assays confirm the silver concentration on the surface. The other elements are not so concentrated, as these would be visible on a survey spectrum. The presence of the S in the same concentration in both samples is from the organic contaminations or from the cleaning process. The N and C atoms are found in higher concentration in the treated samples as was expected from the complex polymer since these are the main elements of the ligand L1.

**Figure 3.2-38:** XPS spectra of the gold substrate treated 2mM/14d





#### ***3.2.5 Coatings on titanium and steel restorative implant materials***

For metallic implants, e.g. hips and knees, either titanium or stainless steel is used in western countries. In this study, both of these materials were tested. The previously described silver polymer network is used to build up a coating on the surface of these materials. Regarding the geometry of the substrates two different forms, disk and cylinders, have been coated for *in vitro* and *in vivo* biological assays. Cages prepared from the same material developed for implantation were used for *in vivo* experiments. Two different roughnesses were tested of each material. Since the roughness of the material influences, the biofilm formation [108,24] the experiments were carried out on rough titanium (TiR), smooth titanium (TiS), rough stainless steel (StR) and polished stainless steel (StPol) surfaces. The materials used for cages, disks and cylinders were anodized commercial pure titanium (cpTi; ISO 5832-2) and electro polished and grid-blasted stainless steel (SS; 1.4441, ISO 5832-1). A smooth finished surface was obtained by vibratory finish and electro polishing. A rough surface was achieved by grid blasting with white corundum ( $\text{Al}_2\text{O}_3$ , grain size 0.84–1.2 mm). The original surface passivation method of these materials determines the elemental construction of the surface. Thus different pre-treatment methods for choosing the anchor molecule, were tried (e.g. several acids, as the isonicotinic acid used for the dental Ti substrate). To choose the appropriate concentration and treating time, numerous samples were prepared with different treating conditions and tested by a microbiological assay in order to find out which are the most antimicrobial potent samples. (The microbiological assays are covered in Chapter 3.3.1.2.4) After discovering the appropriate treatment method, a time dependent screening was carried out. SEM measurements were done to analyse the surface topography of the treated substrates and dissolution tests in order to understand the solubility and the stability of the coating on these surfaces.

##### **3.2.5.1 Titanium rough and smooth restorative implant materials**

The substrates treated with different methods were tested by microbiological assay. (The detailed description of these experiments are found later in Chapter 3.3.1.2.4) The best result is obtained by the simple *in-situ* crystallisation method without any pre-treatment. In contrast to the polished titanium dental implant, which has a simple  $\text{TiO}_2$  surface, these restorative implant materials are treated differently. This can be the reason that the previously used method works less well here than the simple crystallisation. In the time dependent trials, the screening window was from 3h to 10 days and the microbiological assays showed that the

maximal effect was already reached after 3 days. For the further experiments, mainly titanium disks were used since this geometry is more convenient for the *in-situ* crystallization. The cylinders showed higher inhomogeneity in the microbiological results, probably due to their different positions and thus irregular coatings during the crystallisation. The different samples, treated for 3days with *in-situ* crystallization, were studied by SEM and the silver loading was determined. After incubation in different biological media analysis were made for both, on the titanium disks and in the media after 24h.

#### SEM measurements

For the tests, two different concentrations were used, namely 1mM and 2mM of AdI7 and 3days treating time. The following images show the coated rough Ti disks:

**Figure 3.2-39a,b,c:** Ti rough (TiR) treated 1mM/3d

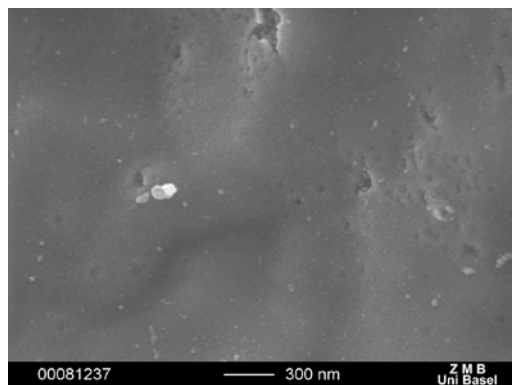
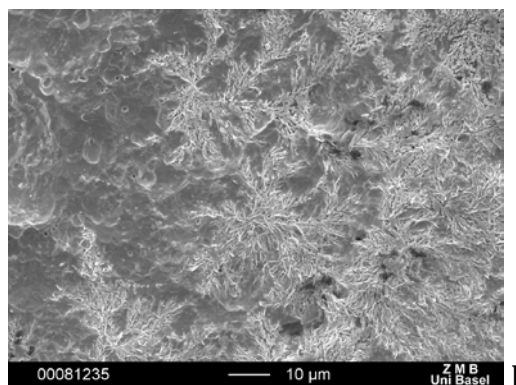
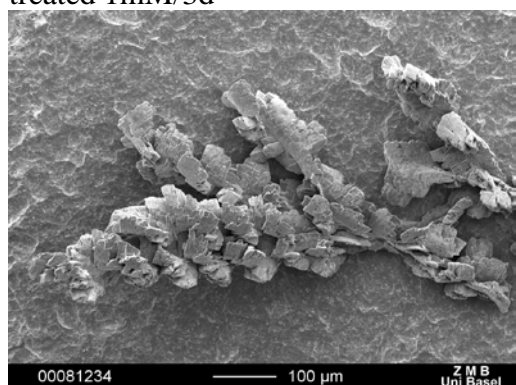
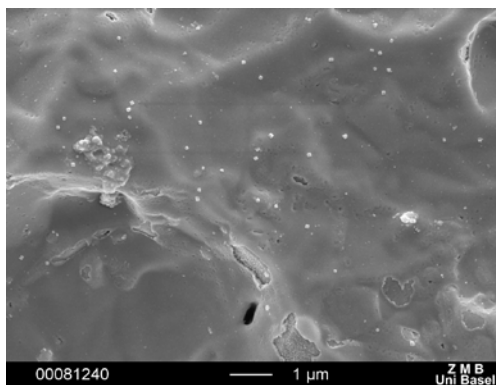
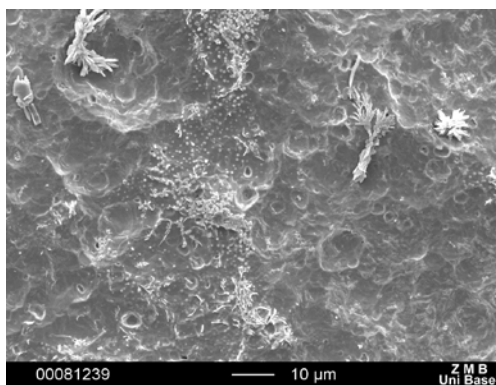
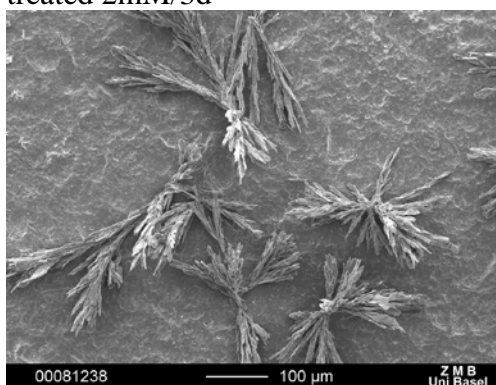


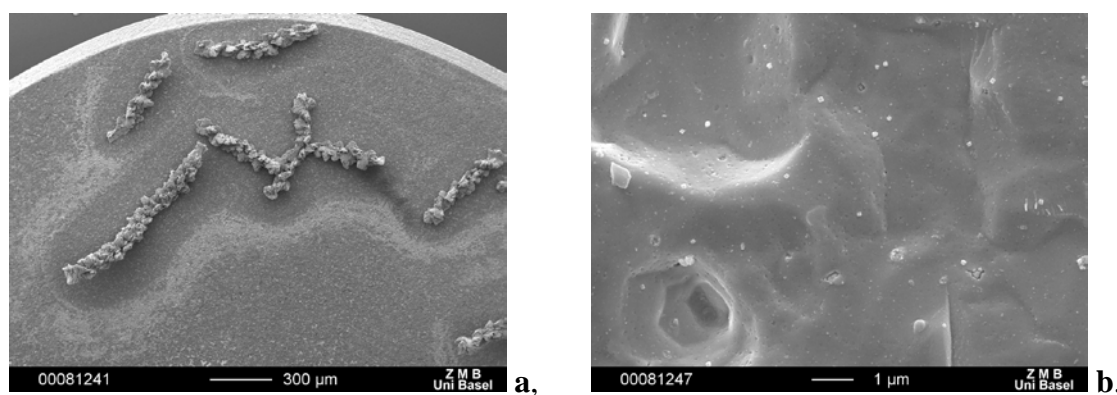
**Figure 3.2-40a,b,c:** Ti rough (TiR) treated 2mM/3d





The typical structures are present: macro crystals of several hundreds of micrometers, flat aggregates of smaller compact crystals of 10-100 micrometers and nanostructures with crystals under 100 nm. The two smaller scale structures are similar in both concentrations in their occurrence and form, while the form of the macro-crystals shows a remarkable difference. More compact crystals form from the 1mM concentration solution thanks to the slower crystallisation process. The occurrence of the macro-structures seemed also different during the SEM measurements: fewer macro crystals have been found on the surface of the 1mM treated disks. The AAS measurement to determine the silver quantity on a surface confirms this hypothesis. (**Table 3.2-5**)

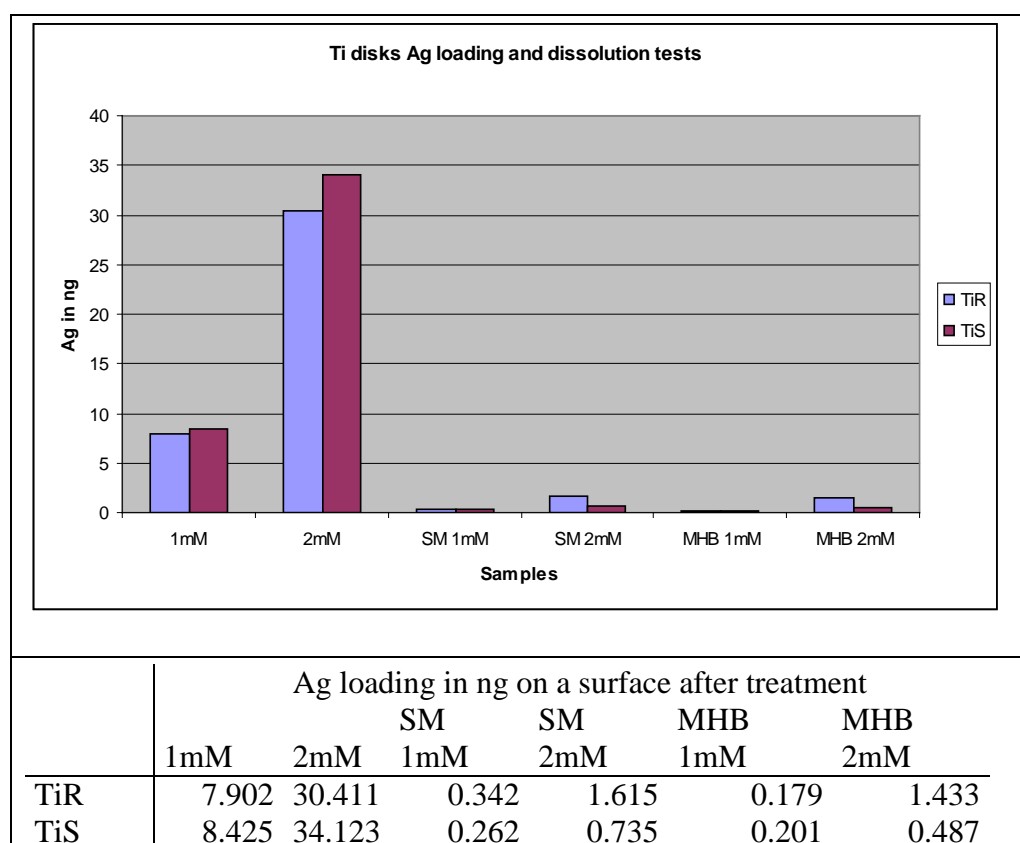
The smooth titanium disks show a high similarity to the rough ones regarding their topography and the loading. The typical size distribution of the compound could be observed on the smooth surface. In addition, the form of the macro crystals of the different concentration treated samples varies as described previously. Thus, just some images are presented here to show the existence of the nanostructures **Fig.3.2-41b**. In order to demonstrate that the crystallisation process follows the classical way: the Ostwald ripening motifs around the macro-crystals are clearly visible **Fig.3.2-41a**.



**Figure 3.2-41a,b:** Treated Ti smooth (TiS) 1mM/3d

The SEM measurements show similar images of the coating for the two substrates with different surface roughnesses. In addition, the AAS measurements determine similar value for the silver concentration on the surface: the smooth plates are just slightly less loaded.

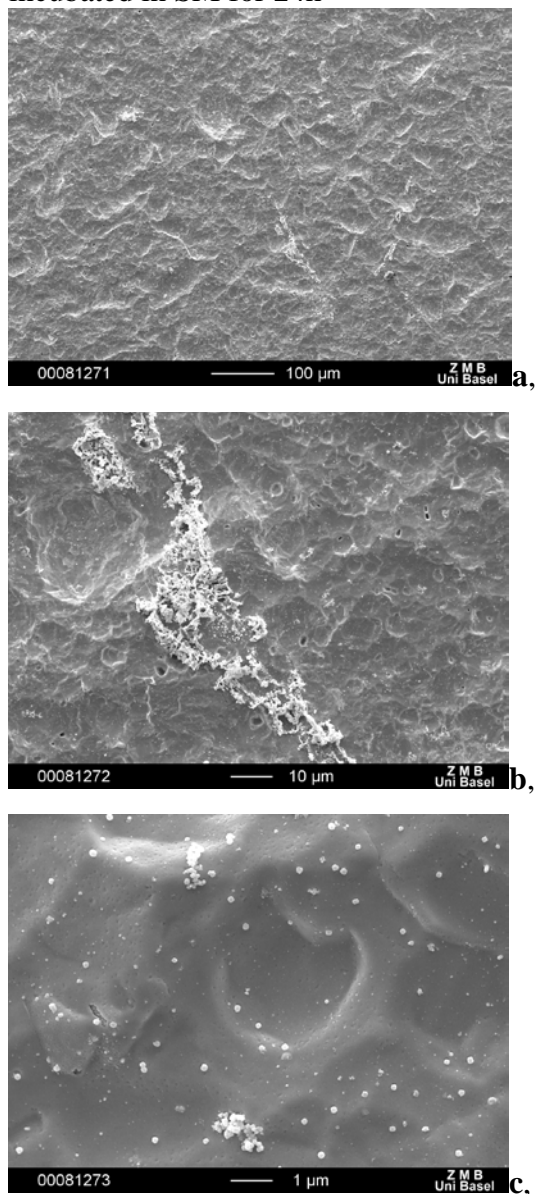
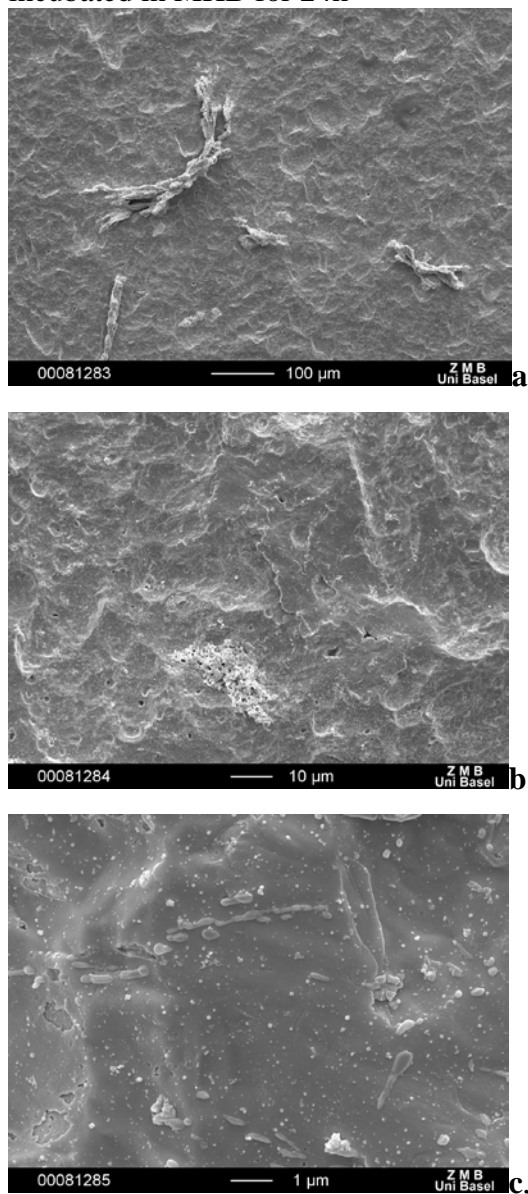
The loadings of the Ti substrates are listed in the **Table 3.2-5**. The loading increase with concentration is similar for both titanium substrates with different roughnesses.

**Table 3.2-5:** Surface loading of the titanium substrates before and after dissolution test

### *Dissolution tests*

For the dissolution tests, the same method as previously described by the gold surface was used. TiR and TiS disks were used, each treated with two different concentrations, 1mM and 2mM, for three days. The dried coated samples were submerged in two different biological media and after 24h removed from the solution, dried and analysed by SEM. The silver quantity on the surface was determined.

The titanium rough samples don't show a significant difference after the incubation in the two media **Fig.3.2-42,43a,b,c**. The quantity of the silver complex remaining on the surface is similar, and so it is for the topography. The here presented sample (2mM / 3days treatment) incubated on the media show only a minor variance. The sample removed from SM contains a little bit less macrostructures and more middle-sized aggregates than the substrate from the Müller-Hinton medium. The nanostructure seems intact in both cases **Fig.3.2-42,43c**.

**Figure 3.2-42a,b,c:** TiR disks 2mM/3d incubated in SM for 24h**Figure 3.2-43a,b,c:** TiR disks 2mM/3d incubated in MHB for 24h

The silver loading determination shows also that the 1mM treated samples behave in a similar way in the two media, and only the nanostructure remains on the surface. As has been observed, during the previous measurements the surface coating of the macrocrystals is significantly damaged by the biological media, and these crystals are covered by AgCl precipitation. This is more pronounced in the case of the synthetic medium. (**Fig.3.2-44a,b,**)

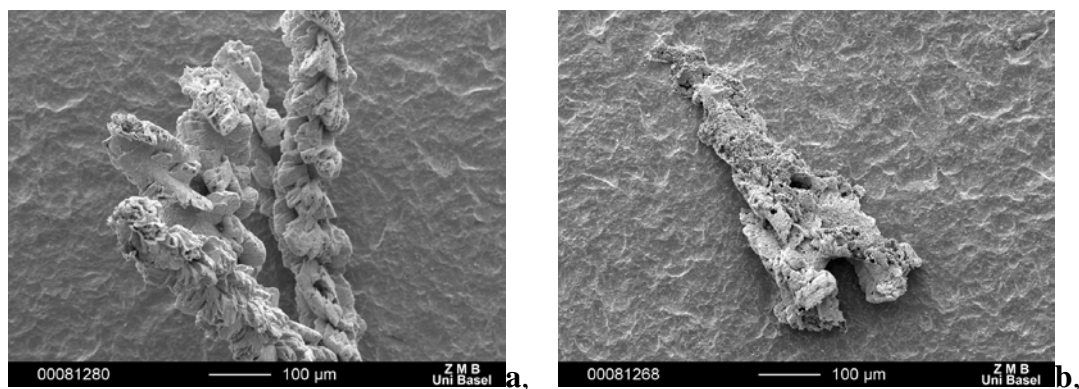


**Figure 3.2-44a,b:** Surface of the macro crystal after 24h incubation in MHB (a) and in SM (b)

Concerning the smooth titanium disks, the dissolution tests were carried out in the same way, and the results can be seen in **Table 3.2-5** comparing to the titanium rough disks. Although, after the crystallisation, the treated smooth and the rough surfaces look much the same, their dissolution tests show a significant difference. On a 1mM treated smooth surface after the dissolution test in both media, no macrocrystals are found and the medium size structures are also absent. Only some nanostructures remain on the substrates removed from the MHB. The concentration of the silver during the AAS measurements was just slightly above the detection limit of the machine.

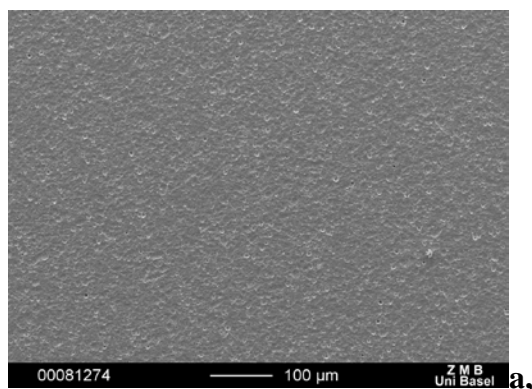


**Figure 3.2-45a,b:** TiS disks 1mM/3d incubated in SM for 24h

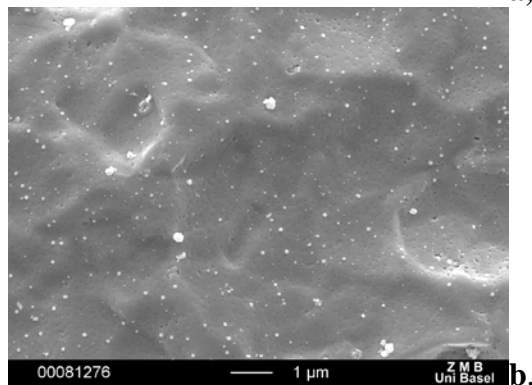
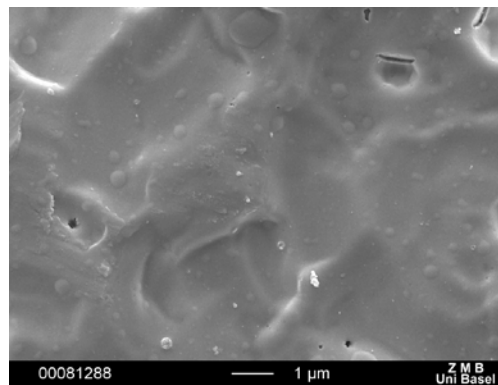


**Figure 3.2-46:** TiS disks 1mM/3d incubated in MHB for 24h



In the case of the 2mM samples the situation is not so critical as the SEM images show:

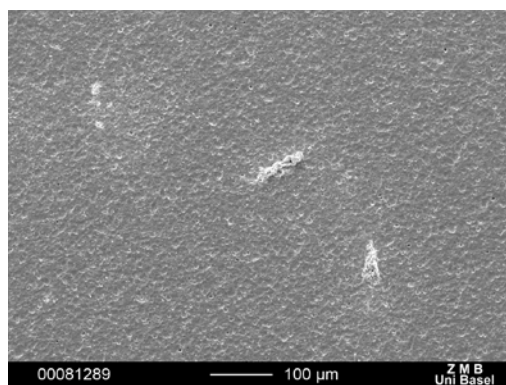


**Figure 3.2-47a,b:** TiS disks 2mM/3d incubated in MHB for 24h

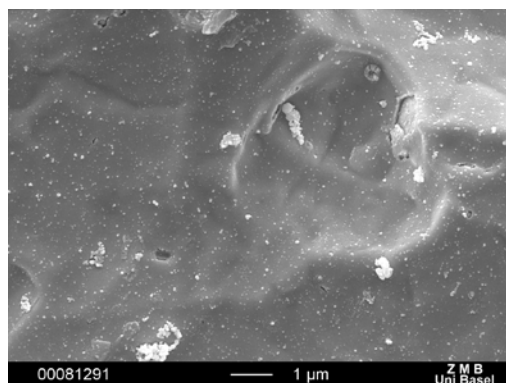
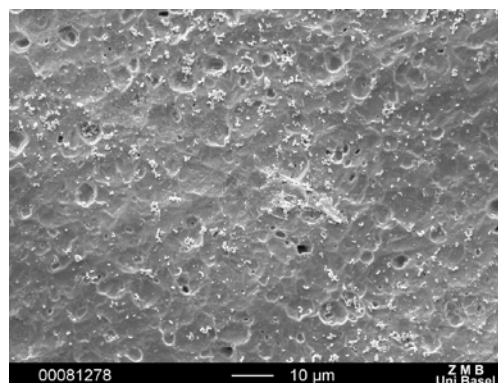


**Figure 3.2-48:** TiS disks 2mM/3d incubated in SM for 24h



This observation is confirmed by the AAS measurements: the silver concentration after incubation in biological media. On a rough surface, there is more than double of compound than on a smooth surface.

The crystallisation process is independent of the roughness of the surface, but the chemical and mechanical stability are higher on a rough surface. The different sizes of crystals hold stronger on a rough surface and are washed out less easily.

#### *Silver release during the dissolution test*

The silver concentration in different media after the incubation of the Ti disks was determined. (**Fig.3.2-48** and **Table 3.2-6**) Results of both roughnesses show the same clear tendency: the silver concentration in a medium is much higher in the case of the 2mM samples, which is explained by on the much higher original loading of these samples as compared to the 1mM samples. The silver concentration is significantly higher in all cases in the Müller-Hinton medium, this also follows the previously observed higher solubility of the compound in this medium.

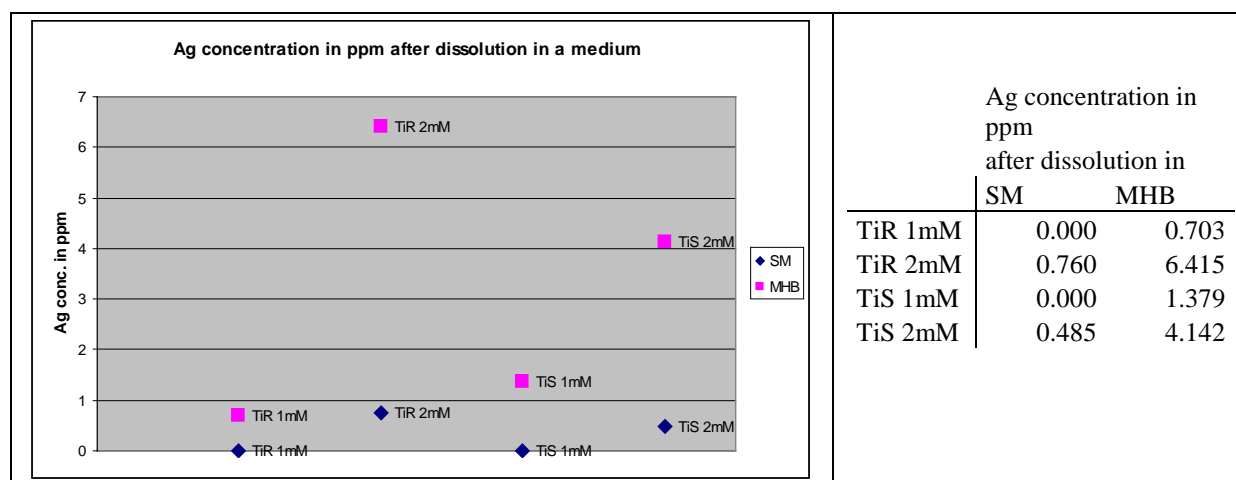


**Figure 3.2-49** and **Table 3.2-6**: Silver concentration in the media after 24h incubation of the different coated substrates

This tendency is more significant than it has been observed previously for the gold plates. The absence of the attaching anchor molecule could be a possible explication of this phenomenon. The compound behaves more as the free compound.

### 3.2.5.2 Smooth and rough stainless steel restorative implant materials

Although the microbiological tests of the steel samples (shown in Chapter 3.3.1.2.4) did not show as good results as the titanium substrates, the silver loading on a surface was determined and some SEM measurements were carried out. In the SEM images of the treated rough steel substrates, the surface appears very similar to the titanium samples. The crystalline structures with three sizes are present. The nanostructure in the case of 1mM treatment is very sparse and difficult to distinguish from the structure of the untreated surface.

This fact can indicate that the silver compound doesn't attach in a strong way on the steel surface. The silver loading measurements (**Table 3.2-7**) seem to confirm this supposition since the loading is appreciably lower than on the titanium or the gold surface loading.

**Table 3.2-7**: Silver concentration on steel disks

	Ag loading on a surface (ng)	
	1mM	2mM
StR	3.942	10.448
StPol	4.400	20.347

**Figure 3.2-50a,b,c:** StR disks coated 1mM/3d

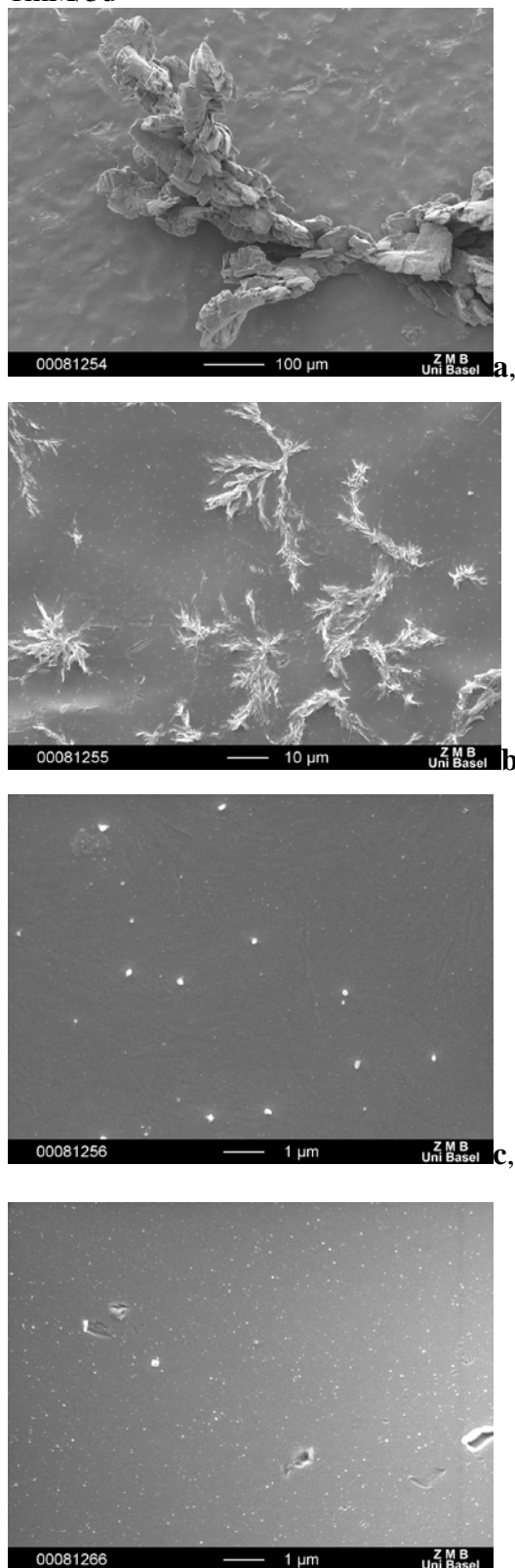


**Figure 3.2-51a,b,c:** StR disks coated 2mM/3d

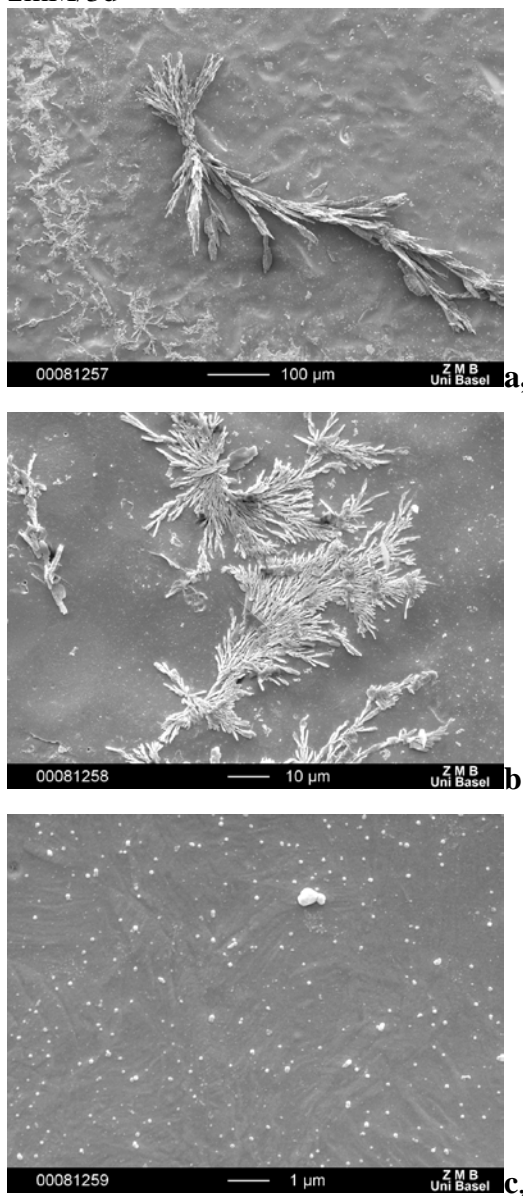


**Figure 3.2-52:** StR disks uncoated

On the surface of the polished steel samples other differences have been observed. The nanostructure is absent in the case of the 1mM treated samples, but present at higher



concentrations. The middle size crystals and aggregations are not as well formed as on the previous substrates.

**Figure 3.2-53a,b,c:** StPol disks coated 1mM/3d

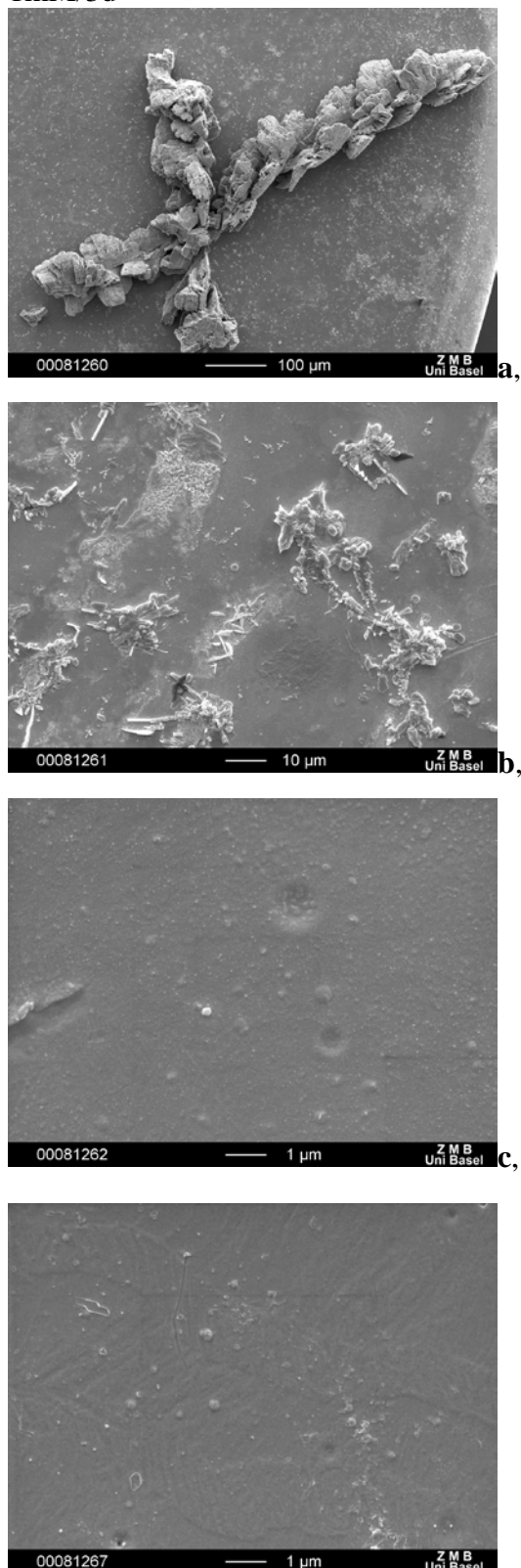


**Figure 3.2-54a,b,c:** StPol disks coated 2mM/3d

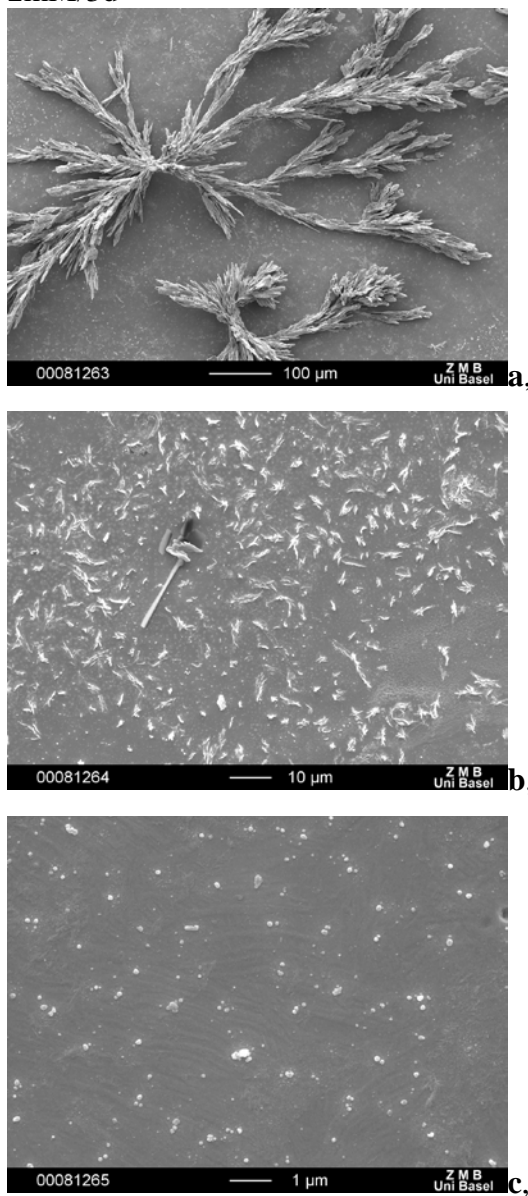


**Figure 3.2-55:** StPol disks coated



### 3.2.6 Coating on other surfaces

The implantable medical devices are not only composed of metal parts, also other materials like ceramics and polymers are used. Hence, other surfaces than metal were treated with the silver polymer network Adl7.

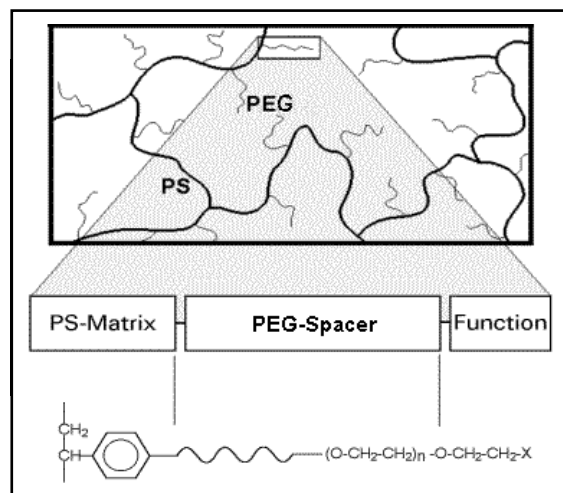


**Figure 3.2-56:** Chemical architecture of T-Gel resins

To simulate a polymer surface like PEG, TentaGel resin was used, as is generally used in a solid state peptide synthesis (see Chapter 3.4.3). Polystyrol beads with grafted PEG surface are suitable to couple amino acids or other acids on the surface. (**Fig.3.2-56**)

The isonicotinic acid coupled T-Gel resin (detailed description is shown in Chapter 3.4.1) behaves as a polymer surface covered with isonicotinic acid. The acidic side of the molecule is connected via a peptide bond to the surface of the bead and the pyridine end remains free. The isonicotinic acid functions as an anchor molecule and plays the same role as the disulfide in a case of the gold plate namely to attach the first silver ion. The so prepared surface was used to build up a coating as previously described. Both of the coating methods, *in-situ* and dip coating were used. The *in-situ* crystallisations took place in a weak concentration solution (0.2mM) to avoid crystallisation other than on the surface. For comparison, the multilayer method was used to build up a crystalline structure on the surface.

Some SEM images of the beads surfaces were taken and EDAX spectra recorded to prove the presence of the silver compound on the surface.

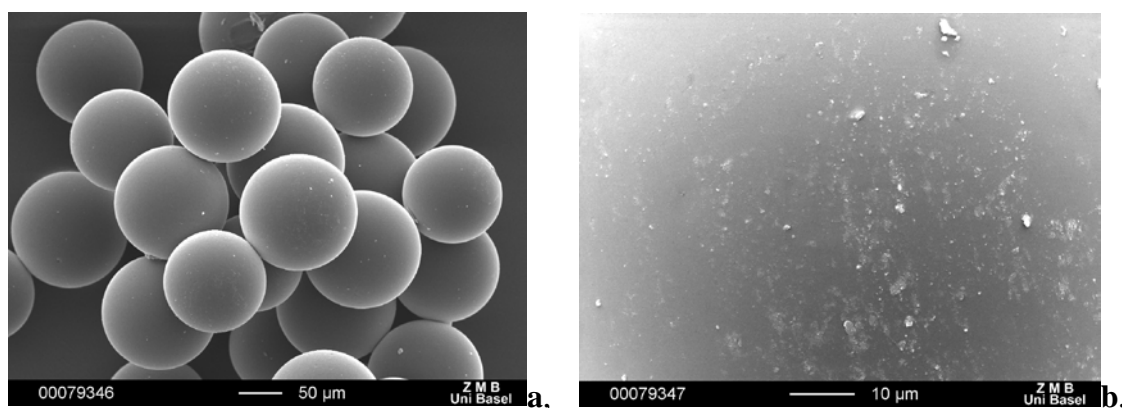


**Figure 3.2-57a,b:** Isonicotinic acid coupled T-Gel resin, layer-by-layer method (12xAgNO<sub>3</sub>→L →...)

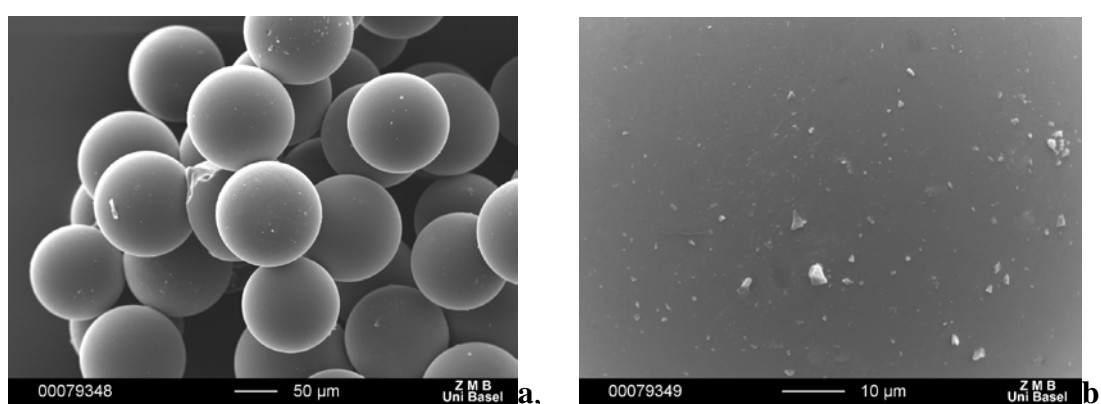


**Figure 3.2-58a,b:** Isonicotinic acid coupled T-Gel resin, in-situ crystallisation (0.2mM/14days)

As it can be observed on the images, both methods worked and allow building up a crystalline coating on the surface. The multilayer method results in a higher but less crystalline coverage. The *in-situ* crystallisation shows better formed and larger sized crystals rising up from the surface.

In addition to isonicotinic acid coupled beads, other peptide coupled T-Gel resins were tested. The Ac-L-His-*rac*-ACHC-L-Tyr-NH-T-Gel tripeptide (detailed description see in Chapter 3.4.3) shows a good complexation with silver (see Chapter 3.4.3), hence, it is apparently a good anchor molecule. This tripeptide coupled T-Gel was subject of the *in-situ* crystallisation (2mM/14days).

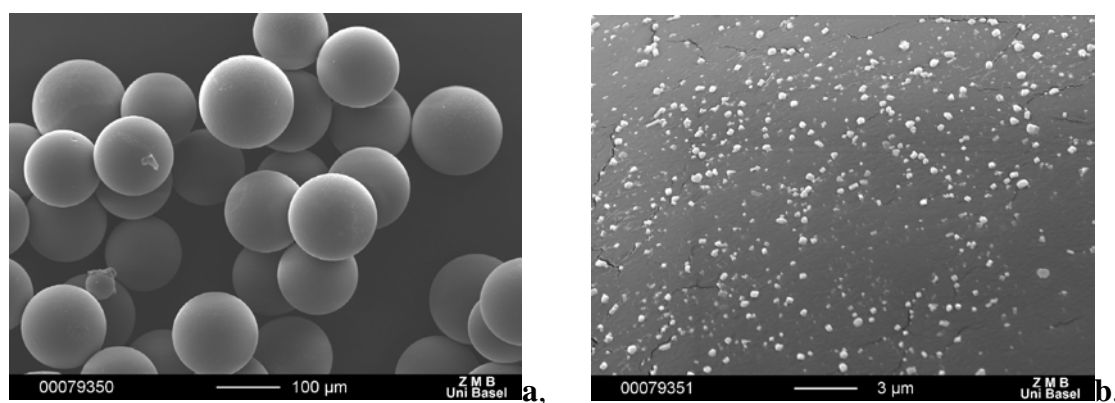


**Figure 3.2-59a,b:** Peptide coupled T-Gel resin, *in-situ* crystallisation (0.2mM/14 days)

Small 20-50nm crystals are covering the surface in a nice homogenous distribution on a T-Gel bead. The loading of the T-Gel resins were measured by AAS and shown in **Table 3.2-8**.

	mgAg/m <sup>2</sup>	LOADING	
		mg Ag/mg beads	mM Ag/mM molecule
TGIso_cryst	80	0.004	0.09
TGIso_LbL	263	0.014	0.31
TG440_cryst	84	0.005	0.10

**Table 3.2-8:** Surface loading of the different coating on T-Gel beads: isonicotinic acid coupled *in-situ* crystallized (TGIso\_cryst) and layer-by-layer treated (TGIso\_LbL) and peptide coupled *in-situ* crystallized coatings.

The loading received by the dipcoating method is much higher than it is in the *in-situ* crystallisation. The silver concentration on the surface obtained by layer-by-layer deposition is similar than on the gold plate treated with 1mM Adl7complex solution for 1d. The *in-situ* crystallisation results in a similar loading than on the gold surface after a 7days treatment of 0.5mM Adl7 solution. All of the coated T-Gel beads were tested for their antimicrobial activity (shown in Chapter 3.3.1.1.1)

These examples show that the described two methods are able to build up the coating on other than metal surfaces. Thus, varying the silver complexing anchor molecule, the silver polymer network can be grown on numerous surfaces.

#### 3.2.7 Conclusions

The different substrates coated with the AdI7 silver polymer network were analysed with different surface analysis methods, like AFM, SEM, XPS and powder X-ray measurements. The silver amount on surfaces was determined by AAS. The change of the coating with the treating time on one hand and the increase of the complex concentration of the treating solution on the other hand was followed with the above mentioned methods. Tests were carried out to study the behaviour of the surface coating against biological media.

The coating on Au(111) is described in detail since all of the analytical methods are suitable for this surface. The here obtained results are extrapolated, compared and confirmed for other substrates by appropriate methods. Depending on the chemical composition of the surface the coating method is slightly adapted for each substrate. In every case that the AdI7 polymer network was applied only the pre-treatment methods were changed, so that the attachment of the polymer network could be optimized.

Concerning the **topography** of the surface after treatment, these following general conclusions can be made for all tested substrates:

- Nanocrystals build up on the surface, which have a compact form and are small in size (50nm). This nanostructure is very homogenous on an Au(111) surface. Most of the nanocrystals seen by AFM and SEM are ca. 10–20 nm in height and have a mean diameter of 10–20 nm, hence the loading of the surface containing this nanostructure could be calculated: the estimated nanocoating for silver is roughly  $3.04 \text{ mg/m}^2$  ( $12.5 \text{ mg/m}^2$  for the compound).
- Middle size crystalline structures with some tens micrometers fall under this second group. These are larger compact crystals or flat aggregates covering the surface after a long enough treating time (at least 1 day for 0.5mM AdI7) or with higher concentration of the treating solution ( $\geq 1.0 \text{ mM}$  for AdI7).
- The macro structures, big well designed crystals of several 100 micrometers, appear when higher concentrations of the treating solution are used ( $\geq 1.0 \text{ mM}$  for AdI7). These crystals are more frequent, but less compact using the highest concentration, 2mM, for the compound.

Besides the surface topography of the substrates, the **silver loading** of the surfaces is the main determining factor concerning the future medical use. Comparing the loading of the Ti plates and the gold surface, the concentration is calculated in  $\text{mg/m}^2$  units and shown in **Table 3.2-9**.

Ag loading in mg/m <sup>2</sup> on the surface after treatment	Table 3.2-9: The surface loading comparing all substrates treated for 3 days		
	0.5mM/3d	1mM/3d	2mM/3d
TiR		403	1549
TiS		429	1738
Auplate	23	424	1747
StR		201	532
StPol		224	1037

TiR: rough titanium; TiS: smooth titanium; Auplate: Au(111) surface; StR: rough steel; StPol: polished steel;

The gold and titanium restorative implant materials have very similar values in contrast to the steel substrates, which have a definitely lower loading. The treatment with 0.5mM Adl7 solution results in a complete covering with nanostructures and some middle size aggregates. The loading is determined by these two types of structures. The 1.0 mM solution results, besides of a fully coverage by the nanostructure, mainly in middle size structures and some rare, compact, well-designed structures on the surface. Thus, the loading is determined mainly by the middle size structures. The surfaces treated with the highest concentration solution show mainly fine, well-designed macro-crystals jointly with the nanocrystals and the middle size structures. Since the macrostructures represent a big mass of the compound, these macrocrystals determine then the loading.

**Dissolutions tests** were carried out to study the stability of the coating against dissolution effects in biological media. The summary of these tests is presented in the **Table 3.2-10**

Ag LOADING IN mg/m<sup>2</sup> ON A SURFACE AFTER TREATMENT

	0.5mM	1mM	2mM	SM 1mM	in %	SM 2mM	in %	MHB 1mM	in %	MHB 2mM	in %
TiR		403	1550		17 4.3	82	5.3	9	2.3	73	4.7
TiS		429	1739		13 3.1	37	2.2	10	2.4	66	3.8
Auplate	23	424	1748		198 46.7	325	18.6	144	34.1	662	37.9
StR		201	532								
StPol		224	1037								

**Table 3.2-10:** Comparative table of the dissolution tests of the different substrates

TiR: rough titanium; TiS: smooth titanium; Auplate: Au(111) surface; StR: rough steel; Stpol: polished steel; SM: synthetic medium; MHB: Müller-Hinton medium

The more Adl7 silver polymer network is present initially on a surface, the more remains after the incubation in a biological medium. The percentage of the compound remaining on a surface is around 2-5% in the case of the Ti surfaces. A higher quantity of the remaining compound in the case of the gold surface can be explained by the used of anchor molecules (disulfide pre-treatment). This molecule guarantees the strong attachment of the compound on

the surface. Although the volume of medium versus the treated surface size ratio was higher in the case of the titanium plates, it cannot explain the large difference. Hence, the positive effect of the anchor molecule is obvious.

Concerning the **chemical changes** taking place on the surface during the incubation in biological media, some observations could be made. In both media, the silver chloride precipitation is significant. This is the main product remaining on the surface of the substrates as well as on the macrostructures after the incubation. Microscopically sized Adl7 crystals are damaged by the solution, their surface is covered by the AgCl, and the major part of the macrostructures is washed out from the surface. This is also true for the medium size structures. The nanostructures seem to resist best against the biological media.

The **silver concentration in media** after 24h the incubation is listed in the **Table 3.2-11**.

	Ag concentration in ppm after dissolution in:	
	SM	MHB
TiR 1mM	0.000	0.703
TiR 2mM	0.760	6.415
TiS 1mM	0.000	1.379
TiS 2mM	0.485	4.142
AuPlate 1mM	0.568	1.760
AuPlate 2mM	3.158	4.346

**Table 3.2-11:** Ag concentration in two different media after 24h incubation of the treated samples

TiR: rough titanium; TiS: smooth titanium; Auplate: Au(111) surface; StR: rough steel; Stpol: polished steel; SM: synthetic medium; MHB: Müller-Hinton medium

As expected, the silver concentration was higher in the Müller-Hinton medium and was in a same region as it was determined for the free compound. It was also anticipated that the silver concentration of the solution is increasing with the quantity of compound on the surface. The less loaded samples (1mM treating solution) have a release of less than 2ppm for silver, which is important information from the biological point of view. The silver concentration is clearly higher, around 5ppm, in the case of the 2mM treated samples. These dissolution tests serve as a model for the biological environment and test the stability of the coating without taking into consideration the flow and other mechanical effects. The microbiological assays will answer the question as to which concentration is necessary to reach a good antimicrobial effect without any toxic side-effects.

In any case, the **Adl7 crystalline coating** has a low solubility, a limited release and a good stability on the surface. These favourable characteristics are more pronounced with the use of an anchor molecule. It's easy to design the coating respectively to the silver loading on the

surface, which makes this silver polymer network a suitable candidate for further microbiological assays. The topography and the loading determine the silver release, thus the 1mM/3h, 2mM/3days treatment is used for small surfaces. In the case of larger surfaces or substrates destined to external use other methods are used. For Au and Ti dental implant materials –external use- 2mM/14days treatment is used to increase the surface loading. For Ti cages (*in vivo* assays) 1mM/3days is applied to avoid the high local Ag concentration.

### 3.3 Microbiological *in vitro* and *in vivo* assays

The purpose of the silver coating is to avoid the biofilm formation on the surface of the implant material, and thus to prevent the septic loosening of the implant. Forming an antimicrobial coating can hinder the preliminary bacterial adhesion and further bacterial multiplication causing septic failure [109,110,167, 140]. The developed silver coordination polymer coating was tested with different microbiological methods to prove the antibacterial efficiency of the coating. First, the free compound, Adl7 is tested by the isothermic micro- and nano- calorimetric method. This method follows the heat of the bacterial growth as a function of time. This is a good way to get information of the antibacterial effect, also of insoluble materials such Adl7 and Ag-treated T-Gel beads. For this kind of material, the classical way of the MIC determination, plating in agarose gel, is not suitable. During IMC measurements, *S.epidermidis* bacterial stain was used in BHI (Brain Heart Infusion) medium. Some complementary tests were done with *S.Aureus*. The inhibition zone experiments were carried out with AgNO<sub>3</sub> solution, followed by some preliminary assays, and the different treated substrates as the Au(111) surface, the titanium, and steel restorative implant materials. In these assays, several bacterial strains were tested, *S.epidermidis*: wild type and ica, *S.Aureus* and also *E.Coli* to compare the effect of the silver on *gram+* and *gram-* bacteria. The microbiological characterization of the treated dental implant materials (gold alloy and pure titanium plates) were carried out in a flow-chamber, which is a typical method in oral microbiology to test the adherent dead and living bacteria on the different substrates. In these assays, *S.Sanguinis*, as one of the known early dental colonizers, suspended in sterilized human saliva, was used. The *in vivo* experiments were carried out on treated titanium cages designed for this aim using the same material as the titanium disks and cylinders in the plating experiments.

#### *Sterilization*

Since some of these methods require a preliminary sterilisation of the coated substrates, different sterilisation methods have been tried on the coating. If the coated plate is rinsed with EtOH (70%), the coating remains intact. Indeed the rinsing of the substrates after the removal from the crystallization solution is made with EtOH. This sterilisation method is generally used during the *in vivo* experiments. Autoclaving (110°C for 1/2h) has been tested on treated titanium dental implant sample and around 10-20% of the coating remains on the surface.

#### **(Fig.3.3-1)**



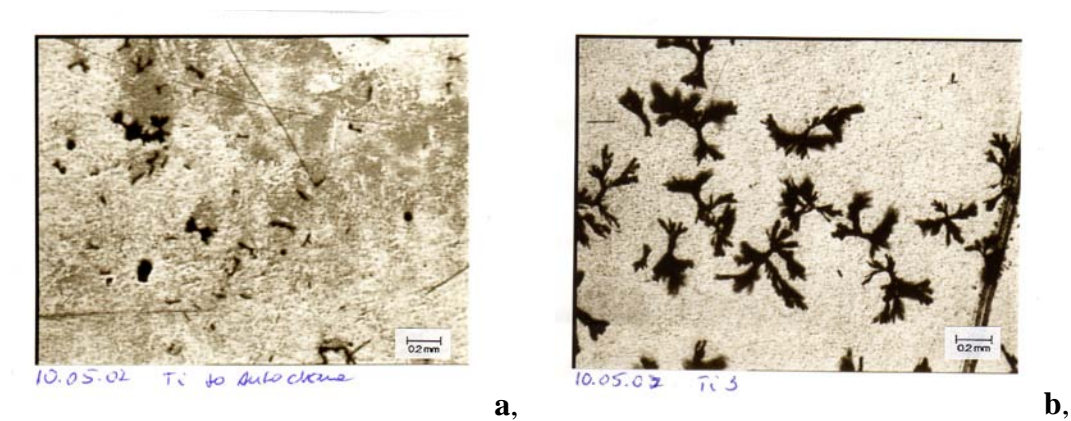


**Figure 3.3-1:** Titanium plates after (a,) and before (b,) autoclaving

In this chapter all of these previously mentioned microbiological methods are described, together with their results for the silver compounds on different substrates. The complementary chemical tests, such as the silver concentration determination in the inhibition zone or in the bacterial fluid, are also presented.

#### **3.3.1 *In vitro* experiments**

##### 3.3.1.1 Isothermal microcalorimetry (IMC) experiments

Calorimetry is attracting increased attention in life sciences [111], because heat flux accompanying action of the living microorganisms is tightly connected with both kinetic and thermodynamic processes [112]. In microbial investigations, calorimetry is particularly valuable because it can provide insights into rapid metabolic changes and allows the velocity and efficiency of growth and product formation to be quantified in a non-invasive way. The enthalpy balance can reveal the formation of unknown, unexpected by-products. These days, calorimetry is a well-established method and a broad spectrum of devices is commercially available, including vessels ranging in volume from a few micro litres to several millilitres (nano and micro calorimeters) or even litres. However, most calorimetric determinations of velocity and efficiency of microbial growth and product formation are highly complicated [113] and therefore not widely used in microbiological laboratories. The simplest calorimetric set-up follows the heat flux of microorganisms growing in a static, sealed ampoule. Critics against to use this approach in microbiological determinations include problems as oxygen supply limitations, pH shifts, lack of homogeneity and sedimentation [114]. Other studies indicate that the simplest calorimetric set-up can be used to obtain reliable and reproducible data about the kinetics of anaerobic growth processes [115].

The application of calorimetry as a routine method in microbiology laboratories seems to have a promising future, given exciting recent developments in miniaturised ‘nanocalorimeters’ [116] or integrated circuit calorimeters [118] with the increasing commercial availability of multi-channel calorimeters [119]. At the beginning of the years of 2000, the calorimetric method was proposed to measure and quantify bacterial growth as a function of different feeding and environmental factors. For the growth of chemoorganoheterotrophic bacteria -which have the potential to catalyse the degradation of harmful organics and synthesise harmless, valuable products- the bacteria have to adjust their utilisation of Gibbs energy, and thus their heat flux and network of reaction fluxes, to cope with sub- or supra-optimal environmental factors, which frequently fluctuate with varying amplitude and frequency. The heat of the growing process was measured, and using the measured enthalpy with the help of special mathematical tools the changes of metabolic fluxes in response to specific stresses could be quantified. [120]

At the University of Basel, the Laboratory of Orthopaedic Biomechanics offers the facility to use this technique to determine microbiological processes on surfaces. The IMC

measurements were made in close collaboration with the group of Prof. A.U.Daniels. The IMC method was first developed by A.U. Daniels to study why by some patients, subject of implant loosening. The main cause of this problem is the micron-size wear polymer and metal particles generated by the mechanical use of the hip implant surfaces. These particles, sometimes, elicit a persistent inflammatory response, eventually leading to bone absorption around the implant and clinical failure due to implant loosening. The response of cultured macrophages to small particles did indeed differ for metal and polymeric hip implant materials [121]. Further microcalorimetric experiments showed that heat flow growth curves in a given culture medium are different for different microorganisms, and heat flow curves for a given microorganism are different in different media. This means that IMC also has potential for identification of the type of microorganism present in a specimen. [122] In general, IMC can be several times faster than conventional culture plate methods, and also simple and safe. Other works were made on microbial contamination in blood platelet products. [123]. The heat of adhesion of bacteria to surfaces of dental implant surfaces was measured with success. [124] In this work, glass beads were used to model the enamel surface. The heat produced by the growing of the *S.Sanguinis* cells, suspended in human saliva, in presence of different quantities of glass beads was determined by the calorimeter. This heat was compared with the growing heat of the stationary microorganisms, thus the adhesion on the glass surface could be determined. Other works were made studying the antibacterial effect of  $Ag^+$ . The MIC values of silver nitrate on *E.Coli* and *S.Aureus* were determined by the microcalorimetric method. The MIC of silver nitrate in LB (Luria-Bertani broth) for *E.coli* ( $10^4$ CFU/ml) is 8 mg /l as determined by the broth dilution method. The MIC of silver nitrate in BHI for *S.aureus* ( $10^4$ CFU/ml) is 256 mg/l as determined by the broth dilution method. Both methods, microcalorimetry and visual interpretation, returned the same results [125].

All the IMC measurements were performed on TAM III™ thermostats, equipped with multi channel microcalorimetry. This calorimeter, a heat flow type calorimeter, works by channelling the heat produced or consumed by a reaction in the sample through heat flow sensors comprised of thermoelectric modules, and converse the heat on an electrical signal which is proportional with the heat change. The TAM III thermostat maintains the outside temperature hence the outstanding sensitivity. The calorimeter is a twin type (Fig.3.3-2), consisting of both a sample and a reference side. The measured value is the difference in heat flow between sample and reference. This twin principle reduces baseline noise by eliminating any small fluctuations of the thermostat resulting a good sensitivity and reliability.

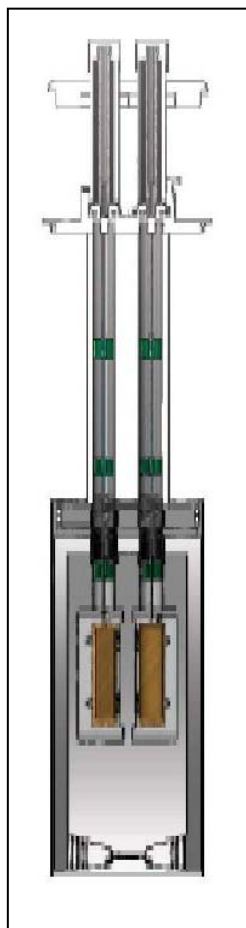
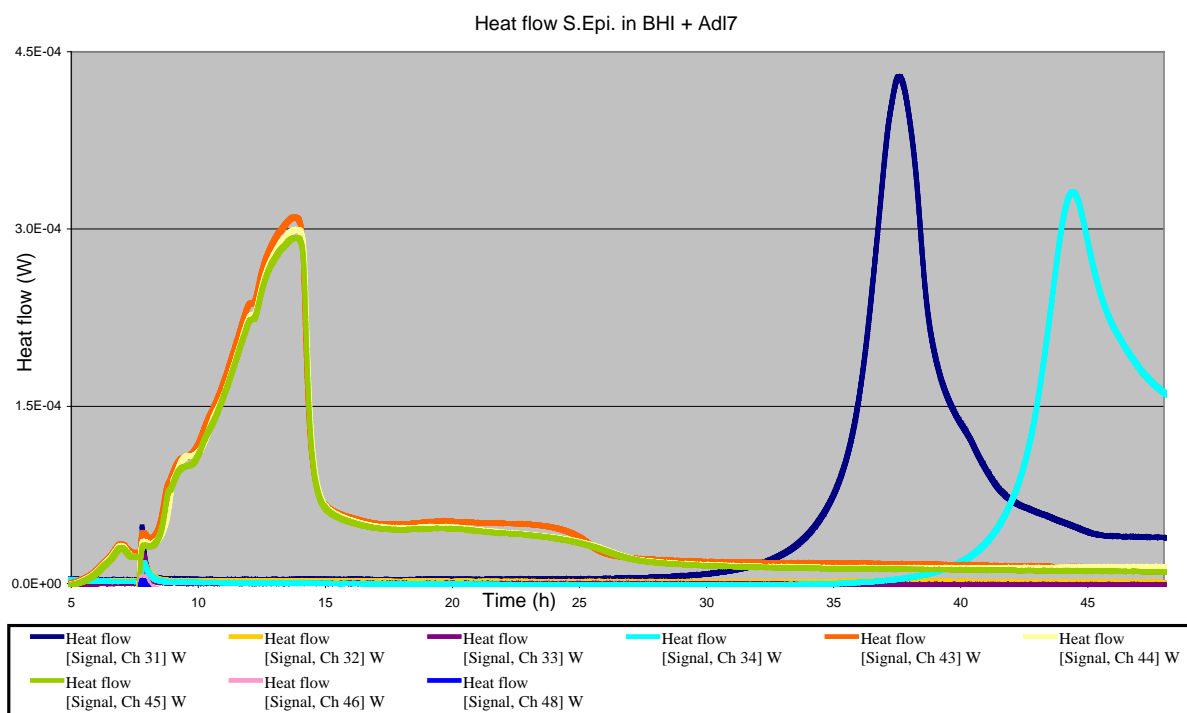


**Figure 3.3-2:** Scheme of the twin type calorimeter

This technique was used to determine the antimicrobial activity of the insoluble compound Adl7 against *S.epidermidis* in BHI. The same conditions were applied during the measurements of the TGel samples. One part of these samples has Adl7 built on the surface by crystallisation or layer-by-layer method. TGel samples having silver nanoparticles generated on the surface by peptides were also tested. The results are presented in the following chapters.

#### ***3.3.1.1.1 IMC measurements on silver coordination polymers***

In figure **Fig.3.3-3** the heat flow curves of the growth of the *S.epidermidis* in BHI medium are presented and compared with the heat flow of the bacterial solution in presence of Adl7 compound. A weighted amount of Adl7 was suspended in the BHI medium, then the bacterial strain was added and the vessel was sealed and put directly into the calorimeter. Adl7 was present in 4 vessels in different concentrations.

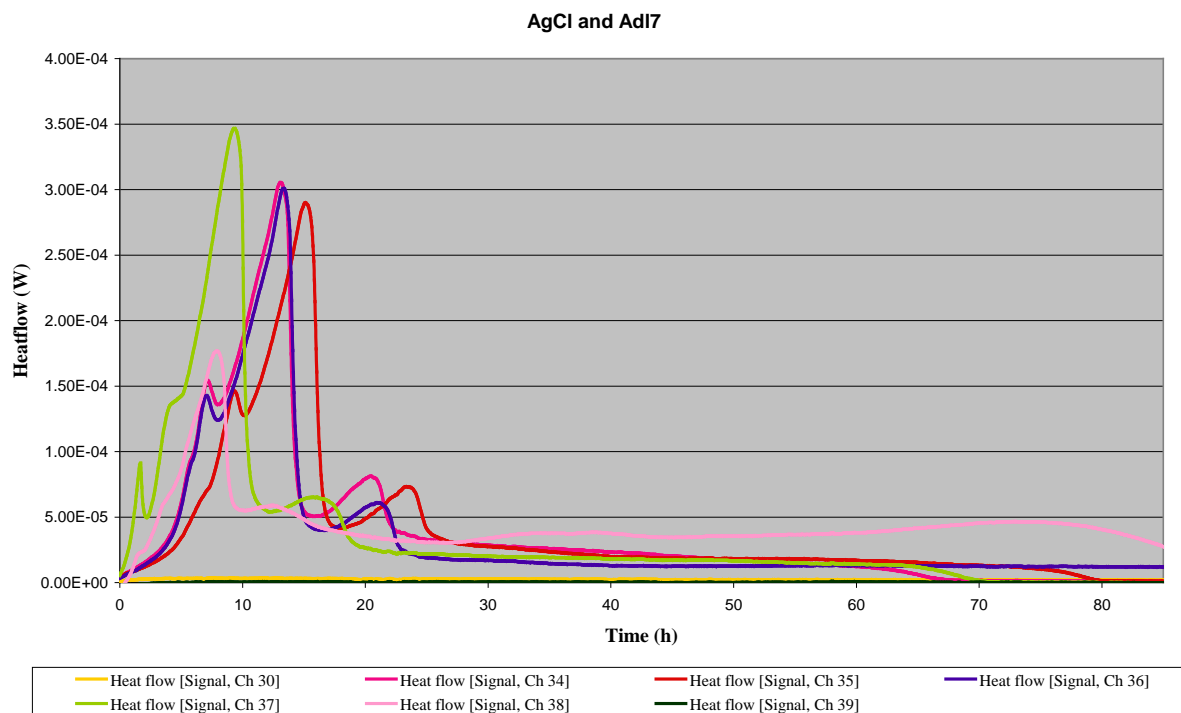


Channel	Compound
Ch 31	Adl7, 4.1 mg
Ch 32	Adl7, 4.3 mg
Ch 33	Adl7, 5.4mg
Ch 34	Adl7, 8.5 mg
Ch 43	<i>S.epidermidis</i>
Ch 44	<i>S.epidermidis</i>
Ch 45	<i>S.epidermidis</i>
Ch 46	BHI
Ch 48	BHI

**Figure 3.3-3:** Heat flow curves of bacterial growth of *S.epidermidis* in presence and without Adl7 compound

From these 4 vessels, bacterial growth can be observed after 36h in one and after 42h in a second vessel. In the two other vessels, no bacterial growth took place during the 48hours of the measurement. This is a very good result, supposing a good antimicrobial effect for Adl7 since this compound, in this concentration, inhibits the bacterial growth for at least 20h, or, in the better case, it can block their growth.

Adl7 was compared with the most common silver precipitate, AgCl, since this is the main product after the dissolution of Adl7 in synthetic and biological media. By the dissolution tests and SEM measurements, the AgCl precipitate forms on the surface of the crystals. It would be preferably to exclude the doubt if only the antibacterial effect of the AgCl could be observed during the measurements or if it is a real effect of Adl7. Therefore, Adl7 was compared to different amounts of AgCl, bacteria alone and blank.



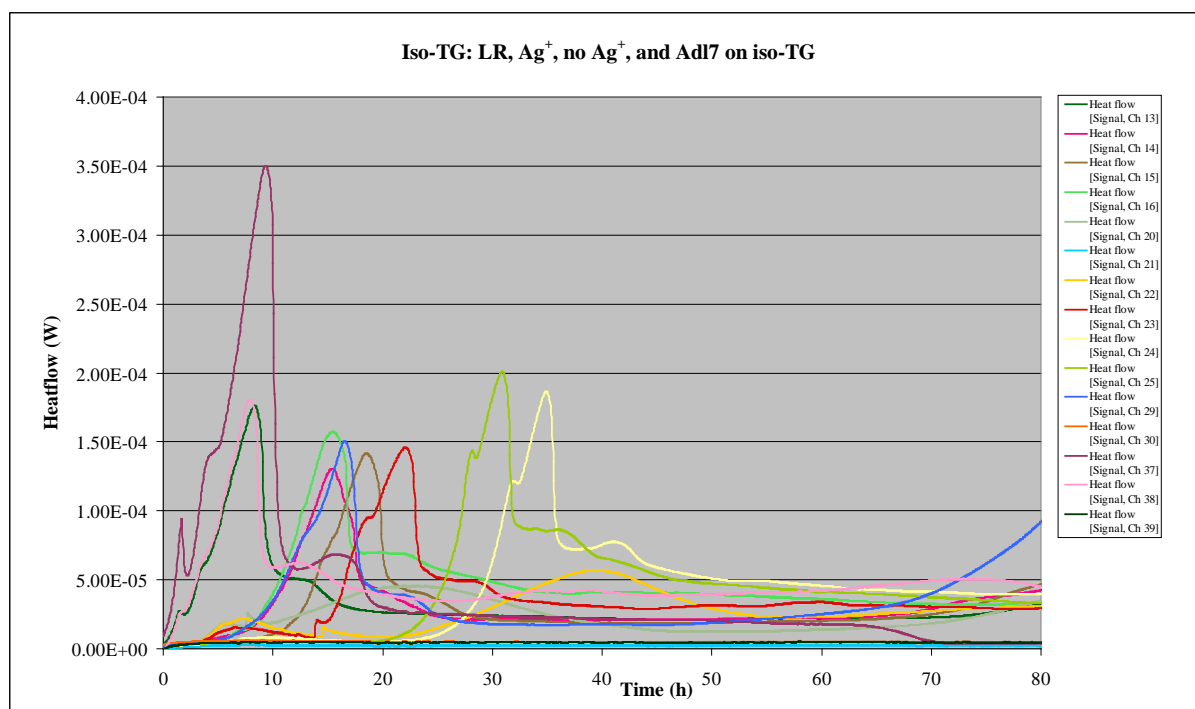
Channel	Compound	Ag conc. mM
Ch 30	Adl7; 3.7mg	0.008
Ch 23	AgCl; 4.9mg	0.034
Ch 24	AgCl; 5.4mg	0.038
Ch 25	AgCl; 4.8mg	0.034
Ch 37	<i>S.epidermidis</i> (3ml)	-
Ch 38	<i>S.epidermidis</i> (1ml)	-
Ch 39	Sterility control (BHI)	-

**Figure 3.3-4:** Heat flow curves of bacterial growth of *S.epidermidis* in presence of Adl7 compound and AgCl salt

The results (**Fig.3.3-4**) obviously show that AgCl has just a weak effect (the bacterial growth is delayed by some hours) against *S.epidermidis*, contrary to Adl7, which inhibits the bacterial growth during the 85 hours of the measurements.

Since the Adl7 has an antimicrobial activity, it is preferable to test the surfaces coated with this compound. The Au(111) plates are too large to test them in these vessels of the calorimeters. Therefore, the Adl7 compound attached on a T-Gel surface was tested. This IMC technique is suitable to measure if the compound attached on polymer beads has the same effect as the free Adl7. For classical microbiological assays, the plating method is not suitable for testing these small particles.

The prepared, dried and weighed T-Gel beads were suspended in the BHI medium, then the bacterial strain was given into the vessel, which is sealed directly and put into the calorimeter. The samples of the two surface treatment methods to build up the Adl7 on isonicotinic acid coupled T-gel are compared with the untreated, iso-TG, the Ag<sup>+</sup> incubated but not reduced iso-TG, the light reduced iso-TG and the free Adl7, as shown on **Fig.3.3-5**.



Channel	Compound
Ch 13	iso-TG; 5.3mg
Ch 14	Ag <sup>+</sup> iso-TG; 3.1mg
Ch 15	Ag <sup>+</sup> iso-TG; 4.9mg
Ch 16	Ag <sup>+</sup> iso-TG; 4.8mg
Ch 20	Adl7 on iso-TG (LbL); 5.9mg
Ch 21	Adl7 on iso-TG (LbL); 5.6mg
Ch 22	Adl7 on iso-TG (LbL); 6.3mg
Ch 23	Adl7 on iso-TG (cryst); 5.9mg
Ch 24	Adl7 on iso-TG (cryst); 7.0mg
Ch 25	Adl7 on iso-TG (cryst); 5.0mg
Ch 29	LR iso-TG; 5.5mg
Ch 30	Adl7; 3.7mg (3ml)
Ch 37	<i>S.epidermidis</i> (3ml)
Ch 38	<i>S.epidermidis</i> (1ml)
Ch 39	Sterility control (BHI)

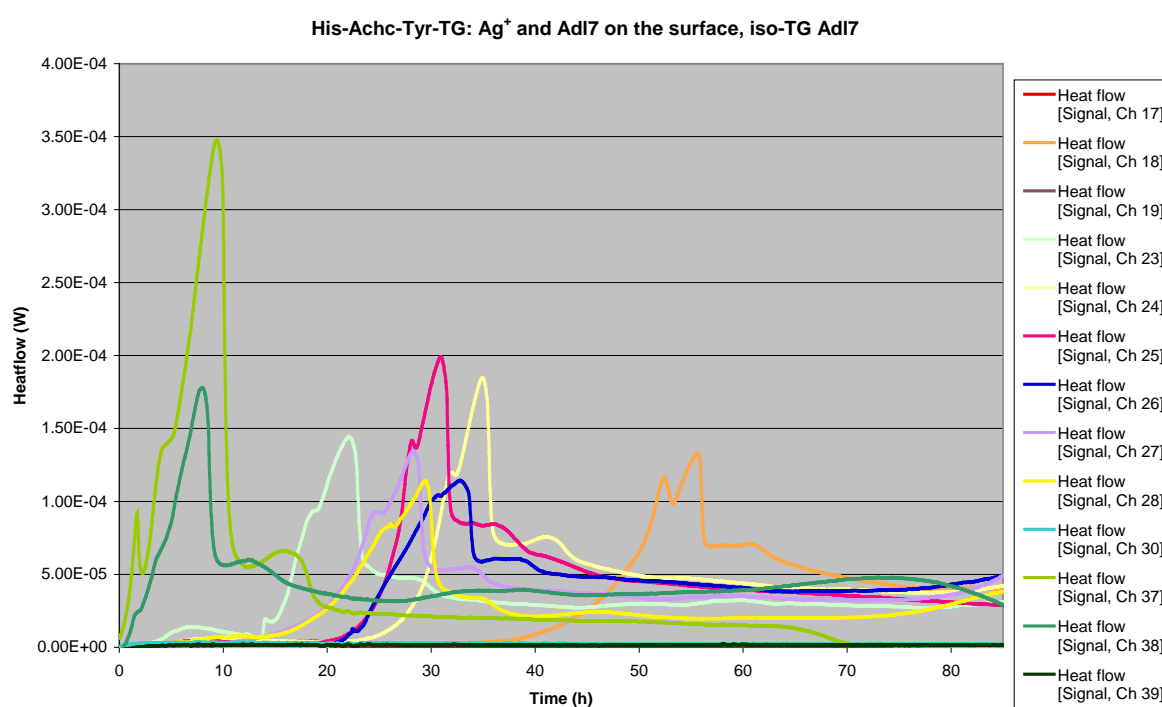
**Figure 3.3-5:** Heat flow curves of bacterial growth of *S.epidermidis* in presence of bulk Adl7 compound compared to the heat flow curves in presence of the differently coated polymer surfaces:  
 Ag<sup>+</sup> iso-TG: isonicotinic acid coupled TG beads complexed with Ag<sup>+</sup>  
 Adl7 on iso-TG(LbL): isonicotinic acid coupled TG beads coated with Adl7, layer-by layer method  
 Adl7 on iso-TG(cryst): isonicotinic acid coupled TG beads coated with Adl7, *in-situ* crystallization method  
 LR iso-TG: isonicotinic acid coupled TG beads complexed with Ag<sup>+</sup>, AgNPs generation by light reduction

The no silver containing iso-TG has no effect on the bacterial growth, as it was expected. The best antibacterial effect has the Adl7 coating, which was built up with the dip coating method on iso-TG. This has the same effect as the free Adl7, and the bacterial growth is blocked by these products during the time of the measurements. The other method used to treat the iso-TG surface with the Adl7, namely the crystallisation method, has a weaker antibacterial effect than the previous one. In anyway, there is a microbiological activity for both Adl7 coated iso-TG. The difference of the two coating methods should be an explanation of this variation in the bacterial growth. The fact that the loading resulting from the dip coating method is almost 3 times higher than the loading after the classical crystallization on iso-TG is supposed to be

### 3 Results and discussion

the cause of this difference, because the  $Ag^+$  release of the sample is proportional with the loading. The  $Ag^+$  incubated and the light reduced iso-TG has the same antibacterial effect. It is much weaker (the bacterial growth is just delayed by 6-8hours) than the Adl7 containing beads. The silver concentration on the surface is much lower, thus the release of  $Ag^+$  is also lower.

A different anchor molecule, His-Achc-Tyr-TG, is also used to build up the Adl7 on the surface of the T-Gel beads. These beads were also tested and compared with the simple  $Ag^+$  incubated peptide-TG and with similarly prepared samples using isonicotinate anchor molecule (**Fig.3.3-6**)



Channel	Compound
Ch 17	$Ag^+$ His-Achc-Tyr-TG; 5.3mg
Ch 18	$Ag^+$ His-Achc-Tyr-TG; 4.4mg
Ch 19	$Ag^+$ His-Achc-Tyr-TG; 7.7mg
Ch 23	Adl7 on iso-TG (cryst); 5.9mg
Ch 24	Adl7 on iso-TG (cryst); 7.0mg
Ch 25	Adl7 on iso-TG (cryst); 5.0mg
Ch 26	Adl7 on His-Achc-Tyr-TG (cryst); 6.4mg
Ch 27	Adl7 on His-Achc-Tyr-TG (cryst); 5.3mg
Ch 28	Adl7 on His-Achc-Tyr-TG (cryst); 5.6mg
Ch 30	Adl7; 3.7mg (3ml)
Ch 37	<i>S.epidermidis</i> (3ml)
Ch 38	<i>S.epidermidis</i> (1ml)
Ch 39	Sterility control (BHI)

**Figure 3.3-6:** Heat flow curves of bacterial growth of *S.epidermidis* in presence of bulk Adl7 compound compared to the heat flow curves in presence of the differently coated polymer surfaces:

$Ag^+$  His-Achc-Tyr-TG: His-Achc-Tyr coupled TG beads complexed with  $Ag^+$

Adl7 on His-Achc-Tyr-TG(cryst): His-Achc-Tyr coupled TG beads coated with Adl7, *in-situ* crystallization method; Adl7 on iso-TG(cryst): isonicotinic acid coupled TG beads coated with Adl7, *in-situ* crystallization method



The peptides incubated with  $\text{Ag}^+$  have a higher effect against the bacterial growth: two out of the three parallel samples were completely blocking the growing process during the time of the measurements. The effect is high thanks to the silver, present in ionic form on the surface and in a high concentration (high uptake), thus easy to release. The samples with the two different anchor molecules are behaving in a same way. These samples delay the bacterial growth by ca. 15-18h on average. This is the same result as received in the previous measurements. The two samples have the same Adl7 loading on the surface, which results in a similar antibacterial effect.

To conclude the measurements regarding the Adl7, some principal remarks should be made:

-The free Adl7 has a very good antibacterial effect on *S.epidermidis* in BHI, much higher than the common AgCl precipitation. The surface passivation of Adl7 by the AgCl has not a remarkable effect.

-The Adl7 attached on polymer surface has also a good impact on the bacterial growth. The effect depends on the loading on the surface hence the concentration of the Adl7.

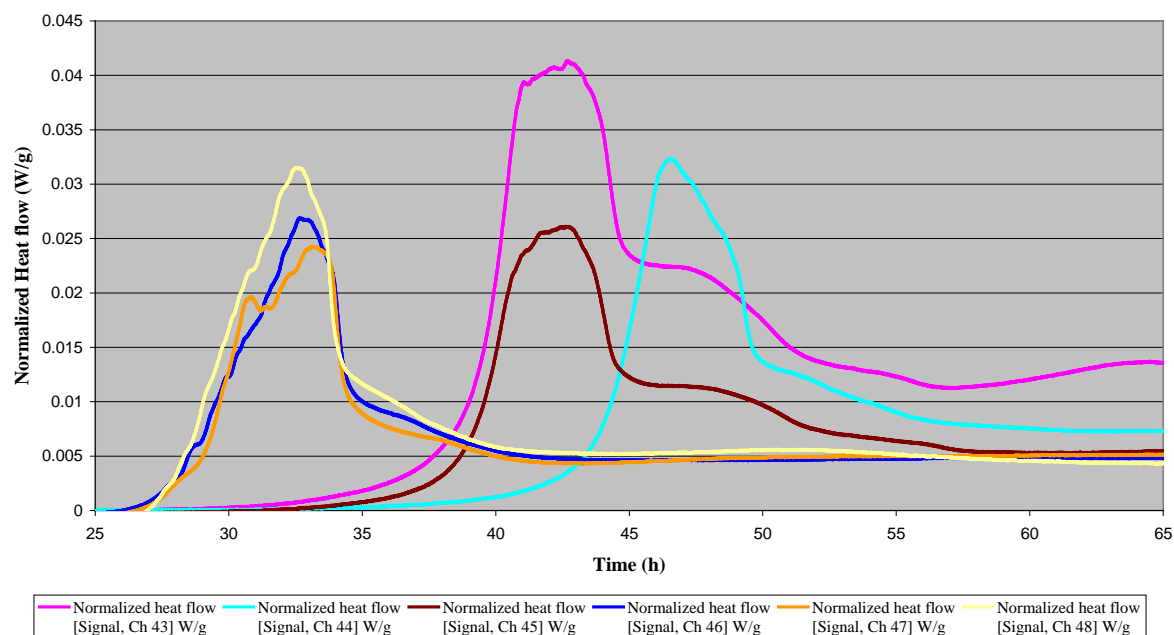
-The antibacterial effect seems to be a direct factor of the silver ion concentration in the solution, because the  $\text{Ag}^+$  incubated samples, where just ions are present on the surface (and these ions are easy to release) show a high activity.

Further IMC investigations were done on other T-Gel beads to test the antimicrobial effect of the AgNPs generated by solid state peptides.

### 3.3.1.1.2 IMC measurements on AgNPs generated on solid surface by peptides

IMC measurements carried out on TG samples focus on the sequence AcHis-Achc-TyrNH-TG. This sequence has good photo reducibility, thus the two reducing methods could be compared. The uptake of the peptide is rather high, resulting in a high  $\text{Ag}^+$  concentration on the surface. The different samples,  $\text{Ag}^+$  incubated, light reduced (LR) and chemically reduced (CR) samples were prepared. The dried beads were weighed directly into the IMC glass vessel, then it was suspended in the BHI medium. The bacterial suspension was added, the vessel sealed and the measurements could begin. In the first step, the chemical and light reduced beads were compared. (**Fig.3.3-7**)

**Normalized Heat flow of LR and CR His-Achc-Tyr-TG**



Channel	Compound
Ch 43	LR His-Achc-Tyr-TG, 4.8 mg
Ch 44	LR His-Achc-Tyr-TG, 4.6 mg
Ch 45	LR His-Achc-Tyr-TG, 4.8 mg
Ch 46	CR His-Achc-Tyr-TG, 7.2 mg
Ch 47	CR His-Achc-Tyr-TG, 7.1 mg
Ch 48	CR His-Achc-Tyr-TG, 5.9 mg

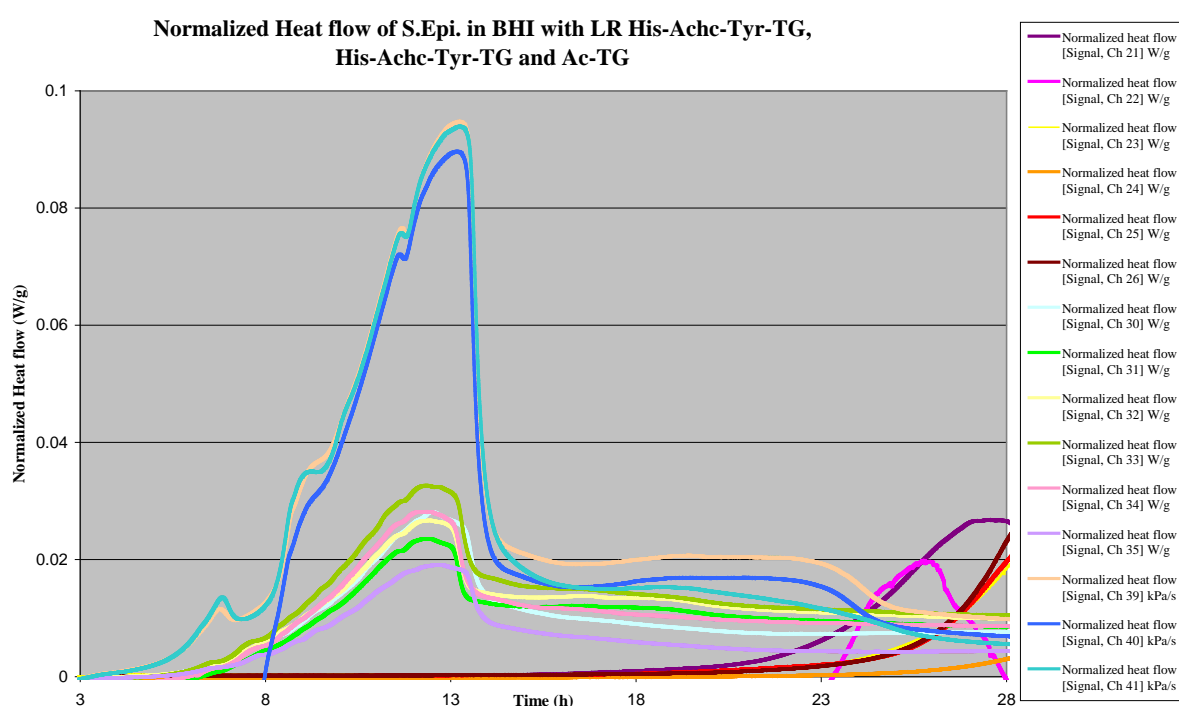
**Figure 3.3-7:** Normalized heat flow curves of bacterial growth of *S.epidermidis* in presence of AgNPs containing TG-beads

LR His-Achc-Tyr-TG: His-Achc-Tyr coupled TG beads complexed with  $\text{Ag}^+$ , AgNPs generation by light reduction

CR His-Achc-Tyr-TG: His-Achc-Tyr coupled TG beads complexed with  $\text{Ag}^+$ , AgNPs generation by chemical reduction

As it can be observed in **Fig.3.3-7**, the light reduced samples have a higher activity than the chemically reduced ones. This higher activity is probably due to the remaining, non-reduced silver ions present on the surface beside of AgNPs, since the reduction is not complete in the case of the LR. Due to the silver ions, the Ag release of these beads is higher and increases the antimicrobial effect.

To exclude the possibility that peptide coupled T-Gel beads and the not coupled, only acetylated T-Gel beads have some activity against bacteria, both were tested in comparison with the LR His-Achc-Tyr-TG. The normalized heat flow values in function of the time are presented on a **Fig.3.3-8**.



Channel	Compound
Ch 21	LR His-Achc-Tyr-TG
Ch 22	LR His-Achc-Tyr-TG
Ch 23	LR His-Achc-Tyr-TG
Ch 24	LR His-Achc-Tyr-TG
Ch 25	LR His-Achc-Tyr-TG
Ch 26	LR His-Achc-Tyr-TG
Ch 30	His-Achc-Tyr-TG
Ch 31	His-Achc-Tyr-TG
Ch 32	His-Achc-Tyr-TG
Ch 33	Ac-TG
Ch 34	Ac-TG
Ch 35	Ac-TG
Ch 39	<i>S.epidermidis</i> (x3)
Ch 40	<i>S.epidermidis</i> (x3)
Ch 41	<i>S.epidermidis</i> (x3)

**Figure 3.3-8:** Normalized heat flow curves of bacterial growth of *S.epidermidis* in a presence of AgNPs containing TG-beads

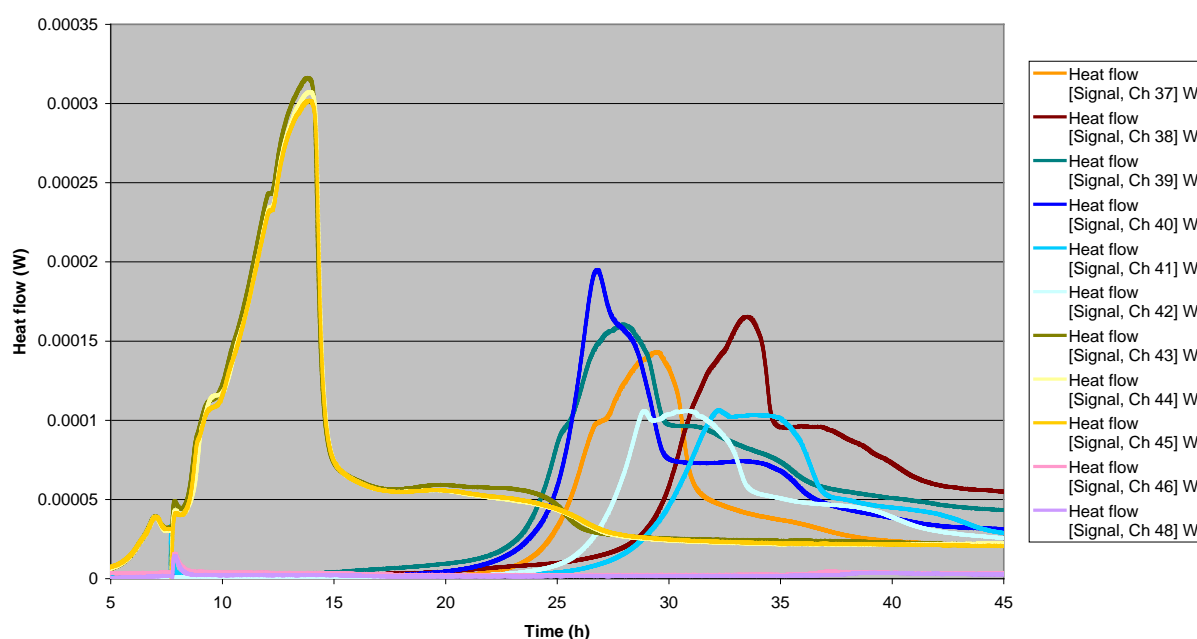
LR His-Achc-Tyr-TG: His-Achc-Tyr coupled TG beads complexed with Ag<sup>+</sup>, AgNPs generation by light reduction

His-Achc-Tyr-TG: His-Achc-Tyr coupled TG beads

Ac-TG: Acetylated TG beads

As the results show, none of the control samples has any antibacterial effect, the bacterial growth takes place at the same time even if acetylated or peptide coupled T-Gel beads are present in the bacterial suspension. This is in contrast with the LR His-Achc-Tyr-TG, which has a clear activity. Since this antibacterial effect depend on the concentration of the active substance (e.g. antibiotics), various quantities of the LR His-Achc-Tyr-TG were tested in parallel and the results are represented in a heat flow vs. time graph (F.3.3-9)

**Heat flow S.Epi. in BHI with LR His-Achc-Tyr-TG**



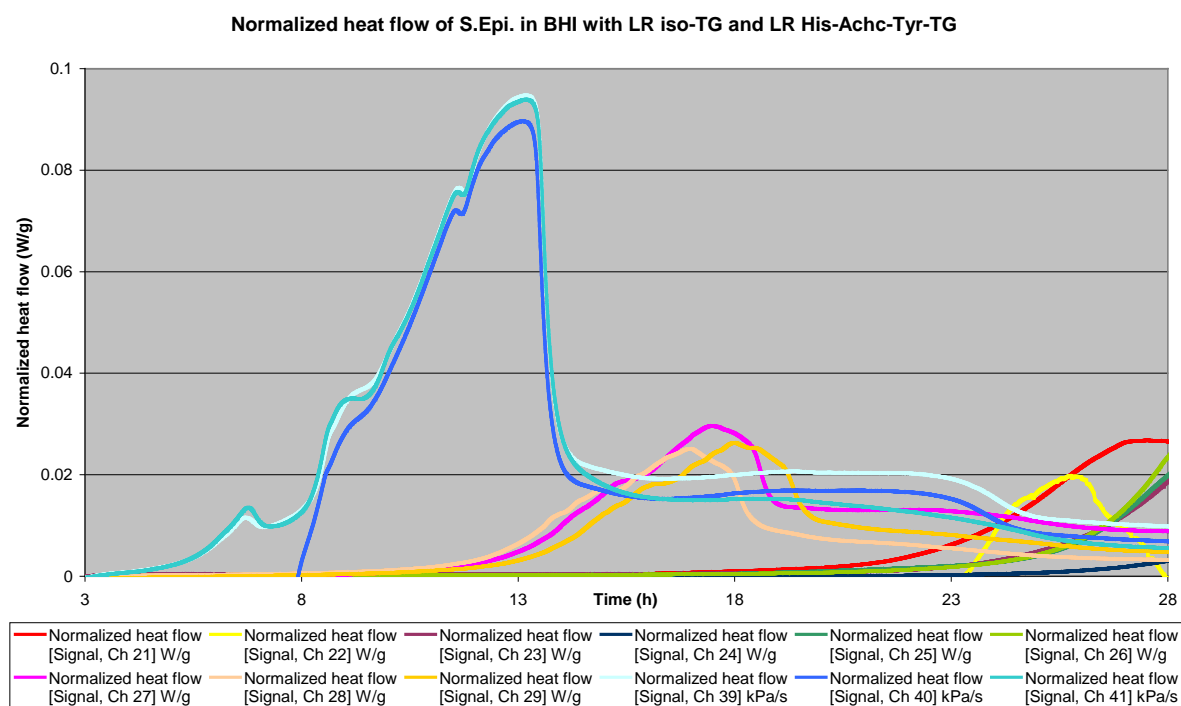
Channel	Compound
Ch 37	LR His-Achc-Tyr-TG, 4.8 mg
Ch 38	LR His-Achc-Tyr-TG, 4.6 mg
Ch39	LR His-Achc-Tyr-TG, 4.8 mg
Ch 40	LR His-Achc-Tyr-TG, 7.2 mg
Ch 41	LR His-Achc-Tyr-TG, 7.1 mg
Ch 42	LR His-Achc-Tyr-TG, 5.9 mg
Ch 43	<i>S.epidermidis</i>
Ch 44	<i>S.epidermidis</i>
Ch 45	<i>S.epidermidis</i>
Ch 46	BHI
Ch 48	BHI

**Figure 3.3-9:** Heat flow curves of bacterial growth of *S.epidermidis* in a presence of AgNPs containing TG-beads LR His-Achc-Tyr-TG: His-Achc-Tyr coupled TG beads complexed with Ag<sup>+</sup>, AgNPs generation by light reduction

Unfortunately, no relation could be found between the beads concentration (in the range of 4-7mg) and their activity against *S.epidermidis*. This surprising result is probably due to the inhomogeneity of the light reduced samples. Since the sample is not stirred during the irradiation, the AgNPs formation is inhomogeneous. AAS measurements revealed a high dispersion in the concentration of the silver ions versus the AgNPs on the surface after light

reduction. Hence, the silver ion concentration seems to be the main responsible for the antibacterial activity, and it can show a high variation on the surface.

The iso-TG has been tested in connection with the Ad17 attached on T-Gel surface, and it would be interesting to compare it with LR His-Achc-Tyr-TG, setting up a bridge between the two measurement series. The **Fig.3.3-10** presents the results of this comparing measurement.



Channel	Compound
Ch 21	LR His-Achc-Tyr-TG
Ch 22	LR His-Achc-Tyr-TG
Ch 23	LR His-Achc-Tyr-TG
Ch 24	LR His-Achc-Tyr-TG
Ch 25	LR His-Achc-Tyr-TG
Ch 26	LR His-Achc-Tyr-TG
Ch 27	LR iso-TG
Ch 28	LR iso-TG
Ch 29	LR iso-TG
Ch 39	<i>S.epidermidis</i> (x3)
Ch 40	<i>S.epidermidis</i> (x3)
Ch 41	<i>S.epidermidis</i> (x3)

**Figure 3.3-10:** Normalized heat flow curve of bacterial growth of *S.epidermidis* in a presence of AgNPs containing TG-beads

LR His-Achc-Tyr-TG: His-Achc-Tyr coupled TG beads complexed with  $Ag^+$ , AgNPs generation by light reduction

LR iso-TG: isonicotinic acid coupled TG beads complexed with  $Ag^+$ , AgNPs generation by light reduction

The light reduced His-Achc-Tyr-TG shows a higher effect to inhibit the bacterial growth than iso-TG prepared in the same way. The LR iso-TG delays the bacterial growth by ca 7h (the same time was determined for this sample during the previous measurements) contrary to the ca 15h delay caused by the LR His-Achc-Tyr-TG. The measured silver uptake is much higher

by the second peptide, which can explain this difference in the activity. The antibacterial effect of the LR His-Achc-Tyr-TG is comparable with the effect of the TG samples having Adl7 on the surface by crystallisation method. The loading of the latter is much higher regarding the silver concentration but there is a big difference in the form of the silver. In the case of the LR His-Achc-Tyr-TG peptide, induced AgNPs and Ag<sup>+</sup> can be found on the surface. The Adl7(cryst) on iso-TG contains only silver ions in the coordination polymer. Hence the determining factor for the antimicrobial activity seems to be the Ag<sup>+</sup> present in the reaction solution.

#### ***3.3.1.1.3 Conclusion of the IMC measurements***

The antimicrobial activity of different samples was tested using the microcalorimetric method. *S.epidermidis*, as the main responsible bacteria for the biofilm formation, was used in BHI medium. The free Adl7 as well as the surface attached compound show a good activity against these bacteria, contrary to the AgCl precipitate, which has a very weak effect. The AgNPs containing T-Gel beads show activity against bacteria only if there are some free silver ions, which can be found on the surface beside of the AgNPs. The silver release of the AgNPs as well as of the AgCl is so weak that it is not enough to show any antimicrobial effect. The antimicrobial activity is in a direct relation with the silver concentration in the reaction suspension, hence the silver release of the substance. These results are encouraging the further *in vitro* and *in vivo* microbiological testing of the coated substrates.

#### 3.3.1.2 *In vitro* microbiological assays: inhibition zone experiments

In the previous chapter, it has already been mentioned that the variety of the microbiological assays is large, and the most suitable testing method should be chosen especially for the defined sample. In the case of the insoluble Adl7 compound and the T-Gel beads, the inhibition zone assays seemed to be suitable. To test the antimicrobial effect of the coated substrates, another, less specific method is needed. As the susceptibility of the antibiotics is often tested by the classical plating method, this method seems to be appropriate for our purpose as well. Using this technique, several bacterial strains in different concentrations can be used and a large number of samples can be screened. It gives the opportunity to test sample series on the different substrates offering the same conditions. A large screening of the coated samples, prepared in different conditions (treating time, treating concentration) was done. Several bacterial strains were used, e.g. gram+ and gram- bacteria, different strains of *S.epidermidis* etc.

##### 3.3.1.2.1 *General description*

Many methods were developed to test bacterial cells, yeast cells and antibiotics. The plating method is one of them and it is generally used in microbiology. This technique is suitable to determine the presence of different bacterial strains in a sample, to count these bacteria or colonize them. It is also often used to determine the concentration of an active substance where this inhibits the bacterial growth.

An agar plate is a sterile Petri dish that contains a growth medium: typically agar plus especially developed nutrients, used to culture microorganisms. Not only the composition of the nutrients is destined to the target microorganism but selective growth compounds may also be added to the media, such as antibiotics.[126] Individual microorganisms/bacteria placed on the plate will grow into individual colonies. A bacterial colony is defined as a cluster of organisms growing on or within a solid medium, which is cultured from a single cell. The participants of the colony are genetically identical to the individual starting organism (except for the unavoidable, generally low rate of mutation,). The growth of the colony is depending on the nutrient and the environmental circumstances. Like other growth media, the compositions of agar used in plates may be classified as either defined or undefined. The defined medium is being synthesized from the individual chemicals as required by the organism so that the exact molecular composition is known, as e.g. the synthetic medium (SM) used and described for the dissolution tests. The undefined medium is made up from natural products such as beef infusion, where the precise composition is unknown.

Agar plates may be formulated as either permissive, allowing the growth of all present bacteria, or restrictive or selective, with the purpose to allow the growth of a particular participant of the present organisms. This correlates to some degree with defined and undefined media. Undefined media are made from natural products and contain an unknown combination of organic molecules. These are typically more permissive than the defined media in terms of serving the needs of a wider variety of microorganisms. Defined media can be precisely designed, to determine organisms with very specific properties.

Müller-Hinton agar is a microbiological growth medium that is commonly used for antibiotic susceptibility testing. It typically contains [127]:

Conc. (g/l)	Composant	
2	beef infusion	pH adjusted to neutral at 25°C. *when susceptibility testing is done on Streptococcus species
17.5	acid digest of casein	
0.15	starch	
17	agar	
50	sheep blood*	

In the case of Adl7 coated substrates, the assays take place on permissive agar plates where the inhibition of the bacterial growth around the substrates is measured. The agar plates are prepared using 15ml liquid MHA agar (or SM agar in the case of AgNO<sub>3</sub> solution and the bacterial count of adherent and planktonic bacteria), cooled to a temperature of approximately 50°C, which is mixed with different concentrated bacterial suspensions. The aimed bacterial concentrations are 10<sup>4</sup>, 10<sup>6</sup> and 10<sup>7</sup> CFU/ml (CFU: colony-forming unit, this is a measure of viable bacterial numbers, which allows to know the bacterial load). This 15ml mixture is layered on a Petri dish, the coated or uncoated samples are placed into the middle of the suspension, under the agar and the plate is covered. The plates are incubated for 24h at 37°C. Then, the inhibition zone around the samples is measured. The bacteria present in the medium begin their multiplication thanks to the nutrients and the appropriate temperature. Where a substance, which blocks the bacterial multiplication, is present, no bacterial growth can be observed. In this area, the agar suspension remains clear contrary to where the bacterial growth takes place, and the suspension becomes turbid. The area of the inhibition becomes visible and easy to measure. The **Fig.3.3-11** shows the principle of the technique:



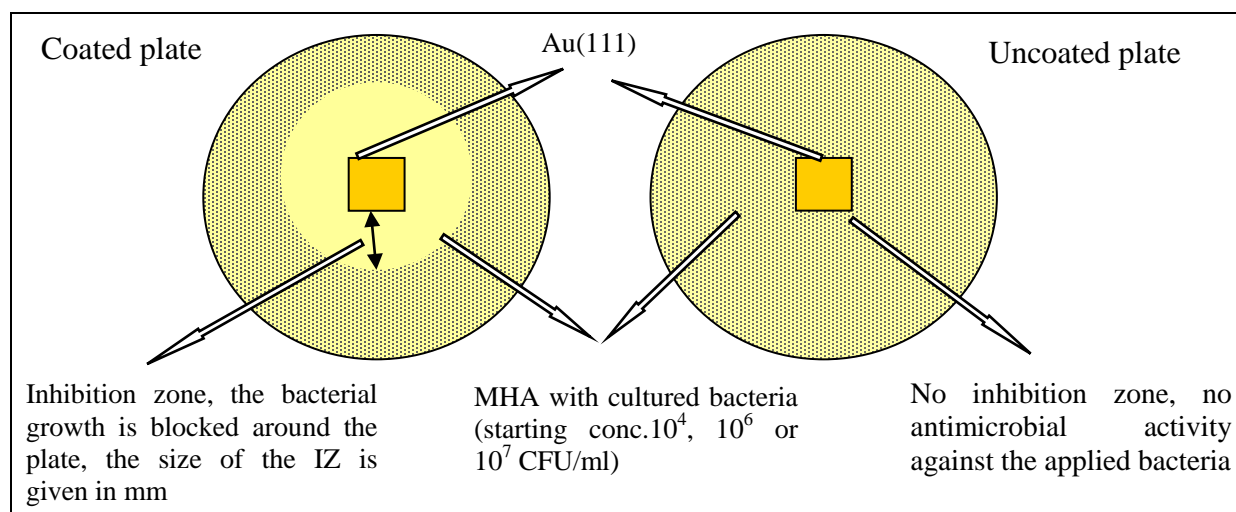


**Figure 3.3-11:** Scheme of the plating experiment, around the coated plate an inhibition zone can be observed where the bacterial growth is inhibited.

The inhibition zone around the plate was measured and the results of the different coated substrates were compared. During the assays, several bacterial strains were tested.

The *Staphylococcus* strains: *S.epidermidis*, *S.aureus*. These bacteria are mainly responsible for the biofilm formation and the post operative infections of the implants. *Staphylococcus* is a genus of Gram-positive bacteria. Under the microscope, they appear round and form in grape-like clusters contrary to *streptococcus* forming linear clusters. The *Staphylococcus* genus includes just thirty-three species. [128] Most are harmless and can be found normally on the skin and mucous membranes of humans and other organisms. Although, *S.epidermidis* is usually non-pathogenic, patients with a weak immune system are often at risk for developing infections. These infections can be both nosocomial (from hospitals) and community acquired, but they are more prevalent in hospital patients. *S.epidermidis* is also a major trouble for people with catheters or other surgical implants because it is known to cause biofilms that grow on these devices causing infections. [129] The capability to form biofilms on implanted devices is a major virulence factor for *S.epidermidis*. The capsule of the surface proteins (binding blood and extra cellular matrix proteins together) known as polysaccharide intercellular adhesion (PIA), is made up of sulfonated polysaccharide and allows other bacteria to bind to the already existing biofilm, creating a multilayer biofilm. The biofilm of *staphylococci* is mainly composed of polysaccharide intercellular adhesin (PIA), whose biosynthesis is encoded by four *ica* genes [130]. Currently, *ica* is considered to be the main responsible for staphylococcal biofilm. Rupp et al. have shown, in a catheter model, that biofilm-negative (*ica*) *staphylococci* are less virulent than isogenic wild-type (WT), *ica*-positive strains. [131]. Landman et al tested the susceptibility of titanium and steel implant

materials to WT and ica- *S. aureus* and *S.epidermidis*. They measured the minimal infective dose and the number of planktonic and adherent bacteria *in vitro* and *in vivo* on the devices. [108] This study revealed that the presence of ica genes had a strong effect on biofilm *in vitro* and a weak effect *in vivo*. The bacterial adhesion and multilayer clustering on titanium and stainless steel was affected strongly by biofilm *in vitro* and weakly *in vivo*. The implant material has just a weak effect on biofilm formation. Both WT strains, but not ica- strains, showed multilayered biofilm formation. *S.epidermidis*, despite its known stronger ica RNA expression and PIA production than the *S.aureus* [131], produced just slightly higher CFU numbers of planktonic and adherent bacteria after injection with WT (ica+) than with ica- bacteria. The effect of the ica genes was only weakly visible in *S. aureus* infection. The biofilm formation doesn't play an exclusive role in the implant-associated infections. *S. aureus* caused a persistent infection only with a very small number of bacteria, which was independent of biofilm formation. In contrast, *S.epidermidis* caused an infection only if a considerable bacterial load was introduced during surgery so that a multilayered biofilm could be formed.

As the importance of the ica genes is not negligible in biofilm formation and thus in infection, our experiments were made with both ica- and WT strains of *S.epidermidis* and *S.aureus*. Beside of these Gram-positive bacteria one Gram-negative strain *E.Coli* was also tested. Most *E. coli* strains are harmless and part of the normal human intestinal flora. The bacteria can be grown easily and its genetics are relatively simple and easily manipulated, hence it is the best-studied, prokaryotic model organisms. These characteristics and because it is a Gram-negative strain makes it a good test bacteria for our aim.

Some complementary experiences were also carried out to determine the adherent and planktonic bacteria on and above the treated implant materials. In this assay the different substrates were incubated for 4 h in a determined concentration bacterial solution in SM. Then the sample is removed, and the bacteria present in the solution are counted as well as the bacteria adhered on the surface (by removing the attached bacteria by sonication from the surface).

The assays were carried out first using AgNO<sub>3</sub> solution. To determine the most appropriate sample preparation method and find out the best loading regarding the antimicrobial activity of Adl7 on the different substrates, several experiments were done. After the evaluation of the results of the method development, more assays were done with the most active samples. Since the diversity of the substrates, Au(111) plates, Ti disks and cylinders with two roughnesses, stainless steel disks and cylinders with two roughnesses would result in a high

repetition number, these assays were focused on the Au(111) substrate, as model surface, and Ti rough disks, because it is the same material as the Ti cages used for the *in vivo* experiments.

The microbiological assays are completed by chemical measurements to determine the silver concentration in the inhibition zone in order to assess the antimicrobial effect of the silver.

### 3.3.1.2.2 Preliminary $\text{AgNO}_3$ assays

As previously described, the *ica* genes have a main role in the biofilm formation, and so the isogenic biofilm negative strains ( $\Delta\text{ica}$ ) and the WT of both bacteria were tested. Different concentrations of  $\text{AgNO}_3$  solution in EtOH were tested. The concentrations of the solutions were 200, 100, 10, 5 and 2,5  $\mu\text{g/ml}$  for  $\text{AgNO}_3$  (127, 63, 6,3, 3,2 and 1,6  $\mu\text{g/ml}$  respectively of silver). The results of the measurements are shown in **Fig.3.3-12-13**.

**Figure 3.3-12a:** Silver inhibited growth of *S.epidermidis* (strains1457; WT and *ica*) **b:** Silver inhibited growth of *S.epidermidis* (strains 047 Wt and *ica*), three bacterial concentration were used:  $10^4$ ,  $10^6$  and  $10^7$  CFU/ml

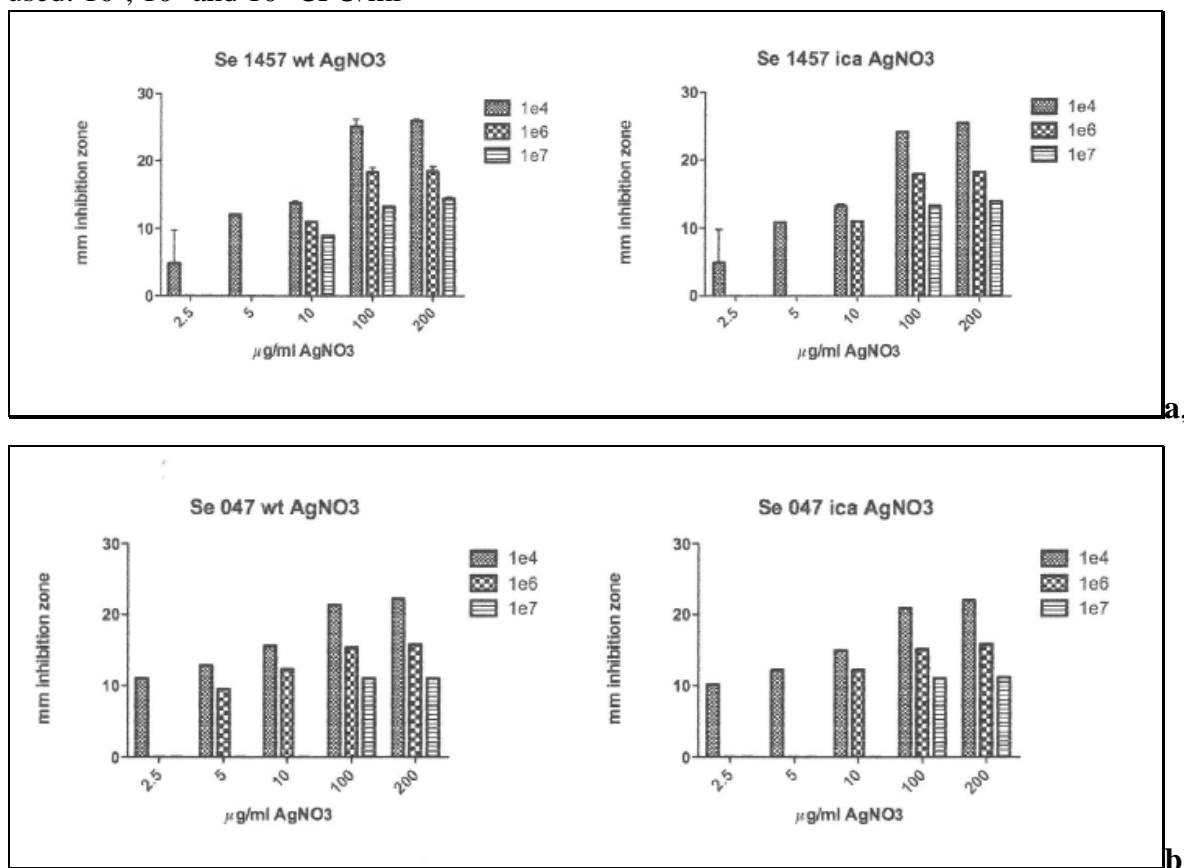
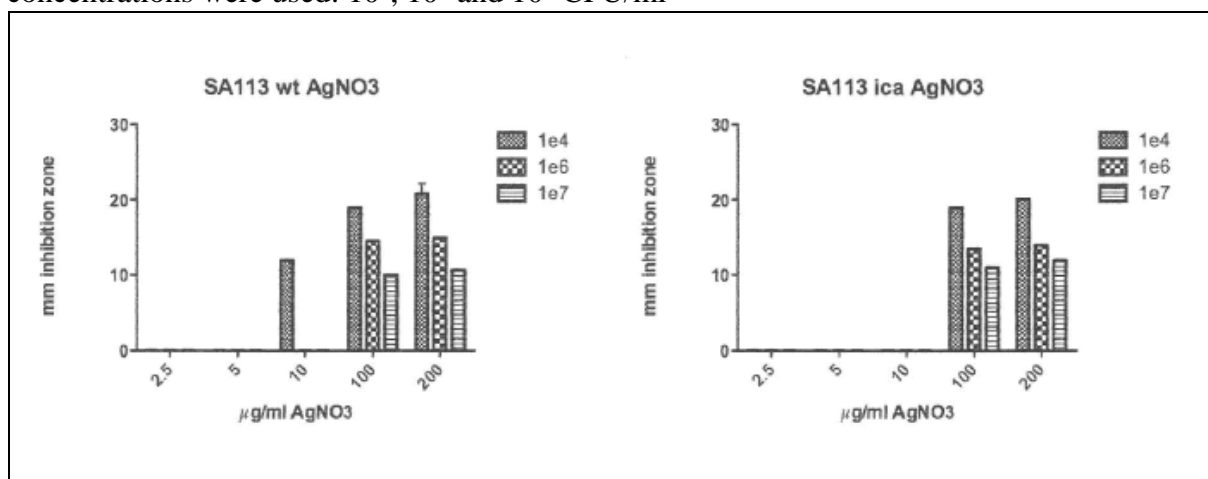


**Figure 3.3-13:** Silver inhibited growth of *S.aureus* (strain 113; WT and ica), three bacterial concentrations were used:  $10^4$ ,  $10^6$  and  $10^7$  CFU/ml



In figures **Fig.3.3-12,13**, it can be observed that the silver has a higher activity on *S.epidermidis* than on *S.aureus*. In the case of *S.epidermidis*, the 2,5 µg/ml concentration of AgNO<sub>3</sub> solution inhibits the bacterial growth, while *S.aureus* is not sensitive to this concentration, but only as of 10 µg/ml AgNO<sub>3</sub> concentration. For both bacterial strains, no significant difference can be observed between the WT and ica bacterial strains. This observation points out that the silver is efficient against bacteria ready to generate biofilm and against bacteria that do not build up biofilms. Hence, the protective biofilm formation, which hinders the efficiency of certain antibiotics against biofilms, does not appear in the case of silver. Concerning the silver concentration in the solutions the, 1,6 µg/ml silver corresponds to 1,6 ppm silver (this unit is used by the AAS measurements to determine the silver concentration in solution). If this value is compared with the silver release values measured previously during the dissolution tests: the 1mM/3d treated samples (Au(111),TiR,TiS) release silver in the same concentration region: 0,7-1,8 ppm in MHB solution without bacterial suspension. The 2mM/3d treated samples reach the active silver concentration against *S.aureus* (4,1-6,4 ppm) in MHB. These results encouraged us to do further experiments on the coated substrates.

### 3.3.1.2.3 Microbiological assays on Au(111) substrate

During the surface characterisation, the coated Au(111) plates were used as model substrate. After the complete chemical and topographic analysis of the coated gold surfaces, it is important to test their antimicrobial activity. Although, gold is not used as restorative implant material (some gold containing material is used in dental applications), testing the activity of the coating serves as important information and can be extrapolated to other materials. Some

preliminary assays were done on Au(111) plates and the 1mM concentration has been chosen. Then, time-dependent screening was done for the disulfide pre-treated and not pre-treated 1mM samples. The results of the assays are shown in **Fig.3.3-14**.

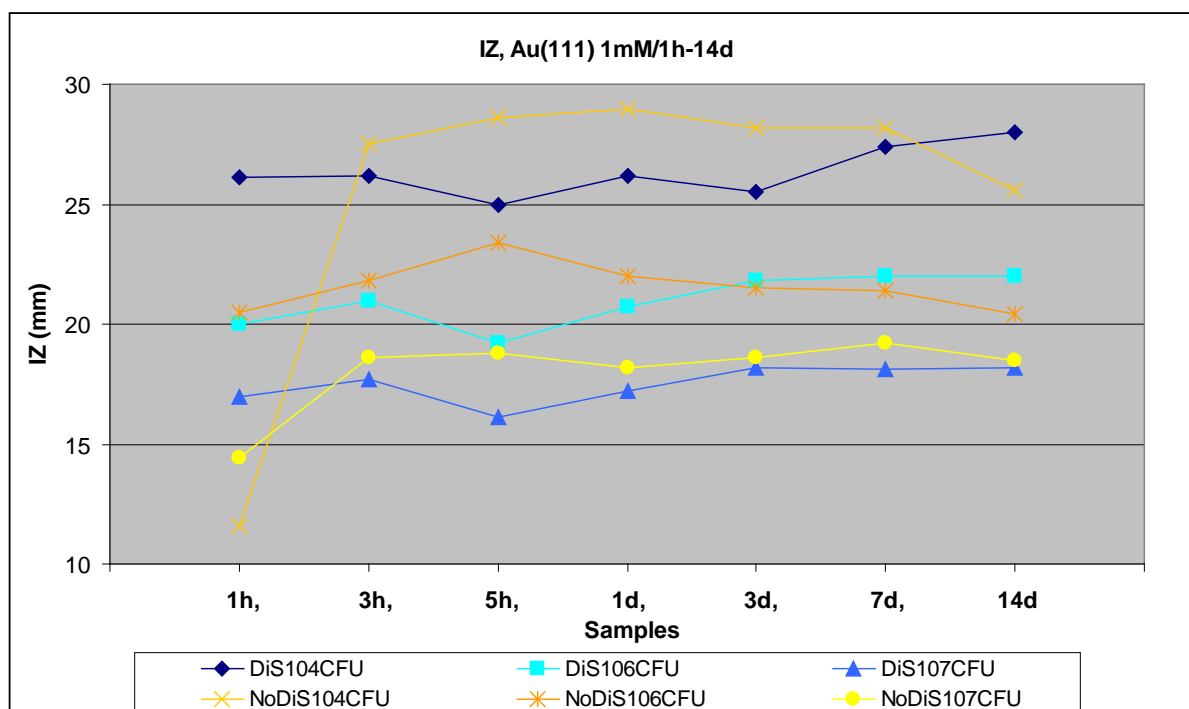


**Figure 3.3-14:** Inhibition zone as a function of the treating time of the coated plates (pre-treated: Dis, and without pre-treatment: NoDis) using three different bacterial concentration,  $10^4$ ,  $10^6$  and  $10^7$  CFU/ml

It is interesting to observe on the graphic that the inhibition zone around the gold plate does not change dramatically with the time of the coating treatment. In the case of the disulfide pre-treated samples, the curve generally ascends slightly and the slope slows down at around 3 days. In contrast, the not pre-treated samples seem to have less activity after 14 days of treatment than the 7 days samples. Not only the form of the curve is different for the two sample preparation methods but also the inhibition zones are generally larger in the case of the not pre-treated samples, except for the descending part of the curve. A probable explication of this difference can be that the absence of the anchor molecule makes the coating easier to release the silver, yet at the same time it becomes less stable. Thus, with a very high loading, the coating loosens and has a weaker effect. Thus, the stable coating (with anchor molecule) results in a more homogeneous silver release. To understand the method of action of these coatings better, the silver concentrations in the inhibition zone were determined by AAS measurements. During the sample preparation the dissolved agar was split in two, one part was filtered, removing the bacteria, and the other part was measured without any filtering. The results of the measurements are shown in the three graphics of **Fig.3.3-15**.

### 3 Results and discussion

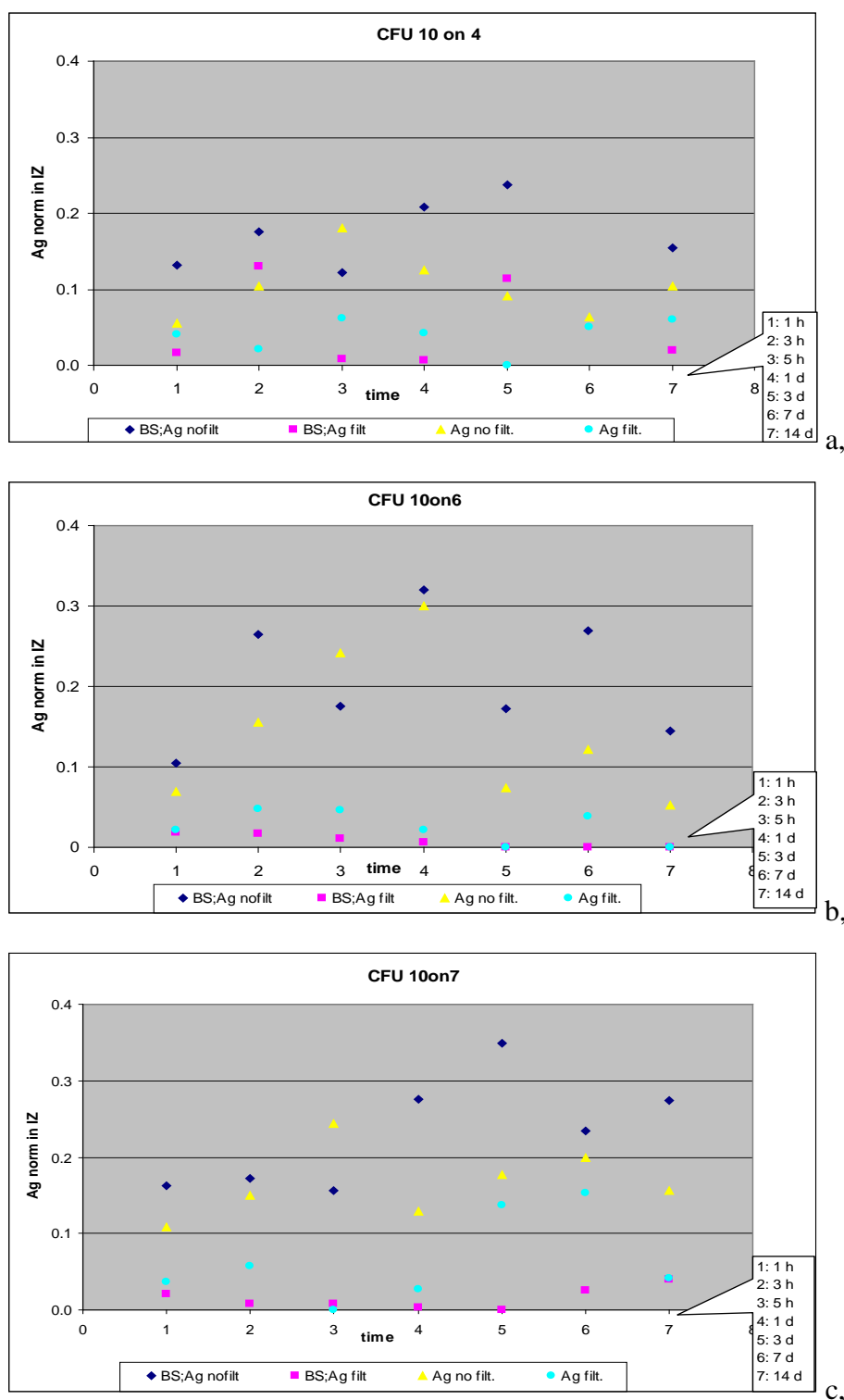


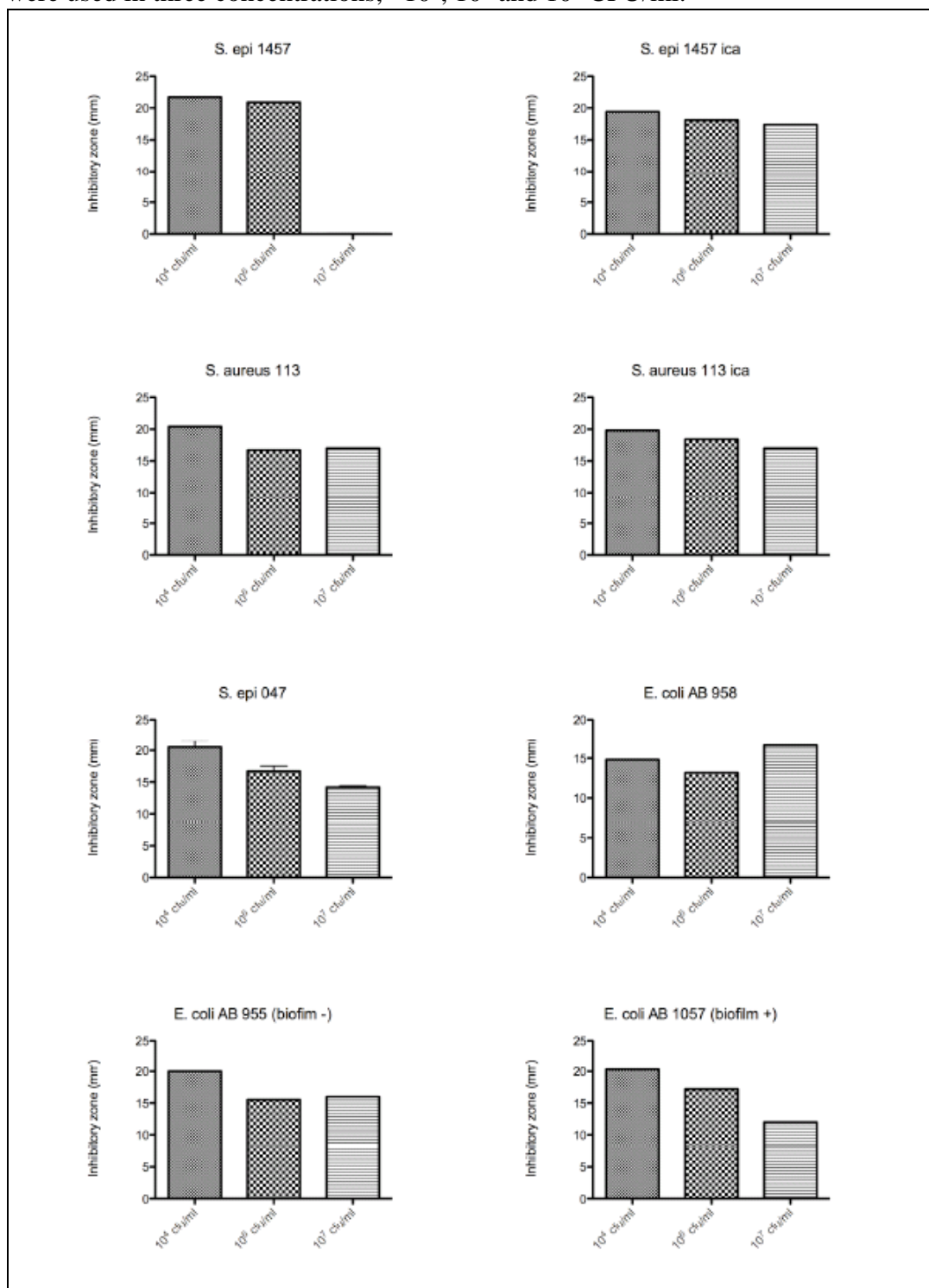
**Figure 3.3-15:** Silver concentration in the inhibition zone as function of the treating time of the plates, measured for filtered and unfiltered solutions. The plates were treated with two methods, with (BS) and without pre-treatment. Three bacterial concentrations were used  $10^4$  (a),  $10^6$  (b) and  $10^7$  (c) CFU/ml.

Some principal observations can be made from the graphs. Generally the filtered samples contain much less silver than the respective unfiltered samples. (The silver concentration of filtered samples is often around the detection limit of the AAS.) In the filtered samples, the bacteria and particles larger than  $40\mu\text{m}$  are removed, so that only the ionic silver and/or its

small complexes are present. In the unfiltered samples, all of the silver containing residues are present and measured. The variation of the filtered and unfiltered samples is coming from the  $\geq 22 \mu\text{m}$  silver containing material. Principally, the silver ions seem to attach to the bacteria since only the inhibition zone was removed and the Ag concentration measured. The fact, that for the  $10^4$  CFU/ml bacterial concentrations, the samples contain less silver in the inhibition zone than the samples of the two higher concentrations, confirms that the major part of the silver is bacterial attached silver. Another general remark can be made regarding the samples with different coating methods. Analysing the silver concentration of the filtered samples, the pre-treated samples show less silver in the inhibition zone. Since the value of the filtered samples is representative of the ionic silver, the samples without any anchor molecule release more ionic silver than the samples having a well attached coating. Although the loading of the gold plates varies between 2 and 60 ng Ag/plate, the silver concentration in the inhibition zone is maximal 0,4 ng. That means that the silver release is controlled by the solubility of the compound in the medium and only slightly influenced by the bacterial concentration.

After these successful assays with *S.epidermidis*, other bacterial strains were tested, such as the biofilm negative and positive strains of the gram positive *S.epidermidis* and *S.aureus* and the gram negative *E.Coli*. The coating of the gold plates was made as follows: after the disulfide pre-treatment, the crystallisation was made in 1mM Adl7 solution for 3h. The results of the agar plate experiments are shown in **Fig.3.3-16**.

**Figure 3.3-16:** Inhibition zones around the coated Au(111) plate (1mM AdI7 treated for 3h). *S.epidermidis*, WT and ica, *S.aureus*, WT and ica, *E.Coli*, biofilm + and – bacterial strains were used in three concentrations,  $10^4$ ,  $10^6$  and  $10^7$  CFU/ml.



Although all the used bacterial strains are susceptible to the silver coating, the gram positive bacteria show slightly larger inhibition zones around the coated plates than the gram negative *E.Coli*, but the difference is not significant. The same minor difference is present between the behaviour of the WT and the ica negative strains of the same type of bacteria towards the silver. The silver coordination polymer coating seems to be equally active on biofilm



producing bacterial strain (WT) and ica type strains. This is true for the *S.epidermidis*, known for having a more pronounced biofilm forming ability. The same observation was made previously for the AgNO<sub>3</sub> experiments. It means that the Adl7 released silver ions are behaving the same way and having the same antimicrobial activity as the silver ions of a soluble salt. It is a big benefit that our Adl7 coating releases silver ions at a determined level while it does not load the organism with a too high concentration of heavy metal.

#### ***3.3.1.2.4 Microbiological assays on coated titanium and stainless steel implant material***

The Au(111) substrates were used as a model surface and give good results, encouraging further assays on other implant materials. The titanium and stainless steel restorative implant materials were described previously and the coatings on these substrates were characterized. The aim of the microbiological assays is to choose the most active coating against bacteria. Similar methods (classical plating method and adhesive and planktonic bacterial count) are used to test the antimicrobial effect of the coating as previously shown. First, several treatment methods were tested to choose the direction of the further experiments. Then, the method development was fine tuned: the time of the treatment is determined. Further experiments with different bacterial strains are planned to confirm the results of the gold plate experiments.

The different treatment methods were tested against *S.epidermidis* and the inhibition zone experiments are shown in the **Fig.3.3-17**. The M1 and M2 samples were pre-treated with isonicotinic acid solution (5mM) for 3 and 8 days respectively, then the crystallisation was done on the surface from 2mM [Ag(L1)NO<sub>3</sub>] solution during 10 days for the M1 samples and from 1mM [Ag(L1)NO<sub>3</sub>] solution during 20 days for the M2 samples. The M5 samples were prepared the same way as M2 but the pretreating was done with pyridine-4-boronic acid instead of the isonicotinic acid. The simplest preparation method was M4, where the coatings were made by *in-situ* crystallisation from 2mM [Ag(L1)NO<sub>3</sub>] solution during 14 days.

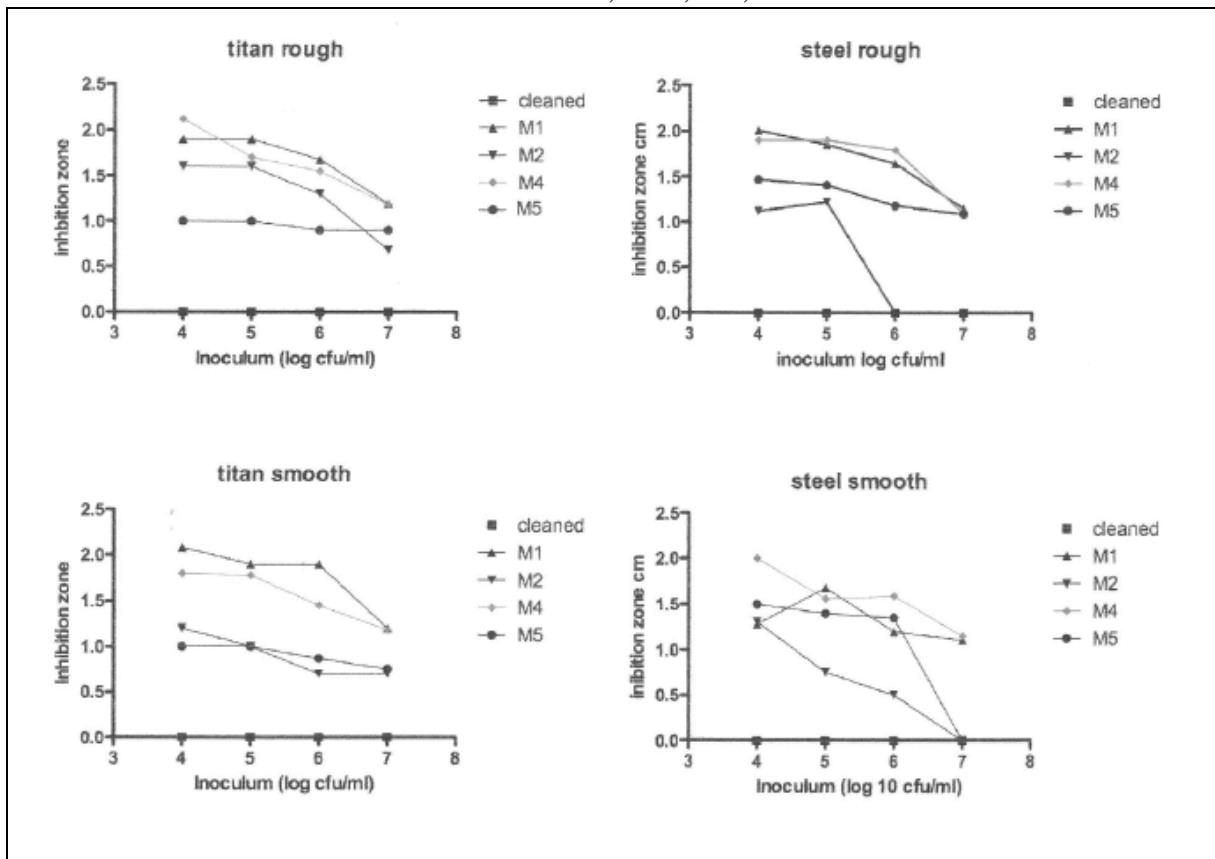
The samples are

---

M1:	Isonic. acid 5mM/3d + Ladl/AgNO <sub>3</sub> 2mM/10d
M2:	Isonic. acid 5mM/8d + Ladl/AgNO <sub>3</sub> 1mM/20 days
M4:	Ladl/AgNO <sub>3</sub> cryst, 2 mM/14d
M5:	Pyridine-4-boronic acid 5mM/8 days+ Ladl/AgNO <sub>3</sub> 1 mM/20 days

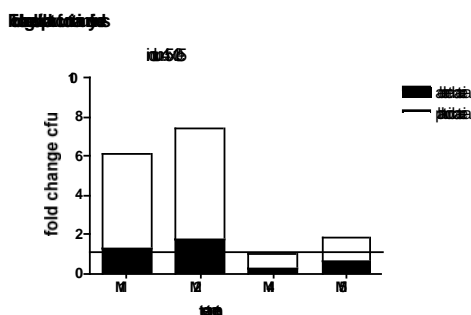
---

**Figure 3.3-17:** Inhibition zones around the different coated Au(111) plate. *S.epidermidis* bacterial strain was used in four concentrations,  $10^4$ ,  $10^5$ ,  $10^6$  and  $10^7$  CFU/ml.



The inhibition zone experiments show that M1 and M4 demonstrate the best activity against *S.epidermidis*. The concentration of the treating solution seems to be clearly the key factor; hence the loading of the surface determines the antimicrobial activity. Although the plating method doesn't show a difference between the samples prepared with these two methods, the bacterial count assays (the bacterial CFU of the *S.epidermidis* is determined after infection and incubation on the surface, adherent bacteria, and in the bacterial suspension, planktonic bacteria) showed a significant difference. In **Fig.3.3-18** just one example is shown:

**CFU linear change**



**CFU log change**

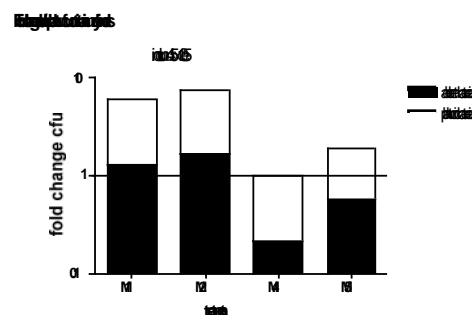


**Figure 3.3-18:** Planktonik and adherent bacterial number around and on the different coated Au(111) plates. *S.epidermidis* bacterial strain was used in  $4.5 \times 10^5$  CFU/ml

### 3 Results and discussion

The M4 shows a clear advantage over the M1, in not only keeping the surface clean of bacteria but also blocking the bacterial growth in the solution. This experiment definitely favours the M4 sample preparation method. This is an interesting observation because it contradicts the expected result, namely that the sample preparation method using an anchor molecule results in a more stable coating than without anchor molecule. Interestingly, there is also no difference between the 1mM (M2) or 2mM (M1) treated samples regarding the bacterial count. To find the optimum sample preparation, all the results were taken into consideration and the M4 designed as the best method. Now that the treatment method was fixed, the 2mM complex solution was used to crystallize the AdI7 compound on different substrate surfaces (TiS, TiR, StPol, StR) during various time intervals: between 3 hours to 10 days. Examples of the inhibition zone experiments of these samples are shown in **Fig.3.3-19**.

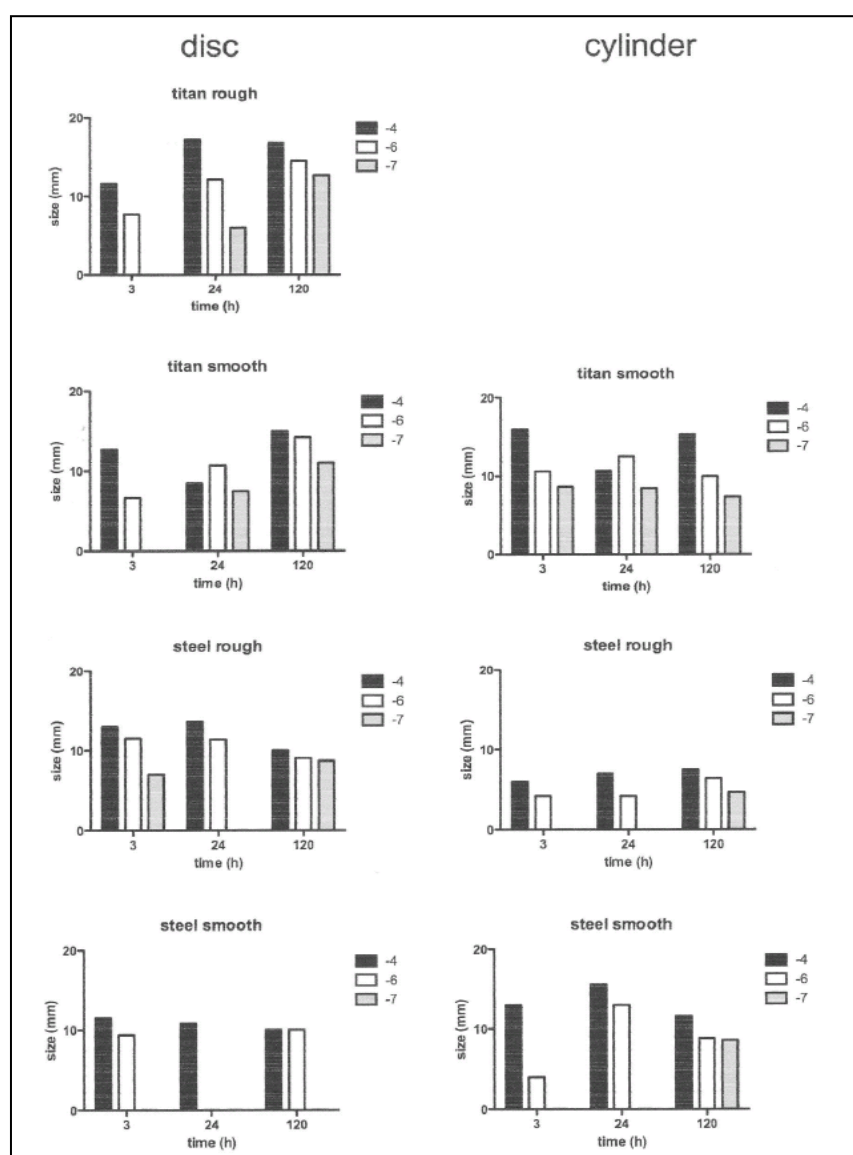


**Figure 3.3-19:** Inhibition zones around the different coated titanium and steel discs and cylinders. The substrates were coated with  $[Ag(L1)NO_3]$  for 3h to 10days. *S.epidermidis* bacterial strain was used in three concentrations,  $10^4$ ,  $10^6$  and  $10^7$  CFU/ml.

On titanium, increased inhibition of *S.epidermidis* growth can be observed with prolonged crystallization. On steel, smaller inhibition zones were observed than on titanium, and there is no enhancement of the growth inhibition with increased crystallization time. Comparing the different surfaces, the coated rough Ti samples have a slightly higher effect than the smooth samples and the same is true for the steel rough disks versus the smooth disks. The contrary is true for the steel cylinders. There is a significant difference between the bacterial growth inhibition of the titanium samples and the steel samples. Generally the coated titanium has much higher effect than the coated steel samples. If the loading of these samples are recalled, this is not surprising as the loading of the titanium samples are almost the double than of the steel sample. Although the loading of the smooth samples is slightly higher than the loading of the rough samples, the antimicrobial effect does not reflect this difference. Here, probably the stability of the coating (higher by the rough samples than by the smooth samples) plays a determining role. The cylinders show the different results and can not be interpreted because the form of the samples hinder the homogenous crystallization, hence a homogenous coating on the surface. Further experiments will be done on treated titanium disks samples with different bacterial strains to confirm the coating efficiency on the titanium surface.

#### ***3.3.1.2.5 Conclusions on in vitro inhibition zone experiments***

The classical plating technique was used to test the antimicrobial activity of the silver coatings. AgNO<sub>3</sub> solution was used for preliminary tests. As model surface, the Au(111) plates were tested in different conditions and several bacterial strains were used. The silver coating is efficient against all of the used bacterial strains (*S.epidermidis*, *S.aureus*, *E.Coli*). Biofilm positive and biofilm negative strains were compared. In the case of the *S.epidermidis* the silver coating has a slightly higher activity against the biofilm positive (wild type) strains, while by the *S.aureus* the difference is minor. Generally, there is no significant difference between the efficiency of the coating against biofilm positive and negative strains. Regarding the silver concentration in the inhibition zone of the bacterial growth, the silver concentration is increasing with the bacterial CFU of the agar. The silver concentration of the filtered samples does not show this tendency, hence the major part of the silver is attached to bacteria. The coatings, which used anchor molecules to fix the Ad17 crystalline layer, release less ionic (not bacterial attached) silver. For real restorative implant materials, titanium and stainless steel, the sample preparation method was optimized and the most efficient coating method was determined. The importance of the loading is proven. The more silver is present on the

surface, the larger the inhibition zone around the substrates. This effect is not visible in the bacterial count of the adherent and planktonic bacteria. Here, the quality rather than the silver concentration of the loading plays the major role in the antimicrobial activity. Taking into consideration all the results the sample preparation method was fixed for the further *in vitro* and *in vivo* experiments. The material and the surface of the titanium cages used for the *in vivo* experiments are identical to the titanium disks/cylinders of the *in vitro* experiments.

#### 3.3.1.3 Flow chamber experiments

Flow chamber experiments are a generally used method in oral microbiology for the study of dental plaque formation. All of these experiments were carried out in a close collaboration with Prof. Jürg Meyer and Dr. Irmgard Hauser-Gerspach (Institute of Preventive Dentistry and Oral Microbiology, University of Basel)

Adhesion, colonization and growth of oral bacteria on tooth surfaces lead to the oral biofilm, called dental plaque [132]. Depending on the composition of the plaque, it can be the cause of dental caries and periodontal diseases [133]. The first step of the oral biofilm formation is the same as for the biofilm formation namely bacterial adhesion. The early bacterial adhesion may determine the later plaque composition [134]. *Streptococcus sanguinis* is one of the early colonizers on exposed tooth surfaces and dental materials [135]. Thus this species was used during the flow chamber experiments. The first adhered bacteria are of great importance in the subsequent stages of dental plaque formation, determining sites for attachment, or modifying the environment for the further colonizers. Plaque is not only present on natural teeth but also on the surface of the dental restorative materials and other implant components. Adhesion of *S. sanguinis* to human enamel, glass slides and commonly-used dental restorative materials has been observed *in vitro* during one hour in a flow chamber [136]. In this study, the bacterial adhesion was observed as an isolated process. Further IMC measurements were carried out to describe the bacterial adhesion process on glass surfaces [137]. Other flow chamber experiments were done to study several orthodontic bonding materials. The biofilm formation initial step, the bacterial adhesion, was tested on these materials and the efficiency of their antimicrobial treatment was studied in parallel flow chambers [138].

The experiments take place in a flow chamber where 4 plates can be measured at the same time. The treated samples are always measured in parallel with an untreated sample from the same substrate and a glass plate as a blank. The scheme of the flow chamber is presented in **Fig.3.3-20**.

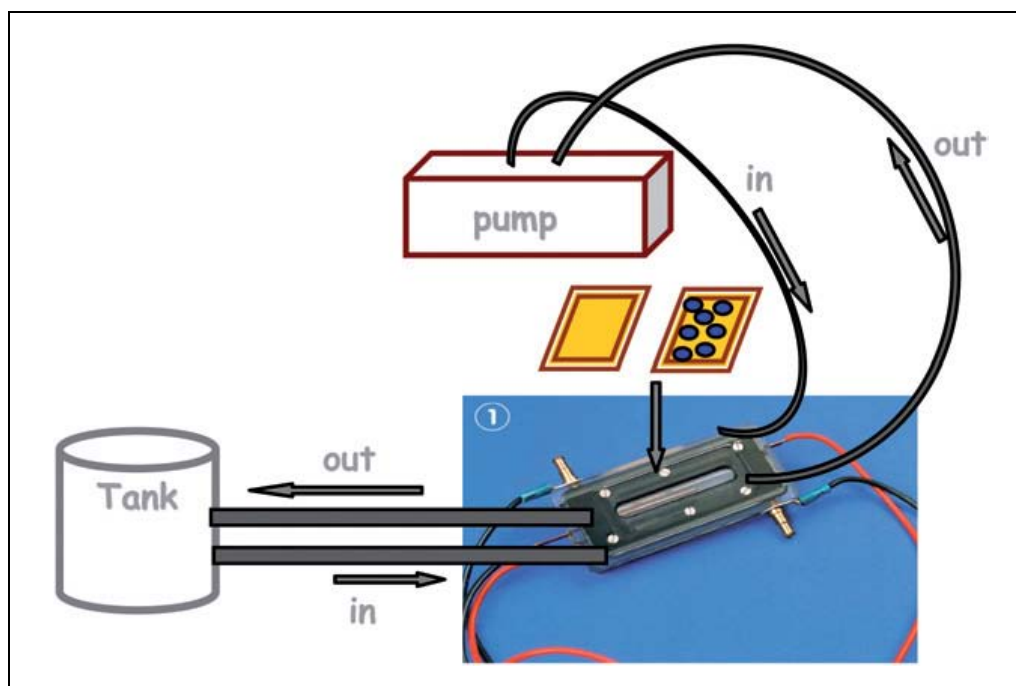


**Figure 3.3-20:** Scheme of the flow chamber experiment

This flow chamber is suitable for anti-microbial testing on dental materials [139]. In a reservoir (Tank), a single bacterial strain, *Streptococcus sanguinis* DSM 20068 (German Collection of Microorganisms and Tissue Culture Cells, Braunschweig, Germany), suspended in sterilized human saliva, collected from volunteers, was added. The saliva collection and treatment is made as described previously [142]. The treated samples, together with non-treated blanks, were exposed during 60 min at room temperature to a flow rate of the bacteria saliva suspension of 0.8 ml/min, which corresponds roughly to physiological oral conditions of low shear [143]. The flow is maintained by the pump and the system is placed on a shaker adjusted to 260 impulses/min in order to maintain the homogeneity of the bacterial suspension.[144] Thereafter, the plates, treated and untreated equally, are removed and analyzed microscopically. The vitality of adhered bacteria is evaluated by applying a dual fluorescent staining (Live/Dead BacLight Bacterial Viability Kit; MoBiTec, Lucerne, Switzerland) according to Decker et al., [145,146] which allows differentiation between vital and dead bacterial cells. The tested plates are removed from the flow chamber and carefully dipped into distilled water in order to eliminate planktonic and loosely attached cells and the detached compound from the surface. After rinsing the plates, they are covered with 7.5 ml of staining solution for 15 min at room temperature in the dark in order to colour the bacteria attached on the surface. The cells were analyzed by epifluorescence microscopy (PROVIS AX70, Olympus AG, Volketswil, Switzerland). A total of twelve digital images (ColorView, Olympus AG, Volketswil, Switzerland) using two filters [blue excitation at 450–490 nm

(FITC) and green excitation at 546 nm (rhodamine)] are obtained for each sample and the percentage of dead adherent cells are calculated.

To find out how the anti-bacterial activity of the Ad17 treatment on the dental restorative materials changes with the treatment method, several different treatment conditions were tested. The treated plates were placed into the flow chamber, then the results were evaluated and the best conditions found. The best treatment method for the gold plate is a 14 days crystallisation in a 2mM [Ag(L1)]NO<sub>3</sub> in THF/EtOH (1/1) solution. The titanium plates are pre-treated with 5mM isonicotinic acid in CH<sub>2</sub>Cl<sub>2</sub>/EtOH (1/1) solution for 5 days, then the EtOH washed plates are placed in 2mM [Ag(L1)]NO<sub>3</sub> in THF/EtOH (1/1) solution for 14 days for crystallization. The detailed description of the coating is shown in the Chapter 3.2.4. The loading of the plates is 2000mg/m<sup>2</sup>, which is high, but these samples are for external use. The treated samples were photographed before and after flow chamber (F-C) experiment (Fig.3.3-21,22):

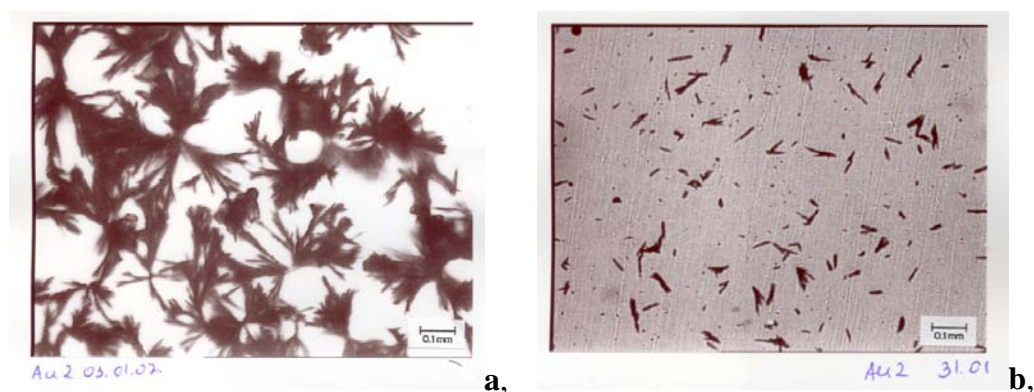


**Figure 3.3-21a,b:** Coated gold plates before (a) and after (b) F-C experiment

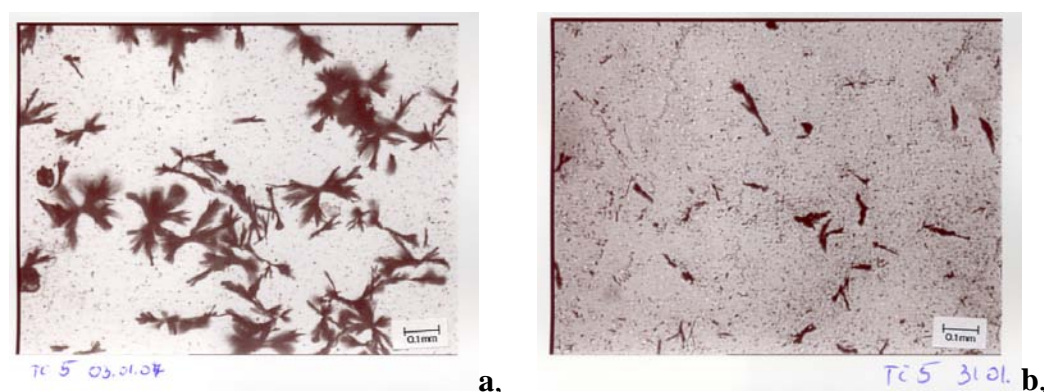


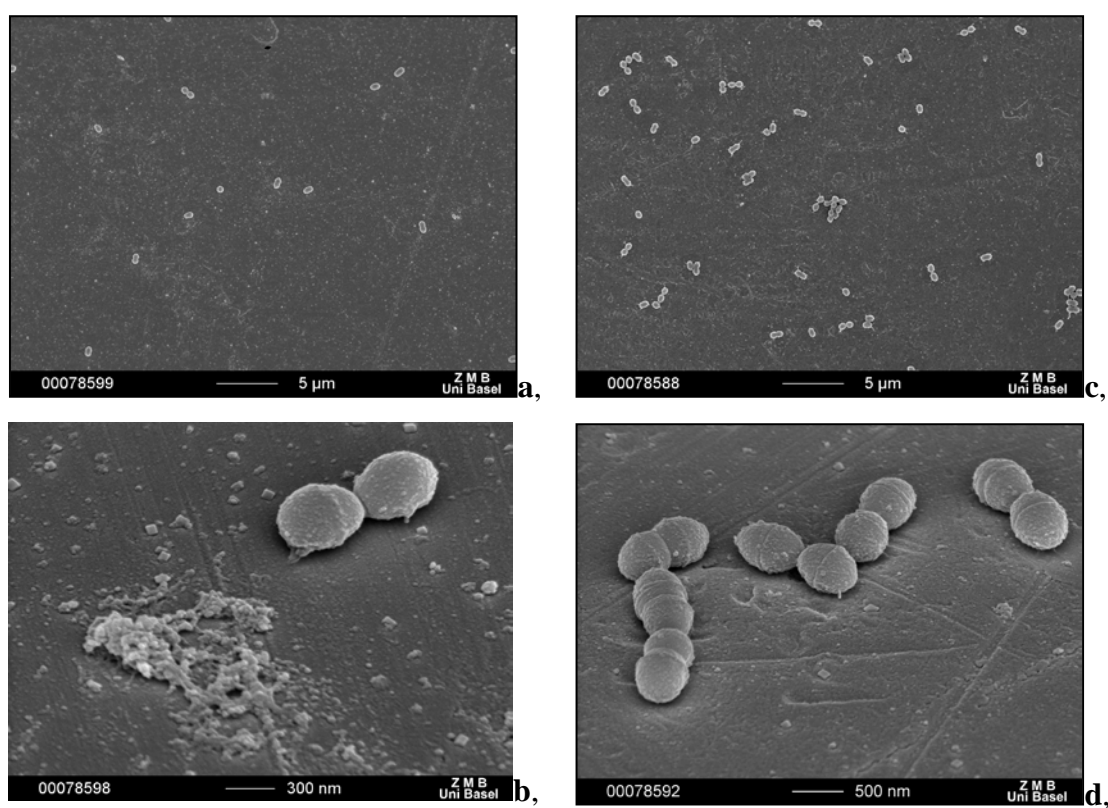
**Figure 3.3-22a,b:** Coated titanium plates before (a) and after (b) F-C experiment

As shown in Fig.3.3-21,22, the majority of the big crystals were washed out, but a good portion remained attached on the surface. The previously described AAS assay show that the silver concentration of the non filtered chamber suspension is 10 times higher. This could

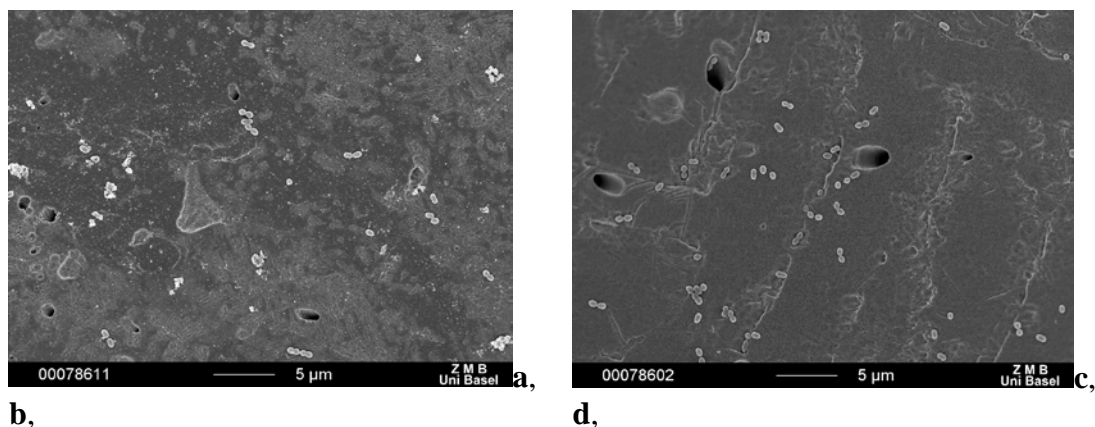


mean that a part of the silver ions are attached to the bacteria and removed by the 0.22 $\mu$ m filter. There are probably larger crystalline residues in the suspension, but these are not present in the decanted AAS sample, yet the middle sized floating aggregates can increase the signal. After the surface treatment method was fixed, each material was tested in at least four independent experiments to reach a reliable result.

The coated and uncoated samples were also evaluated by SEM measurements. With a special fixation method, the bacteria were fixed on the surface while the other components of the saliva suspension were removed. The plates were dried and SEM images were done. (**Fig3.3-23,24**).



**Figure 3.3-23:** Adl7 coated Au-alloy substrate (left **a,b**) and uncoated Au-alloy substrate (right **c,d**) after F-C experiment





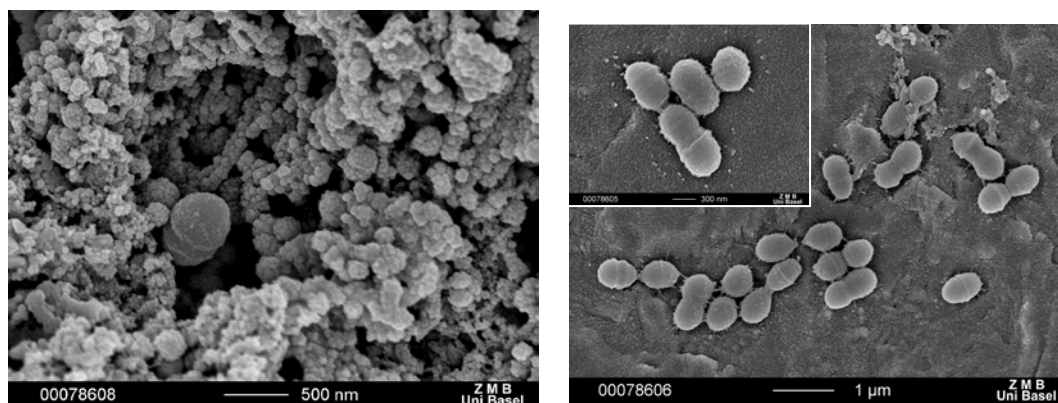


**Figure 3.3-24:** Adl7 coated titanium sample (left **a,b**) and uncoated titanium sample (right **c,d**) after F-C experiment

The number of attached bacteria on the surface is obviously higher in the case of the uncoated samples (both gold and titanium substrates). The bacteria have a tendency to colonize on the untreated samples. Although, the SEM images do not give information about the bacteria being dead or alive at the moment of removal from the flow chamber, the aggregation of the bacteria on the surface can be an indication that these were living bacteria. On the coated samples, more single, or pairs of bacteria can be observed, and, besides of the cells, the residue of the original coating is present. Since this method is not capable to differentiate the living and dead bacteria, the previously described microscopic method was used to evaluate the results.

The epifluorescence microscopic images of the treated and untreated substrates after the flow chamber experiment are shown in **Fig.3.3-25,26**. The images of the representative sectors of both dental materials are presented. Many bacteria, attached to the untreated materials, were stained green because they were still alive. On the treated samples most bacteria were stained red, indicating that they were dead at the time of staining.

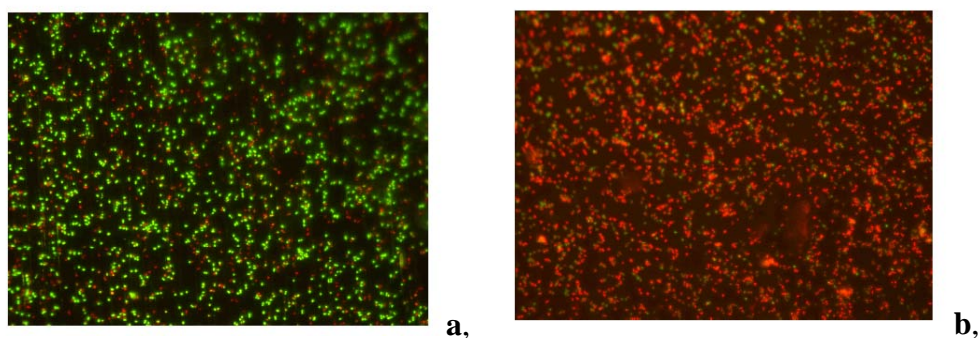


**Figure 3.3-25a,b:** Uncoated (**a**) and coated (**b**) Au-alloy substrate

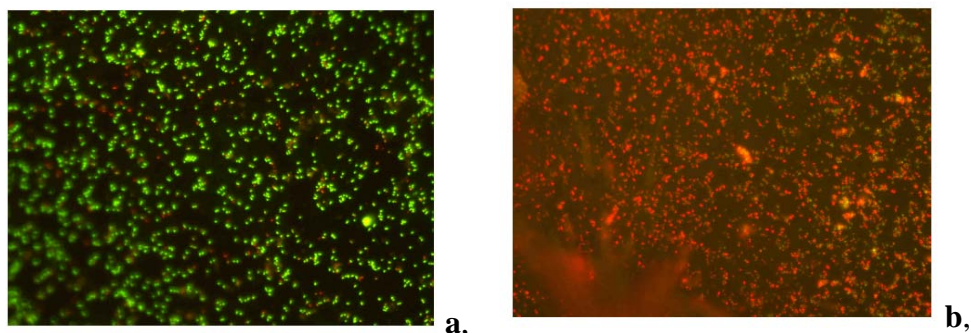


**Figure 3.3-26a,b:** Uncoated (**a**) and coated (**b**) titanium substrate

From the analysis of dead and alive bacteria on the treated metal surfaces, it can be concluded that compound Adl7 has definitely an anti-bacterial effect on *S.Sanguinis* cells under the given conditions. The treated substrates show a reduction of adherent live bacteria of more than 90% for gold alloy and for titanium as compared to the corresponding non-treated samples. Based on the SEM measurements, not only the living and dead bacteria ratio is strongly decreased thanks to the surface coating, but the number of the attached bacteria is also diminished on the treated surfaces as compared to the untreated samples.

#### 3.3.1.4 Conclusions

The different *in vitro* experiments all confirmed the antimicrobial effect of the silver coordination polymer, Adl7, against several bacterial strains. The silver concentrations measured in the different bacterial suspensions were in a safe range of 1-15 ppm encouraging the further *in vivo* experiments of this compound.

### 3.3.2 *In vivo* experiments

*In vivo* experiments were carried out based on the previous work of Prof. R. Landmann [108]. The same mice and tissue cage models were used with the coated titanium cages as previously described. The experiment is shortly described: with EtOH sterilized coated and uncoated titanium cages are subcutaneously implanted in the back of a mouse. Then, inocula, a bacterial suspension  $10^6$  CFU *S.Epidermidis*/cage, is injected percutaneously preoperatively. The tissue cage fluid is removed after 2, 6, 9, and 15 days after the implantation and the bacteria present in the fluid are counted and the silver concentration is determined.

Preliminary experiments were done using coated Ti disks placed into the cage, but the surface of the disks is much smaller compared to the surface of the cage, hence the effect of the coating was not perceptible. Then, the titanium cages were treated to build up the Ad17 coating on it. 1mM concentration of  $[\text{Ag}(\text{L}1)\text{NO}_3]$  treating solution was used for 3 days crystallisation. Then, the cages were removed from the solution, rinsed with EtOH, and dried under vacuum. The loading of the cage is  $27\text{mg}/\text{mm}^2$ , which is much less than the loading of the 1mM/3d treated titanium disks (ca.  $400\text{mg}/\text{mm}^2$ ). The crystallisation on the cage is not so ideal and the surface/treating solution ratio is 5 times less than in the case of the titanium disks. These two unfavourable conditions could cause this decrease of the loading. Although the loading is not high, the coating contains 54 ng silver/cage, which can be enough to have a local antimicrobial effect. The results of the *in vivo* experiments are shown in a **Fig.3.3-27**.

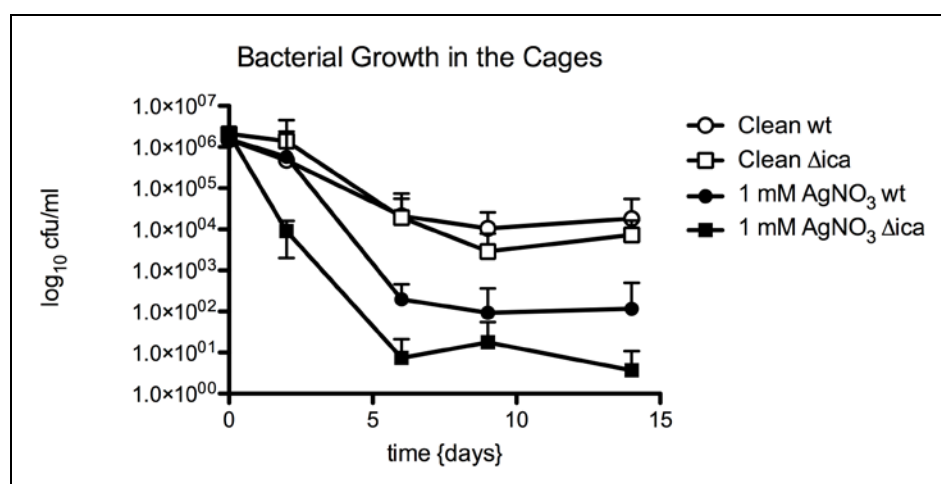


**Figure 3.3-27:** Combined data of the cage experiments: clean (uncoated) WT (biofilm+), clean (uncoated) Δica (biofilm-), AgNO<sub>3</sub> (coated) WT, AgNO<sub>3</sub> (coated) Δica

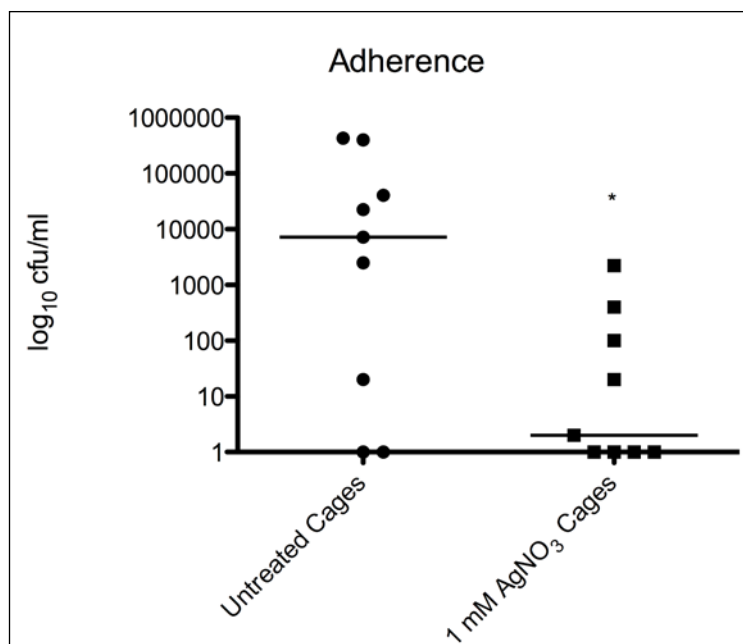
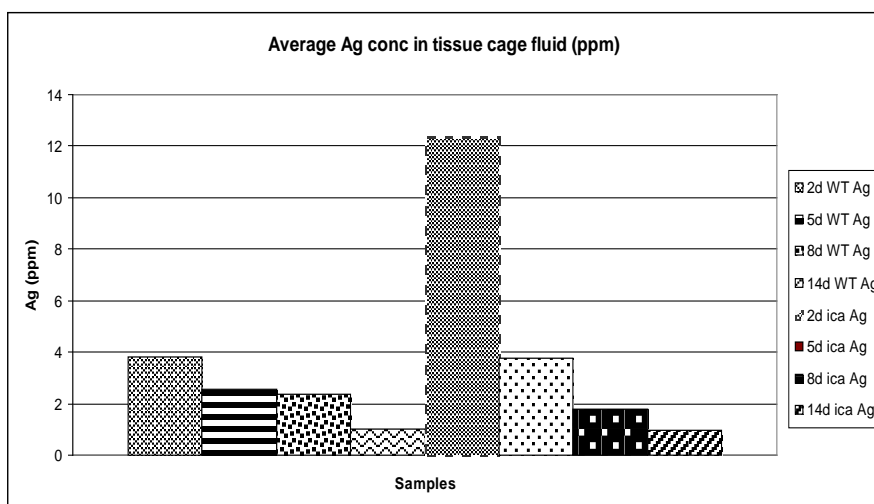


**Figure 3.3-28:** Combined data (WT and ica) of the surface adhered *S.epidermidis* bacteria numbers on coated and uncoated cages after explantation.

The microbiological assays show a significant antimicrobial effect of the coating after 9 days, when no bacteria could be found in the tissue cage fluid. The adherent bacteria count was very low on the treated cages in the case. No adherent bacteria were found in the case of 5 treated cages.

Concerning the silver concentration measurements, the two measurements gave rather different results. The average values are presented in the **Fig.3.3-29**.



Sample	Ag conc. (ppm)	Stdev
WT clean	0	-
WT clean	0	-
WT clean	0	-
WT clean	0	-
ica clean	0	-
ica clean	0	-
ica clean	0	-
ica clean	0	-
WT Ag	3.80	3.12
WT Ag	2.55	1.45
WT Ag	2.36	2.41
WT Ag	1.02	1.11
ica Ag	12.36	10.61
ica Ag	3.76	3.37
ica Ag	1.79	1.73
ica Ag	0.95	0.75

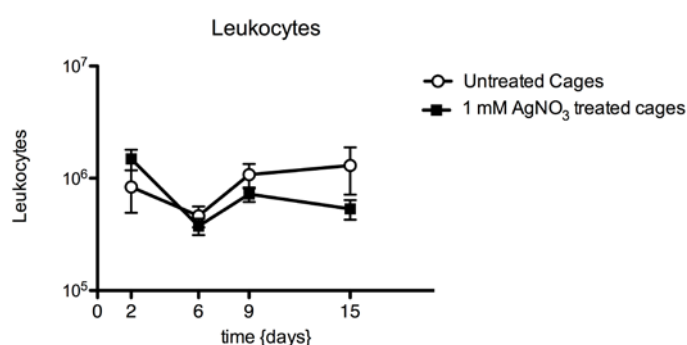
**Figure 3.3-29:** Silver concentration of the tissues cage fluids after implantation, 2, 6, 9, 15 days, in the case of ica and WT bacterial strains

Although the standard deviation of the results is high which is generally the case on biological assays some tendencies are remarkable. The concentration of the silver is decreasing with the time but does not reach zero at the end of the 2 weeks. This means that the slow leakage of

the silver is not finished after two weeks. The removed cages were tested to measure the silver remained on the surface. It means that with acid treatment we remove the possibly remained coating after the in vivo experiments. These measurements also showed a rather big variance between the cages: the remaining silver concentration on the surface was 1 and 9 mg/mm<sup>2</sup> with an average of 4 mg/mm<sup>2</sup>. These results are very promising but further investigations are necessary to confirm the data of the chemical measurements.

The leukocyte cells were also investigated, to study the influence of the AdI7 on the immune system (Fig.3.3-30).

**a,**



**b,**

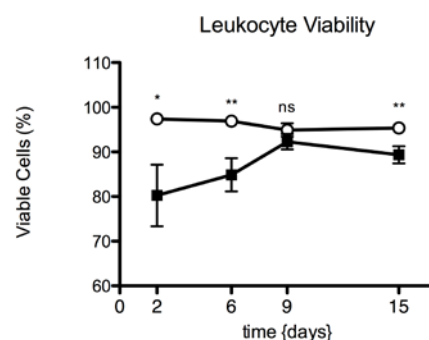


**Figure 3.3-30:** Total leukocyte numbers (a) and viability (b) in the cage fluid after implantation 2,6,9 and 15 days

After a short decrease of the viable leukocytes and their number in the tissue cage fluid, their number and viability increases again after ca. 3-6 days. This shows that our samples have good bio integration in the case of the coated Ti cages, thus a good biocompatibility with the host immune system.

### 3.3.3 Conclusions

All different microbiological assays confirmed the anti-microbial characteristics of AdI7 bulk compound and coating. Several different substrates were tested, from polymer surface to dental implant materials. The efficiency of the coating depends on the silver loading and the stability of the coating. The AdI7 coating shows higher antimicrobial affinity than the silver nanoparticles generated on polymer surface. The antibacterial effect depends on the released silver ions in the solution. Although the silver nanoparticles are small enough to have good contact with the surrounding solution, they do not release enough silver ions to have a good antimicrobial effect. In contrast, if silver ions are present on the surface, as for the silver coordination polymer or by the silver ions attached by the peptides, the anti-microbial activity is significant. The silver release of the coating was 1-15 ppm depending on the loading and

the used microbiological assays. The major part of the silver released by the coating is attached to the bacteria and just a minor part remains in ionic form in the solution. Thus the toxicity of the coating might be low. This should be confirmed by further cell viability assays. The higher stability of the coating, prepared by methods using an anchor molecule, is confirmed by the inhibition zone assays of the gold plates: less ionic silver could be found in the bacterial free solution. The most tested bacteria strain was the *S.epidermidis*, which is the main responsible for the biofilm formation and implant related infections. The biofilm positive and negative strains were tested and the two strains seem to be susceptible against silver, with no significant difference between the two. This is true for both *S.epidermidis* and *S.aureus* bacterial strains. It means that the biofilm is rather not protective against silver. To complete the list of the bacterial strains, the gram negative *E.Coli* was tested in the inhibition zone assays and one strain of *Streptococcus Sanguinis* was tested in the flow chamber experiments. Both experiments confirmed the general antimicrobial activity of the silver polymer complex. This characteristic makes Adl7 a perfect candidate for the further *in vivo* assays. The *in vivo* assays made on mouse models gave a positive result for *S.epidermidis*. No more bacteria could be found in the fluid around the implanted Adl7 coated titanium cages after 9 days from the implantation and infection. In addition, the number of the adhering bacteria was decreased dramatically.

All these microbiological results propose to continue, making further assays such as cell viability and toxicity assays with the aim to use the silver coordination compound as coating for implant materials. Such tests were carried out by another PhD student of our group, Priscilla Brunetto. They show that Adl7 is also a potent antimicrobial compound against yeast cells, and that fibroblast cells survive and proliferate in presence of Adl7 coated Au(111) plates and Ti disks. The detailed results will be described in P.Brunetto's thesis.

## 3.4 Molecular mechanism of Ag<sup>+</sup>

To learn more about the molecular mechanism of silver ions, it is important to know which amino acids play a role in the process of the attachment and transport of the silver ions in the cell. Histidine is the most studied amino acid in connection with silver. Its function in the silver resistance is well known [79]. Detailed description of the silver resistance is presented in the Introduction (Chapter 1). Other amino acids could also have an impact regarding the silver transport into the cell.

The purpose of the experiments in this chapter is to find out which amino acids or short amino acid sequences could be involved in silver ion binding and/or transport. In our studies, the nanoparticle formation will be used for the detection of bound silver. The idea is to reduce the attached silver to make it visible, and thus use it like a marker. This method is not only useful to determine the affinity of the different amino acid sequences towards the silver. At the same time, other analyses are carried out to characterize the AgNPs (silver nanoparticles will be abbreviated by AgNPs) regarding their size and distribution and test their antimicrobial effects (Chapter 3.3.1.1.). Attaching AgNPs on a surface via peptides can also be a solution to render an implant surface antimicrobial. The size and form of the nanoparticles are expected to be the determining factors for the microbiological characteristics. Creating a surface coating by size-controlled nanoparticle generation, the microbiological properties of the surface could be tuned.

Over the last decade, a lot of progress has been made in the development of methods for synthesizing and controlling the size and shape of metallic nanocrystals. [148] Nobel metal particles have been used in several different applications such as catalysis, biological diagnostics, imaging and other optical applications, for their unique optical properties [147,149,150]. The most studied Nobel metal is the gold and much less work is focusing on AgNPs. Although the silver plays an important role in medicinal and photochemical applications, is somehow neglected due to the lack of comprehension of its role in the involved processes.

Several different ways are known for the preparation of AgNPs,. The particle synthesis usually starts from a soluble metal salt, which is treated with a reducing agent. A stabilizing agent is used to prevent the further growth and aggregation. One of the simplest ways to fabricate Nobel metal nanoparticles called citrate reduction where citrate acts both as a reducing and stabilizing agent [151]. Photochemical methods are also known to induce the formation of AgNPs [153,154] In this case, the use of a separate stabilising agent is necessary.



The development of the biologically inspired processes for nanoparticle synthesis is currently in the focus of interest. The fungus, *Aspergillus flavus*, treated with silver nitrate solution, accumulates AgNPs on the surface of its cell wall [155] and several strains of the fungus *Fusarium oxysporum* can fabricate nanoparticles as well [156,212]. These methods are rather slow, but other rapid microbiological methods using bacteria can be found in the literature. [157] The role of the stabilizing agent can be played by the organic matrix of the bacteria [158]. Looking at less complex biological systems, different natural and artificial proteins are used in the fabrication of nanoparticles, for example nitrate reductase [160] engineered protein cages [161] or different oligopeptides [162-164]. The common point of these last examples is that the peptides contain tyrosine whose reducing character is well known [165,166]. These peptides can stabilise the nanoparticles and/or serve as supramolecular gelators [164] to decrease the mobility of the particles. Thus, Shinkai and co-workers used supramolecular organogels as templates to form helical nanofibers [168-170]. Using the same technique, Hanabusa and Stupp developed transition metal nanotubes [171-173]. Except for these latter examples, most of the research is done in solution. Other works dealing with biological structures and silver are more focused on its use [174] than on the synthesis of the NPs or on the selectivity of the proteins regarding their effect to generate AgNPs. Since the use of AgNPs is increasing due to the renaissance of silver as antimicrobial agent, the nanoparticle generation *in-situ* on a surface could be an interesting subject also for a possible medical use. This chapter has therefore two main objectives:

- studying short peptide sequences, bound on solid phase, regarding their affinity to silver ions, which can help to understand the molecular mechanism of the antimicrobial property of Ag<sup>+</sup>
- analysing the AgNPs generated on the surface of polymer beads, their size distributions and microbiological effects to suggest a further medical or even technical use.

As a first step, a model experiment was built up to develop an effective method for the detection of the silver ions attached on the surface. A good silver complexing model molecule (isonicotinic acid) was coupled to a TentaGel resin. The method development was done on this substrate. Two reduction pathways of silver were investigated to detect the attached silver ions and generate AgNPs on the surface. A combinatorial chemistry approach helped to determine the active amino acids and short amino acid sequences (tripeptides) that are able to bind silver ions. Then, several tripeptides were synthesized to analyse the AgNP size and distribution as a function of the amino acid combinations.



Combinatorial experiments and other experiments concerning solid state bound peptides were made in close collaboration with Prof. Helma Wennemers and her group, Dr. Kirsten Belser, Dr. Gregory Upert and Conelious Pfumbidzai.

#### ***3.4.1 Preliminary experiments with isonicotinate grafted T-Gel resin***

To find the appropriate method to study the affinity of the different peptides for silver ions, a model system was prepared. To a TentaGel resin, which is generally used for solid state peptide synthesis, isonicotinic acid was coupled. This substrate has been described in a previous chapter. Since the affinity of the pyridine tail of the isonicotinic acid to the silver ions is well known [93], this T-gel resin was used as an active substrate able to bind silver ion. T-gel resin is incubated in a 0.05M AgNO<sub>3</sub> aq. solution for 15 min, in a volume of the solution that the Ag<sup>+</sup> concentration is approx. 10x higher regarding the isonicotinic acid loading on the resin to guarantee a 100% uptake. Typically, for 30mg coupled T-Gel beads, 2ml 0.05M AgNO<sub>3</sub> aq. solution is used. If the quantity of the treated beads is reduced, the volume of the silver nitrate solution is reduced respectively. The incubated resin was then washed 5 times to remove the remaining free silver ions, and the reduction of the silver was carried out. The photochemical (light) reduction method (generally abbreviated further as LR) means that the wet resin is irradiated with normal light, 15W, for 8h from a 10cm distance. For the chemical reduction method (generally abbreviated further as CR), the wet resin is mixed together with 0.05M Na-ascorbate aq. solution, then the resin is washed to remove the excess of the ascorbate.

Some control experiments were first carried out to demonstrate the efficiency of this method in detecting attached silver on a surface. Acetylated T-gel resin was prepared as a negative control since the carbonyl group coordinates weakly to the silver ions. The original T-gel resin, which has an amino group, was used as a positive control as the amino group coordinates well with the silver ions. Acetylated T-gel resin (Ac-TG) was mixed to the isonicotinic acid coupled T-gel resin (Iso-TG) and the NH<sub>2</sub>-terminated T-gel resin (NH<sub>2</sub>-TG) in similar ratios. Then, the mixture was treated with AgNO<sub>3</sub> and irradiated with light.

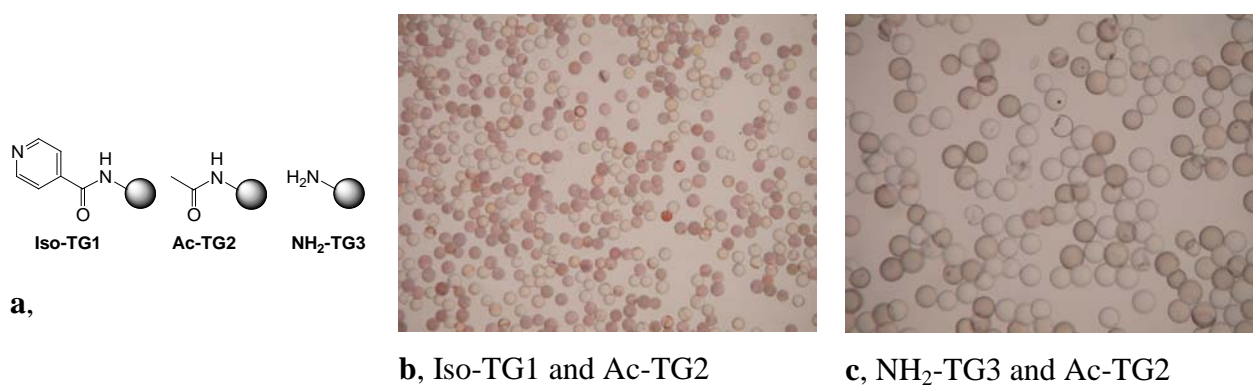


**Figure 3.4-1a,b,c:** Scheme of the isonicotinic acid coupled (iso-TG1), acetylated (Ac-TG2) and amino functionalized (NH<sub>2</sub>-TG) T-gel beads (**a**), and their mixture after incubation in AgNO<sub>3</sub> solution and irradiation (**b,c**)

In **Fig.3.4-1** can be observed that the isonicotinic acid coupled T-gel (iso-TG) beads have a nice reddish colour after the light treatment (light reduction abbr. LR) and a greyish colour for the amino functionalized T-gel beads (NH<sub>2</sub>-TG). The number of the coloured and colourless beads is around 50% each. This experiment encourages further investigations using the reduction method to detect silver. Thus, the colour change of the beads is a good sensor for the attached silver. The coloured beads indicate also nanoparticle generation on the surface.

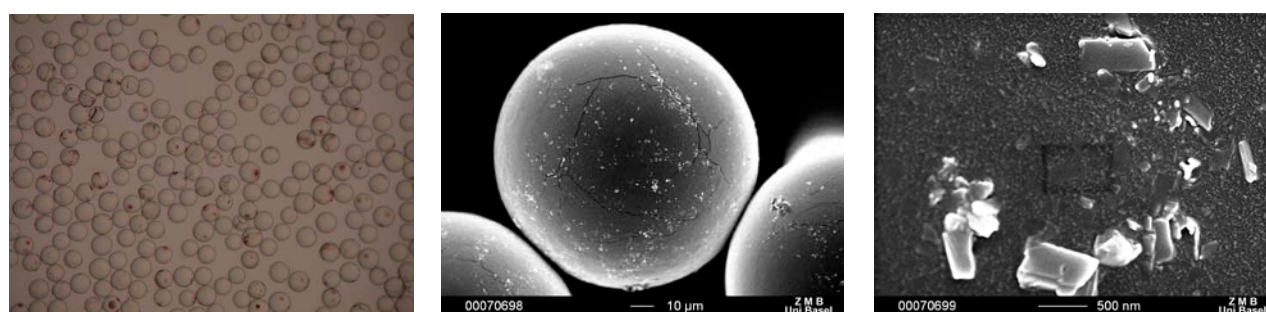


**Figure 3.4-2:** Optical microscopic and SEM images of Ag<sup>+</sup> incubated, light reduced (LR) iso-TG

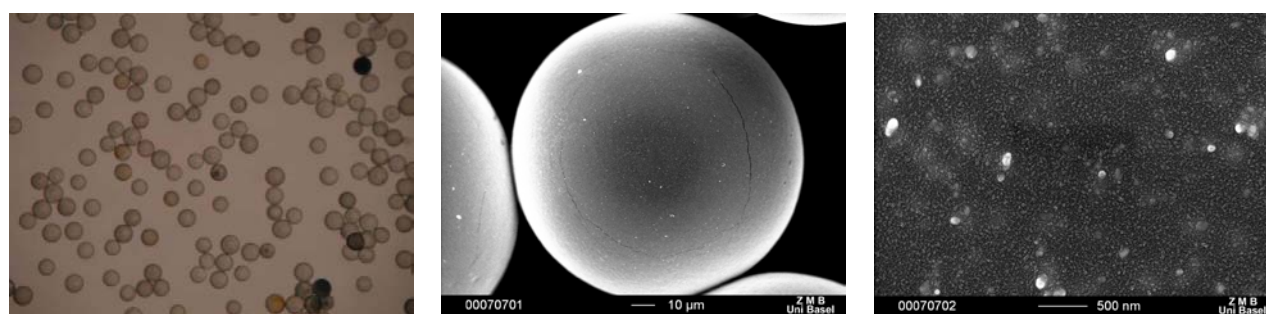


**Figure 3.4-3:** Optical microscopic and SEM images of Ag<sup>+</sup> incubated, chemically reduced (CR) iso-TG

The optical microscopic images (**Fig.3.4-2,3**) show a neat difference: the light reduced (LR) beads are red and spotted, while the chemically reduced (CR) are grey and more homogeneous. The colour of the nanoparticles depends on their shape and size [175]. The SEM images (**Fig.3.4-2,3**) confirm the size difference of the AgNPs on different coloured beads. The light reduced beads are inhomogeneous and the size distribution of the particles is also inhomogeneous (100-1000nm). Some hundreds of nm crystals can be found on the surface with bigger well designed crystals. On the other hand, the chemically reduced beads show a homogeneous coverage with nanoparticles of a size around 50nm, always arranged in big flat aggregates. Identically loaded beads show different NP formation, depending on the used reduction method. The reduction characteristics of the light and the Na ascorbate method are dissimilar. The speed of the LR, which takes place over 8h, is slow in comparison with the fast chemical reduction (minutes). Thus, during the light reduction, there is enough time for the crystal formation resulting in well designed silver crystals. The almost immediate nanoparticle formation through CR does not allow slow crystallisation, resulting in small nanoparticles.

The fast reduction does not allow for the silver ions to move on the surface in order to group together and build up larger structures. The autocatalytic reduction of the silver ions towards nanoparticles, well known from photography, is also negligible. Since the photo reduction is a long process and irradiation is not homogeneous on the surface of the beads(only from the top), the reduction of the silver ions is probably not complete in the case of LR.

#### 3.4.1.1 XPS measurements

XPS measurements were carried out to learn more about silver behaviour on the surface and during the reduction process. This measurement reveals the chemical environment and the oxidation state of silver in different reduced and not reduced samples. Other chemical elements present on the surface (the ligand atoms principally), were also analyzed.

Four samples were prepared for the measurement: isonicotinic acid coupled polymer, Ag treated, light reduced, and chemically reduced isonicotinic acid coupled polymer. Overview spectra show that spectra all used elements can be found. (**Fig.3.4-4**)

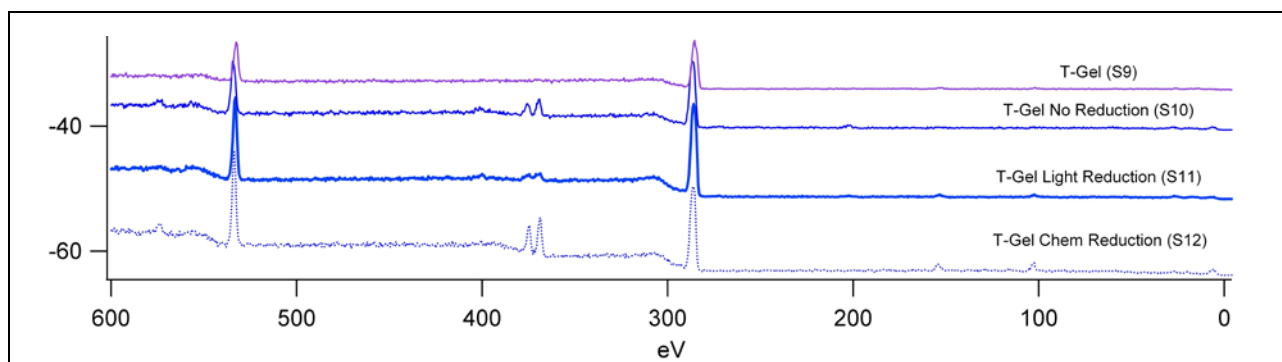


**Figure 3.4-4:** XPS survey spectra of the iso-TG, the  $\text{AgNO}_3$  incubated iso-TG (no reduction), the  $\text{AgNO}_3$  incubated and light reduced iso-TG and the  $\text{AgNO}_3$  incubated and chemically reduced iso-TG

To learn more about the atomic state of the elements, the peaks were measured one by one (**Fig.3.4-5**) and compared with literature data. Almost all of the spectra show shifted peaks due to the charging effect (conducting Si wafer+insulating beads and ligand). The shifts have been corrected to the charging effect. The correction is based on the value of the C1s peaks. The position of the most intense carbon peak was assigned according to what was expected given the known composition of the material. All of the other peak positions were corrected with respect to this peak. The shift corrections were between 0.4-0.9 eV, which is an acceptable shift resulting from the charging effect.

The **Ag3d** peaks in the case of the chemically reduced beads are not broad, and only one component is present. The position of this peak shows a good correspondence with the bulk silver with 367,8 eV binding energy (=BE). The relative concentration of the silver seems much higher in this sample, compared with the light reduced or not reduced samples although the real concentration is the same in all Ag-treated samples. The probable explanation of this phenomenon is that during the chemical reduction, the previously ligand complexed silver ions move to the surface of the beads, making large aggregates of silver metal nanoparticles (as confirmed by the previous SEM measurements). The escape depth of the  $e^-$  being  $\sim 5$  nm, that means that silver attached inside the functionalized PEG spacer (**Fig.3.2-56** in Chapter 3.2.6) is invisible for the X-rays, hence the measured silver concentration on the surface is much lower.

The unreduced sample reveals a Ag3d peak with a slightly higher BE level (368.1eV) in good agreement with the results of the previous measurements on the Ad17 silver complex polymer compound (Chapter 3.2.3.4). The lines are broad, probably due to a second component of silver that can be recognized at BE 369.0 eV. This can be attributed to an Ag cluster upon cluster formation due to a reduction of the Ag-ions caused by the X-ray radiation during the XPS recording. The light reduced beads show a much more complicated Ag3d spectrum with

at least two different silver compounds, one of them with a binding energy of 368.4 eV. This compound can be a silver cluster with an inferior size of clusters than in the previous sample. The second component, with binding energy of 371.1eV, is a silver having a changed chemical environment in which the electronic density must be much higher than for  $\text{Ag}^+$  in a complex bond. This big shift can be explained by the formation of a very small cluster (3-4 Ag) or dimers. Supposing to have  $\text{Ag}^+-\text{Ag}^+$  interactions which is already half way to the reduced  $\text{Ag}^0$ , this can resemble the Ag-Ag pairs observed in other Ag-coordination polymer networks described by us [207][93].

The **N1s** peaks are on the same place by all of the samples, at 399.7-9eV. These peaks are so broad that they might correspond to two types of N present in the molecule. These are the pyridine N of the isonicotinic tail and the N of the peptide bond through the isonicotinic acid, which is bonded to the T-Gel beads.

The **C1s** peaks show two different components of ca. 50% distribution each. One peak at 284.8 eV is attributed to C=C/C-C bonds (carbons in aromatic/aliphatic environment) and the second one at 286.5 eV BE is attributed to the C-N/C=O bonds.

The **O1s** spectrum shows everywhere a single broad peak around 532.8eV binding energy. We should always see the O1s from the substrate  $\text{SiO}_x$ , as is confirmed by the Si 2p spectra. There is probably overlap with a O1s signal from other compounds. These different oxygen atoms have a binding energy in the same area. The value of 532.8eV is higher than the value expected for the C=O oxygen atoms (around 532eV), but is slightly lower than these of the absorbed  $\text{H}_2\text{O}$  oxygen atoms. It can be more attributed to a C-O or an H-bonded O. The area covered by this broad O1s peak from ~531.6 to 534.0eV and can thus afford no further information.

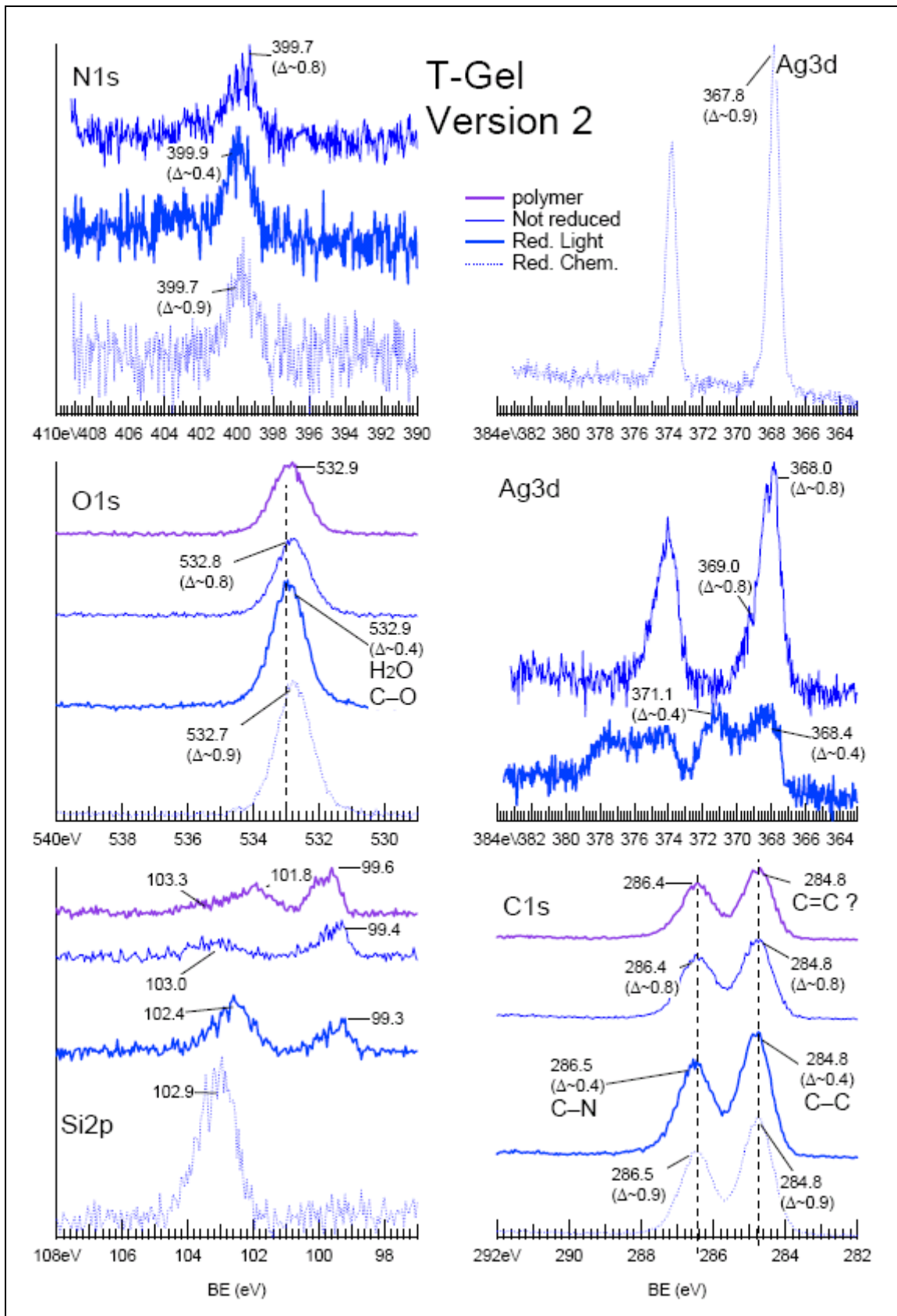


**Figure 3.4-5:** N1s, O1s, Si2p, C1s, Ag3d peaks of the four samples

#### 3.4.1.2 Conclusions

Following the preliminary experiments, some important remarks should be made:

-both reduction methods are suitable to detect the silver ions attached to the surface of the beads: colouration of the beads signifies the AgNPs formation from the silver ions

-after reduction, the colour of the beads is different in case of the two reduction methods, LR (light reduction) generates red, while CR (chemical reduction) generates grey colour in the case of iso-TG. In addition, the obtained nanoparticles causing the colour of the beads are different depending on the two methods.

-the nanoparticle size, form and distribution are representative of the reduction method: the light reduction results in well designed crystalline nanoparticles, while the chemical reduction generates well distributed small aggregates on the surface;

-the LR method represents a partial reduction of the silver ions. Crystalline structures (some 100 nm) of small clusters and ions can be found on the surface of the beads. This is in contrast to the CR, where the AgNPs are formed within minutes.

In further investigations, both reduction methods are used. First a combinatorial assay with a tripeptide library was carried out, and the reduction methods are used as marker reaction during the screening. Then, the analysis of the library, the active sequences, were determined and the synthesized tripeptides were tested regarding their silver affinity and AgNP formation.

#### ***3.4.2 Combinatorial experiments***

As a simple biological model, tripeptides were used to study the selectivity of the different structures regarding their affinity to silver ions and to better understand the role of the amino acids in the AgNPs formation. For the nanoparticle formation, the silver ions attached to a surface were reduced in two different ways: with the light reduction (LR) method and the chemical reduction (CR) method. To gain insight into molecular interactions of silver ions with peptides, we used a combinatorial approach and prepared an encoded split-and-mix peptide library (library1) [176, 177] split-and-mix synthesis [178, 179]. Here, a short description is given to explain the basics of the combinatorial approach and the synthesis of an encoded split and mix library.

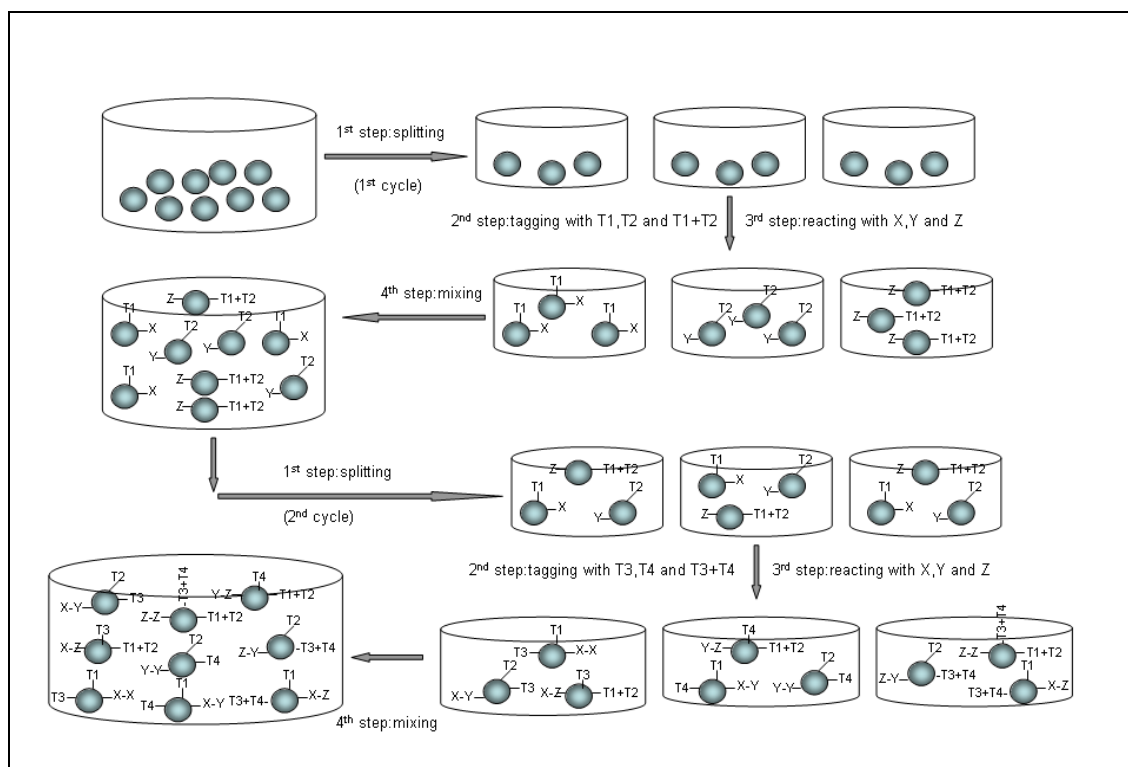
##### **3.4.2.1 Solid phase peptide synthesis and combinatorial chemistry**

Since the Nobel Prize winner Merrifield pioneered solid phase synthesis in 1963, the peptide synthesis has changed radically. Merrifield's Solid Phase synthesis concept, first developed for biopolymers, is used in every field where organic synthesis is involved. Merrifield developed a series of chemical reactions that can be used to synthesize proteins. The direction of synthesis is opposite to that used in solution. The intended carboxy terminal amino acid is anchored to a solid support. Then, the next amino acid is coupled to the first one. To prevent further chain growth at this point, the amino acid, which is added, has its amino group protected. After the coupling step, the protecting block is removed from the primary amino group and the coupling reaction is repeated with the next amino acid. The process continues until the peptide or protein is completed. Then, the molecule can be cleaved from the solid support and any groups protecting amino acid side chains are removed. Finally, the peptide or protein is purified to remove partial products and products containing errors. For this purpose, a RinkAmid resin is used. The peptide can also be left on the solid support. Just the side chain protecting group are removed and peptide containing beads are used for further experiments. TentaGel resin is used for this aim.

Combinatorial synthesis on solid phase can generate very large numbers of products, using a method described as mix and split synthesis. This technique was pioneered by Furka and has since been exploited by many others since its first disclosure. The method works as follows: a sample of resin support material is divided into a number of equal portions (x) and each of these is individually reacted with a single different reagent/amino acid. After completion of the reactions, and subsequent washing to remove excess reagents, the individual portions are



recombined; the whole is thoroughly mixed, and may then be divided again into portions. Reaction with a further set of activated reagents/amino acids gives the complete set of possible dimeric units as mixtures and this whole process may then be repeated as necessary (for a total of  $n$  times). The number of compounds obtained arises from the geometric increase in potential products; in this case  $x$  to the power of  $n$ . A simple example of a  $3 \times 3 \times 3$  library gives all 27 possible combinations of trimeric products. If X, Y and Z were amino acids, the final products would be tripeptides. The compounds can be tested whilst still attached to the bead or as a mixture following cleavage from the solid phase. The library is then tested to determine the most active sequences. As the quantity of the substance present on one bead is very low (ca. 100 pmol), defining the sequences present on a bead would need a complicated analytical method. To facilitate this step, an encoded library is prepared. The encoded library contains several tag molecules as a marker. These molecules are representatives for the determined reagent/amino acid in a determined position. The present tag molecules will give the information which reagents/amino acids are on the beads and in which order. These tag molecules should be easy to work with and to detect with an analytical method. Other characteristics of these molecules are also important, namely that during the reaction it should be inert and detectable in small quantity. [180] It should be also easy to cleave from the beads. These tag molecules were developed [176] containing a polyhalogenated aromatic alcohol residue and a photo-cleavable part. The polyhalogenated aromatic alcohol residue can easily be determined by EC-GC. The sensitivity of the EC method for this type of molecule is so high that only 2% of one bead surface should be loaded with it. The scheme of an encoded library synthesis is presented on **Fig.3.4-6**. To encode the library, a binary code is necessary: every reaction is coded by one or several tag molecules. In the presented example, two tags are used to code three reactions in both two cycles. E.g.: if after analysis, the T1, T2, and T4 are detected, that means that on the beads, the Z was in the first and Y in the second position. Using the binary code,  $N$  tag molecules can encode  $2^N - 1$  reactions. [176]

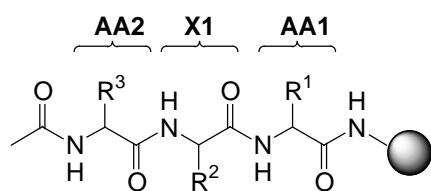


**Figure 3.4-6:** Scheme of the preparation of an encoded split-and-mix library

The “one-bead-screening“ method is an efficient way to test a large number of different molecules to find out the active sequences. In this method, all participants of the library are tested at the same time. The screening reaction is made with the library and a simple visible reaction taking place on the active beads. The typical size and shape dependent coloration of Ag-NPs [181-187] was anticipated to allow for an easy identification of active library members. Then, the coloured beads are removed and analysed. The sequence on a bead is determined by detecting the present tag molecules.

### 3.4.2.2 Combinatorial experiments

The synthesized tripeptide library (by Dr. Kirsten Belser), contains seven different linkers and seven different L- and D- amino acids in positions AA1 and AA2, hence the library **1** consisted maximally of  $7^3 = 343$  different peptides. In the three variable positions, the library **1** contains the amino acids D/L-Asp, D/L-His, D/L-Ser, L-Tyr (**AAn**), and a linker, which can be a linear spacer like Gly,  $\beta$ -Ala, aminohexanoic acid (Ahx) or a turn inducing rigid motive like Pro-Gly, Pro-Aib and *trans*-2-aminocyclohexane carboxylic acid (turnrac, Achc;) (**Xn**).

**Figure 3.4-7:** Encoded split-and-mix library **1**

**AA<sub>n</sub>:** *L-Asp, D-Asp, L-His, D-His, L-Ser, D-Ser, L-Tyr*

**X<sub>n</sub>:** *no motif, Ahx, Pro-Aib, Gly, Pro-Gly, β-Ala, trans-2-aminocyclohexane carboxylic acid*

Regarding the choice of the peptides, which are present in the library **1**, some principle considerations should be made. The histidine amino acid plays a key role in the mechanism of the silver resistance process of the cell, thus the presence of this amino acid was necessary. The tyrosine is well known for its photo activity and reducing behaviour [189-191], which can be beneficial during the light reduction. The serine and aspartame can function as good oxygen donor complexing agents since silver ions; in absence of N donors are readily complexed with carboxyl or hydroxyl oxygen atoms. The sulphur containing amino acids were avoided because their silver complexation is expected to be so strong that no other complexing effect can be observed. The strong interaction between the sulphur containing group and the silver ions probably hinders the NP formation.

The role of the linker is to predetermine the form of the amino acid chain. Thus, the spatial arrangement of the side chains AA1 and AA2 can either help or hinder the complexation of the metal ion. Indeed, the importance of turn-inducing linkers in peptides binding to metal ions other than Ag<sup>+</sup> has been already observed [192]

The library **1** is incubated with 0.05M AgNO<sub>3</sub> so that the silver ion concentration is in large excess (around 10 times higher than the peptide receptor concentration on the solid support). After 15 min sonication with the silver nitrate solution, the beads are washed 5 times with nanopure water to wash out the non complexed, free silver ions. The wet beads are reduced either with light (8h with a 15W electrical lamp, from a distance of 10cm) or with 0.05M sodium ascorbate solution (chemical reduction). After the chemical reduction, the beads were again washed 5 times with nanopure water. The light microscopic images are made using wet samples. For the SEM measurements, the samples are dried under vacuum.

The images of the library **1** are shown in a **Fig.3.4-8**, (light reduced samples), and in **Fig.3.4-10** (chemically reduced samples).

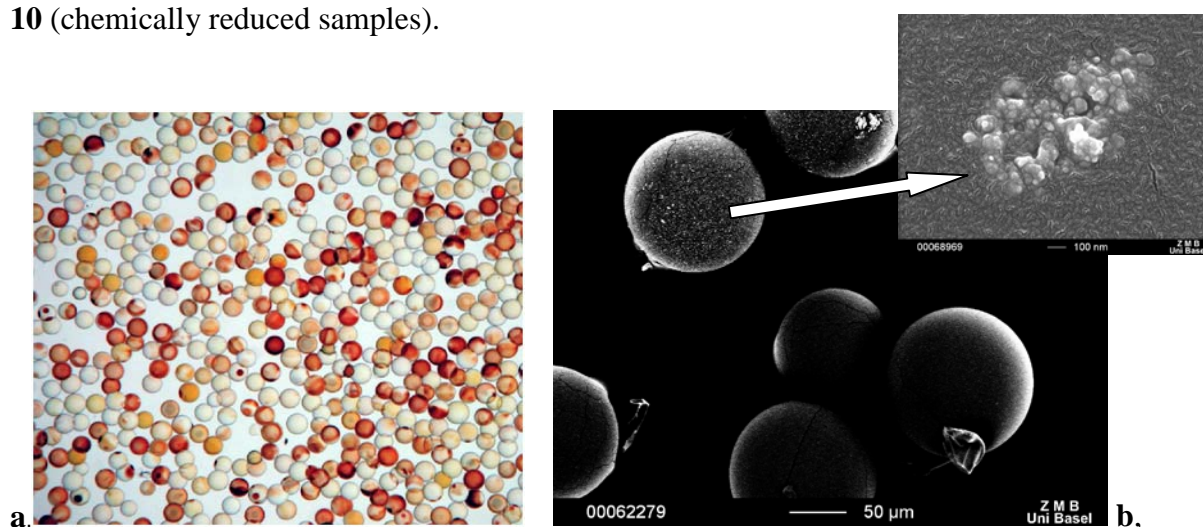


**Figure 3.4-8a,b:** Library **1** after  $\text{Ag}^+$  incubation and light reduction (LR), light microscopic (a) and SEM images (b)

The light reduction generates several red, dark red or spotted beads and many colourless or slightly coloured beads. Similar but lighter colours have been observed for the light reduced isonicitinic acid coupled T-gel (iso-TG) sample. The SEM image shows also differences between the beads. Some beads are covered with nanoparticles corresponding to the dark red coloured beads. No particles can be found on the colourless beads. The fact that coloured and colourless beads are present after the reduction means that some tripeptide sequences react well with silver ions and others do not interact with  $\text{Ag}^+$ . The silver ions attached on the surface by the tripeptides are reduced by the light generating nanoparticles. The energy dispersive X-ray analysis (EDAX) of the solid particles confirms the presence of metallic silver. (**Fig.3.4-9**)

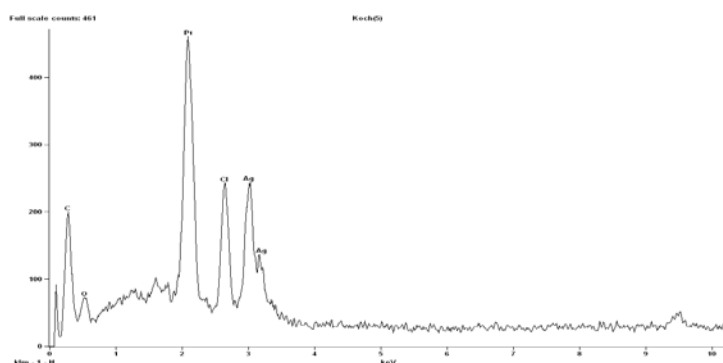


**Figure 3.4-9:** EDAX spectrum of the  $\text{Ag}^+$  incubated and light reduced library **1**,

Indeed, on the EDAX spectrum the signal of the Pt, used as sprinkled metal, is observed as main peak. The C and O from the organic molecules and the Cl (since the library was

prepared using polychlorinated tag molecules to determine the tripeptide sequences present in one bead) can also be observed.

The colouration of the beads is more pronounced using chemical reduction. There are different coloured beads present after the reduction: dark red, red, orange and yellow beads are found next to the colourless beads. (Fig.3.4-10a)

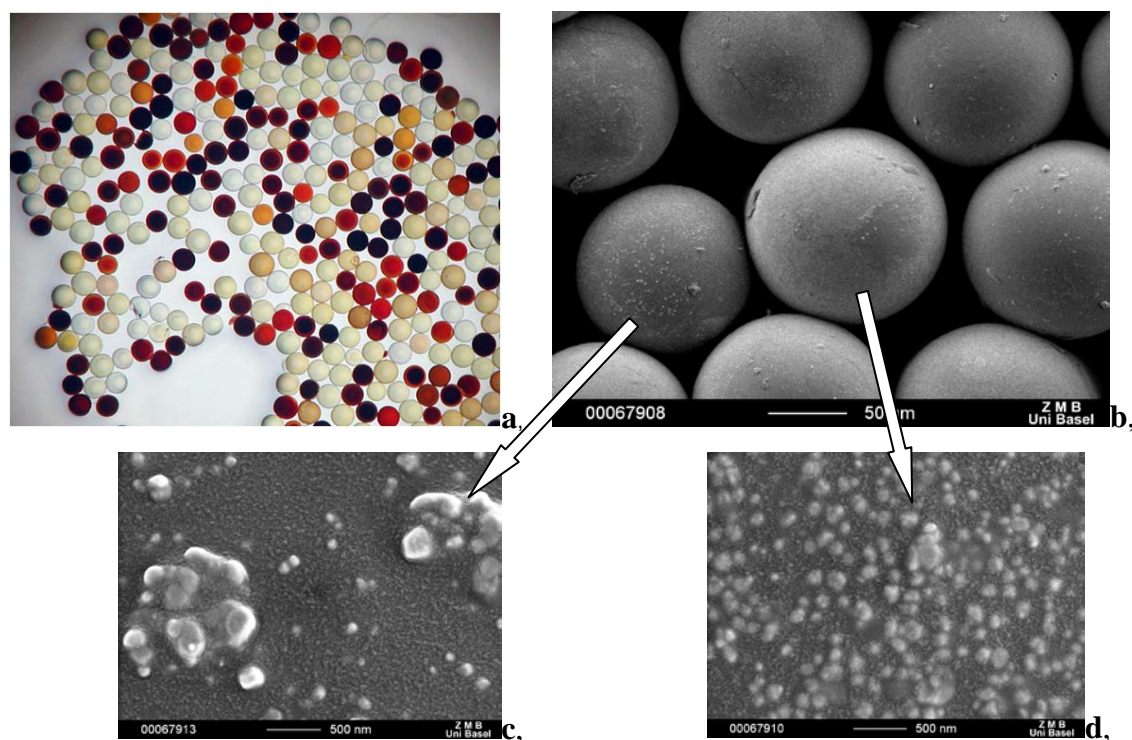


**Figure 3.4-10a,b:** Library 1 after  $\text{Ag}^+$  incubation and chemical reduction (CR), light microscopic (a) and SEM images (b,c,d)

The SEM images show different sized AgNPs on the different beads. Since the colour of the AgNPs changes with their size, the different coloured beads have different sized NPs on the surface. This suggests that beads, containing certain tripeptide sequences, have a higher affinity to silver, resulting in more and larger AgNPs. The colour diversity of the beads suggests higher selectivity in the case of the chemical reduction method.

To answer the question of the selectivity, namely if there are tripeptide sequences having higher affinity for silver ions, the coloured beads were analysed by EC-GC technique. Isolation of several of the coloured beads from both LR and CR assays, and analysis of the peptides on them, revealed the following main consensus sequences listed in **Table 3.4-1** and **3.4-2**.

**Table 3.4-1:** AgNPs formation by reduction of Ag<sup>+</sup> with light (light reduction, LR), most often found sequences after GC analysis

Colour	AA1	X1 (linker)	AA2
Red	Ac-D/L-His	Achc	L-Tyr
	Ac-D/L-Ser	Achc	L-Tyr
	Ac-L-Tyr	Achc	D/L-Ser

Analysing these sequences, which are active for light reduction, some general remarks can be made, namely the importance of the tyrosine amino acid is significant. The tyrosine, being a photoactive molecule, possibly helps the reduction of the silver ions to nanoparticles during LR. Histidine, being a good complexing agent for silver, and the serine seem to be also important. Their role is probably to attach the silver ions on the surface and coordinate them for the reduction. Since the two effects, the attachment of silver ions and the reduction, should take place near each other, the spatial arrangement of the tripeptide seems to be crucial. This can be the explanation why turn linker motifs have a higher occurrence in the GC results than the linear flexible linkers (see the detailed table of the GC results in the experimental part).

The chemically reduced library **1** has a higher diversity in colour of the beads the same is true for the tripeptide sequences found after GC analysis. (**Table 3.4-2**).

**Table 3.4-2:** AgNPs formation by reduction of Ag<sup>+</sup> with sodium ascorbate (chemical reduction, CR), most often found sequences after GC analysis (“X”: random linker)

Colour	AA1	X1 (linker)	AA2
Dark red/red/ dark orange beads	Ac-D/L-His	X	D/L-His
	Ac-D/L-His	X	D/L-Asp
	Ac-D/L-Asp	X	D/L-His
	Ac-D/L-His	X	L-Tyr
	Ac-L-Tyr	X	D/L-His
	Ac-D/L-His	X	D/L-Ser
	Ac-D/L-Ser	X	D/L-His
yellow/light orange beads	Ac-D/L-Asp	X	D/L-Asp
	Ac-D/L-Ser	X	L-Tyr
	Ac-L-Tyr	X	D/L-Ser
	Ac-D/L-Asp	X	D/L-Ser
	Ac-D/L-Ser	X	D/L-Asp

The occurrence of the histidine amino acid is very high, as well the aspartate and the serine. These amino acids have a high affinity towards the silver ions. This seems to be the determining factor for the colouration of the beads. Compared with the LR, the rigid turn-inducing linkers and the tyrosine have lost their predominant important role during the reduction with sodium ascorbate.

### 3.4.3 Silver affinity and AgNP generation of tripeptides on solid support

After the evaluation of the results of library **1**, further investigations were done on some active tripeptide structures using SEM, EDAX and powder X-ray spectroscopy techniques to characterize the particles, their size and distribution, and to understand the formation of the nanoparticles. To determine the loading of silver on the different T-gel beads, the AAS technique was used.

The synthesized tripeptide sequences are split into different groups. In the first group, tripeptides contain the sequences that were found to be positive after analysing the LR library **1**. The prepared positive sequences contain histidine, serine and tyrosine and a rigid turn-inducing linker (Achc). Some negative control sequences were also synthesized; these are not present among the sequences found by GC analysis. In the second group, tripeptide sequences are present with amino acids found in a high occurrence after the GC analysis of the CR library **1**. Those tripeptide sequences, found in the last group, were prepared for another purpose, for example as the model sequences or tripeptides for solution experiments.[2] All sequences were completely analyzed independently of which group they belong to and are attached on the beads. The tripeptides synthesized in TG are treated in a same way as the library **1**. The beads are incubated in  $\text{AgNO}_3$  solution, then washed and reduced by light or sodium ascorbate. Then the samples were photographed, dried, and SEM measurements were done. The silver ion uptake of the beads was calculated by measuring the remaining silver ion concentration in the treating solution, using AAS. Some reduced T-gel beads were measured by powder X-ray to identify the nanoparticles on the surface **Fig.3.4-11**. These measurements could be made only on samples with the coverage high enough to detect the crystalline structure on the surface.

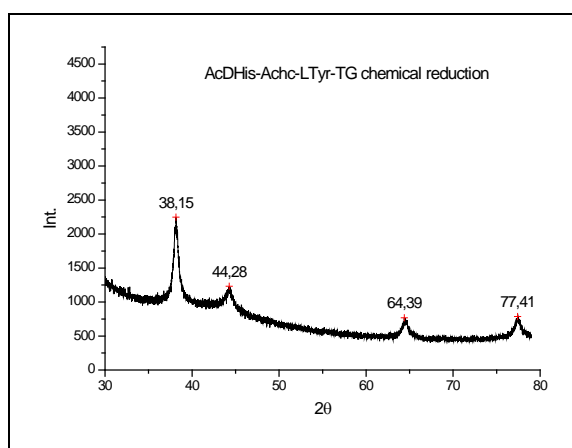


**Figure 3.4-11:** Example of powder X-ray spectra of the AgNPs on the beads

## 3.4.3.1 Light reduction

The results of the first group of the tripeptides are listed in **Table 3.4-3**, and some representative images are shown in **Fig.3.4-12**. The compositions of the sequences have been chosen accordingly to the GC analysis of the light reduced library **1** and the representative sequences were synthesized. Negative control sequences were also synthesized to compare the affinity for silver and the behaviour toward light reduction.

Peptides-NHTG	Light reduction		Chemical reduction		Uptake mMAg/ mM pept
	Color	NP size (nm)	Color	NP size (nm)	
AcDHis-Achc-LTyr	Red	300-500nm	Dark red	100-200nm	0.67
AcLHis-Achc-LTyr	Red	300-500nm	Dark red	100-200nm	0.60
AcLSer-Achc-LTyr	Orange	>500nm cryst.	Yellow	≤ 50nm	0.33
AcDSer-Achc-LTyr	Orange	> 1 μm cryst.	Yellow	≤ 50nm	0.35
AcLTyr-Achc-DSer	Orange	> 1 μm cryst.	Yellow	≤50nm	0.34
AcDHis-proAib-LTyr	Colourless	-	Dark red	200-300nm	0.68
AcLSer-proAib-LTyr	Colourless	>700nm rare	Colourless	Rare 100 isol.	0.18
AcLSer-proAib-LSer	Colourless	> 1 μm cryst.	Colourless	-	0.23
AcLTyr-LTyr	Colourless	500-1000nm rare	Colourless	> 1 μm rare	0.23
AcLTyr-LGly-LTyr	Colourless	>1 μm isol.cryst.	Colourless	-	0.31
AcDAsp-βAla-DAsp	Colourless	> 400nm aggr.	Grey	250-1000nm	0.37
Tripeptide sequences, positive and negative controls, for light reduction					
AcDHis-Gly-LTyr	Grey	2-300nm	Dark red	cov. agg.+100nm	0.80
AcDHis-LTyr	Grey	500nm cryst.	Red	100-200nm	0.44
AcDHis-LHis	Red	1-200nm isol.	Dark red	1-200nm aggr.	0.81
Tripeptide sequences to test the spacial effect on the NP generation					

**Table 3.4-3:** The first 14 tripeptide sequences, synthesized as positive and negative controls for light reduction, and their complete analysis

The results confirm a very high selectivity for a turn inducing linker and tyrosine. **Fig.3.4-12a,b,c** show the optical microscope images of two active sequences: AcDHis-Achc-LTyr-TG and AcLSer-Achc-LTyr-TG and the negative control sequence AcDHis-LHis-TG.



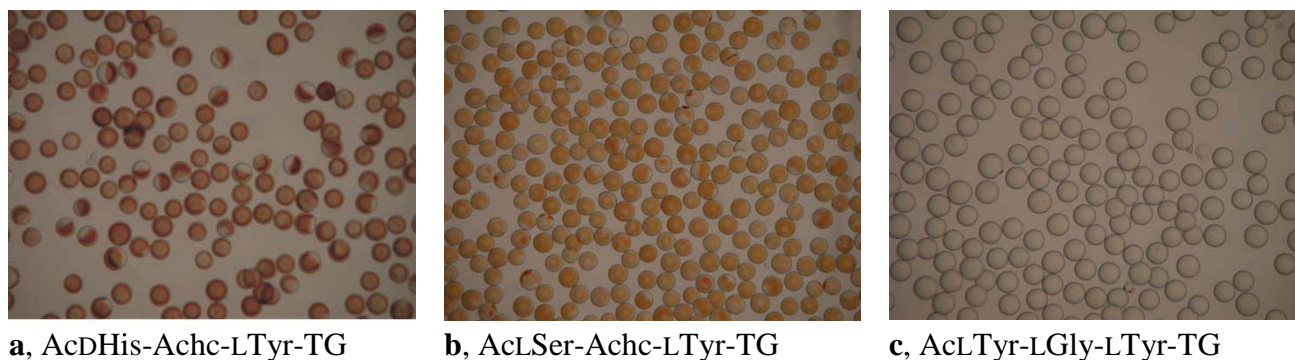


**Figure 3.4-12a,b,c:** Optical microscopic images of the  $\text{Ag}^+$  incubated and light reduced (LR) different tripeptide containing beads

The colour of the beads is darker in the case of the AcDHis-Achc-LTyr-NHTG than that other active sequence AcLSer-Achc-LTyr-NHTG. Silver uptake measurements were done to measure the affinity of the tripeptide sequences towards silver ions. The AcDHis-Achc-LTyr-NHTG has a higher uptake, thus higher affinity to silver ions than the AcLSer-Achc-LTyr-NHTG. Also, the first peptide shows darker coloured beads than the second one. (Darker colour means generally larger NPs.) The most active sequence AcDHis-Achc-LTyr-NHTG contains a good silver complexing molecule, His and a photoactive residue, Tyr. Their special spatial arrangement is controlled via the Achc turn inducing linker. This suggests that the collective presence of the three influencing factors namely: a good complexing amino acid, a photoactive residue and good spatial arrangement, results in  $\text{Ag}^+$  uptake and thus the AgNPs formation. If one of these conditions is missing, the tripeptide would not favour the AgNP formation by light, as for instance the negative control sequence AcLTyr-LGly-LTyr-NHTG. Although the AcLTyr-LGly-LTyr-NHTG has a photoactive residue, the affinity towards silver ions is not high enough and does not show colouration by this reducing method. The sequences presented in the **Table 3.4-3** confirm that the tripeptide sequence should fulfil the three conditions described above simultaneously to generate AgNPs on the surface via light reduction. If the tripeptide doesn't contain any photoactive residue as the AcDAsp- $\beta$ Ala-DAsp-NHTG or AcLSer-proAib-LSer-NHTG there is also no AgNPs formation on the surface. The sequences missing a good silver complexing group, AcLTyr-LTyr-NHTG and AcLTyr-LGly-LTyr-NHTG or having an unfavourable spatial arrangement, AcLSer-proAib-LTyr-NHTG and AcDHis-proAib-LTyr-NHTG are also inactive for the light reduction. If all of the three conditions are fulfilled, the affinity of the tripeptide seems to be the colour determining factor. The darker the colour, the larger are the AgNPs, which are present. The uptake measurements determine the quantity of the silver ions remaining on the surface after

incubation in  $\text{AgNO}_3$  solution, and are thus representative for the silver affinity of the tripeptide.

The uptake measurements show a significant affinity of the sequences containing histidine amino acid. The two histidine containing tripeptides have such a high affinity, uptake (0.81 mM  $\text{Ag}/\text{mM}$  peptide) that the light reduction takes place even without any photoactive residue. The silver ions are probably attached so close to each other that the light initiates the autocatalytic photo reduction. The above described results demonstrate the weakness of this reducing method, namely that it is not possible to detect all of the sequences attaching silver ions.

Before analysing the tripeptide sequences prepared to study the reduction with sodium ascorbate, **Fig.3.4-13,14** presents an example comparing the two methods in case of the photo reducible tripeptide AcDHis-Achc-LTyr-NHTG.

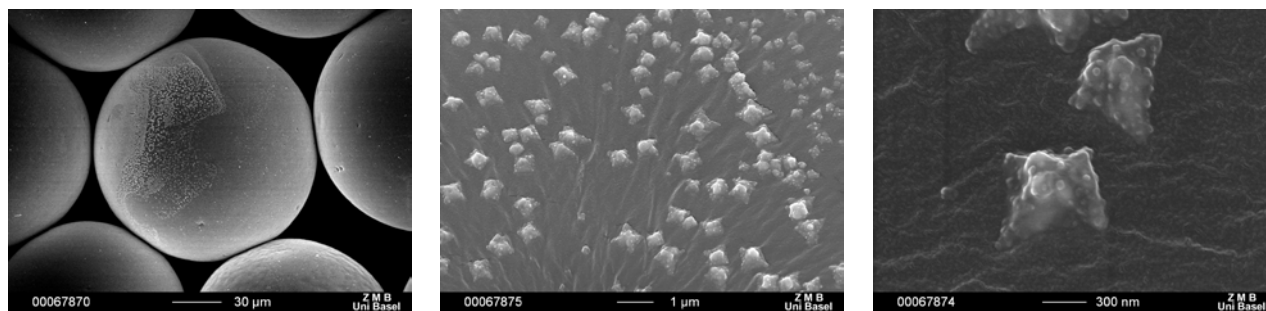


**Figure 3.4-13:** SEM images of the AcDHis-Achc-LTyr-TG, tripeptide after  $\text{Ag}^+$  incubation and light reduction (LR)

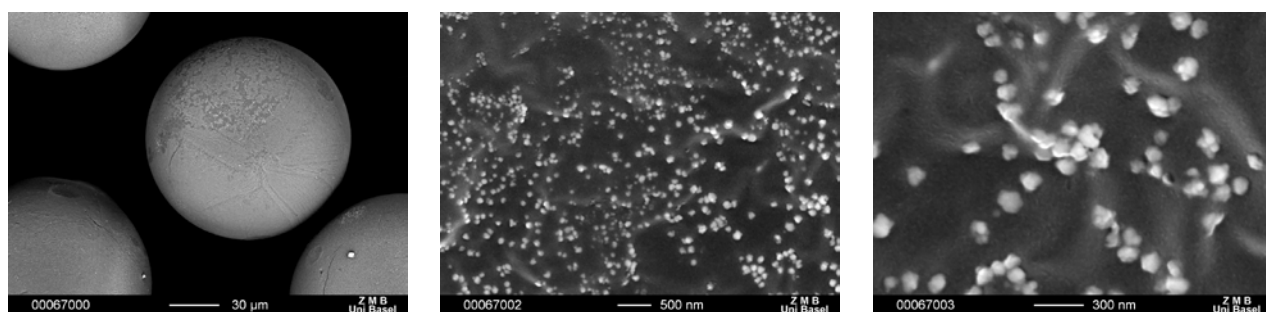


**Figure 3.4-14:** SEM images of the AcDHis-Achc-LTyr-TG, tripeptide after  $\text{Ag}^+$  incubation and chemical reduction (CR)

The SEM images show a big difference between the two samples. The most remarkable difference can be observed in the shape of the AgNPs. In the case of the light reduced sample, 500nm size crystalline AgNPs can be observed in inhomogeneous distribution. This is in contrast to the light reduced sample, where the bigger aggregates of small AgNPs are covering homogeneously the whole surface. This difference can be explained by the mechanism of the two reducing methods. The light reduction takes place during 8 hours, which is a long process allowing enough time for the crystallisation.

Since the samples are irradiated from the top of the sample, the reduction effect is inhomogeneous, thus the AgNPs formation will be strong on the irradiated side of the bead and weaker on the shaded side. The reduction achieved in this way is not complete. To prove this incompleteness of the reduction, further AAS measurements were carried out. The measurements show that the percentage of the unreduced silver ions can vary between 78% for AcLHis-Gly-LHis-NHTG and 25% for AcDHis-LHis-NHTG. The iso-TG has around 50% ionic silver after light reduction. The light reduced beads are not photostable since no fixation process for the AgNPs, as it is generally used in photography to remove unreduced silver ions, was done, thus the ionic/metal silver ratio can change with the time and the AgNPs formation continues further when exposed to light.

### 3.4.3.2 Chemical reduction

Comparing the SEM images of the two reduction methods of the tripeptide AcDHis-Achc-LTyr-NHTG **Fig.3.4-13,14**, the main differences become visible. As opposed to the photo reduction, the chemical reduction takes place in some minutes in the solution of sodium ascorbate. Hence, the reducing effect is homogenous and fast, there is no time for a crystallisation process. Some small aggregates are formed covering the surface. As this tripeptide forms different AgNPs after chemical reduction from those of light reduction, the other peptides also react differently. Library 1 shows higher diversity in colour and this increases the diversity in AgNP size. To study the AgNPs generation of the tripeptides by chemical reduction, the following sequences, listed in **Table 3.4-4**, were synthesized.

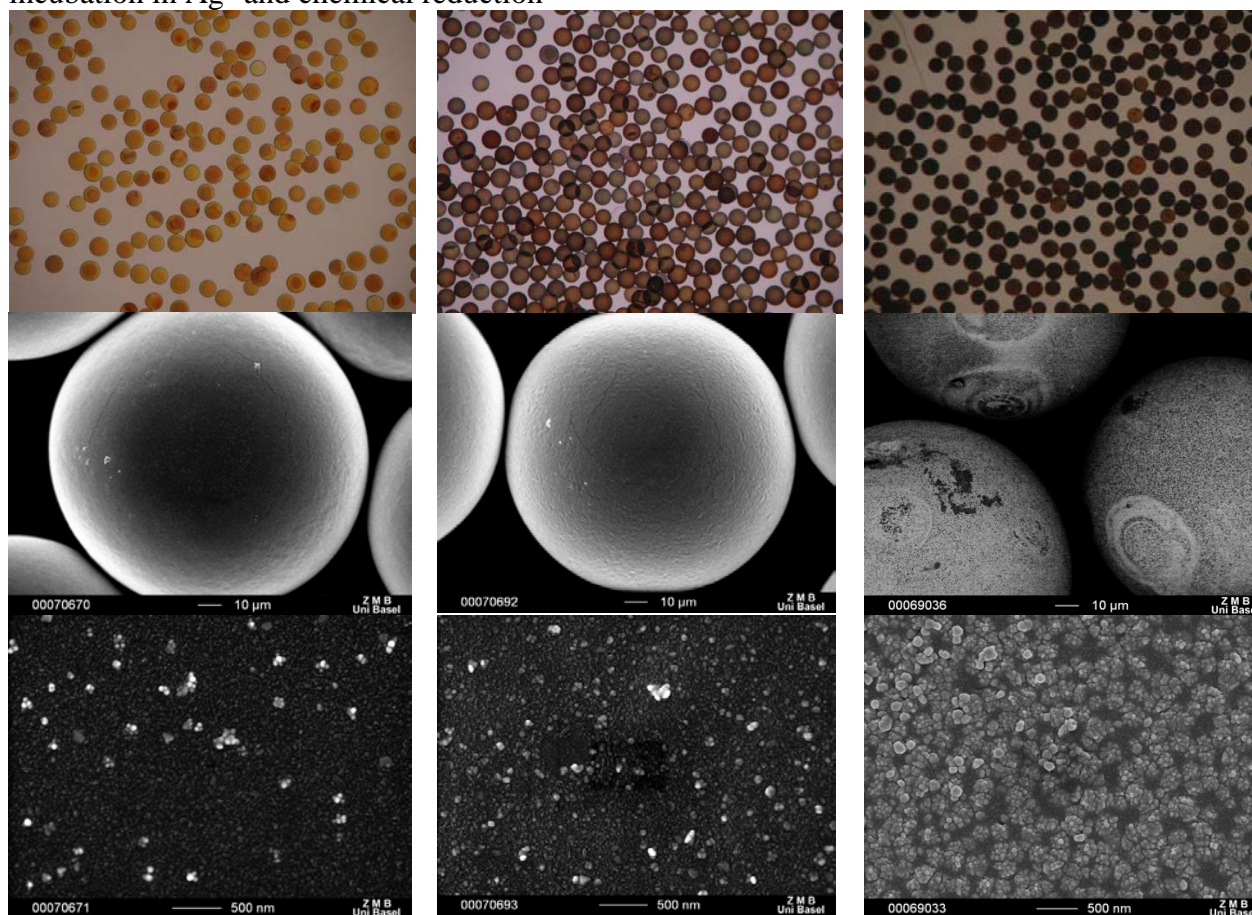
Peptides-NHTG	Light reduction		Chemical reduction		Uptake mMAg/ mM pept
	Colour	NP size (nm)	Colour	NP size (nm)	
AcLAsp-ProGly-LAsp	Colourless	>1 $\mu$ m isol.	D. grey	400-1000nm aggr.	0.57
AcLHis-Gly-LHis	Red	500nm isol.	D. red	100-200nm	0.71
AcDHis-ProAib-LAsp	Colourless	1-300nm cryst.	D. yellow	<100nm aggr.	0.44
AcDHis-Gly-DAsp	Colourless	>500nm isol.	D. orange	1-200nm aggr.	0.58
AcLHis-ProGly-DAsp	Colourless	2-300nm cryst.	Orange	2-500nm aggr.	0.64
AcLAsp- $\beta$ Ala-DHis	Colourless	2-400nm	D. yellow	1-200nm cov.	0.59
AcLSer- $\beta$ Ala-LHis	Red-grey	1-200nm isol.	Red	1-200nm cov.	0.70
AcLAsp-Achc-LTyr	L.rosa	-	Grey	~400nm aggr.	0.37

Tripeptide sequences for chemical reduction

**Table 3.4-4:** Second 8 tripeptide sequences, synthesized as positive controls for chemical reduction, and their complete analysis

To analyse the results, the tripeptides of the first group (**Table 3.4-2**) were also used. The first important observation should be made regarding the colour of the beads. The synthesized sequences show the same diversity in colour as in library **1**. In **Fig.3.4-15**, three peptides are shown comparing their colours, their SEM images, AgNP size and distribution.

**Figure 3.4-15a,b,c:** Optical microscopic and SEM images of the three tripeptide sequences **a:** AcDHis-ProAib-LAsp-TG, **b:** AcLSer- $\beta$ Ala-LHis-TG and **c:** AcDHis-LHis-TG after incubation in  $\text{Ag}^+$  and chemical reduction



**a,** AcDHis-ProAib-LAsp-TG, **b,** AcLSer- $\beta$ Ala-LHis-TG, CR **c,** AcDHis-LHis-TG, CR  
CR

The AgNPs present on the surface of the different coloured beads show a big difference in their size and diversity. The light yellow, coloured beads of AcDHis-ProAib-LAsp-NHTG have aggregates of maximum 100nm on the surface. The red beads of the AcLSer- $\beta$ Ala-LHis-NHTG have larger aggregates and higher coverage on the surface, but the coverage does not reach the level of that of the AcDHis-LHis-NHTG peptide. There, the complete coverage can be observed by the dark beads of the AcDHis-LHis-NHTG, and the size of the AgNPs is difficult to determine. Ca. ~50nm sized grains stick together, covering the whole surface. This is a good example for the fact that the colour of the beads is determined by the size and the

distribution of the AgNPs. The other important observation concerns the relationship between the colour of the beads after the chemical reduction and the silver affinity of the peptides.

**Table 3.4-5:** Summary of the colour of the TG beads, 20 different tripeptide sequences, after CR and their Ag<sup>+</sup> uptake

Peptide-NHTG	Colour after CR	Uptake	NPs on the surface
AcLSer-proAib-LTyr	Colourless	0.18	Rare 100 isol.
AcLSer-proAib-LSer	Colourless	0.23	-
AcLTyr-LTyr	Colourless	0.23	> 1 $\mu\text{m}$ rare
AcLSer-Ahx-LTyr	Yellow	0.26	<50nm cov
AcLSer-Achc-LTyr	Yellow	0.33	$\leq 50\text{nm}$
AcDSer-Achc-LTyr	Yellow	0.35	$\leq 50\text{nm}$
AcLTyr-Achc-DSer	Yellow	0.34	$\leq 50\text{nm}$
AcDHis-ProAib-LAsp	D. yellow	0.44	<100nm aggr.
AcDHis-Gly-DAsp	D.orange	0.58	1-200nm aggr.
AcLHis-Ahx-LAsp	D.orange	0.55	1-300nm aggr.
AcLHis-ProGly-LAsp	D.orange	0.47	50-200nm cryst..
AcDHis-LTyr	Red	0.44	100-200nm
AcDHis-Achc-LTyr	Dark red	0.67	100-200nm
AcLHis-Achc-LTyr	Dark red	0.60	100-200nm
AcDHis-proAib-LTyr	Dark red	0.68	200-300nm
AcLHis-Gly-LHis	Dark red	0.71	100-200nm
AcDHis-Gly-LTyr	Dark red	0.80	cov. aggr.+100nm
AcDHis-LHis	Dark red	0.81	1-200nm aggr.
AcLAsp-Achc-LTyr	Grey	0.37	$\sim 400\text{nm}$ aggr.
AcDAsp- $\beta$ Ala-DAsp	Grey	0.37	250-1000nm

**Table 3.4-5** shows, that contrary to the light reduction method, the reduction with sodium ascorbate detects silver ions attached on the surface, independently on the conformation of the peptide or the presence of a photoactive residue. Therefore, this method is more sensitive on silver ions but much less specific for the tripeptide sequences than the photo reduction method. The colour of the beads has a direct relationship with the silver affinity of the peptides. The higher the uptake means darker colour of the beads. The uptake for the colourless, yellow, orange and dark red beads are around 0.20, 0.30, 0.50 and 0.70 mM Ag/mM peptide, respectively. The size of the aggregates of NPs on the surface is increasing in the same way. Interestingly, in the histidine containing tripeptides, the grain size of the AgNPs is more or less the same, but the size of the aggregates and coverage is increasing with the uptake and the colour gets darker. If the sequence does not contain any histidine, the size of the AgNPs and thus the colour of the beads is different: e.g. for AcLAsp-Achc-LTyr-TG and AcDAsp- $\beta$ Ala-DAsp-TG sequences. Although the uptake of these sequences is not so high, around 0.40 mM Ag/mM peptide, the dark colour is present, but in a different tone: not

yellow-orange but grey, and the size of the AgNPs is also larger than in the case of the histidine containing peptides. The other peptides, containing different amino acids than histidine, are the serine containing peptides. As the affinity towards silver ions of these peptides is weaker, the uptake is low and the AgNPs size is also small, thus the colour of these beads is light.

### 3.4.3.3 Other complementary experiments with the solid phase tripeptide sequences

The previously made observations are confirmed by the last group of the tripeptide sequences on T-gel listed in **Table 3.4-6**. The colour of the beads after chemical reduction depends on the uptake, and only the two histidine containing tripeptides show some colour after light reduction.

**Table 3.4-6:** Other complementary tripeptide and model sequences and their analysis

Peptides-TG	Light reduction		Chemical reduction		Uptake mMAg/ mM pept
	Colour	NP size (nm)	Colour	NP size (nm)	
AcLHis-Ahx-LAsp	Colourless	No cryst. mater.	D.orange	1-300nm aggr.	0.55
AcLHis-ProGly-LAsp	Colourless	No cryst. mater.	D.orange	50-200nm cryst..	0.47
AcLHis-Ahx-LHis	L.red	>500 aggr.	D.red	50-100nm cov.	0.38
AcLHis-ProGly-LHis	Red	50-100nm cov.	D.red	>100 aggr.cov.	0.64
AcLSer-Ahx-LTyr	Colourless	>1 $\mu$ m isol.cryst.	Yellow	<50nm cov	0.26
AcLSer-ProGly-LTyr	Colourless	>100nm isol.	Yellow	<30nm cov	0.19
Tripeptide sequences prepared by C.P* for solution experiments					
Isonicotinic acid	Red spot	2-700nm cryst.	Grey	1-200nm aggr.	0.46
Ac-TGel	Colourless	> 1 $\mu$ m cryst.	Colourless	> 1 $\mu$ m	0.29
Model sequences					

Regarding the conformation of the rigid turn-inducing motif, all possible diastereoisomers of peptides AcDHis-Achc-LTyr-NHTG, AcDSer-Achc-LTyr-NHTG and Ac-LTyr-Achc-DSer-NHTG were re-synthesized and examined. The performed experiments, LR, CR, silver uptake measurements and SEM, of these sequences show essentially the same results, demonstrating that the absolute configuration of the amino acids is of minor importance for their activity. The same is true for the configuration of the amino acids. During the GC analysis of the library **1**, independently of the reduction method, any linker was found suggesting that the relative orientation of the two amino acids towards each other is not crucial for their activity. In both assays, no pronounced selectivity for L- or D-configured amino acids was observed. Cysteine containing tripeptide was also synthesized, to test a sulphur containing amino acid sequence with silver treatment and both reduction methods. The measured uptake was not as



high as by histidine containing tripeptides (0.36 mM Ag/mM peptide). The SEM measurements did not show any AgNPs on the surface of the light reduced beads (colourless beads), and just some very small AgNPs (less than 30nm) after reduction with sodium ascorbate. The cysteine attaches the silver probably so strongly that it hinders the AgNP formation and blocks the silver ion movement to build up larger aggregates.

#### ***3.4.4 Complementary experiments in solution***

Besides the tests on solid phase peptides, some other experiments were done in solution. The **TEM** and **UV** studies [194] show the AgNPs formation also in solution phase.

**NMR** studies were done on AcDHis-*rac*Achc-LTyr-NH<sub>2</sub> tripeptide to determine which groups are involved in the NP generation and which are the silver binding sites of the peptide. For this purpose, the NMR spectra of 2.2mM peptide in D<sub>2</sub>O/H<sub>2</sub>O with different equivalents of Ag<sup>+</sup> (AgNO<sub>3</sub> solution) in H<sub>2</sub>O, were measured. As the racemic mixture of the Achc molecule was used, both diastereomers can be found in the sample solution. Using different equivalents of Ag<sup>+</sup>, the proton signal of the binding sites will be shifted with the increase of the silver concentration. In **Fig.3.4-16,17** and **Table 3.4-7**, the most important signal and their shifts are presented.

**Figure 3.4-16:** Schema of the conformation of the AcDHis-*rac*Achc-LTyr-NH<sub>2</sub> tripeptide

**Figure 3.4-17:** Chemical shifts of the <sup>1</sup>H signals without Ag<sup>+</sup> and 700 eq. concentration Ag<sup>+</sup>

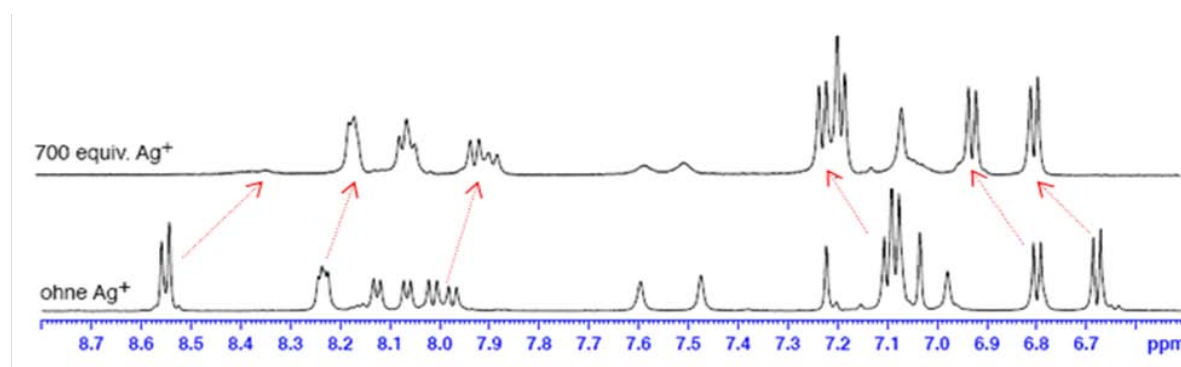


**Table 3.4-7:** Shift of some  $^1\text{H}$  signals in function of the  $\text{Ag}^+$  concentration

	Eqv. $\text{Ag}^+$	$\text{H}\epsilon$ -TyrSS	$\text{H}\epsilon$ -TyrRR	NH-turnRR	$\text{H}\delta$ -TyrSS	$\text{NH}\epsilon$ -HisRR
Ref.signal [ppm]	0	6.80	6.68	8.02	7.10	8.54
Shift [Hz]	4.91	2.83	2.43	1.41	2.43	2.94
	24.6	4.99	4.86	7.17	5.38	18.2
	98.0	13.7	12.3	20.9	14.3	48.6
	250.8	31.2	28.7	35.5	32.0	77.6
	490.6	59.0	56.6	52.1	59.8	99.9
	702.4	70.9	69.4	57.2	71.2	108.3

The results show a significant shift of the  $\epsilon$  proton of the imidazole side chain, the proton of the peptide bond between the Achc linker, and the histidine and the different protons of the tyrosine side chain. This latter suppose the interaction between the silver ion and the aromatic ring of the tyrosine, having a contact between the  $\pi$  system and the  $\text{Ag}^+$ . The shift of the histidine imidazol proton confirms the previous observation, that the main binding site is the histidine with its two N donor atoms. Different studies were done to describe the complexing behaviour of histidine towards silver ions [195] Generally, the silver tends to prefer coordination with N donor atoms compared to O atoms. In the histidine molecule, there are 3 nitrogen atoms (1 amine and 2 imidazole). From the imidazol N-atoms only one is able to coordinate silver at a time so it means one possible coordination site, thus two N sites are available, one imidazole and one on the amino N-atom. There are two carboxylic oxygen atoms that could be available sites and interact with the metal. Depending on the pH, it gives many possibilities to form complexes resulting in different structures. Nomiya et al. [195] prepared a histidine silver polymer  $[\text{Ag} - \text{His}]_n$  from  $\text{Ag}_2\text{O}$  under basic conditions where the crystal structure formed a 1-D chain consisting of a 2-coordinated silver(I) atom linking with the N-amino atom in one His - ligand and the N-imidazole atom in a different His - ligand, in which the carboxylic oxygen atoms do not participate in the coordination to the silver(I) centre. This type of structure formation is confirmed by the works of Mirolo [196]. Under basic condition silver histidine complex from  $\text{AgNO}_3$  was prepared, it contains silver

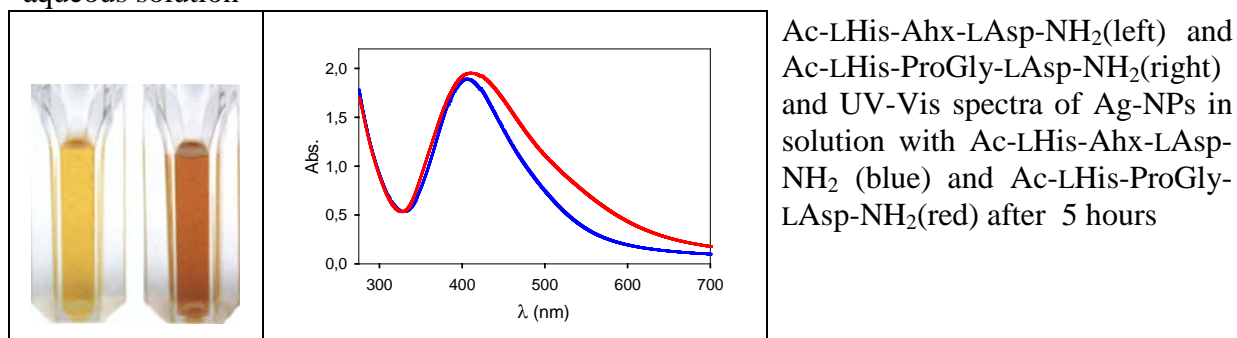


atom coordinating with one histidine by the amino group and to another histidine by its imidazole nitrogen, which is similar structure as the polymer prepared with  $\text{Ag}_2\text{O}$  by Nomiya. In the silver histidine complex prepared under neutral conditions from  $\text{AgNO}_3$  [ $\text{Ag}(\text{LHistidine})(\text{NO}_3)_2 \cdot 2\text{H}_2\text{O}$ ], the silver is attached to two imidazol nitrogen atoms from two different histidine molecules. If the silver complex is prepared in acidic solution, the silver forms a network with histidine  $\{[\text{Ag}(\text{LHistidine})(\text{NO}_3)_2] \cdot 2\text{H}_2\text{O}\}_n$  through complexation with the only available atoms, the carboxylic oxygen donors. The pH of the solution during the crystallisation has thus a big impact as it determines the possible coordination sites for the silver.

As for NMR measurements, the experiments were carried out at neutral pH, thus the binding of the silver by the imidazol N of the histidine is confirmed by the previous results. Using the NMR measurements, the binding constant of the peptide to  $\text{Ag}^+$  was calculated. The determined very weak complexation constant of 2.13M is probably due to the TFA salt, which was used during the measurement. To determine the binding constant of the free peptide, further investigations should be done.

Other solution experiments were done by Conelious Pfumbidzai: analyze if the identified peptides are also able to induce the formation of Ag-NPs in solution phase. Experiments were done with  $\text{Ac-L-His-Ahx-L-Asp-NH}_2$  and  $\text{Ac-L-His-ProGly-L-Asp-NH}_2$  peptides. Upon mixing of aqueous solutions of these peptides with  $\text{AgNO}_3$  (0.1 equiv.) followed by addition of sodium ascorbate (0.12 equiv.) the solutions turned yellow and orange respectively (**Figure 3.4-18**). These colours are indicative of solutions containing Ag-NPs. This is supported by the absorption maximum at 408 nm observed in the UV-Vis spectra of the Ag-NPs derived from these peptides, which is typical for Ag-NPs.

**Figure 3.4-18:** AgNPs formation by tripeptide in aqueous solution



### 3.4.5 Conclusions

The developed two reduction methods, light reduction and chemical reduction with sodium ascorbate, are suitable to detect silver ions attached on the surface of the solid-phase bound peptides. Both methods operate with nanoparticle generation. The size and distribution of the AgNPs depend on which tripeptide sequences are used. Both reduction methods have their advantages and disadvantages:

The light reduction method is suitable to detect higher uptakes and light sensitive structures, such as Tyr containing sequences. The spatial conformation of these sequences is also important; if the turn linker keeps the complexing site, e.g. His, close to the photoactive site, Tyr, of the peptide, the photo reduction is more pronounced, and thus the AgNP formation is more developed. The reduction of the silver ions through light is slow, allowing enough time for crystallisation, which results in larger, well designed structures. The silver ion reduction to  $\text{Ag}^0$  is not complete and part of the  $\text{Ag}^+$  remains in ionic form attached to the surface.

The reduction with sodium ascorbate results in a complete reduction of the ions to NPs. The colour of the beads depends of the size of the NP and their aggregates. Since the size and distribution of the AgNPs depends directly on the quantity of the silver ions present on the surface before reduction, the colour of the beads is a good indicator of the silver affinity to the tripeptide sequences. Different tripeptide sequences attach the silver in different quantity, the AgNP size and distribution depend on the tripeptide sequences. That means: using defined tripeptide sequences, different sized AgNPs can be generated.

The control of the AgNPs by tripeptides points out a further biological utilisation. Generally, the AgNPs in medicine should be size controlled, and attaching these AgNPs on the surface of the material can foster an antimicrobial effect to the surface.

Regarding the affinity of the different amino acids to silver, the histidine is the most significant although both serine and aspartate have an affinity to the  $\text{Ag}^+$ . The tripeptides containing no histidine can show quite high uptake and also light reducible characteristics. This means that the histidine is not the only powerful Ag-binding amino acid (after the sulphur containing amino acids). The amino acids serine and aspartate can also play a role, probably much less significant than the histidine, in the different biological processes in the context of silver.

## 4 Conclusions

This thesis reports on novel antimicrobial silver containing coatings for implant materials. Several materials were successfully coated with silver coordination polymers and their antimicrobial activity was positively tested. In **Table 4-1**, a short summary of the results is presented:

Substrate	Active compound on the surface	Loading mg Ag/m <sup>2</sup>	Antimicrobial effect
Au(111) model surface	Silver coordination polymer	424	++
Titanium rough disks	Silver coordination polymer	403	++
Titanium smooth disks	Silver coordination polymer	429	++
Steel rough disks	Silver coordination polymer	201	+
Steel polished disks	Silver coordination polymer	224	+
Isonicotinate grafted polymer (crystallisation)	Silver coordination polymer	80	+
Isonicotinate grafted polymer (dip coating)	Silver coordination polymer	263	++
AcDHis-Achc-LTyr-N- peptide grafted polymer	Silver coordination polymer	84	+
Isonicotinate grafted polymer	AgNPs and/or Ag ions	390	AgNPs -/ Ag ions +
AcDHis-Achc-LTyr-N- peptide grafted polymer	AgNPs and/or Ag ions	568	AgNPs -/ Ag ions ++

**Table 4-1:** Short summary of the different coatings on various substrates

### Surface treatment and analysis

After preliminary tests, one of the previously described silver coordination networks of ethanediyl bis(isonicotinate) ligand (Adl7) has been chosen as surface coating. Different substrates were coated following the principle to attach the coating to the surface with covalent bonds. For this purpose, a disulfide molecule (bis 2-((4-pyridinylcarbonyl)oxy)ethyl disulfide) for the gold surface, isonicotinic acid molecule for some titanium samples and surface grafted isonicotinate or tripeptide (AcDHis-Achc-LTyr-N-) for polymer surfaces were used. Other surfaces (steel and some titanium substrates) were coated via electrostatic interaction between the surface and the coating. After the attachment of the anchor molecule,

the silver coordination polymer was built up on a surface using *in-situ* crystallisation or the alternating dip coating method. The coated surface shows a nanostructure of the silver compound. This nanostructure, with individual peaks from 10-100nm, is very homogenous for the coating attached with covalent bonds, and existing, but less homogenous for electrostatically attached coatings. There is a group of middle sized structures (1-50 $\mu$ m intervals) and another group of macro sized (up to 100 $\mu$ m), well designed crystals that are present on the surface. The crystallisation conditions, namely the crystallization time and the concentration of the treating solution determine the quantity of silver compound grafted on the surface according to the surface loading. **Fig.4-1** shows the example of the gold surface treatment by *in-situ* crystallisation:

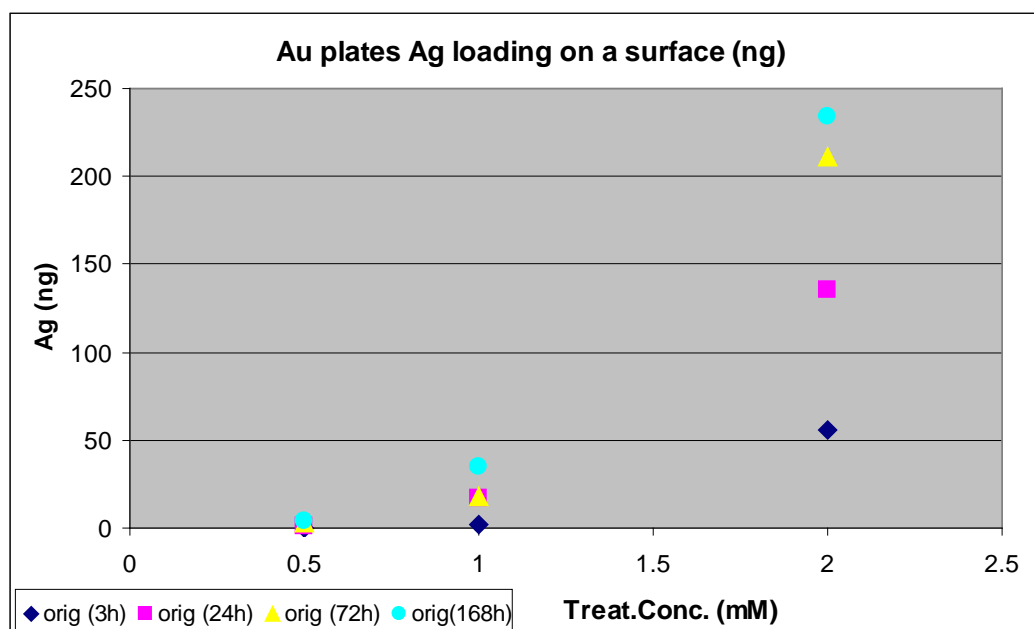


**Figure 4-1:** Ag loading on gold plate in function of the treating solution concentration and the crystallisation time

The longer the treating time and/or higher the concentration of the crystallization solution, the higher is the loading of the surface. Higher surface loading results in higher silver ion concentration in the solution above the coating. **Fig.4-2** shows the example of the different substrates having varying loading on the surface and respectively their silver release in Müller-Hinton biological medium. Choosing the appropriate crystallisation conditions, as the crystallisation time and concentration, the loading of the substrate can be determined and the silver release can be controlled.

## 4 Conclusion

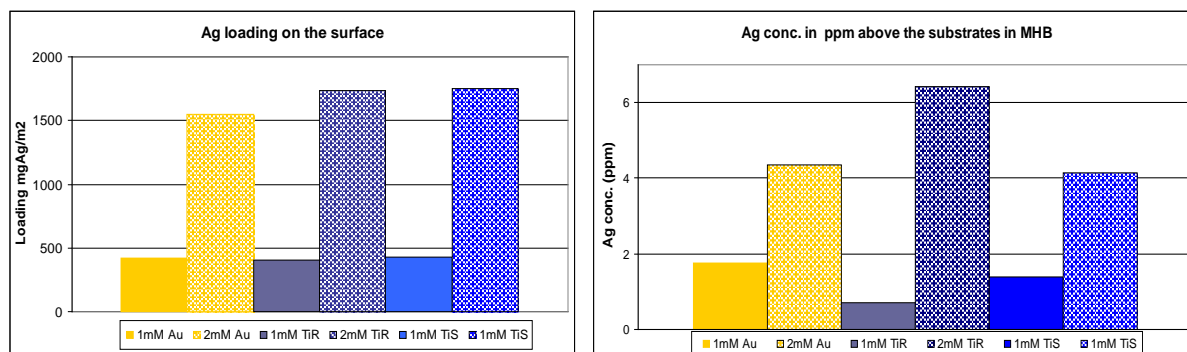


**Figure 4-2:** Silver loading on the surface and relating silver concentration in the solution above the coated sample

The silver ion concentration released by the material determines the effect of the coating: it is either inactive or active against the bacteria or eventually toxic for the living organism. The surface treatment method was optimized on each substrates and the best treatment conditions for each substrate and/or application are listed in **Table 4-2**.

Substrate	Application	Pre-treatment	Treatment
Au(111) model surface	<i>in vitro</i> microbiological assays	5mM disulfide in CH <sub>2</sub> Cl <sub>2</sub> /EtOH for 5 days	<i>In-situ</i> crystallization from 1mM [Ag(L1)NO <sub>3</sub> ] in EtOH/THF for 3 hours
Titanium rough (TiR) and smooth (TiS) disks	<i>in vitro</i> microbiological assays	-	<i>In-situ</i> crystallization from 2mM [Ag(L1)NO <sub>3</sub> ] in EtOH/THF for 3 days
Steel polished (StPol) and rough (StR) disks and cylinders	<i>in vitro</i> microbiological assays	-	<i>In-situ</i> crystallization from 2mM [Ag(L1)NO <sub>3</sub> ] in EtOH/THF for 3 days
Titanium rough (TiR) cages	<i>in vivo</i> microbiological assays	-	<i>In-situ</i> crystallization from 1mM [Ag(L1)NO <sub>3</sub> ] in EtOH/THF for 3 days
Gold alloy dental implant material	Flow chamber experiment	-	<i>In-situ</i> crystallization from 2mM [Ag(L1)NO <sub>3</sub> ] in EtOH/THF for 14 days
Titanium dental implant material	Flow chamber experiment	5mM isonicotinic acid in CH <sub>2</sub> Cl <sub>2</sub> /EtOH for 7 days	<i>In-situ</i> crystallization from 2mM [Ag(L1)NO <sub>3</sub> ] in EtOH/THF for 14 days

**Table 4-2:** Summary of the different substrates + application and their treatments

### Nanoparticles generation

Isonicotinate and peptide grafted polymers have been used to generate silver nanoparticles (AgNPs) on the surface. This was made for two purposes:

- to build up an antimicrobial coating from nanoparticles
- to study the molecular mechanism of the  $\text{Ag}^+$ .

For this goal, a combinatorial chemistry method was used. For the identification of peptides able to attach silver ions and induce the formation of AgNPs, a split-and-mix library was used. The different reducing methods serve to detect the attached silver on the surface as AgNP formation results in a colour change of the sample. The library and different peptide sequences on solid support were incubated in  $\text{AgNO}_3$  aq. solution and then two reducing methods were used: light and chemical reduction to generate AgNPs from the surface attached silver ions. The light reducing method was efficient on sequences fulfilling three conditions:

- they should contain a good silver complexing agent (as His or Ser),
- a photosensitive molecule and
- the spatial conformation of the sequences to allow the reduction of the ions.

AcD/LHis-Achc-LTyr-N- and AcD/LSer-Achc-LTyr-N- peptide sequences meet these conditions, having a red and yellow colour, respectively, after reduction. The distribution of the light generated AgNPs is neither homogenous nor is the reduction complete, however the AgNPs have well developed crystalline structures. This is issued from the characteristics of the illumination, which is inhomogeneous and slow enough to give time for crystallisation. The reduction with sodium ascorbate (chemical reduction) takes only few minutes in solution, which is a homogenous and fast reaction way, thus a complete reduction and poorly crystallized particles were generated. By this method, the photo sensibility of the sequence is not a requirement for the reduction to take place. The AgNPs generation depends on the concentration of the attached silver on the surface. Thus, this is a direct method to determine the silver affinity of the different tripeptide sequences. Here, all of the sequences having higher silver uptake than 0.25 mM Ag/ mM peptide show colouration. The colour of the surface due to the AgNPs becomes darker from yellow/grey to dark red/black with silver uptakes from 0.25 to 0.80 mM Ag/mM peptide, respectively. The different sizes of AgNPs result in this variety of the colours. This is more accentuated for the chemically reduced samples since there are no restrictive conditions for the AgNP generation. Generally, different peptides allow for the formation of AgNPs with different sizes using either light or a chemical reducing agent (sodium ascorbate). Regarding the molecular mechanism of the  $\text{Ag}^+$ , some main observations can be made: the key role of the His amino acid is confirmed. All of the histidine containing sequences showed affinity towards silver ions. Both, the serine and the

aspartame amino acid, attached the silver ions, due to their carboxyl containing side chains, which is a good complexing group for the silver ions. Although these amino acids have lower affinity towards silver than histidine, they could also play a role in the silver transport on a cellular level.

### Microbiological assays

Different *in vitro* microbiological assays have been done to test the antimicrobial properties of the developed coating. Isothermal microcalorimetric measurements determine the bacterial multiplication heat. This method was used to measure the activity of the free compound and the treated polymer surfaces against *S.epidermidis*. The antimicrobial activity of the silver polymer network coating on polymer surface depends on the loading of the surface and does not depend on the quality of the anchor molecule. Regarding the nanoparticle loaded surfaces, if only AgNPs are present on the surface (chemical reduced samples), no antimicrobial activity is observed. If the reduction is not complete and some silver ions remain on the surface (light reduced samples), the coated surface has antimicrobial properties. To achieve biologically active silver containing coatings, a release of oxidized form silver (Ag(I)) from the surface is thus necessary. The coated implant materials and gold plates were tested with the classical plating method in agar. Several bacterial strains were used, such as the gram positive *S.epidermidis* and *S.aureus*, the two principal responsible strains for the biofilm formation and infection of the implants, and the gram negative strain *E.Coli*. All of the coated implant materials were tested positively against the different bacterial strains. Coated titanium cages were used for *in vivo* assays. The after implantation, with *S.epidermidis* infected coated cages did not show any bacterial activity on the surface after one week. Some complementary microbiological assays were done on coated titanium and gold dental implant materials in a flow chamber, where the treated and untreated substrates were exposed to *S.sanguinis* (normal habitant of the oral flora, causing among others cavities) in sterilized saliva. The tests showed a dramatically decreased bacterial number on the coated substrates. The untreated samples showed ca.80% more living bacteria on the surface comparing to the silver treated samples. All these microbiological experiments confirm the general antimicrobial efficiency of the developed silver coordination network coatings on implant materials. Regarding the silver action mechanism inside of the cells, it seems that silver acts in several levels of the cells, probably disturbs the TCA cycle, hence the respiratory chain, but also acts at the level of DNA. To prove these theories, further investigations are required.

### Outlook

Following this study, further investigation should be done to improve the mechanical stability of these coatings. Since the silver coordination networks have a large diversity, other compounds, could be tried to tune the three important characteristics of the coating: structure, stability and solubility. Copper is also known for its antimicrobial activity [198] and ability to form coordination networks, hence, its ability to build up antimicrobial coatings should be studied. Further investigations could be done to work on the coating of different polymer surfaces. Regarding the biological assays, cell viability tests with fibroblasts are currently under investigation. Other trials with osteoblast cells should be done because the osseointegration of the implant is a crucial step towards healing.



## 5 Experimental part

### Abbreviations

Ac	acetyl
Ac <sub>2</sub> O	aceticacid anhydrid
Achc	<i>trans</i> -2-Aminocyclohexan Carbonacid
AcN	acetonitril
Ahx	aminohexanacid
Aib	$\alpha$ -Methylalanin
$\beta$ -Ala	$\beta$ -Alanin
Asc	ascorbate (Vitamin C)
Asp	aspartate
Aq.	aquoeus
BE	binding energy (eV)
Bead	Tenta-gel bead
BHI	brain-heart-infusion serum/medium
CR	chemically reduced
Cys	cystein
Disulfide	bis 2-((4-pyridinylcarbonyl)oxy)ethyl disulfide
DMAP	<i>N,N</i> -Dimethylaminopyridin
DMF	<i>N,N</i> -Dimethylformamide
DMSO	dimethylsulfoxid
EC-GC	electroncapture Gaschromatography
EDAX	energydispersiv Röntgenanalysis
ESI	Electron Spray Ionisation
eq	equivalent
EtOH	ethanol
EtOAc	ethylacetat
Et <sub>3</sub> N	etriethylamin
Et <sub>2</sub> O	diethylether
Fmoc	9-Fluorenylmethoxycarbonyl
GC	gaschromatography
Gly	glycin
h	hour(s)
HCTU	<i>O</i> -( <i>1H</i> -6-chlorobenzotriazol-1-yl)1,1,3,3-tetramethyluronium hexafluorophosphat
His	histidin
HPLC	High Pressure Liquid Chromatography
ica	isogenic biofilm negative bacterial strains
IMC	Isothermal Microcalorimetry
iso-TG	isonicotinic acid coupled tenta-gel beads
u. v.	under vacuum
<i>J</i>	coupling constant in Hertz
kcal	kilocalorie
LR	light reduction
MeOH	methanol
MHA	Müller-Hinton agar
MHB	Müller-Hinton medium
MHz	megahertz

min	minute(s)
MRSA	methicilin-resistant <i>Staphylococcus Aureus</i>
MRSE	methicilin-resistant <i>Staphylococcus epidermidis</i>
MS	mass spectrometry
m/z	mass/charge
nm	nanometer
NMR	Nuclear Magnetic Resonance
NP	nanoparticle
ppb	parts per billion
ppm	parts per million
quant.	quantitative
rac	racemic
RT	room temperature
SAM	self assembled monolayer
SEM	Scanning Electron Microscopy
SM	synthetic medium
StR	rough steel restorative implant material
StPol	polished steel restorative implant material
TFA	2,2,2- trifluoroacetic acid
TG, T-Gel	TentaGel-Resin
THF	tetrahydrofuran
TiR	rough titanium restorative implant material
TiS	smooth titanium restorative implant material
TRIS HCl	tris(hydroxymethyl)aminomethan hydrochlorid
turn	structure determinative Element
Tyr	tyrosin
UV-Vis	ultraviolet-visible
W	watt

## 5.1 Equipments and materials

### 5.1.1 Analytical equipments

**<sup>1</sup>H-NMR** Bruker Avance 400 (400 MHz), Bruker 500 DRX (500 MHz)

Chemical shifts ( $\delta$ ) are given in ppm and refer to Tetramethylsilan as internal Standard ( $\delta_{\text{TMS}} = 0.00$  ppm) or the solvent signal of  $\text{CDCl}_3$  ( $\delta = 7.26$  ppm),  $d_6$ -DMSO ( $\delta = 2.50$  ppm) or  $\text{CD}_3\text{OD}$  ( $\delta = 3.31$  ppm). All spectra of 1D or 2D experiments were analysed (COSY, NOESY, TOCSY) and the coupling constants ( $J$ ) are given in Hertz (Hz). The signals are indicated as follows: s = singlet, brs = broad singlet, d = doublet, brd = broad doublet, t = triplet, brt = broad triplet, q = quartet, quin = quintet, m = multiplet,  $\psi$  = pseudo. All the deuterated solvents were purchased from *Cambridge Isotope Laboratories*.

**<sup>13</sup>C-NMR** Bruker Avance 400 (101.1 MHz), Bruker 500 DRX (125.6 MHz)

Chemical shifts ( $\delta$ ) are given in ppm and refer to the solvent signal of  $\text{CDCl}_3$  ( $\delta = 77.1$  ppm),  $d_6$ -DMSO ( $\delta = 39.5$  ppm) or  $\text{CD}_3\text{OD}$  ( $\delta = 49.3$  ppm). All spectra are <sup>1</sup>H-coupled and assigned by 1D or 2D Experiments (DEPT, HMBC, HMQC). Quarternary C-Atoms are indicated as Cq.

**Mass spectroscopy** Bruker Esquire 3000 plus, Finnigan MAT LCQ (octapol)

The samples are 0.01 mg/mL or 0.1 mg/mL solutions in MeOH,  $\text{CH}_2\text{Cl}_2$  or  $\text{H}_2\text{O}$  and directly injected. The ion generation is made by electron spray ionisation (ESI). The values are given in atom mass per charge (m/z).

**Atomic Absorption Spectroscopy (AAS)** Shimadzu AA-6300

For all silver measurements, a combined Au/Ag lamp was used. The measurements were carried without any background correction; a simple standard method was used for the silver concentration determination. The standard concentrations are varied from 0.1 ppm to 8 ppm. All of the solutions contain  $\text{HNO}_3$  to keep the silver ions in solution, the concentration of the acid depending on the sample. In all of the measurements, appropriate blank solutions are measured.

**Scanning Electron Microscopy (SEM)** Philips ESEM XL 30 FEG and Hitachi S-4800

All of the measurements were made in the Zentrum für Mikroskopie in Pharmazentrum, Basel by Gianni Morson, Marcel Düggelein, Daniel Mathys or Eva Bieler and in the Department für Geowissenschaften in Fribourg. The T-Gel samples were sputtered with 5 nm Pt or Au and measured at 5 kV. The images were measured in two different modes namely: contrast or

back-scattering modus depending on the sample. Some EDAX spectra were taken with the same device.

### **Powder diffractometer** *STOE STADI P automatic Diffractometer*

Powder diffraction for all samples was measured on a STOE STADI P automated diffractometer, with CuK source, graphite monochromator, by using quartz sample holders; for the pure reagents, 10-25 mg of substance were used. The program PowderCell 2.2[23d] was used for calculation of X-ray powder patterns based on the single crystal structure determinations. Experimental and calculated patterns were then compared.

### **XPS** *Leybold EA 10N*

Equipped with an Mg K $\alpha$  (1253.6eV) X-ray source and with an experimental resolution of 0.8eV. The energy position of each spectrum was calibrated with reference to the 4f<sub>7/2</sub> level of a clean gold sample (84.9eV). Mathematical analysis of the XPS data was done using the software UNIFIT. XPS measurements were carried out at the Physics department of Basel by Dr. Teresa de los Arcos. For the T-Gel measurements, we used a Si(110) surface, for the others the previously mentioned substrates.

### **AFM** *PycoLE System*

Tapping mode AFM was performed, molecular imaging, with silicon nitride cantilevers, k ¼ 42 N/m, at a force set point 3.8 V and a scan rate of 1 line 1/s. Different positions on the sample were monitored. All experiments were performed on dry sample at room temperature.

### **Crystallography** *STOE IPDS-II diffractometer*

The measurement was done on a STOE IPDS-II diffractometer with monochromated graphite Mo K $\alpha$  radiation,  $\lambda = 0.71073 \text{ \AA}$ , equipped with an Oxford Cryosystems open flow cryostat [199]. The structure was solved with the SIR 2004 program [200] and refined by full-matrix least-square on F2 with SHELX-97 [201]. The non-H atoms were refined anisotropically and the hydrogen atoms were simulated and refined. The different representations of the compound were drawn with the Diamond program using a Pov Ray representation.

### **Microscope (reflection)** *Leitz Aristomet, Leica optic (Dept. of Physics of Univ. Basle)*

### **Microscope (transmission)** *Olympus Microscope SXZ12,*

### **Microscope-Camera** *Olympus Camedia C-3000 Zoom*

### **Peptide Synthesizer** *Syro I MultiTech GmbH*

**Isothermic Microcalorimetry** *TAM III-48, Waters-TA Instruments, New Castle DE, USA, 48 parallel Channels.* The measurements were carried out in the group of Prof. A.U. Daniels, LOB, University of Basel by Dr. Ueli von Ah and Dr. Olivier Braissant

### ***5.1.2 Solvents and chemicals***

All of the used chemicals and solvents were purchased in the highest quality. The solvents used for the chromatography were previously distilled. The water (nanopure water) used for all of the experiments and measurements, was filtered through a Barnstead Ultrapure Water System. TentaGel-NH<sub>2</sub>-Resin was bought from RAPP Polymere GmbH Tübingen (Deutschland) and the Rink-Amid-Polystyrolresine from Novabiochem (Schweiz). The protected amino acids were purchased from Bachem AG (Schweiz) and Novabiochem (Schweiz). Coupling reagents, isonicotinic acid, AgNO<sub>3</sub> and other chemicals (acids, NH<sub>3</sub> etc.) were bought from Fluka, Acros or Bachem AG. 1000 ppm silver standard solution was purchased from Fluka and Acros, the Au(111) plates from Arrandee.

## 5.2 Synthesis and chemical characterisation

### 5.2.1 *Ligand*

Isonicotinic acid (15 g, 0.122 mol) is stirred in SOCl<sub>2</sub> (40 mL) in the presence of DMF (0.6 mL) at 60°C for 12h. Excess thionyl chloride is removed *in vacuo*. Dried ethylene glycol (3.4 mL, 0.061 mol) is added. After the evolution of hydrogen chloride ends, the mixture is heated at 150°C for a few hours. The mixture is dissolved in water, and NH<sub>4</sub>OH is added. After filtration, recrystallization in ethyl acetate gives white crystals of **L**.

Yield 5,4 g (35%). Analysis calculated for C<sub>14</sub>H<sub>12</sub>N<sub>2</sub>O<sub>4</sub>: C 61.76, H 4.44, N 10.29; found: C 61.12, H 4.52, N10.11%. <sup>1</sup>H NMR (300MHz, CDCl<sub>3</sub>, 293 K):(ppm) 8.73 (4 H, m, H-pyr), 7.82 (4H, m, H-pyr), 4.69 (4H, s, H-ethyl).

### 5.2.2 *Bis 2-((4-pyridinylcarbonyl)oxy)ethyl disulfide*

Synthesis: DCC (4.13 g, 20.02 mmol) was added to a concentrated solution of isonicotinic acid 2.24 g, 18.20 mmol), 2-hydroxyethyl disulfide (1.404 g, 9.10 mmol), and DMAP (0.22 g, 1.82 mmol) in 20 mL of dichloromethane at 0 °C. After 1 h, the solution was allowed to warm to room temperature, and stirring was continued for 4 day. After removal of the precipitated dicyclohexylurea (DCU) by filtration, the product was recovered by extraction with CH<sub>2</sub>Cl<sub>2</sub>. After the CH<sub>2</sub>Cl<sub>2</sub> extract was washed twice with water, it was dried with magnesium sulfate and then evaporated on the rotavap. The bis 2-((4-pyridinylcarbonyl)oxy)ethyl disulfide was obtained by evaporation under reduced pressure and recrystallization with ethanol. The product was dissolved in methylene chloride and chromatographed on silica gel with ethyl acetate. Yield: 0.56g (17%) M: 364.0558 (C<sub>16</sub>H<sub>16</sub>N<sub>2</sub>O<sub>4</sub>S<sub>2</sub>); <sup>1</sup>H NMR (300MHz, CDCl<sub>3</sub>, 293 K):(ppm) 8.80 (d, 4H), 7.87 (d, 4H), 4.68 (t, 4H), 3.13 (t, 4H)

Elementary analysis calculated for (C<sub>16</sub>H<sub>16</sub>N<sub>2</sub>O<sub>4</sub>S<sub>2</sub>): C 52.73, H 4.43, N 7.69 and O 17.56, found: C 53.03 / 52.97 H 4.40 / 4.45 and N 7.54 / 7.58 %.

The single crystal X-ray measurements: Crystals of the disulfide were measured at the University of Basle and Fribourg by Laurent Mirolo. Diffractometer is a STOE IPDS-II diffractometer with monochromated graphite Mo K $\alpha$  radiation,  $\lambda=0.71073\text{\AA}$ , equipped with an Oxford Cryosystems open flow cryostat [199] with an absorption correction by analytical integration [200] The structure was solved with direct methods and refined by full-matrix least-square on F<sup>2</sup> with the SHELX-99 package [201].

**Table 5-1:****A - Crystal data and structure refinement for disulfide.**

Empirical formula	C <sub>16</sub> H <sub>16</sub> N <sub>2</sub> O <sub>4</sub> S <sub>2</sub>	
Formula weight	364.43	
Temperature	200(2) K	
Wavelength	0.71073 Å	
Crystal system	Monoclinic	
Space group	P2(1)/c	
Unit cell dimensions	a = 18.3640(4) Å	$\alpha = 90^\circ$
	b = 10.9400(4) Å	$\beta = 99.887(4)^\circ$
	c = 8.5540(9) Å	$\gamma = 90^\circ$
Volume	1692.99(19) Å <sup>3</sup>	
Z	4	
Density (calculated)	1.430 Mg/m <sup>3</sup>	
Absorption coefficient	0.337 mm <sup>-1</sup>	
F(000)	760	
Crystal size	0.23 x 0.19 x 0.11 mm <sup>3</sup>	
Theta range for data collection	2.18 to 26.75 °	
Index ranges	-23 ≤ h ≤ 22, 0 ≤ k ≤ 13, 0 ≤ l ≤ 10	
Reflections collected	13192	
Independent reflections	3580 / 3580 [R(int) = 0.0000]	
Completeness to theta = 26.75°	99.4 %	
Absorption correction	None	
Refinement method	Full-matrix least-squares on F <sup>2</sup>	
Data / restraints / parameters	3580 / 0 / 217	
Goodness-of-fit on F <sup>2</sup>	0.918	
Final R indices [I > 2σ(I)]	R1 = 0.0411, wR2 = 0.0868	
R indices (all data)	R1 = 0.0643, wR2 = 0.0935	
Largest diff. peak and hole	0.256 and -0.355 e.Å <sup>-3</sup>	

**Table 5-2.** Atomic coordinates ( $\times 10^4$ ) and equivalent isotropic displacement parameters ( $\text{\AA}^2 \times 10^3$ ) for disulfide.  $U(\text{eq})$  is defined as one third of the trace of the orthogonalized  $U_{ij}$  tensor.

	x	y	y	U(eq)
C(1)	3543(1)	-170(2)	-688(3)	45(1)
C(2)	4072(1)	290(2)	507(2)	36(1)
C(3)	4017(1)	1499(2)	933(2)	34(1)
C(4)	3426(1)	2182(2)	166(3)	48(1)
C(5)	2926(1)	1627(2)	-1003(3)	57(1)
C(6)	4585(1)	2105(2)	2146(2)	35(1)
C(7)	5639(1)	1779(2)	4125(3)	38(1)
C(8)	6043(1)	691(2)	4909(3)	41(1)
C(9)	8075(1)	724(2)	4850(3)	43(1)
C(10)	8223(1)	-345(2)	5957(3)	45(1)
C(11)	8682(1)	-692(2)	8666(3)	38(1)
C(12)	9528(1)	-250(2)	12939(3)	47(1)
C(13)	9205(1)	-808(2)	11548(3)	44(1)
C(14)	9022(1)	-105(2)	10192(2)	35(1)
C(15)	9167(1)	1140(2)	10307(3)	40(1)
C(16)	9483(1)	1609(2)	11765(3)	48(1)
N(1)	2976(1)	470(2)	-1447(3)	54(1)
N(2)	9671(1)	944(2)	13066(2)	49(1)
O(1)	4630(1)	3190(2)	2365(2)	53(1)
O(2)	5051(1)	1293(1)	2936(2)	41(1)
O(3)	8510(1)	-1755(2)	8539(2)	58(1)
O(4)	8596(1)	105(1)	7472(2)	41(1)
S(1)	6761(1)	1124(1)	6549(1)	42(1)
S(2)	7541(1)	1966(1)	5520(1)	44(1)

**Table 5-3.** . Bond lengths [ $\text{\AA}$ ] and angles [ $^\circ$ ] for disulfide

C(1)-N(1)	1.328(3)	N(1)-C(1)-C(2)	124.3(2)
C(1)-C(2)	1.379(3)	C(3)-C(2)-C(1)	118.09(19)
C(2)-C(3)	1.380(3)	C(2)-C(3)-C(4)	118.59(19)
C(3)-C(4)	1.387(3)	C(2)-C(3)-C(6)	122.31(18)
C(3)-C(6)	1.494(3)	C(4)-C(3)-C(6)	119.06(19)
C(4)-C(5)	1.378(3)	C(5)-C(4)-C(3)	118.4(2)
C(5)-N(1)	1.329(3)	N(1)-C(5)-C(4)	123.8(2)
C(6)-O(1)	1.202(3)	O(1)-C(6)-O(2)	123.90(19)
C(6)-O(2)	1.334(2)	O(1)-C(6)-C(3)	124.59(19)
C(7)-O(2)	1.451(2)	O(2)-C(6)-C(3)	111.49(17)
C(7)-C(8)	1.499(3)	O(2)-C(7)-C(8)	105.96(17)
C(8)-S(1)	1.815(2)	C(7)-C(8)-S(1)	112.15(15)
C(9)-C(10)	1.500(3)	C(10)-C(9)-S(2)	115.56(16)
C(9)-S(2)	1.825(2)	O(4)-C(10)-C(9)	107.91(18)
C(10)-O(4)	1.444(2)	O(3)-C(11)-O(4)	124.6(2)
C(11)-O(3)	1.205(3)	O(3)-C(11)-C(14)	124.0(2)
C(11)-O(4)	1.332(3)	O(4)-C(11)-C(14)	111.43(18)
C(11)-C(14)	1.493(3)	N(2)-C(12)-C(13)	123.6(2)
C(12)-N(2)	1.334(3)	C(12)-C(13)-C(14)	118.9(2)
C(12)-C(13)	1.378(3)	C(13)-C(14)-C(15)	118.1(2)
C(13)-C(14)	1.384(3)	C(13)-C(14)-C(11)	119.9(2)
C(14)-C(15)	1.388(3)	C(15)-C(14)-C(11)	122.09(19)



C(15)-C(16)	1.380(3)	C(16)-C(15)-C(14)	118.3(2)
C(16)-N(2)	1.325(3)	N(2)-C(16)-C(15)	124.3(2)
S(1)-S(2)	2.0277(8)	C(1)-N(1)-C(5)	116.7(2)
		C(16)-N(2)-C(12)	116.7(2)
		C(6)-O(2)-C(7)	116.52(16)
		C(11)-O(4)-C(10)	116.15(17)
		C(8)-S(1)-S(2)	104.88(8)
		C(9)-S(2)-S(1)	104.78(8)

Symmetry transformations used to generate equivalent atoms: #1 -x+1,-y+1,-z+2 #2 -x+1,-y+1,-z+1 #3 -x,-y+1,-z+1

**Table 5-4.** Anisotropic displacement parameters ( $\text{\AA}^2 \times 10^3$ ) for disulfid The anisotropic displacement factor exponent takes the form:  $-2 \pi^2 [ h^2 a^{*2} U11 + \dots + 2 h k a^* b^* U12 ]$

	U11	U22	U33	U23	U13	U12
C(1)	51(1)	34(1)	46(1)	-4(1)	-1(1)	-1(1)
C(2)	38(1)	33(1)	38(1)	2(1)	5(1)	2(1)
C(3)	33(1)	35(1)	33(1)	0(1)	4(1)	0(1)
C(4)	48(1)	35(1)	55(1)	-5(1)	-5(1)	9(1)
C(5)	48(1)	51(2)	63(2)	-7(1)	-15(1)	10(1)
C(6)	33(1)	34(1)	37(1)	1(1)	7(1)	0(1)
C(7)	32(1)	37(1)	42(1)	-4(1)	1(1)	-4(1)
C(8)	34(1)	38(1)	48(1)	5(1)	-1(1)	-7(1)
C(9)	35(1)	56(1)	38(1)	-6(1)	1(1)	0(1)
C(10)	42(1)	45(1)	43(1)	-12(1)	-5(1)	3(1)
C(11)	34(1)	34(1)	45(1)	-3(1)	1(1)	2(1)
C(12)	48(1)	53(2)	40(1)	3(1)	3(1)	10(1)
C(13)	45(1)	37(1)	48(1)	3(1)	5(1)	3(1)
C(14)	27(1)	36(1)	41(1)	-1(1)	5(1)	3(1)
C(15)	42(1)	33(1)	44(1)	1(1)	5(1)	0(1)
C(16)	52(1)	41(1)	50(1)	-8(1)	5(1)	-6(1)
N(1)	52(1)	47(1)	53(1)	-6(1)	-13(1)	1(1)
N(2)	48(1)	54(1)	44(1)	-9(1)	0(1)	2(1)
O(1)	52(1)	33(1)	66(1)	-9(1)	-9(1)	2(1)
O(2)	36(1)	33(1)	49(1)	0(1)	-8(1)	-3(1)
O(3)	74(1)	36(1)	59(1)	-3(1)	-6(1)	-9(1)
O(4)	41(1)	39(1)	39(1)	-3(1)	-5(1)	-2(1)
S(1)	34(1)	56(1)	35(1)	3(1)	3(1)	-2(1)
S(2)	33(1)	41(1)	57(1)	3(1)	4(1)	-4(1)

**Table 5-5.** Hydrogen coordinates ( $\times 10^4$ ) and isotropic displacement parameters ( $\text{\AA}^2 \times 10^3$ ) for disulfide.

	x	y	z	U(eq)
H(1)	3586	-981	-983	54
H(2)	4455	-200	1012	43
H(4)	3369	2996	434	57
H(5)	2529	2088	-1511	68
H(7A)	5436	2266	4895	45
H(7B)	5969	2287	3632	45
H(8A)	6264	242	4131	49
H(8B)	5694	153	5297	49
H(9A)	7813	431	3837	52
H(9B)	8545	1050	4673	52
H(10A)	7762	-737	6076	54
H(10B)	8531	-940	5538	54
H(12)	9654	-734	13839	57
H(13)	9111	-1644	11520	52
H(15)	9055	1646	9425	48
H(16)	9569	2447	11839	57

### 5.2.3 Ag coordination networks

*Synthesis of Adl7:* Small crystals are obtained at room temperature, in the dark, after 1-2 days in a closed vessel from a mixture of 25ml 4mM AgNO<sub>3</sub> in THF/EtOH 1/1 solution and 25ml 4mM L THF/EtOH 1/1 solution. After 5 days, the crystals are filtered and washed with EtOH. Yield: 30 mg (68%). The crystallisation takes place also in different concentrations, starting at 0.2mM complex concentration the crystal formation is reached. Depending on the concentration of the starting solution, the size of the crystals can be influenced.

*Synthesis of Adl3:* Small crystals are obtained at room temperature from AcN/EtOH 1 to 1. The Adl7 crystals are completely dissolved in AcN/EtOH 1 to 1. After slow evaporation in the dark, Adl3 precipitates on a bottom of the recipient.

*Powder X-ray measurements:* Since, only the crystalline structures are differing and only the powder X-ray spectra can serve as reliable information and identification of the compound. This technique is used routinely to identify the compounds. Some mg of the compound are put into the sample holder, and with continuously rotation, the sample is measured between 3 to 80° theta. The time and the taken points of the measurement depend on the desired resolution. The spectra are then compared to the simulated powder spectra of the compounds obtained from the single crystal data.

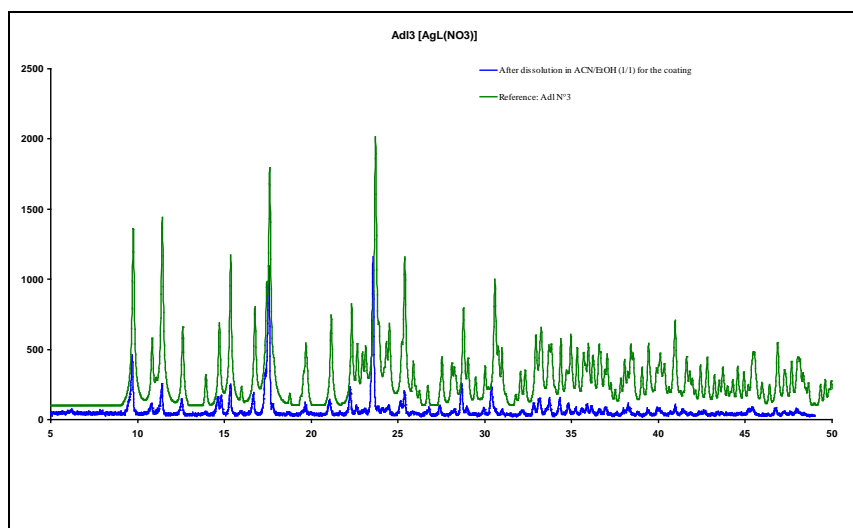


**Figure 5-1:** Powder X-ray spectra of synthesized Adl3 and from the single crystal data simulated powder X-ray spectra of Adl3

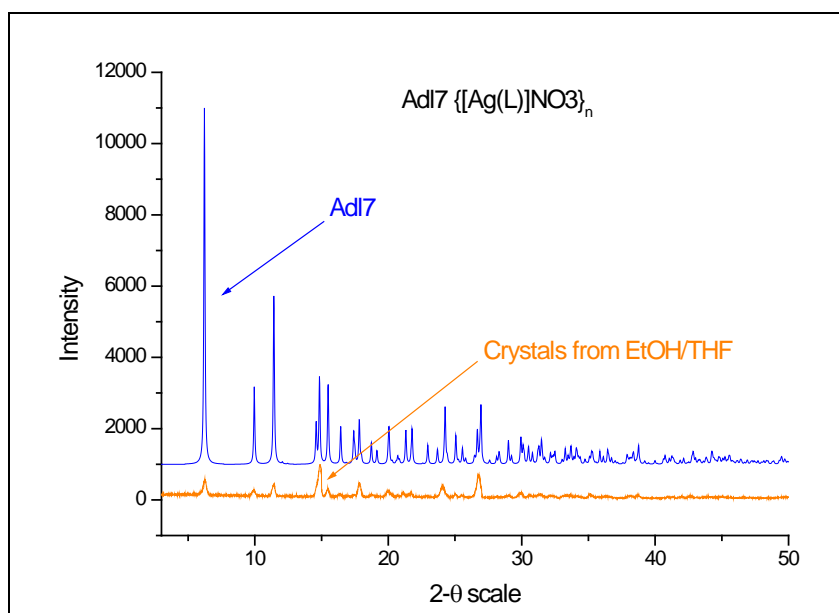


**Figure 5-2:** Powder X-ray spectra of synthesized Adl7 and from the single crystal data simulated powder X-ray spectra of Adl7

*Dissolution studies:* For the dissolution studies, the coordination polymer compounds were synthesized in a previously described way. AgCl was prepared freshly by precipitation of a mixture of molar equivalents of concentrated NaCl and AgNO<sub>3</sub> aq. (nanopure water) solutions. The precipitate was dried and used for further experiments. 4-5mg of compound are weighed into small (5ml) vessels. 2ml of the medium are added on top, then the vessel is closed and shaken (5 sec sonication) and stored in the dark. The solution is removed and filtered on a 0.40μm disposable filter (Millipore, Millex GS, 0.40μm). To 0.5 ml of the filtrate, 0.5 ml 10% HNO<sub>3</sub> solution is added and diluted to 10ml with water for the silver

determination by AAS. The precipitation was washed 3 times with EtOH, then dried in vacuum, and a powder spectrum is taken.

Two biological media for microbiological assays are used for the dissolution tests. The Müller-Hinton medium was proposed by MUELLER and HINTON (1941) for testing the sensitivity of clinically important pathogens towards antibiotics or sulfonamides and is composed of beef infusion, casamino acids, and starch. (Typical Composition (g/litre): Meat infusion 2.0; casein hydrolysate 17.5; starch 1.5.) This medium mixed with agar is used for further microbiological assays. The synthetic medium is an artificial medium, used for bacterial growth inhibition tests of *S.aureus*; the exact composition is shown in **Table 5-6**.

**Table 5-6:** The composition of the synthetic medium

Synthetic Medium for <i>S.aureus</i> Newman			
<b>Solution 1 products</b>	g/L (2x)	<b>Solution 2 products</b>	M
Na <sub>2</sub> HPO <sub>4</sub>	3.54	citrate	1
KH <sub>2</sub> PO <sub>4</sub>	2.72	(tri Na)	
MgSO <sub>4</sub> ·7H <sub>2</sub> O	0.4	<b>Solution 5 amino acids</b>	g/100 mL (50x)
NH <sub>4</sub> Cl	1	alanine	0.8
NaCl	1	valine	0.8
<b>Solution 4 products</b>	g/L (25x)	leucine	0.8
MOPS	209.26	isoleucine	0.8
	pH 7.0	aspartate	0.8
<b>Solution 7 trace elements</b>	mM (1000x)	glutamate	0.8
ZnCl <sub>2</sub>	0.51	serine	0.8
MnCl <sub>2</sub>	0.5	threonine	0.8
H <sub>3</sub> BO <sub>3</sub>	0.097	cysteine	0.8
CoCl <sub>2</sub>	1.46	arginine	0.8
CuCl <sub>2</sub>	0.015	lysine	0.8
NiCl <sub>2</sub>	0.1	proline	0.8
NaMoO <sub>4</sub>	0.148	phenylalanine	0.8
		tryptophane	0.8
		histidine	0.8
		glycine	8
<b>Solution 3 products</b>	% (w/v)	<b>Solution 6 vitamins</b>	mM (1000x)
glucose	20	cyanocobalamine	0.036
		p-aminobenzoate	0.29
		biotin	0.04
		nicotinic acid	0.81
		Ca-D-pantotheic ac.	0.21
		pyridoxamine hydrochloride	0.62
		thiaminium dichloride	0.29
		riboflavin	0.26
		<b>Solution 8 product</b>	mM
		FeCl <sub>2</sub>	0.5
		in 2N HCl	
		<b>Solution 9 product</b>	
		NaOH 2N	

*Light sensibility tests:* The test based on the preliminary assay is described in [202] The Adl3 and Adl7 are prepared as described previously. The other compounds were synthesized according to [93] Adl8 and Adl10 and [207] J11. 0.01 M solutions in CH<sub>3</sub>CN are prepared and filter paper (ø:3cm) was impregnated with the different solutions. The filter papers are

first dried in the dark and are then illuminated with a 15W electric lamp from a distance of 10 cm. The colour change of the different filter papers is compared after 5h illumination.

### 5.2.4 Peptide synthesis

#### 5.2.4.1 General procedures of the peptide synthesis

Synthetic steps follow the same procedure according to the sections below. Peptides containing AHC group and the isonicotinic acid coupled T-Gel are prepared manually, the others were prepared by the automatic peptide synthesizer.

##### 5.2.4.1.1 Manual peptide synthesis on solid support

###### *Synthesis on TentaGel Resin*

For the synthesis 200 mg TentaGel Resin (0.09 mmol, 1.0 eq) was used.

A, Fmoc-aminoacid is coupled with an amino-functionalised TentaGel-Resin with HCTU.  $\text{CH}_2\text{Cl}_2$  suspension of the T-Gel resin are mixed with an aminoacid (1.5–3 eq) solution and HCTU (3.0 eq) in 1 mL DMF in a Merryfield vessel and is shaken for 2 min. Then  $i\text{Pr}_2\text{NEt}$  (3.0–6.0 eq) is added and the mixture is shaken for 2h. After removing all the reactant, the resin is washed 3 times with  $\text{CH}_2\text{Cl}_2$  and the degree of coupling is controlled with a Kaiser [204] or TNBS-Test [205].

B, After the aminoacid coupling, the Fmoc protecting group is removed: The resin is mixed with 20 % (v/v) piperidin in DMF and shaken for 2 min. Then, the piperidin solution is removed. The same solution is once more given to the resin and shaken again for 10 min. Finally, the resin is washed three times with DMF and five times with  $\text{CH}_2\text{Cl}_2$ , and the completeness of coupling is controlled with a Kaiser [204] or TNBS-Test [205].

C, After the deprotection, the free amines are acetylated: The resin is suspended in 5 ml  $\text{CH}_2\text{Cl}_2$ . The suspension is mixed with  $\text{NEt}_3$  (100 eq) and shaken for 2 min, than  $\text{Ac}_2\text{O}$  (50 eq) is given to the mixture and shaken again for 1 h. After the removal of all the reactants the resin was 3 times washed with  $\text{CH}_2\text{Cl}_2$  and the completeness of acetylation is controlled with a Kaiser [204] or TNBS-Test [205].

D, The side chain protecting groups of the T-Gel resin are cleaved: The resin is mixed with a mixture of 95 % TFA, 2.5 % TIS und 2.5 %  $\text{H}_2\text{O}$  and shaken for 2 h. Than, the resin is washed three times with  $\text{CH}_2\text{Cl}_2$ , five times with 10 %  $\text{Et}_3\text{N}$  in  $\text{CH}_2\text{Cl}_2$  and ten times with  $\text{CH}_2\text{Cl}_2$ .

###### *Synthesis on Rink Amid Resin*

For the synthesis, 200 mg Rink-amid resin (0.14 mmol, 1.0 eq) were used.

A, Fmoc-aminoacid is coupled on an amino-functionalised Rink-amid resin with HCTU.  $\text{CH}_2\text{Cl}_2$  suspension of the Rink-amid resin are mixed with an aminoacid (1.5–3 eq) solution and HCTU (3.0 eq) in 1 mL DMF in a Merryfield vessel and is shaken for 2 min. Then  $i\text{Pr}_2\text{NEt}$  (3.0–6.0 eq) is added and the mixture is shaken for 2h. After removing all the reactants, the resin is washed 3 times with  $\text{CH}_2\text{Cl}_2$  and the degree of coupling is controlled with a Kaiser [204] or TNBS-Test [205].

B, After the aminoacid coupling, the Fmoc protecting group is removed: The resin is mixed with 20 % (v/v) piperidin in DMF and shaken for 2 min. Then, the piperidin solution is removed. The same solution is once more given to the resin and shaken again for 10 min. Finally, the resin is washed three times with DMF and five times with  $\text{CH}_2\text{Cl}_2$ , and the level of the deprotection is controlled with a Kaiser [204] or TNBS-Test [205].

C, After the deprotection, the free amines are acetylated: The resin is suspended in 5 ml  $\text{CH}_2\text{Cl}_2$ . The suspension is mixed with  $\text{NEt}_3$  (100 eq) and shaken for 2 min, then  $\text{Ac}_2\text{O}$  (50 eq) is given to the mixture and shaken again for 1 h. After the removal of all reactants, the resin was washed 3 times with  $\text{CH}_2\text{Cl}_2$  and the degree of acetylation is controlled with a Kaiser [204] or TNBS-Test [205].

E, End up cleavage of the side chain protecting groups and the synthesized peptide from the Rink-Resin: The resin is mixed with a mixture of 95 % TFA, 2.5 % TIS und 2.5 %  $\text{H}_2\text{O}$  and shaken for 2 h. Then, the resin is washed three times with  $\text{CH}_2\text{Cl}_2$ . After that the solvent is removed and the oily product is washed several times with  $\text{Et}_2\text{O}$  and precipitated. The white precipitation is dried.

### ***5.2.4.1.2 Peptide synthesis on solid support with automatic synthesizer***

The description of the automatic way of the synthesis concerns both resins (TentaGel and Rink Amid resin).

A, Fmoc-Aminoacid coupling: The aminoacid (4 eq) and HCTU (4 eq) are dissolved in DMF (ca. 5 mL / g aminoacid) and mixed with an  $i\text{Pr}_2\text{NEt}$  (12 eq) in N-Methylpyrrolidon (3 M) solution. The mixture is shaken for 1.5 h, then the reagent is removed from the resin and the resin is washed with DMF.

B, Fmoc-Cleavage: The resin is mixed with 40 % (v/v) piperidin in DMF and shaken for 2 min. After the solution is removed from the resin, it is shaken for 10 min with 20 % (v/v) piperidin in DMF. Then, the resin was washed five times with DMF.

C, Acetylation of the free amins: After the last deprotection the resin is suspended with 2 ml  $\text{CH}_2\text{Cl}_2$  and first mixed with  $\text{NEt}_3$  (100 eq) then with  $\text{Ac}_2\text{O}$  (50 eq) and the mixture is shaken for 1 h. All reagents are removed and the resin is washed five times with  $\text{CH}_2\text{Cl}_2$ .

In the case of the synthesis on Rink amid resin, the last step is followed by the cleavage of the side chain protecting groups and the peptide from the resin. (step E)

## 5.2.4.2 Peptide synthesis for Nanoparticle generation

The following **Table 5-7** shows the quantity of the different amino acids and coupling reagents for the synthesized peptides. For the automatic synthesis 4.0 eq for the manual 3.0 eq of the substances is used.

**Table 5-7:** Quantity of the different amino acids and coupling reagents for the synthesized peptides

	Substance	Eq	n	m	V
			[mmol]	[mg]	[mL]
TentaGel	Fmoc-D/L-His(Trt)-OH	3.0	0.26	159.9	
		4.0	0.34	213.3	
	Fmoc- <i>trans</i> -2-Aminocyclohexane acid <i>rac</i>	3.0	0.26	100.0	
	Fmoc- <i>trans</i> -( <i>R,R</i> )-Aminocyclohexane acid	3.0	0.26	100.0	
	Fmoc- <i>trans</i> -( <i>S,S</i> )-Aminocyclohexane acid	3.0	0.26	100.0	
	Fmoc-L-Tyr( <sup>t</sup> Bu)-OH	3.0	0.26	120.0	
		4.0	0.34	158.3	
	Fmoc-D/L-Ser( <sup>t</sup> Bu)-OH	3.0	0.26	99.9	
		4.0	0.34	131.9	
	Fmoc-L-Pro-OH	4.0	0.34	116.1	
	Fmoc-Aib-OH	4.0	0.34	111.9	
	Fmoc-Gly-OH	4.0	0.34	102.3	
	Fmoc-D/L-Asp(OtBu)-OH	3.0	0.26	111.0	
		4.0	0.34	141.6	
	Fmoc-β-Ala-OH	3.0	0.26	80.0	
		4.0	0.34	107.1	
	Fmoc-Ahx-OH	4.0	0.34	121.6	
	Fmoc-L-Phe-OH	3.0	0.26	110.0	
	Fmoc-L-Cys-OH	4.0	0.34	201.5	
	Fmoc-L-Ala-OH	4.0	0.34	107.1	
	Isonicotinicacid	3.0	0.34	31.8	
	HCTU	3.0	0.26	107.0	
		4.0	0.34	142.3	
	<sup>i</sup> Pr <sub>2</sub> NEt	6.0	0.52		0.09
		12.0	1.03		0.18
	NEt <sub>3</sub>	100	8.6		1.20
Ac <sub>2</sub> O	50	4.3		0.41	



	Substance	Eq	n [mmol]	m [mg]	V [mL]
	<b>Rink</b>	Fmoc-D/L-His(Trt)-OH	3.0 4.0	0.43 0.57	264.0 353.2
Fmoc- <i>trans</i> -2-Aminocyclohexane acid <i>rac</i>		3.0	0.43	155.5	
Fmoc- <i>trans</i> -( <i>R,R</i> )-Aminocyclohexane acid		4.0	0.43	155.5	
Fmoc- <i>trans</i> -( <i>S,S</i> )-Aminocyclohexane acid		4.0	0.43	155.5	
Fmoc-L-Tyr( <sup>t</sup> Bu)-OH		3.0 4.0	0.43 0.57	196.0 261.9	
Fmoc-D/L-Ser( <sup>t</sup> Bu)-OH		3.0 4.0	0.43 0.57	163.0 218.6	
Fmoc-L-Pro-OH		4.0	0.57	192.3	
Fmoc-Aib-OH		4.0	0.57	185.5	
Fmoc-Gly-OH		4.0	0.57	168.9	
Fmoc-D/L-Asp(OtBu)-OH		3.0 4.0	0.43 0.57	175.0 233.7	
Fmoc-β-Ala-OH		3.0 4.0	0.43 0.57	133.0 176.8	
Fmoc-Ahx-OH		4.0	0.57	200.7	
Fmoc-L-Phe-OH		3.0	0.43	170.0	
Fmoc-L-Cys-OH		4.0	0.57	337.2	
Fmoc-L-Ala-OH		4.0	0.57	176.8	
HCTU		3.0 4.0	0.43 0.57	176.0 235.8	
<sup>i</sup> Pr <sub>2</sub> NEt		6.0 12.0	0.43 1.70		0.15 0.29
NEt <sub>3</sub>		100	14.2		2.0
Ac <sub>2</sub> O		50	7.1		0.67

## Isonicotinic acid TentaGel

Synthesis on TentaGel: Isonicotinic acid is coupled on amino functionalised TentaGel-Resin with HCTU:

CH<sub>2</sub>Cl<sub>2</sub> suspension of the T-Gel resin is mixed with isonicotinic acid (1.5–3 eq) solution and HCTU (3.0 eq) in 1 mL DMF in a Merryfield vessel and is shaken for 2 min. Then <sup>i</sup>Pr<sub>2</sub>NEt (3.0–6.0 eq) is added and the mixture is shaken for 2h. After removing all of the reactants, the resin is washed 3 times with CH<sub>2</sub>Cl<sub>2</sub> and dried.

The following table (**Table 5-8**) shows the characteristics of the synthesised peptides:

**Table 5-8:** Characterisation of the synthesised tripeptide sequences

Peptide	Structure	MW (g/mol)	Yield (mg)	<sup>1</sup> H-NMR	<sup>13</sup> C-NMR	ESI-MS (m/z)
Ac-D-His- <i>rac</i> -ACHC-L-Tyr-NH-TG/H 92a/b		C <sub>24</sub> H <sub>32</sub> N <sub>6</sub> O <sub>5</sub> 484.24	79.0	<sup>1</sup> H-NMR (400.0 MHz, CD <sub>3</sub> OD, 25°C): δ (ppm) = 8.76 (s, 1H, CH <sub>Imi</sub> ), 7.3 (s, 1H, CH <sub>Imi</sub> ), 7.2 (s, 2H, CH <sub>Imi</sub> ), 7.05 (d, J = 8.6 Hz, 2H, ArH <sub>Tyr</sub> ), 7.03 (d, J = 8.3 Hz, 2H, ArH <sub>Tyr</sub> ), 6.62 (d, J = 8.6 Hz, 2H, ArH <sub>Tyr</sub> ), 4.66 (dd, J = 8.1 Hz, 6.1 Hz, 1H, CHα <sub>His</sub> ) 4.55 (dd, J = 8.8 Hz, 5.6 Hz, 2H, CHα <sub>His</sub> , CHα <sub>Tyr</sub> ), 4.49 (dd, J = 9.8 Hz, 4.8 Hz, 1H, CHα <sub>Tyr</sub> ), 3.99 (dt, J = 11.2 Hz, 4.3 Hz, 1H, CHβ <sub>ACHC</sub> ), 3.85 (dt, J = 11.6 Hz, 4.8 Hz, 1H, CHβ <sub>ACHC</sub> ), 3.19 (dd, J = 15.4 Hz, 6.1 Hz, 1H, CH <sub>2</sub> β <sub>His</sub> ), 3.06 (m, 3H, CH <sub>2</sub> β <sub>His</sub> ), 2.96 (dd, J = 15.2 Hz, 7.8 Hz, 1H, CH <sub>2</sub> β <sub>Tyr</sub> ), 2.78 (m, 2H, CH <sub>2</sub> β <sub>Tyr</sub> ), 2.69 (dd, J = 15.1 Hz, 6.1 Hz, 1H, CH <sub>2</sub> β <sub>Tyr</sub> ), 2.26 (m, 2H, CHα <sub>ACHC</sub> ), 1.99 (s, 3H, CH <sub>3</sub> <sub>Ac</sub> ), 1.88 (s, 3H, CH <sub>3</sub> <sub>Ac</sub> ), 1.71 (m, 5H, CH <sub>2</sub> <sub>ACHC</sub> ), 1.33 (m, 8H, CH <sub>2</sub> <sub>ACHC</sub> );	<sup>13</sup> C-NMR (100.6 MHz, CD <sub>3</sub> OD, 25°C): δ (ppm) = 177.1/176.2/173.4/171.1/170.9/168.5/ 165.7 (CO), 157.4 (C <sub>Ar</sub> -OH), 134.8 (CH <sub>Imi</sub> ), 134.7 (CH <sub>Imi</sub> ), 131.3 (Cq <sub>Imi</sub> ), 131.4 (CH <sub>Ar</sub> <sub>Tyr</sub> ), 131.2 (CH <sub>Ar</sub> <sub>Tyr</sub> ), 130.5 (Cq <sub>Imi</sub> ), 129.6 (Cq <sub>Tyr</sub> ), 128.9 (Cq <sub>Tyr</sub> ), 118.7 (CH <sub>Imi</sub> ), 118.6 (CH <sub>Imi</sub> ), 116.2 (CH <sub>Ar</sub> <sub>Tyr</sub> ), 55.5 (CHα <sub>Tyr</sub> ), 53.7 (CHα <sub>Tyr</sub> ), 53.1 (CHα <sub>His</sub> ), 51.9 (CHα <sub>His</sub> ), 50.9 (CHα <sub>ACHC</sub> ), 50.5 (CHβ <sub>ACHC</sub> ), 38.5 (CH <sub>2</sub> β <sub>Tyr</sub> ), 38.2 (CH <sub>2</sub> β <sub>Tyr</sub> ), 33.5 (CH <sub>2</sub> <sub>ACHC</sub> ), 31.3 (CH <sub>2</sub> <sub>ACHC</sub> ), 30.5 (CH <sub>2</sub> <sub>ACHC</sub> ), 28.7 (CH <sub>2</sub> β <sub>His</sub> ), 28.2 (CH <sub>2</sub> β <sub>His</sub> ), 26.0 (CH <sub>2</sub> <sub>ACHC</sub> ), 26.0 (CH <sub>2</sub> <sub>ACHC</sub> ), 25.9 (CH <sub>2</sub> <sub>ACHC</sub> ), 25.8 (CH <sub>2</sub> <sub>ACHC</sub> ), 22.7 (CH <sub>3</sub> <sub>Ac</sub> ), 22.5 (CH <sub>3</sub> <sub>Ac</sub> );	calculated : 484.24; found: 485.2 [M+H] <sup>+</sup> .
Ac-L-His- <i>rac</i> -ACHC-L-Tyr-NH-TG/H 93a/b		C <sub>24</sub> H <sub>32</sub> N <sub>6</sub> O <sub>5</sub> 4 84.24	53.0 77%	<sup>1</sup> H-NMR (400.0 MHz, CD <sub>3</sub> OD, 25°C): δ (ppm) = 8.76 (s, 1H, CH <sub>Imi</sub> ), 7.30 (s, 1H, CH <sub>Imi</sub> ), 7.08 (dd, J = 8.3 Hz, 4.8 Hz, 4H, ArH <sub>Tyr</sub> ), 6.70 (dd, J = 8.3 Hz, 4.5 Hz, 4H, ArH <sub>Tyr</sub> ), 4.60 (m, 2H, CHα <sub>His</sub> ) 4.55 (dd, J = 9.3 Hz, 5.3 Hz, 1H, CHα <sub>Tyr</sub> ), 4.45 (dd, J = 8.1 Hz, 6.6 Hz, 1H, CHα <sub>Tyr</sub> ), 3.95 (dt, J = 11.3 Hz, 3.5 Hz, 1H, CHβ <sub>ACHC</sub> ), 3.82 (dt, J = 11.6 Hz, 4.3 Hz, 1H, CHβ <sub>ACHC</sub> ), 3.14 (dd, J = 15.2 Hz, 6.3 Hz, 1H, CH <sub>2</sub> β <sub>His</sub> ), 2.99 (m, 4H, CH <sub>2</sub> β <sub>His</sub> , CH <sub>2</sub> β <sub>Tyr</sub> ), 2.81 (m, 2H, CH <sub>2</sub> β <sub>Tyr</sub> ), 2.32 (m, 1H, CHα <sub>ACHC</sub> ), 2.23 (m, 1H, CHα <sub>ACHC</sub> ), 1.96 (s, 3H, CH <sub>3</sub> <sub>Ac</sub> ), 1.88 (s, 3H, CH <sub>3</sub> <sub>Ac</sub> ), 1.72 (m, 6H, CH <sub>2</sub> <sub>ACHC</sub> ), 1.29 (m, 8H, CH <sub>2</sub> <sub>ACHC</sub> );	<sup>13</sup> C-NMR (100.6 MHz, DMSO, 25°C): δ (ppm) = 173.5/173.4/172.9/172.6/169.2/169.1/168.9/168.7 (CO), 155.6 (C <sub>Ar</sub> -OH), 133.7 (CH <sub>Imi</sub> ), 133.5 (CH <sub>Imi</sub> ), 132.7 (Cq <sub>Imi</sub> ), 129.9 (CH <sub>Ar</sub> <sub>Tyr</sub> ), 129.8 (CH <sub>Ar</sub> <sub>Tyr</sub> ), 129.1 (Cq <sub>Imi</sub> ), 127.9 (Cq <sub>Tyr</sub> ), 127.8 (Cq <sub>Tyr</sub> ), 116.7 (CH <sub>Imi</sub> ), 114.7 (CH <sub>Ar</sub> <sub>Tyr</sub> ), 54.8 (CHα <sub>Tyr</sub> ), 53.6 (CHα <sub>His</sub> ), 51.9 (CHα <sub>His</sub> ), 48.8 (CHα <sub>ACHC</sub> ), 48.5 (CHβ <sub>ACHC</sub> ), 36.9 (CH <sub>2</sub> β <sub>Tyr</sub> ), 36.6 (CH <sub>2</sub> β <sub>Tyr</sub> ), 32.2 (CH <sub>2</sub> <sub>ACHC</sub> ), 32.1 (CH <sub>2</sub> <sub>ACHC</sub> ), 30.6 (CH <sub>2</sub> <sub>ACHC</sub> ), 29.4, (CH <sub>2</sub> <sub>ACHC</sub> ), 28.7 (CH <sub>2</sub> β <sub>His</sub> ), 28.0 (CH <sub>2</sub> β <sub>His</sub> ), 27.9 (CH <sub>2</sub> <sub>ACHC</sub> ), 27.7 (CH <sub>2</sub> <sub>ACHC</sub> ), 24.3 (CH <sub>2</sub> <sub>ACHC</sub> ), 22.4 (CH <sub>3</sub> <sub>Ac</sub> ), 22.3 (CH <sub>3</sub> <sub>Ac</sub> );	calculated : 484.24; found: 485.2 [M+H] <sup>+</sup> .

## 5 Experimental part

Peptide	Structure	MW (g/mol)	Yield (mg)	<sup>1</sup> H-NMR	<sup>13</sup> C-NMR	ESI-MS (m/z)
Ac-D-Ser- <i>rac</i> -ACHC-L-Tyr-NH-TG/H 94a/b		C <sub>21</sub> H <sub>30</sub> N <sub>4</sub> O <sub>6</sub> 434.49	38.0 (62%)	<sup>1</sup> H-NMR (400.0 MHz, d <sub>6</sub> -DMSO, 25 °C): δ (ppm) = 7.05 (d, J = 7.1 Hz, 4H, ArH <sub>Tyr</sub> ), 6.67 (dd, J = 8.6 Hz, 2.5 Hz, 4H, ArH <sub>Tyr</sub> ), 4.39 (s, 2H, CH <sub>α</sub> <sub>Tyr</sub> ) 4.35 (dd, J = 9.1 Hz, 5.1 Hz, 1H, CH <sub>α</sub> <sub>Ser</sub> ), 4.24 (m, 3H, CH <sub>α</sub> <sub>Ser</sub> , CH <sub>β</sub> <sub>ACHC</sub> ), 3.51 (m, 4H, CH <sub>2</sub> β <sub>Ser</sub> ), 2.92 (ddd, J = 13.3 Hz, 7.1 Hz, 5.3 Hz, 2H, CH <sub>2</sub> β <sub>Tyr</sub> ), 2.71 (m, 2H, CH <sub>2</sub> β <sub>Tyr</sub> ), 2.26 (dt, J = 11.1 Hz, 3.6 Hz, 1H, CH <sub>α</sub> <sub>ACHC</sub> ), 2.17 (dt, J = 12.1 Hz, 3.6 Hz, 1H, CH <sub>α</sub> <sub>ACHC</sub> ), 1.97 (s, 3H, CH <sub>3</sub> <sub>Ac</sub> ), 1.89 (s, 3H, CH <sub>3</sub> <sub>Ac</sub> ), 1.80 (m, 2H, CH <sub>2</sub> <sub>ACHC</sub> ), 1.61 (m, 6H, CH <sub>2</sub> <sub>ACHC</sub> ), 1.20 (m, 8H, CH <sub>2</sub> <sub>ACHC</sub> );	<sup>13</sup> C-NMR (100.6 MHz, d <sub>6</sub> -DMSO, 25 °C): δ (ppm) = 174.4/173.9/173.8/173.7/170.8/170.6/169.8/169.5 (CO), 155.9 (C <sub>Ar</sub> -OH), 130.6 (CH <sub>Ar</sub> <sub>Tyr</sub> ), 128.3 (C <sub>q</sub> <sub>Tyr</sub> ), 115.2 (CH <sub>Ar</sub> <sub>Tyr</sub> ), 62.2 (CH <sub>2</sub> β <sub>Ser</sub> ), 62.0 (CH <sub>2</sub> β <sub>Ser</sub> ), 55.7 (CH <sub>α</sub> <sub>Ser</sub> ), 55.1 (CH <sub>α</sub> <sub>Ser</sub> ), 54.8 (CH <sub>α</sub> <sub>Tyr</sub> ), 54.1 (CH <sub>α</sub> <sub>Tyr</sub> ), 50.1 (CH <sub>α</sub> <sub>ACHC</sub> ), 49.8 (CH <sub>α</sub> <sub>ACHC</sub> ), 49.3 (CH <sub>β</sub> <sub>ACHC</sub> ), 48.6 (CH <sub>β</sub> <sub>ACHC</sub> ), 37.0 (CH <sub>2</sub> β <sub>Tyr</sub> ), 36.9 (CH <sub>2</sub> β <sub>Tyr</sub> ), 32.7 (CH <sub>2</sub> <sub>ACHC</sub> ), 32.5 (CH <sub>2</sub> <sub>ACHC</sub> ), 29.3 (CH <sub>2</sub> <sub>ACHC</sub> ), 24.8 (CH <sub>2</sub> <sub>ACHC</sub> ), 24.7 (CH <sub>2</sub> <sub>ACHC</sub> ), 23.0 (CH <sub>3</sub> <sub>Ac</sub> ), 22.8 (CH <sub>3</sub> <sub>Ac</sub> );	calculated: 434.49; found: 457.2 [M+Na] <sup>+</sup> .
Ac-L-Ser- <i>rac</i> -ACHC-L-Tyr-NH-TG/H 95a/b		C <sub>21</sub> H <sub>30</sub> N <sub>4</sub> O <sub>6</sub> 434.49	38.0 (62%)	<sup>1</sup> H-NMR (400.0 MHz, D <sub>2</sub> O, 25 °C): δ (ppm) = 7.12 (dd, J = 8.3 Hz, 3.8 Hz, 4H, ArH <sub>Tyr</sub> ), 6.80 (dd, J = 8.1 Hz, 6.1 Hz, 4H, ArH <sub>Tyr</sub> ), 4.57 (dd, J = 8.8 Hz, 5.6 Hz, 1H, CH <sub>α</sub> <sub>Tyr</sub> ) 4.45 (t, J = 7.6 Hz, 1H, CH <sub>α</sub> <sub>Tyr</sub> ), 4.29 (m, 2H, CH <sub>α</sub> <sub>Ser</sub> ), 3.88 (m, 1H, CH <sub>β</sub> <sub>ACHC</sub> ), 3.71 (m, 5H, CH <sub>β</sub> <sub>ACHC</sub> , CH <sub>2</sub> β <sub>Ser</sub> ), 2.85 (m, 2H, CH <sub>2</sub> β <sub>Tyr</sub> ), 2.28 (m, 2H, CH <sub>α</sub> <sub>ACHC</sub> ), 2.03 (s, 3H, CH <sub>3</sub> <sub>Ac</sub> ), 1.98 (s, 3H, CH <sub>3</sub> <sub>Ac</sub> ), 1.85 (m, 2H, CH <sub>2</sub> <sub>ACHC</sub> ), 1.74 (m, 5H, CH <sub>2</sub> <sub>ACHC</sub> ), 1.29 (m, 9H, CH <sub>2</sub> <sub>ACHC</sub> );	<sup>13</sup> C-NMR (100.6 MHz, d <sub>6</sub> -DMSO, 25 °C): δ (ppm) = 173.3/172.8/172.7/169.7/169.0/168.9 (CO), 155.6 (C <sub>Ar</sub> -OH), 155.5 (C <sub>Ar</sub> -OH), 129.97 (CH <sub>Ar</sub> <sub>Tyr</sub> ), 129.93 (CH <sub>Ar</sub> <sub>Tyr</sub> ), 127.9 (C <sub>q</sub> <sub>Tyr</sub> ), 127.8 (C <sub>q</sub> <sub>Tyr</sub> ), 114.7 (CH <sub>Ar</sub> <sub>Tyr</sub> ), 114.6 (CH <sub>Ar</sub> <sub>Tyr</sub> ), 64.8 (CH <sub>2</sub> β <sub>Ser</sub> ), 61.8 (CH <sub>α</sub> <sub>Ser</sub> ), 54.8 (CH <sub>α</sub> <sub>Tyr</sub> ), 49.1 (CH <sub>β</sub> <sub>ACHC</sub> ), 48.8 (CH <sub>β</sub> <sub>ACHC</sub> ), 36.9 (CH <sub>2</sub> β <sub>Tyr</sub> ), 36.9 (CH <sub>2</sub> β <sub>Tyr</sub> ), 33.6 (CH <sub>2</sub> <sub>ACHC</sub> ), 32.6 (CH <sub>2</sub> <sub>ACHC</sub> ), 32.5 (CH <sub>2</sub> <sub>ACHC</sub> ), 28.5 (CH <sub>2</sub> <sub>ACHC</sub> ), 28.5 (CH <sub>2</sub> <sub>ACHC</sub> ), 24.32 (CH <sub>2</sub> <sub>ACHC</sub> ), 24.31 (CH <sub>2</sub> <sub>ACHC</sub> ), 22.5 (CH <sub>3</sub> <sub>Ac</sub> ), 22.4 (CH <sub>3</sub> <sub>Ac</sub> );	calculated: 434.49; found: 457.9 [M+Na] <sup>+</sup> .

## 5 Experimental part

Peptide	Structure	MW (g/mol)	Yield (mg)	<sup>1</sup> H-NMR	<sup>13</sup> C-NMR	ESI-MS (m/z)
Ac-L-Tyr-rac-ACHC-D-Ser-NH-TG/H 96a/b		<b>C<sub>21</sub>H<sub>30</sub>N<sub>4</sub>O</b>  5  434.49	51.2  (83%)	<sup>1</sup> H-NMR (400.0 MHz, d <sub>6</sub> -DMSO, 25°C): δ (ppm) = 7.04 (dd, J = 8.6 Hz, 6.3 Hz, 4H, ArH <sub>Tyr</sub> ), 6.68 (dd, J = 8.6 Hz, 2.2 Hz, 4H, ArH <sub>Tyr</sub> ), 4.30 (s, 3H, CH <sub>Ar</sub> Tyr), 4.14 (m, 1H, CH <sub>α</sub> Ser), 3.66 (m, 2H, CH <sub>β</sub> ACHC), 3.60 (m, 4H, CH <sub>2</sub> β Ser), 2.87 (dd, J = 13.6 Hz, 5.8 Hz, 1H, CH <sub>2</sub> β Tyr), 2.78 (dd, J = 14.1 Hz, 3.5 Hz 1H, CH <sub>2</sub> β Tyr), 2.51 (m, 2H, CH <sub>2</sub> β Tyr), 2.30 (m, 2H, CH <sub>α</sub> ACHC), 1.79 (2 s, 9H, CH <sub>3</sub> Ac, CH <sub>3</sub> Ac, CH <sub>2</sub> ACHC) 1.67 (m, 5H, CH <sub>2</sub> ACHC), 1.41 (m, 2H, CH <sub>2</sub> ACHC), 1.20 (m, 6H, CH <sub>2</sub> ACHC);	<sup>13</sup> C-NMR (100.6 MHz, d <sub>6</sub> -DMSO, 25°C): δ (ppm) = 174.9/174.9/173.8/173.6/171.8/171.4 (CO), 155.9 (C <sub>Ar</sub> -OH), 130.9 (CH <sub>Ar</sub> Tyr), 128.9 (Cq <sub>Tyr</sub> ), 115.7 (CH <sub>Ar</sub> Tyr), 62.2 (CH <sub>2</sub> β Ser), 62.1 (CH <sub>2</sub> β Ser), 55.7 (CH <sub>α</sub> Ser), 55.1 (CH <sub>α</sub> Ser), 54.8 (CH <sub>α</sub> Tyr), 54.5 (CH <sub>α</sub> Tyr), 50.0 (CH <sub>α</sub> ACHC), 49.9 (CH <sub>α</sub> ACHC), 49.9 (CH <sub>β</sub> ACHC), 49.6 (CH <sub>β</sub> ACHC), 37.8 (CH <sub>2</sub> β Tyr), 37.6 (CH <sub>2</sub> β Tyr), 33.0 (CH <sub>2</sub> ACHC), 29.7 (CH <sub>2</sub> ACHC), 27.5 (CH <sub>2</sub> ACHC), 25.1 (CH <sub>2</sub> ACHC), 24.9 (CH <sub>2</sub> ACHC), 24.4 (CH <sub>2</sub> ACHC), 24.1 (CH <sub>2</sub> ACHC), 23.9 (CH <sub>2</sub> ACHC), 23.1 (CH <sub>3</sub> Ac), 22.9 (CH <sub>3</sub> Ac);	calculated: 434.49; found: 457.2 [M+Na] <sup>+</sup> (100), 435.74 [M+H] <sup>+</sup> (50).
Ac-D-His-ProAib-L-Tyr-NH-TG/H 97a/b		<b>C<sub>26</sub>H<sub>35</sub>N<sub>7</sub>O</b>  6  541.60	76.1  (quant.)	<sup>1</sup> H-NMR (400.0 MHz, CD <sub>3</sub> OD, 25°C): δ (ppm) = 8.56 (s, 1H, CH <sub>Imi</sub> ), 7.28 (s, 1H, CH <sub>Imi</sub> ), 7.06 (d, J = 8.1 Hz, 2H, ArH <sub>Tyr</sub> ), 6.70 (d, J = 8.3 Hz, 2H, ArH <sub>Tyr</sub> ), 4.80 (t, J = 6.7 Hz, 1H, CH <sub>α</sub> Pro), 4.41 (dd, J = 9.6 Hz, 4.8 Hz, 1H, CH <sub>α</sub> His), 4.24 (t, J = 6.8 Hz, 1H, CH <sub>α</sub> Tyr), 3.49 (m, 2H, CH <sub>2</sub> δ Pro), 3.18 (dd, J = 14.1 Hz, 4.5 Hz, 2H, CH <sub>2</sub> β His), 2.95 (m, 2H, CH <sub>2</sub> β Tyr), 2.17 (m, 1H, CH <sub>2</sub> β Pro), 1.99 (m, 1H, CH <sub>2</sub> β Pro), 1.91 (m, 5H, CH <sub>3</sub> Ac, CH <sub>2</sub> γ Pro), 1.38 (s, CH <sub>3</sub> Aib), 1.27 (s, CH <sub>3</sub> Aib);	<sup>13</sup> C-NMR (100.6 MHz, CD <sub>3</sub> OD, 25°C): δ (ppm) = 176.8/174.6/173.2/171.6 (CO), 157.3 (C <sub>Ar</sub> -OH), 135.3 (CH <sub>Imi</sub> ), 131.8 (Cq <sub>Imi</sub> ), 131.3 (Cq <sub>Tyr</sub> ), 129.8 (CH <sub>Ar</sub> ), 118.6 (CH <sub>Imi</sub> ), 116.2 (CH <sub>Ar</sub> Tyr), 62.9 (CH <sub>α</sub> Tyr), 58.2 (CH <sub>α</sub> Pro), 56.6 (CH <sub>α</sub> His), 52.8 (Cq <sub>Aib</sub> ), 37.2 (CH <sub>2</sub> β Tyr), 30.3 (CH <sub>2</sub> δ Pro), 28.1 (CH <sub>2</sub> β His), 26.2 (CH <sub>2</sub> β Pro), 25.9 (CH <sub>2</sub> γ Pro), 24.9 (CH <sub>3</sub> Aib), 24.6 (CH <sub>3</sub> Aib), 22.5 (CH <sub>3</sub> Ac);	calculated: 541.60; found: 542.2 [M+H] <sup>+</sup> .
Ac-L-Ser-ProAib-L-Tyr-NH-TG/H 98a/b		<b>C<sub>23</sub>H<sub>33</sub>N<sub>5</sub>O</b>  7  491.24	77.1  (quant.)	<sup>1</sup> H-NMR (400.0 MHz, CD <sub>3</sub> OD, 25°C): δ (ppm) = 7.10 (d, J = 6.8 Hz, 2H, ArH <sub>Tyr</sub> ), 6.70 (d, J = 6.3 Hz, 2H, ArH <sub>Tyr</sub> ), 4.77 (t, J = 6.3 Hz, 1H, CH <sub>α</sub> Pro), 4.42 (m, 1H, CH <sub>α</sub> Ser), 4.24 (t, J = 6.1 Hz, 1H, CH <sub>α</sub> Tyr), 3.85 (m, 2H, CH <sub>2</sub> β Ser) 3.72 (t, J = 8.1 Hz, 1H, CH <sub>2</sub> δ Pro), 3.48 (m, 1H, CH <sub>2</sub> δ Pro), 3.25 (d, J = 14.1 Hz, 1H, CH <sub>2</sub> β Tyr), 2.93 (t, J = 12.0 Hz, 1H, CH <sub>2</sub> β Tyr), 2.24 (m, 1H, CH <sub>2</sub> β Pro), 1.99 (s, 5H, CH <sub>3</sub> Ac, CH <sub>2</sub> γ Pro), 1.88 (m, 1H, CH <sub>2</sub> β Pro), 1.35 (s, CH <sub>3</sub> Aib), 1.17 (s, CH <sub>3</sub> Aib);	<sup>13</sup> C-NMR (100.6 MHz, CD <sub>3</sub> OD, 25°C): δ (ppm) = 176.9/176.8/174.5/173.4/172.7 (CO), 157.3 (C <sub>Ar</sub> -OH), 131.3 (Cq <sub>Tyr</sub> ), 129.9 (CH <sub>Ar</sub> ), 116.2 (CH <sub>Ar</sub> Tyr), 63.0 (CH <sub>2</sub> β Ser), 62.8 (CH <sub>α</sub> Ser), 58.0 (CH <sub>α</sub> Pro), 56.5 (CH <sub>α</sub> Tyr), 54.5 (Cq <sub>Aib</sub> ), 36.9 (CH <sub>2</sub> β Tyr), 30.4 (CH <sub>2</sub> δ Pro), 26.3 (CH <sub>2</sub> β Pro), 25.9 (CH <sub>2</sub> γ Pro), 24.5 (CH <sub>3</sub> Aib), 22.3 (CH <sub>3</sub> Ac);	calculated: 491.24; found: 514.2 [M+Na] <sup>+</sup> .

## 5 Experimental part

Peptide	Structure	MW (g/mol)	Yield (mg)	<sup>1</sup> H-NMR	<sup>13</sup> C-NMR	ESI-MS (m/z)
Ac-L-Ser-ProAib-L-Ser-NH-TG/H 99a/b		C <sub>17</sub> H <sub>29</sub> N <sub>5</sub> O <sub>7</sub>  415.21	63.1 (quant.).	<sup>1</sup> H-NMR (400.0 MHz, CD <sub>3</sub> OD, 25°C): δ (ppm) = 4.78 (t, J = 6.4 Hz, 1H, CHα <sub>Pro</sub> ), 4.35 (t, J = 7.0 Hz, 1H, CHα <sub>Ser</sub> ), 4.29 (t, J = 4.0 Hz, 1H, CHα <sub>Ser</sub> ), 3.83 (m, 6H, CH <sub>2</sub> β <sub>Ser</sub> , CH <sub>2</sub> β <sub>Ser</sub> , CH <sub>2</sub> δ <sub>Pro</sub> ), 2.29 (m, 1H, CH <sub>2</sub> β <sub>Pro</sub> ), 2.10 (m, 2H, CH <sub>2</sub> β <sub>Pro</sub> , CH <sub>2</sub> γ <sub>Pro</sub> ), 2.00 (brs, 4H, CH <sub>3</sub> <sub>Ac</sub> , CH <sub>2</sub> γ <sub>Pro</sub> ), 1.48 (s, CH <sub>3</sub> <sub>Aib</sub> ), 1.44 (s, CH <sub>3</sub> <sub>Aib</sub> );	<sup>13</sup> C-NMR (100.6 MHz, CD <sub>3</sub> OD, 25°C): δ (ppm) = 176.9/175.3/174.7/173.4/172.6 (CO), 63.1 (CH <sub>2</sub> β <sub>Ser</sub> ), 62.9 (CH <sub>2</sub> β <sub>Ser</sub> ), 62.8 (CHα <sub>Ser</sub> ), 58.2 (CHα <sub>Ser</sub> ), 57.7 (CHα <sub>Pro</sub> ), 54.6 (Cq <sub>Aib</sub> ), 30.4 (CH <sub>2</sub> δ <sub>Pro</sub> ), 26.2 (CH <sub>2</sub> β <sub>Pro</sub> ), 26.0 (CH <sub>2</sub> γ <sub>Pro</sub> ), 25.1 (CH <sub>3</sub> <sub>Aib</sub> ), 22.3 (CH <sub>3</sub> <sub>Ac</sub> );	Calculated 415.21; found: 438.9 [M+Na] <sup>+</sup> .
Ac-L-Tyr-L-Tyr-NH-TG/H 100a/b		C <sub>20</sub> H <sub>23</sub> N <sub>3</sub> O <sub>5</sub>  385.16	61.0 (quant.).	<sup>1</sup> H-NMR (400.0 MHz, CD <sub>3</sub> OD, 25°C): δ (ppm) = 7.00 (dd, J = 11.3 Hz, 8.6 Hz, 4 H, ArH <sub>Tyr</sub> ), 6.67 (dd, J = 8.3 Hz, 2.2 Hz, 4 H, ArH <sub>Tyr</sub> ), 4.48 (m, 2H, CHα <sub>Tyr</sub> ), 3.03 (dd, J = 14.1 Hz, 5.8 Hz, 1H, CH <sub>2</sub> β <sub>Tyr</sub> ), 2.92 (dd, J = 13.8 Hz, 6.0 Hz, 1H, CH <sub>2</sub> β <sub>Tyr</sub> ), 2.79 (dd, J = 14.1 Hz, 8.6 Hz, 1H, CH <sub>2</sub> β <sub>Tyr</sub> ), 2.70 (dd, J = 14.1 Hz, 8.8 Hz, 1H, CH <sub>2</sub> β <sub>Tyr</sub> ), 1.88 (s, CH <sub>3</sub> <sub>Ac</sub> );	<sup>13</sup> C-NMR (100.6 MHz, CD <sub>3</sub> OD, 25°C): δ (ppm) = 175.9/173.5/173.3 (CO), 157.4 (C <sub>Ar</sub> -OH), 157.3 (C <sub>Ar</sub> -OH), 131.5/131.3/129.1/129.0/116.2 (CH <sub>Ar</sub> <sub>Tyr</sub> ), 56.6/55.8 (CHα <sub>Tyr</sub> ), 38.0/37.8 (CH <sub>2</sub> β <sub>Tyr</sub> ), 22.4 (CH <sub>3</sub> <sub>Ac</sub> ).	calculated: 385.16; found: 408.2 [M+Na] <sup>+</sup> .
Ac-L-Tyr-Gly-L-Tyr-NH-TG/H 101a/b		C <sub>22</sub> H <sub>26</sub> N <sub>4</sub> O <sub>6</sub>  442.19	53.0 (84%).	<sup>1</sup> H-NMR (400.0 MHz, CD <sub>3</sub> OD, 25°C): δ (ppm) = 7.08 (dd, J = 8.3 Hz, 3.8 Hz, 4 H, ArH <sub>Tyr</sub> ), 6.75 (dd, J = 8.6 Hz, 2.2 Hz, 4 H, ArH <sub>Tyr</sub> ), 4.50 (dd, J = 8.6 Hz, 5.1 Hz, 1H, CHα <sub>Tyr</sub> ), 4.43 (dd, J = 8.6 Hz, 6.6 Hz, 1H, CHα <sub>Tyr</sub> ), 3.89 (d, J = 16.9 Hz, 1H, CH <sub>2</sub> <sub>Gly</sub> ), 3.66 (d, J = 16.9 Hz, 1H, CH <sub>2</sub> <sub>Gly</sub> ), 3.03 (m, 2H, CH <sub>2</sub> β <sub>Tyr</sub> ), 2.83 (dd, J = 13.8 Hz, 6.0 Hz, 2H, CH <sub>2</sub> β <sub>Tyr</sub> ), 1.93 (s, CH <sub>3</sub> <sub>Ac</sub> );	<sup>13</sup> C-NMR (100.6 MHz, CD <sub>3</sub> OD, 25°C): δ (ppm) = 176.5/174.9/174.3/171.6 (CO), 156.4 (C <sub>Ar</sub> -OH), 156.3 (C <sub>Ar</sub> -OH), 131.4/131.3/129.3/129.1/116.3 (CH <sub>Ar</sub> <sub>Tyr</sub> ), 56.9/56.1 (CHα <sub>Tyr</sub> ), 43.4 (CH <sub>2</sub> <sub>Gly</sub> ), 37.6/37.4 (CH <sub>2</sub> β <sub>Tyr</sub> ), 22.6 (CH <sub>3</sub> <sub>Ac</sub> );	calculated: 442.19; found: 465.2 [M+Na] <sup>+</sup> .
Ac-D-Asp-β-Ala-D-Asp-NH-TG/H 102a/b		C <sub>13</sub> H <sub>20</sub> N <sub>4</sub> O <sub>8</sub>  360.32	61.1 (quant.).	<sup>1</sup> H-NMR (400.0 MHz, CD <sub>3</sub> OD, 25°C): δ (ppm) = 4.73 (dd, J = 7.8 Hz, 5.6 Hz, 1H, CHα <sub>Asp</sub> ), 4.66 (dd, J = 7.1 Hz, 5.8 Hz, 1H, CHα <sub>Asp</sub> ), 3.50 (m, 1H, CH <sub>2</sub> <sub>β-Ala</sub> ), 3.40 (m, 1H, CH <sub>2</sub> <sub>β-Ala</sub> ), 2.78 (m, 4H, CH <sub>2</sub> β <sub>Asp</sub> ), 2.43 (m, 1H, CH <sub>2</sub> <sub>β-Ala</sub> ), 1.99 (s, 3H, CH <sub>3</sub> <sub>Ac</sub> );	<sup>13</sup> C-NMR (100.6 MHz, CD <sub>3</sub> OD, 25°C): δ (ppm) = 174.1/174.1/173.3 (CO), 51.4 (CHα <sub>Asp</sub> ), 51.1 (CHα <sub>Asp</sub> ), 37.1 (CH <sub>2</sub> β <sub>Asp</sub> ), 36.8 (CH <sub>2</sub> <sub>β-Ala</sub> ), 36.6 (CH <sub>2</sub> <sub>β-Ala</sub> ), 22.7 (CH <sub>3</sub> <sub>Ac</sub> );	calculated: 360.32; found: 383.1 [M+Na] <sup>+</sup> .

## 5 Experimental part

Peptide	Structure	MW (g/mol)	Yield (mg)	<sup>1</sup> H-NMR	<sup>13</sup> C-NMR	ESI-MS (m/z)
Ac-L-Tyr-Pro-Gly-L-Tyr-Pro-Gly-L-Ser-NH-TG/H 103a/b		C <sub>37</sub> H <sub>48</sub> N <sub>8</sub> O <sub>1</sub> 780.34	112.0 (quant.)	<sup>1</sup> H-NMR (400.0 MHz, CD <sub>3</sub> OD, 25°C): δ (ppm) = 7.07 (m, 4H, ArH <sub>Tyr</sub> ), 6.72 (m, 4H, ArH <sub>Tyr</sub> ), 4.80 (m, 2H, CHα <sub>Pro</sub> ), 4.36 (m, 3H, CHα <sub>Tyr</sub> ), CHα <sub>Tyr</sub> , CHα <sub>Ser</sub> , 3.84 (m, 8H, CH <sub>2</sub> <sub>Gly</sub> , CH <sub>2</sub> <sub>Gly</sub> , CH <sub>2</sub> δ <sub>Pro</sub> , CH <sub>2</sub> δ <sub>Pro</sub> ), 3.41 (m, 2H, CH <sub>2</sub> β <sub>Ser</sub> ), 3.03 (m, 4H, CH <sub>2</sub> β <sub>Tyr</sub> , CH <sub>2</sub> β <sub>Tyr</sub> ), 2.19 (m, 2H, CH <sub>2</sub> β <sub>Pro</sub> ), 2.03 (m, 6H, CH <sub>2</sub> β <sub>Pro</sub> , CH <sub>2</sub> γ <sub>Pro</sub> ), 1.87 (s, 3H, CH <sub>3</sub> <sub>Ac</sub> );	<sup>13</sup> C-NMR (100.6 MHz, CD <sub>3</sub> OD, 25°C): δ (ppm) = 177.3/175.1/174.8/173.0/172.9/172.8/171.9/171.5 (CO), 131.8 (CH <sub>Ar</sub> ), 131.6 (CH <sub>Ar</sub> ), 128.9 (C <sub>qAr</sub> ), 128.8 (C <sub>qAr</sub> ), 116.6 (CH <sub>Ar</sub> ), 116.3 (CH <sub>Ar</sub> ), 63.3 (CH <sub>2</sub> β <sub>Ser</sub> ), 62.8 (CHα <sub>Pro</sub> ), 62.4 (CHα <sub>Pro</sub> ), 57.2 (CHα <sub>Ser</sub> ), 54.7 (CHα <sub>Tyr</sub> ), 54.3 (CHα <sub>Tyr</sub> ), 44.1 (CH <sub>2</sub> <sub>Gly</sub> ), 43.4 (CH <sub>2</sub> <sub>Gly</sub> ), 37.5 (CH <sub>2</sub> β <sub>Tyr</sub> ), 37.2 (CH <sub>2</sub> β <sub>Tyr</sub> ), 30.3 (CH <sub>2</sub> δ <sub>Pro</sub> ), 26.3 (CH <sub>2</sub> β <sub>Pro</sub> ), 26.2 (CH <sub>2</sub> γ <sub>Pro</sub> ), 22.3 (CH <sub>3</sub> <sub>Ac</sub> );	calculated: 780.34; found: 781.3 [M+H] <sup>+</sup> (100), 803.2 [M+Na] <sup>+</sup> (73).
Ac-L-His-L-His-Pro-Gly-D-His-NH-TG/H 104a/b		C <sub>27</sub> H <sub>36</sub> N <sub>12</sub> O <sub>6</sub> 624.29	88.0 (quant.)	<sup>1</sup> H-NMR (400.0 MHz, CD <sub>3</sub> OD, 25°C): δ (ppm) = 8.80 (s, 3H, CH <sub>Imi</sub> ), 7.40 (s, 1H, CH <sub>Imi</sub> ), 7.32 (s, 1H, CH <sub>Imi</sub> ), 7.21 (s, 1H, CH <sub>Imi</sub> ), 4.89 (m, 1H, CHα <sub>Pro</sub> ), 4.70 (dd, J = 9.1 Hz, 4.8 Hz, 1H, CHα <sub>His</sub> ), 4.66 (dd, J = 8.3 Hz, 5.8 Hz, 1H, CHα <sub>His</sub> ), 4.38(t, J = 7.1 Hz, 1H, CHα <sub>His</sub> ), 3.9 (d, J = 17.1 Hz, 1H, CH <sub>2</sub> <sub>Gly</sub> ), 3.78 (d, J = 17.1 Hz, 2H, CH <sub>2</sub> <sub>Gly</sub> , CH <sub>2</sub> δ <sub>Pro</sub> ), 3.60 (m, 1H, CH <sub>2</sub> δ <sub>Pro</sub> ), 3.30-3.13 (m, 6H, CH <sub>2</sub> β <sub>His</sub> ), 2.28 (m, 1H, CH <sub>2</sub> β <sub>Pro</sub> ), 2.09 (m, 1H, CH <sub>2</sub> β <sub>Pro</sub> ), 1.97 (m, 2H, CH <sub>2</sub> γ <sub>Pro</sub> ), 1.94 (s, 3H, CH <sub>3</sub> <sub>Ac</sub> );	<sup>13</sup> C-NMR (100.6 MHz, CD <sub>3</sub> OD, 25°C): δ (ppm) = 175.5/174.5/173.6/172.1/171.7/170.9 (CO), 135.14/135.12/135.01 (C <sub>qImi</sub> ), 131.3/131.1/130.3 (CH <sub>Imi</sub> ), 118.6/118.5/118.4 (CH <sub>Imi</sub> ), 62.6 (CHα <sub>Pro</sub> ), 53.6 (CHα <sub>His</sub> ), 53.3 (CHα <sub>His</sub> ), 51.9 (CHα <sub>His</sub> ), 43.8 (CH <sub>2</sub> <sub>Gly</sub> ), 30.5 (CH <sub>2</sub> δ <sub>Pro</sub> ), 28.0 (CH <sub>2</sub> β <sub>His</sub> ), 27.7 (CH <sub>2</sub> β <sub>His</sub> ), 27.4 (CH <sub>2</sub> β <sub>His</sub> ), 26.3 (CH <sub>2</sub> β <sub>Pro</sub> ), 26.1 (CH <sub>2</sub> γ <sub>Pro</sub> ), 22.5 (CH <sub>3</sub> <sub>Ac</sub> );	calculated : 624.29; found: 625.2 [M+H] <sup>+</sup> .
Ac-L-Ser-Ahx-L-Asp-Ahx-D-His-NH-TG/H 105a/b		C <sub>27</sub> H <sub>44</sub> N <sub>8</sub> O <sub>9</sub> 624.32	113.0 (quant.)	<sup>1</sup> H-NMR (400.0 MHz, CD <sub>3</sub> OD, 25°C): δ (ppm) = 8.83 (s, 1H, CH <sub>Imi</sub> ), 7.34 (s, 1H, CH <sub>Imi</sub> ), 4.75 (dd, J = 8.8 Hz, 5.3 Hz, 1H, CHα <sub>His</sub> ), 4.67 (t, J = 7.6 Hz, 1H, CHα <sub>Asp</sub> ), 4.37 (t, J = 5.3 Hz, 1H, CHα <sub>Ser</sub> ), 3.76 (d, J = 5.0 Hz, 1H, CH <sub>2</sub> β <sub>Ser</sub> ), 3.19 (m, 5H, NHCH <sub>2</sub> <sub>Ahx</sub> , NHCH <sub>2</sub> <sub>Ahx</sub> , CH <sub>2</sub> β <sub>Asp</sub> ), 3.05 (dd, J = 15.4 Hz, 9.1 Hz, 1H, CH <sub>2</sub> β <sub>Asp</sub> ), 2.85 (dd, J = 16.6 Hz, 5.8 Hz, 1H, CH <sub>2</sub> β <sub>His</sub> ), 2.69 (dd, J = 16.4 Hz, 7.8 Hz, 1H, CH <sub>2</sub> β <sub>His</sub> ), 2.23 (m, 4H, CH <sub>2</sub> CO <sub>Ahx</sub> ), 2.02 (s, 3H, CH <sub>3</sub> <sub>Ac</sub> ), 1.62 (m, 2H, CH <sub>2</sub> <sub>Ahx</sub> ), 1.50 (m, 6H, CH <sub>2</sub> <sub>Ahx</sub> ), 1.34 (m, 2H, CH <sub>2</sub> <sub>Ahx</sub> ), 1.23 (m, 2H, CH <sub>2</sub> <sub>Ahx</sub> );	<sup>13</sup> C-NMR (100.6 MHz, CD <sub>3</sub> OD, 25°C): δ (ppm) = 176.2/176.1/174.8/173.6/169.0 (CO), 135.0 (C <sub>qImi</sub> ), 131.5 (CH <sub>Imi</sub> ), 118.5 (CH <sub>Imi</sub> ), 63.1 (CH <sub>2</sub> β <sub>Ser</sub> ), 57.1 (CHα <sub>Ser</sub> ), 52.9 (CHα <sub>His</sub> ), 51.8 (CHα <sub>Asp</sub> ), 43.8 (CH <sub>2</sub> <sub>Gly</sub> ), 40.3 (NHCH <sub>2</sub> <sub>Ahx</sub> ), 36.7 (CH <sub>2</sub> β <sub>Asp</sub> ), 36.6 (CH <sub>2</sub> CO <sub>Ahx</sub> ), 29.9 (CH <sub>2</sub> β <sub>His</sub> ), 28.4/28.1 (CH <sub>2</sub> β <sub>Ahx</sub> ), 27.6/27.5 (CH <sub>2</sub> <sub>Ahx</sub> ), 26.6/26.5 (CH <sub>2</sub> <sub>Ahx</sub> ), 22.7 (CH <sub>3</sub> <sub>Ac</sub> );	calculated : 624.32; found: 625.2 [M+H] <sup>+</sup> .

## 5 Experimental part

Peptide	Structure	MW (g/mol)	Yield (mg)	<sup>1</sup> H-NMR	<sup>13</sup> C-NMR	ESI-MS (m/z)
Ac-D-His-(R,R)-ACHC-L-Tyr-NH-TG/H 106a/b		C <sub>24</sub> H <sub>32</sub> N <sub>6</sub> O <sub>5</sub> 84.24	49.6 (72%).	<sup>1</sup> H-NMR (400.0 MHz, CD <sub>3</sub> OD, 25°C): δ (ppm) = 8.74 (s, 1H, CH <sub>Imi</sub> ), 7.2 (s, 1H, CH <sub>Imi</sub> ), 7.03 (d, J = 8.3 Hz, 2H, ArH <sub>Tyr</sub> ), 6.62 (d, J = 8.3 Hz, 2H, ArH <sub>Tyr</sub> ), 4.55 (t, J = 5.8 Hz, 1H, CH <sub>His</sub> ), 4.49 (dd, J = 9.8 Hz, 5.0 Hz, 1H, CH <sub>Tyr</sub> ), 3.99 (dt, J = 11.4 Hz, 4.3 Hz, 1H, CH <sub>ACHC</sub> ), 3.09 (dd, J = 15.1 Hz, 5.6 Hz, 1H, CH <sub>2</sub> <sub>His</sub> ), 3.03 (dd, J = 14.1 Hz, 5.1 Hz, 1H, CH <sub>2</sub> <sub>His</sub> ), 2.75 (ddd, J = 13.9 Hz, 9.8 Hz, 6.3 Hz, 2H, CH <sub>2</sub> <sub>Tyr</sub> ), 2.24 (dt, J = 11.6 Hz, 3.0 Hz, 1H, CH <sub>ACHC</sub> ), 1.96 (s, 3H, CH <sub>3</sub> <sub>Ac</sub> ), 1.88 (m, 2H, CH <sub>2</sub> <sub>ACHC</sub> ), 1.75 (m, 2H, CH <sub>2</sub> <sub>ACHC</sub> ), 1.33 (m, 4H, CH <sub>2</sub> <sub>ACHC</sub> );	<sup>13</sup> C-NMR (100.6 MHz, CD <sub>3</sub> OD, 25°C): δ (ppm) = 177.1/175.7/173.1/170.9/167.8 (CO), 157.4 (C <sub>Ar</sub> -OH), 134.7 (CH <sub>Imi</sub> ), 131.3 (CH <sub>Ar</sub> <sub>Tyr</sub> ), 130.5 (C <sub>q</sub> <sub>Imi</sub> ), 129.6 (C <sub>q</sub> <sub>Tyr</sub> ), 118.7 (CH <sub>Imi</sub> ), 116.2 (CH <sub>Ar</sub> <sub>Tyr</sub> ), 53.1 (CH <sub>Ar</sub> <sub>Tyr</sub> ), 51.9 (CH <sub>His</sub> ), 51.1 (CH <sub>ACHC</sub> ), 50.5 (CH <sub>ACHC</sub> ), 38.2 (CH <sub>2</sub> <sub>Tyr</sub> ), 33.5 (CH <sub>2</sub> <sub>ACHC</sub> ), 31.3 (CH <sub>2</sub> <sub>ACHC</sub> ), 28.7 (CH <sub>2</sub> <sub>His</sub> ), 26.08 (CH <sub>2</sub> <sub>ACHC</sub> ), 26.02 (CH <sub>2</sub> <sub>ACHC</sub> ), 22.5 (CH <sub>3</sub> <sub>Ac</sub> );	calculated : 484.24; found: 485.3 [M+H] <sup>+</sup> .
For the NMR Titration this Peptid was alone and also with AgNO <sub>3</sub> in D <sub>2</sub> O measured				<sup>1</sup> H-NMR (600 MHz, D <sub>2</sub> O, 25°C): δ (ppm) = 8.54 (d, J = 1.3 Hz, 1H, CH <sub>Imi</sub> ), 8.23 (d, J = 7.5 Hz, 1H, NH <sub>Tyr</sub> ), 8.12 (d, J = 7.9 Hz, 1H, NH <sub>His</sub> ), 8.01 (d, J = 9.7 Hz, 1H, NH <sub>ACHC</sub> ), 7.48 (s, 1H, NH <sub>2</sub> <sub>Amid</sub> ), 7.08 (s, 2H, ArH <sub>Tyr</sub> ), 7.07 (s, 1H, NH <sub>2</sub> <sub>Amid</sub> ), 7.04 (s, 1H, CH <sub>Imi</sub> ), 6.68 (d, J = 8.8 Hz, 2H, ArH <sub>Tyr</sub> ), 4.43 (dq, J = 7.9 Hz, 5.6 Hz, 1H, CH <sub>His</sub> ), 4.35 (ddd, J = 10.1 Hz, 7.6 Hz, 5.1 Hz, 1H, CH <sub>Tyr</sub> ), 3.86 (m, 1H, CH <sub>ACHC</sub> ), 2.99 (dd, J = 14.7 Hz, 5.1 Hz, 1H, CH <sub>2</sub> <sub>Tyr</sub> ), 2.86 (dd, J = 16.2 Hz, 5.3 Hz, 1H, CH <sub>2</sub> <sub>His</sub> ), 2.79 (dd, J = 14.7 Hz, 10.1 Hz, 1H, CH <sub>2</sub> <sub>Tyr</sub> ), 2.66 (dd, J = 16.2 Hz, 7.9 Hz, 1H, CH <sub>2</sub> <sub>His</sub> ), 2.31 (dt, J = 8.7 Hz, 3.7 Hz, 1H, CH <sub>ACHC</sub> ), 1.92 (s, 3H, CH <sub>3</sub> <sub>Ac</sub> ), 1.83 (m, 1H, CH <sub>2</sub> <sub>ACHC</sub> ), 1.80 (m, 1H, CH <sub>2</sub> <sub>ACHC</sub> ), 1.73 (m, 1H, CH <sub>2</sub> <sub>ACHC</sub> ), 1.69 (m, 2H, CH <sub>2</sub> <sub>ACHC</sub> ), 1.35 (m, 1H, CH <sub>2</sub> <sub>ACHC</sub> ), 1.28 (m, 1H, CH <sub>2</sub> <sub>ACHC</sub> ), 1.24 (m, 1H, CH <sub>2</sub> <sub>ACHC</sub> ), 1.22 (m, 1H, CH <sub>2</sub> <sub>ACHC</sub> );	<sup>13</sup> C-NMR (150 MHz, D <sub>2</sub> O, 25°C): δ (ppm) = 177.4 (CO <sub>Tyr</sub> ), 176.4 (CO <sub>Amid</sub> ), 174.1 (CO <sub>Ac</sub> ), 171.2 (CO <sub>ACHC</sub> ), 154.7 (C <sub>Ar</sub> -OH), 134.4 (CH <sub>Imi</sub> ), 130.6 (CH <sub>Ar</sub> <sub>Tyr</sub> ), 129.7 (C <sub>q</sub> <sub>Imi</sub> ), 128.8 (C <sub>q</sub> <sub>Tyr</sub> ), 117.4 (CH <sub>Imi</sub> ), 115.6 (CH <sub>Ar</sub> <sub>Tyr</sub> ), 55.9 (CH <sub>Ar</sub> <sub>Tyr</sub> ), 52.7 (CH <sub>His</sub> ), 50.1 (CH <sub>ACHC</sub> ), 49.8 (CH <sub>ACHC</sub> ), 36.5 (CH <sub>2</sub> <sub>Tyr</sub> ), 31.9 (CH <sub>2</sub> <sub>ACHC</sub> ), 29.7 (CH <sub>2</sub> <sub>ACHC</sub> ), 27.8 (CH <sub>2</sub> <sub>His</sub> ), 24.4 (CH <sub>2</sub> <sub>ACHC</sub> ), 21.9 (CH <sub>3</sub> <sub>Ac</sub> );	

## 5 Experimental part

Peptide	Structure	MW (g/mol)	Yield (mg)	<sup>1</sup> H-NMR	<sup>13</sup> C-NMR	ESI-MS (m/z)
Ac-D-His-(S,S)-ACHC-L-Tyr-NH-TG/H 107a/b		C <sub>24</sub> H <sub>32</sub> N <sub>6</sub> O <sub>5</sub> 484.24	49.6 (72%)	<sup>1</sup> H-NMR (400.0 MHz, CD <sub>3</sub> OD, 25°C): δ (ppm) = 8.71 (s, 1H, CH <sub>I</sub> mi), 7.3 (s, 1H, CH <sub>I</sub> mi), 7.05 (d, J = 8.1 Hz, 2H, ArH <sub>Tyr</sub> ), 6.62 (d, J = 8.3 Hz, 2H, ArH <sub>Tyr</sub> ), 4.66 (t, J = 6.6 Hz, 1H, CH <sub>α</sub> His), 4.55 (dd, J = 8.6 Hz, 6.1 Hz, 1H, CH <sub>α</sub> Tyr), 3.85 (m, 1H, CH <sub>β</sub> ACHC), 3.19 (dd, J = 14.9 Hz, 5.3 Hz, 1H, CH <sub>2</sub> β His), 3.04 (dd, J = 14.1 Hz, 5.8 Hz, 1H, CH <sub>2</sub> β Tyr), 2.96 (dd, J = 14.9 Hz, 7.8 Hz, 1H, CH <sub>2</sub> β His), 2.80 (dd, J = 13.9 Hz, 9.1 Hz, 1H, CH <sub>2</sub> β Tyr), 2.26 (m, 1H, CH <sub>α</sub> ACHC), 1.99 (s, 3H, CH <sub>3</sub> Ac), 1.88 (m, 1H, CH <sub>2</sub> ACHC), 1.68 (m, 3H, CH <sub>2</sub> ACHC), 1.30 (m, 4H, CH <sub>2</sub> ACHC);	<sup>13</sup> C-NMR (100.6 MHz, CD <sub>3</sub> OD, 25°C): δ (ppm) = 177.1/176.2/173.5/171.2/ (CO), 157.5 (C <sub>Ar</sub> -OH), 134.8 (CH <sub>I</sub> mi), 131.5 (Cq <sub>I</sub> mi), 131.3 (CH <sub>Ar</sub> Tyr), 128.9 (Cq <sub>Tyr</sub> ), 118.6 (CH <sub>I</sub> mi), 116.2 (CH <sub>Ar</sub> Tyr), 55.5 (CH <sub>α</sub> Tyr), 53.7 (CH <sub>α</sub> His), 51.6 (CH <sub>α</sub> ACHC), 50.9 (CH <sub>β</sub> ACHC), 38.5 (CH <sub>2</sub> β Tyr), 33.2 (CH <sub>2</sub> ACHC), 30.5 (CH <sub>2</sub> ACHC), 28.3 (CH <sub>2</sub> β His), 25.9 (CH <sub>2</sub> ACHC), 25.8 (CH <sub>2</sub> ACHC), 22.8 (CH <sub>3</sub> Ac);	calculated : 484.24; found: 485.2 [M+H] <sup>+</sup> .
With the help of the NMR Titration in D <sub>2</sub> O we could the signals of the SS diastereomers from the mixed diastereomers distinguish as showed:				<sup>1</sup> H-NMR (600 MHz, D <sub>2</sub> O, 25°C): δ (ppm) = 8.56 (s, 1H, CH <sub>I</sub> mi), 8.24 (m, 1H, NH <sub>Tyr</sub> ), 8.07 (d, J = 8.1 Hz, 1H, NH <sub>His</sub> ), 7.97 (d, J = 9.7 Hz, 1H, NH <sub>ACHC</sub> ), 7.60 (s, 1H, NH <sub>2</sub> Amid), 7.22 (s, 1H, CH <sub>I</sub> mi), 7.10 (s, 2H, ArH <sub>Tyr</sub> ), 6.98 (s, 1H, NH <sub>2</sub> Amid), 6.80 (d, J = 8.8 Hz, 2H, ArH <sub>Tyr</sub> ), 4.57 (m, 1H, CH <sub>α</sub> Tyr), 4.48 (m, 1H, CH <sub>α</sub> Tyr), 3.75 (m, 1H, CH <sub>β</sub> ACHC), 3.08 (m, 1H, CH <sub>2</sub> β Tyr), 3.06 (m, 1H, CH <sub>2</sub> β His), 2.96 (m, 1H, CH <sub>2</sub> β His), 2.82 (m, 1H, CH <sub>2</sub> β Tyr), 2.24 (m, 1H, CH <sub>α</sub> ACHC), 1.93 (s, 3H, CH <sub>3</sub> Ac), 1.73 (m, 1H, CH <sub>2</sub> ε ACHC), 1.68 (m, 2H, CH <sub>2</sub> γ ACHC, CH <sub>2</sub> δ ACHC), 1.53 (m, 1H, CH <sub>2</sub> ζ ACHC), 1.24 (m, 1H, CH <sub>2</sub> δ ACHC), 1.18 (m, 1H, CH <sub>2</sub> ζ ACHC), 1.13 (m, 1H, CH <sub>2</sub> ε ACHC), 1.09 (m, 1H, CH <sub>2</sub> γ ACHC).	<sup>13</sup> C-NMR (150 MHz, D <sub>2</sub> O, 25°C): δ (ppm) = 176.5 (CO <sub>Tyr</sub> ), 176.1 (CO <sub>Amid</sub> ), 174.1 (CO <sub>Ac</sub> ), 171.2 (CO <sub>ACHC</sub> ), 154.6 (C <sub>Ar</sub> -OH), 134.4 (CH <sub>I</sub> mi), 130.9 (CH <sub>Ar</sub> Tyr), 130.0 (Cq <sub>I</sub> mi), 128.6 (Cq <sub>Tyr</sub> ), 117.5 (CH <sub>I</sub> mi), 115.6 (CH <sub>Ar</sub> Tyr), 54.3 (CH <sub>α</sub> Tyr), 53.5 (CH <sub>α</sub> His), 49.9 (CH <sub>β</sub> ACHC), 49.8 (CH <sub>α</sub> ACHC), 37.1 (CH <sub>2</sub> β Tyr), 31.7 (CH <sub>2</sub> γ ACHC), 29.4 (CH <sub>2</sub> ζ ACHC), 27.8 (CH <sub>2</sub> β His), 24.4 (CH <sub>2</sub> δ ACHC, CH <sub>2</sub> ε ACHC), 21.9 (CH <sub>3</sub> Ac);	



## 5 Experimental part

Peptide	Structure	MW (g/mol)	Yield (mg)	<sup>1</sup> H-NMR	<sup>13</sup> C-NMR	ESI-MS (m/z)
Ac-D-Ser-(R,R)-ACHC-L-Tyr-NH-TG/H 108a/b		C <sub>21</sub> H <sub>30</sub> N <sub>4</sub> O <sub>6</sub> 434.49	42.7 (69%)	<sup>1</sup> H-NMR (400.0 MHz, d <sub>6</sub> -DMSO, 25°C): δ (ppm) = 9.10 (s, 1H, OH), 7.78 (d, J = 8.1 Hz, 1H, NH), 7.70 (d, J = 8.8 Hz, 1H, NH), 7.67 (d, J = 7.8 Hz, 1H, NH), 7.10 (s, 1H, NH), 6.97 (d, J = 8.3 Hz, 2H, ArH <sub>Tyr</sub> ), 6.62 (d, J = 8.1 Hz, 2H, ArH <sub>Tyr</sub> ), 4.61 (m, 1H, CH <sub>α</sub> <sub>Tyr</sub> ) 4.24 (m, 2H, CH <sub>α</sub> <sub>Ser</sub> ), CH <sub>β</sub> <sub>ACHC</sub> , 3.76 (m, 1H, CH <sub>2</sub> β <sub>Ser</sub> ), 3.45 (m, 1H, CH <sub>2</sub> β <sub>Ser</sub> ), 2.81 (m, 1H, CH <sub>2</sub> β <sub>Tyr</sub> ), 2.68 (m, 1H, CH <sub>2</sub> β <sub>Tyr</sub> ), 2.20 (m, 1H, CH <sub>α</sub> <sub>ACHC</sub> ), 1.86 (s, 3H, CH <sub>3</sub> <sub>Ac</sub> ), 1.78 (m, 1H, CH <sub>2</sub> <sub>ACHC</sub> ), 1.62 (m, 3H, CH <sub>2</sub> <sub>ACHC</sub> ), 1.20 (m, 4H, CH <sub>2</sub> <sub>ACHC</sub> );	<sup>13</sup> C-NMR (100.6 MHz, d <sub>6</sub> -DMSO, 25°C): δ (ppm) = 172.9/172.8/169.5/169.1 (CO), 155.5 (C <sub>Ar</sub> -OH), 129.9 (CH <sub>Ar</sub> <sub>Tyr</sub> ), 127.9 (Cq <sub>Tyr</sub> ), 114.7 (CH <sub>Ar</sub> <sub>Tyr</sub> ), 62.2 (CH <sub>2</sub> β <sub>Ser</sub> ), 55.2 (CH <sub>α</sub> <sub>Ser</sub> ), 54.8 (CH <sub>α</sub> <sub>Tyr</sub> ), 49.5 (CH <sub>α</sub> <sub>ACHC</sub> ), 48.8 (CH <sub>β</sub> <sub>ACHC</sub> ), 36.8 (CH <sub>2</sub> β <sub>Tyr</sub> ), 32.3 (CH <sub>2</sub> <sub>ACHC</sub> ), 31.5 (CH <sub>2</sub> <sub>ACHC</sub> ), 28.7 (CH <sub>2</sub> <sub>ACHC</sub> ), 24.4 (CH <sub>2</sub> <sub>ACHC</sub> ), 22.3 (CH <sub>3</sub> <sub>Ac</sub> );	calculated : 434.49; found: 457.2 [M+Na] <sup>+</sup> .
Ac-D-Ser-(S,S)-ACHC-L-Tyr-NH-TG/H 109a/b		C <sub>21</sub> H <sub>30</sub> N <sub>4</sub> O <sub>6</sub> 434.49	37.6 (61%)	<sup>1</sup> H-NMR (400.0 MHz, d <sub>6</sub> -DMSO, 25°C): δ (ppm) = 9.10 (s, 1H, OH), 7.78 (d, J = 8.6 Hz, 1H, NH), 7.70 (d, J = 8.1 Hz, 1H, NH), 7.67 (d, J = 7.8 Hz, 1H, NH), 7.10 (s, 1H, NH), 6.98 (d, J = 8.3 Hz, 2H, ArH <sub>Tyr</sub> ), 6.63 (d, J = 8.1 Hz, 2H, ArH <sub>Tyr</sub> ), 4.61 (m, 1H, CH <sub>α</sub> <sub>Tyr</sub> ) 4.32 (m, 1H, CH <sub>α</sub> <sub>Ser</sub> ), 4.24 (m, 1H, CH <sub>β</sub> <sub>ACHC</sub> ), 3.56 (m, 1H, CH <sub>2</sub> β <sub>Ser</sub> ), 3.45 (m, 1H, CH <sub>2</sub> β <sub>Ser</sub> ), 2.88 (dd, J = 13.9 Hz, 4.8 Hz, 1H, CH <sub>2</sub> β <sub>Tyr</sub> ), 2.65 (dd, J = 13.6 Hz, 8.8 Hz, 1H, CH <sub>2</sub> β <sub>Tyr</sub> ), 2.26 (m, 1H, CH <sub>α</sub> <sub>ACHC</sub> ), 1.88 (s, 3H, CH <sub>3</sub> <sub>Ac</sub> ), 1.82 (m, 1H, CH <sub>2</sub> <sub>ACHC</sub> ), 1.58 (m, 2H, CH <sub>2</sub> <sub>ACHC</sub> ), 1.20 (m, 4H, CH <sub>2</sub> <sub>ACHC</sub> );	<sup>13</sup> C-NMR (100.6 MHz, d <sub>6</sub> -DMSO, 25°C): δ (ppm) = 173.4/173.1/169.3/169.1 (CO), 155.6 (C <sub>Ar</sub> -OH), 129.8 (CH <sub>Ar</sub> <sub>Tyr</sub> ), 127.6 (Cq <sub>Tyr</sub> ), 114.7 (CH <sub>Ar</sub> <sub>Tyr</sub> ), 61.8 (CH <sub>2</sub> β <sub>Ser</sub> ), 54.5 (CH <sub>α</sub> <sub>Ser</sub> ), 53.6 (CH <sub>α</sub> <sub>Tyr</sub> ), 49.5 (CH <sub>α</sub> <sub>ACHC</sub> ), 47.8 (CH <sub>β</sub> <sub>ACHC</sub> ), 36.6 (CH <sub>2</sub> β <sub>Tyr</sub> ), 32.0 (CH <sub>2</sub> <sub>ACHC</sub> ), 30.5 (CH <sub>2</sub> <sub>ACHC</sub> ), 28.5 (CH <sub>2</sub> <sub>ACHC</sub> ), 24.1 (CH <sub>2</sub> <sub>ACHC</sub> ), 22.7 (CH <sub>3</sub> <sub>Ac</sub> );	calculated : 434.49; found: 457.2 [M+Na] <sup>+</sup> .
Ac-L-Tyr-(R,R)-ACHC-D-Ser-NH-TG/H 110a/b		C <sub>21</sub> H <sub>30</sub> N <sub>4</sub> O <sub>5</sub> 434.49	46.7 (75%)	<sup>1</sup> H-NMR (400.0 MHz, d <sub>6</sub> -DMSO, 25°C): δ (ppm) = 7.90 (d, J = 8.8 Hz, 1H, NH), 7.60 (d, J = 8.1 Hz, 1H, NH), 7.52 (d, J = 7.8 Hz, 1H, NH), 7.22 (s, 1H, NH), 6.96 (d, J = 8.3 Hz, 2H, ArH <sub>Tyr</sub> ), 6.62 (d, J = 8.3 Hz, 2H, ArH <sub>Tyr</sub> ), 4.30 (m, 1H, CH <sub>α</sub> <sub>Tyr</sub> ), 4.14 (m, 1H, CH <sub>α</sub> <sub>Ser</sub> ), 3.70 (m, 1H, CH <sub>β</sub> <sub>ACHC</sub> ), 3.60 (dd, J = 10.8 Hz, 5.1 Hz, 1H, CH <sub>2</sub> β <sub>Ser</sub> ), 3.55 (dd, J = 10.8 Hz, 4.8 Hz, 1H, CH <sub>2</sub> β <sub>Ser</sub> ), 2.87 (dt, J = 8.6 Hz, 5.3 Hz, 1H, CH <sub>2</sub> β <sub>Tyr</sub> ), 2.54 (m, 1H, CH <sub>2</sub> β <sub>Tyr</sub> ), 2.29 (m, 1H, CH <sub>α</sub> <sub>ACHC</sub> ), 1.77 (s, 5H, CH <sub>3</sub> <sub>Ac</sub> ), CH <sub>2</sub> <sub>ACHC</sub> 1.62 (m, 2H, CH <sub>2</sub> <sub>ACHC</sub> ), 1.41 (m, 1H, CH <sub>2</sub> <sub>ACHC</sub> ), 1.15 (m, 3H, CH <sub>2</sub> <sub>ACHC</sub> );	<sup>13</sup> C-NMR (100.6 MHz, d <sub>6</sub> -DMSO, 25°C): δ (ppm) = 172.8/172.3/170.0/168.9 (CO), 155.5 (C <sub>Ar</sub> -OH), 129.9 (CH <sub>Ar</sub> <sub>Tyr</sub> ), 127.9 (Cq <sub>Tyr</sub> ), 114.7 (CH <sub>Ar</sub> <sub>Tyr</sub> ), 61.5 (CH <sub>2</sub> β <sub>Ser</sub> ), 55.7 (CH <sub>α</sub> <sub>Ser</sub> ), 54.8 (CH <sub>α</sub> <sub>Ser</sub> ), 53.9 (CH <sub>α</sub> <sub>Tyr</sub> ), 49.1 (CH <sub>α</sub> <sub>ACHC</sub> ), 48.5 (CH <sub>β</sub> <sub>ACHC</sub> ), 37.3 (CH <sub>2</sub> β <sub>Tyr</sub> ), 31.8 (CH <sub>2</sub> <sub>ACHC</sub> ), 29.3 (CH <sub>2</sub> <sub>ACHC</sub> ), 28.7 (CH <sub>2</sub> <sub>ACHC</sub> ), 24.3 (CH <sub>2</sub> <sub>ACHC</sub> ), 22.5 (CH <sub>3</sub> <sub>Ac</sub> );	calculated : 434.49; found: 457.2 [M+Na] <sup>+</sup> .

## 5 Experimental part

Peptide	Structure	MW (g/mol)	Yield (mg)	<sup>1</sup> H-NMR	<sup>13</sup> C-NMR	ESI-MS (m/z)
Ac-L-Tyr-(S,S)-ACHC-D-Ser-NH-TG/H 111a/b		C <sub>21</sub> H <sub>30</sub> N <sub>4</sub> O <sub>5</sub> 434.49	42.6 mg (69%).	<sup>1</sup> H-NMR (400.0 MHz, d <sub>6</sub> -DMSO, 25°C): δ (ppm) = 7.89 (dd, J = 8.6 Hz, 5.1 Hz, 1H, NH), 7.76 (dd, J = 12.1 Hz, 8.6 Hz, 1H, NH), 7.48 (d, J = 8.1 Hz, 1H, NH), 7.24 (s, 1H, NH), 6.99 (t, J = 8.1 Hz, 2H, ArH <sub>Tyr</sub> ), 6.60 (d, J = 8.3 Hz, 2H, ArH <sub>Tyr</sub> ), 4.30 (m, 1H, CH <sub>α</sub> <sub>Tyr</sub> ), 4.17 (m, 1H, CH <sub>α</sub> <sub>Ser</sub> ), 3.72 (m, 1H, CH <sub>β</sub> <sub>ACHC</sub> ), 3.60 (dd, J = 10.6 Hz, 5.1 Hz, 1H, CH <sub>2</sub> β <sub>Ser</sub> ), 3.46 (dd, J = 10.6 Hz, 5.6 Hz, 1H, CH <sub>2</sub> β <sub>Ser</sub> ), 2.71 (m, 1H, CH <sub>2</sub> β <sub>Tyr</sub> ), 2.51 (m, 1H, CH <sub>2</sub> β <sub>Tyr</sub> ), 2.29 (m, 1H, CH <sub>α</sub> <sub>ACHC</sub> ), 1.81 (m, 2H, CH <sub>2</sub> <sub>ACHC</sub> ), 1.72 (s, 3H, CH <sub>3</sub> <sub>Ac</sub> ), 1.64 (m, 2H, CH <sub>2</sub> <sub>ACHC</sub> ), 1.43 (m, 1H, CH <sub>2</sub> <sub>ACHC</sub> ), 1.20 (m, 3H, CH <sub>2</sub> <sub>ACHC</sub> );	<sup>13</sup> C-NMR (100.6 MHz, d <sub>6</sub> -DMSO, 25°C): δ (ppm) = 173.4/172.8/172.0 (CO), 155.5 (C <sub>Ar</sub> -OH), 129.9 (CH <sub>Ar</sub> <sub>Tyr</sub> ), 128.0 (C <sub>q</sub> <sub>Tyr</sub> ), 114.6 (CH <sub>Ar</sub> <sub>Tyr</sub> ), 64.8 (CH <sub>2</sub> β <sub>Ser</sub> ), 55.2 (CH <sub>α</sub> <sub>Ser</sub> ), 54.2 (CH <sub>α</sub> <sub>Ser</sub> ), 54.1 (CH <sub>α</sub> <sub>Tyr</sub> ), 49.2 (CH <sub>α</sub> <sub>ACHC</sub> ), 47.9 (CH <sub>β</sub> <sub>ACHC</sub> ), 36.8 (CH <sub>2</sub> β <sub>Tyr</sub> ), 33.2 (CH <sub>2</sub> <sub>ACHC</sub> ), 28.7 (CH <sub>2</sub> <sub>ACHC</sub> ), 27.4 (CH <sub>2</sub> <sub>ACHC</sub> ), 24.3 (CH <sub>2</sub> <sub>ACHC</sub> ), 22.3 (CH <sub>3</sub> <sub>Ac</sub> );	berechnet: 434.49; gefunden: 457.2 [M+Na] <sup>+</sup> .
Ac-L-His-Gly-L-His-NH-TG/H 112a/b		C <sub>16</sub> H <sub>22</sub> N <sub>8</sub> O <sub>4</sub> 390.40	55.0 (quant.)	<sup>1</sup> H-NMR (400.0 MHz, CD <sub>3</sub> OD, 25°C): δ (ppm) = 8.81 (s, 2H, CH <sub>Imi</sub> ), 7.37 (d, J = 10.8 Hz, 2H, CH <sub>Imi</sub> ), 4.72 (dd, J = 8.5 Hz, 4.7 Hz, 1H, CH <sub>α</sub> <sub>His</sub> ), 4.61 (t, J = 6.9 Hz, 1H, CH <sub>α</sub> <sub>His</sub> ), 3.89 (q, J = 16.7 Hz, 2H, CH <sub>2</sub> <sub>Gly</sub> ), 3.31 (m, 2H, CH <sub>2</sub> β <sub>His</sub> ), 3.14 (dq, J = 15.4 Hz, 8.5 Hz, 2H, CH <sub>2</sub> β <sub>His</sub> ), 1.98 (s, 3H, CH <sub>3</sub> <sub>Ac</sub> );	<sup>13</sup> C-NMR (100.6 MHz, CD <sub>3</sub> OD, 25°C): δ (ppm) = 174.4/173.8/171.8 (CO), 135.0/134.9 (C <sub>q</sub> <sub>Imi</sub> ), 131.1/131.0 (CH <sub>Imi</sub> ), 118.6/118.5 (CH <sub>Imi</sub> ), 53.9 (CH <sub>α</sub> <sub>His</sub> ), 53.4 (CH <sub>α</sub> <sub>His</sub> ), 43.7 (CH <sub>2</sub> <sub>Gly</sub> ), 27.9 (CH <sub>2</sub> β <sub>His</sub> ), 27.7 (CH <sub>2</sub> β <sub>His</sub> ), 22.6 (CH <sub>3</sub> <sub>Ac</sub> );	calculated : 390.40; found: 391.3 [M+H] <sup>+</sup> .
Ac-D-His-Pro-Aib-L-Asp-NH-TG/H 113a/b		C <sub>21</sub> H <sub>31</sub> N <sub>7</sub> O <sub>7</sub> 493.51	70.0 (quant.)	<sup>1</sup> H-NMR (400.0 MHz, CD <sub>3</sub> OD, 25°C): δ (ppm) = 8.80 (s, 1H, CH <sub>Imi</sub> ), 7.39 (s, 1H, CH <sub>Imi</sub> ), 4.67 (m, 2H, CH <sub>α</sub> <sub>Asp</sub> ), 4.28 (t, J = 7.3 Hz, 1H, CH <sub>α</sub> <sub>Pro</sub> ), 3.72 (m, 1H, CH <sub>2</sub> δ <sub>Pro</sub> ), 3.62 (m, 1H, CH <sub>2</sub> δ <sub>Pro</sub> ), 3.21 (dd, J = 15.1 Hz, 5.6 Hz, 1H, CH <sub>2</sub> β <sub>His</sub> ), 3.06 (dd, J = 15.4 Hz, 8.2 Hz, 1H, CH <sub>2</sub> β <sub>His</sub> ), 2.95 (dd, J = 16.7 Hz, 5.6 Hz, 1H, CH <sub>2</sub> β <sub>Asp</sub> ), 2.81 (dd, J = 16.7 Hz, 7.6 Hz, 1H, CH <sub>2</sub> β <sub>Asp</sub> ), 2.26 (m, 1H, CH <sub>2</sub> β <sub>Pro</sub> ), 2.10 (m, 1H, CH <sub>2</sub> β <sub>Pro</sub> ), 1.97 (m, 5H, CH <sub>3</sub> <sub>Ac</sub> , CH <sub>2</sub> γ <sub>Pro</sub> ), 1.48 (s, CH <sub>3</sub> <sub>Aib</sub> ), 1.45 (s, CH <sub>3</sub> <sub>Aib</sub> );	<sup>13</sup> C-NMR (100.6 MHz, CD <sub>3</sub> OD, 25°C): δ (ppm) = 176.8/175.8/174.7/174.6/173.1/170.9 (CO), 134.9 (CH <sub>Imi</sub> ), 131.1 (C <sub>q</sub> <sub>Imi</sub> ), 118.8 (CH <sub>Imi</sub> ), 62.9 (CH <sub>α</sub> <sub>Pro</sub> ), 58.2 (CH <sub>α</sub> <sub>His</sub> ), 57.9 (CH <sub>α</sub> <sub>Asp</sub> ), 51.9 (C <sub>q</sub> <sub>Aib</sub> ), 36.4 (CH <sub>2</sub> β <sub>Asp</sub> ), 30.6 (CH <sub>2</sub> δ <sub>Pro</sub> ), 27.8 (CH <sub>2</sub> β <sub>His</sub> ), 26.2 (CH <sub>2</sub> β <sub>Pro</sub> ), 25.6 (CH <sub>2</sub> γ <sub>Pro</sub> ), 25.6 (CH <sub>3</sub> <sub>Aib</sub> ), 25.4 (CH <sub>3</sub> <sub>Aib</sub> ), 22.4 (CH <sub>3</sub> <sub>Ac</sub> );	calculated : 493.51; found: 494.2 [M+H] <sup>+</sup> .

## 5 Experimental part

Peptide	Structure	MW (g/mol)	Yield (mg)	<sup>1</sup> H-NMR	<sup>13</sup> C-NMR	ESI-MS (m/z)
Ac-D-His-Gly-D-Asp-NH-TG/H 114a/b		C <sub>14</sub> H <sub>20</sub> N <sub>6</sub> O <sub>6</sub> 368.35	63.7 (quant.)	<sup>1</sup> H-NMR (400.0 MHz, CD <sub>3</sub> OD, 25°C): δ (ppm) = 8.78 (s, 1H, CH <sub>I</sub> mi), 7.38 (s, 1H, CH <sub>I</sub> mi), 4.76 (dd, J = 7.3 Hz, 5.6 Hz, 1H, CHα <sub>His</sub> ), 4.70 (t, J = 6.1 Hz, 1H, CHα <sub>Asp</sub> ), 3.92 (s, 2H, CH <sub>2</sub> <sub>Gly</sub> ), 3.24 (dd, J = 16.6 Hz, 5.8 Hz, 1H, CH <sub>2</sub> β <sub>His</sub> ), 3.15 (dd, J = 14.9 Hz, 6.6 Hz, 1H, CH <sub>2</sub> β <sub>His</sub> ), 2.87 (dd, J = 16.9 Hz, 5.3 Hz, 2H, CH <sub>2</sub> β <sub>His</sub> , CH <sub>2</sub> β <sub>Asp</sub> ), 2.76 (dd, J = 16.9 Hz, 7.6 Hz, 1H, CH <sub>2</sub> β <sub>Asp</sub> ), 1.98 (s, 3H, CH <sub>3</sub> <sub>Ac</sub> );	<sup>13</sup> C-NMR (100.6 MHz, CD <sub>3</sub> OD, 25°C): δ (ppm) = 174.0/173.6/172.9/171.8 (CO), 135.1 (CH <sub>I</sub> mi), 130.8 (Cq <sub>I</sub> mi), 118.8 (CH <sub>I</sub> mi), 53.7 (CHα <sub>His</sub> ), 51.2 (CHα <sub>Asp</sub> ), 43.6 (CH <sub>2</sub> <sub>Gly</sub> ), 36.7 (CH <sub>2</sub> β <sub>Asp</sub> ), 28.0 (CH <sub>2</sub> β <sub>His</sub> ), 22.6 (CH <sub>3</sub> <sub>Ac</sub> );	calculated: 368.35; found: 369.1 [M+H] <sup>+</sup> .
Ac-L-His-Pro-Gly-D-Asp-NH-TG/H 115a/b		C <sub>19</sub> H <sub>27</sub> N <sub>7</sub> O <sub>7</sub> 465.46	67.2 (quant.)	<sup>1</sup> H-NMR (400.0 MHz, CD <sub>3</sub> OD, 25°C): δ (ppm) = 8.79 (s, 1H, CH <sub>I</sub> mi), 7.43 (s, 1H, CH <sub>I</sub> mi), 4.97 (t, J = 6.8 Hz, 1H, CHα <sub>His</sub> ), 4.80 (dd, J = 8.3 Hz, 5.6 Hz, 1H, CHα <sub>Asp</sub> ), 4.35 (t, J = 7.1 Hz, 1H, CHα <sub>Pro</sub> ), 4.05 (d, J = 16.6 Hz, 1H, CH <sub>2</sub> <sub>Gly</sub> ), 3.83 (m, 1H, CH <sub>2</sub> δ <sub>Pro</sub> ), 3.77 (d, J = 16.6 Hz, 1H, CH <sub>2</sub> <sub>Gly</sub> ), 3.50 (m, 1H, CH <sub>2</sub> δ <sub>Pro</sub> ), 3.20 (dd, J = 15.1 Hz, 6.8 Hz, 1H, CH <sub>2</sub> β <sub>His</sub> ), 3.07 (dd, J = 15.1 Hz, 6.8 Hz, 1H, CH <sub>2</sub> β <sub>His</sub> ), 2.94 (dd, J = 16.9 Hz, 5.3 Hz, 1H, CH <sub>2</sub> β <sub>Asp</sub> ), 2.83 (dd, J = 16.7 Hz, 8.3 Hz, 1H, CH <sub>2</sub> β <sub>Asp</sub> ), 2.25 (m, 1H, CH <sub>2</sub> β <sub>Pro</sub> ), 2.08 (m, 1H, CH <sub>2</sub> β <sub>Pro</sub> ), 1.97 (m, 5H, CH <sub>3</sub> <sub>Ac</sub> , CH <sub>2</sub> γ <sub>Pro</sub> );	<sup>13</sup> C-NMR (100.6 MHz, CD <sub>3</sub> OD, 25°C): δ (ppm) = 175.7/174.1/173.1/171.6/170.9 (CO), 135.2 (CH <sub>I</sub> mi), 130.4 (Cq <sub>I</sub> mi), 119.1 (CH <sub>I</sub> mi), 62.4 (CHα <sub>Pro</sub> ), 51.7 (CHα <sub>His</sub> ), 51.1 (CHα <sub>Asp</sub> ), 43.9 (CH <sub>2</sub> <sub>Gly</sub> ), 36.7 (CH <sub>2</sub> β <sub>Asp</sub> ), 30.7 (CH <sub>2</sub> β <sub>Pro</sub> ), 27.6 (CH <sub>2</sub> β <sub>His</sub> ), 26.3 (CH <sub>2</sub> β <sub>Pro</sub> ), 25.0 (CH <sub>2</sub> γ <sub>Pro</sub> ), 22.3 (CH <sub>3</sub> <sub>Ac</sub> );	calculated: 465.46; found: 466.2 [M+H] <sup>+</sup> .
Ac-L-Asp-β-Ala-D-His-NH-TG/H 116a/b		C <sub>15</sub> H <sub>22</sub> N <sub>6</sub> O <sub>6</sub> 382.37	54.0 (quant.)	<sup>1</sup> H-NMR (400.0 MHz, CD <sub>3</sub> OD, 25°C): δ (ppm) = 8.81 (s, 1H, CH <sub>I</sub> mi), 7.34 (s, 1H, CH <sub>I</sub> mi), 4.71 (dd, J = 8.1 Hz, 5.8 Hz, 1H, CHα <sub>His</sub> ), 4.61 (dd, J = 7.8 Hz, 6.3 Hz, 1H, CHα <sub>Asp</sub> ), 3.44 (m, 2H, CH <sub>2</sub> <sub>β-Ala</sub> ), 3.28 (dd, J = 15.4 Hz, 5.6 Hz, 2H, CH <sub>2</sub> β <sub>Asp</sub> ), 3.07 (dd, J = 15.4 Hz, 8.1 Hz, 2H, CH <sub>2</sub> β <sub>Asp</sub> ), 2.80 (dd, J = 16.6 Hz, 5.6 Hz, 2H, CH <sub>2</sub> β <sub>His</sub> ), 2.68 (dd, J = 16.9 Hz, 7.8 Hz, 2H, CH <sub>2</sub> β <sub>His</sub> ), 2.41 (dt, J = 6.8 Hz, 2.2 Hz, 2H, CH <sub>2</sub> <sub>β-Ala</sub> ), 1.99 (s, 3H, CH <sub>3</sub> <sub>Ac</sub> );	<sup>13</sup> C-NMR (100.6 MHz, CD <sub>3</sub> OD, 25°C): δ (ppm) = 174.0/173.9/173.5/173.3 (CO), 134.9 (Cq <sub>I</sub> mi), 131.4 (CH <sub>I</sub> mi), 118.5 (CH <sub>I</sub> mi), 53.2 (CHα <sub>His</sub> ), 51.6 (CHα <sub>Asp</sub> ), 36.9 (CH <sub>2</sub> <sub>β-Ala</sub> ), 36.5 (CH <sub>2</sub> <sub>β-Ala</sub> ), 28.0 (CH <sub>2</sub> β <sub>Ser</sub> ), 22.6 (CH <sub>3</sub> <sub>Ac</sub> );	calculated: 382.37; found: 383.2 [M+H] <sup>+</sup> .

## 5 Experimental part

Peptide	Structure	MW (g/mol)	Yield (mg)	<sup>1</sup> H-NMR	<sup>13</sup> C-NMR	ESI-MS (m/z)
Ac-D-His-rac-ACHC-L-Phe-NH-TG/H 117a/b		C <sub>24</sub> H <sub>32</sub> N <sub>6</sub> O <sub>4</sub> 468.55	50.4 (76%t)	<sup>1</sup> H-NMR (400.0 MHz, CD <sub>3</sub> OD, 25°C): δ (ppm) = 8.75 (s, 1H, CH <sub>Imi</sub> ), 7.21 (m, 7H, CH <sub>Imi</sub> , ArH <sub>Phe</sub> ), 4.63 (m, 2H, CH <sub>α</sub> <sub>His</sub> ), 4.52 (m, 2H, CH <sub>α</sub> <sub>Phe</sub> ), 3.97 (dt, J = 11.1 Hz, 3.8 Hz, 1H, CH <sub>β</sub> <sub>ACHC</sub> ), 3.83 (dt, J = 11.6 Hz, 3.8 Hz, 1H, CH <sub>β</sub> <sub>ACHC</sub> ), 3.19 (m, 4H, CH <sub>2</sub> β <sub>His</sub> ), 2.96 (m, 3H, CH <sub>2</sub> β <sub>Tyr</sub> ), 2.70 (dd, J = 15.4 Hz, 6.3 Hz, 1H, CH <sub>2</sub> β <sub>Tyr</sub> ), 2.26 (m, 2H, CH <sub>α</sub> <sub>ACHC</sub> ), 1.99 (s, 3H, CH <sub>3</sub> <sub>Ac</sub> ), 1.87 (m, 2H, CH <sub>2</sub> <sub>ACHC</sub> ), 1.77 (m, 5H, CH <sub>2</sub> <sub>ACHC</sub> ), 1.58 (m, 1H, CH <sub>2</sub> <sub>ACHC</sub> ), 1.30 (m, 8H, CH <sub>2</sub> <sub>ACHC</sub> );	<sup>13</sup> C-NMR (100.6 MHz, CD <sub>3</sub> OD, 25°C): δ (ppm) = 171.0 (CO), 138.8 (C <sub>qPhe</sub> ), 138.3 (C <sub>qPhe</sub> ), 134.8 (C <sub>qImi</sub> ), 130.3 (CH <sub>Imi</sub> ), 129.5 (CH <sub>Ar</sub> <sub>Phe</sub> ), 127.9 (CH <sub>Ar</sub> <sub>Phe</sub> ), 123.4 (CH <sub>Ar</sub> <sub>Phe</sub> ), 118.8 (CH <sub>Imi</sub> ), 55.2 (CH <sub>α</sub> <sub>Phe</sub> ), 55.0 (CH <sub>α</sub> <sub>Phe</sub> ), 53.1 (CH <sub>α</sub> <sub>His</sub> ), 52.9 (CH <sub>α</sub> <sub>His</sub> ), 50.9 (CH <sub>α</sub> <sub>ACHC</sub> ), 50.5 (CH <sub>β</sub> <sub>ACHC</sub> ), 38.9 (CH <sub>2</sub> β <sub>Phe</sub> ), 38.3 (CH <sub>2</sub> β <sub>Phe</sub> ), 33.5 (CH <sub>2</sub> <sub>ACHC</sub> ), 33.1 (CH <sub>2</sub> <sub>ACHC</sub> ), 31.2 (CH <sub>2</sub> <sub>ACHC</sub> ), 30.5 (CH <sub>2</sub> <sub>ACHC</sub> ), 28.7 (CH <sub>2</sub> <sub>ACHC</sub> ), 28.2 (CH <sub>2</sub> β <sub>His</sub> ), 26.0 (CH <sub>2</sub> <sub>ACHC</sub> ), 25.9 (CH <sub>2</sub> <sub>ACHC</sub> ), 22.8 (CH <sub>3</sub> <sub>Ac</sub> ), 22.5 (CH <sub>3</sub> <sub>Ac</sub> );	calculated: 468.55; found: 469.3 [M+H] <sup>+</sup> .
Ac-D-His-Gly-L-Tyr-NH-TG/H 118a/b		C <sub>19</sub> H <sub>24</sub> N <sub>6</sub> O <sub>5</sub> 416.43	63.7 (quant.)	<sup>1</sup> H-NMR (400.0 MHz, CD <sub>3</sub> OD, 25°C): δ (ppm) = 8.78 (s, 1H, CH <sub>Imi</sub> ), 7.36 (s, 1H, CH <sub>Imi</sub> ), 7.07 (d, J = 8.1 Hz, 2H, ArH <sub>Tyr</sub> ), 6.69 (d, J = 7.8 Hz, 2H, ArH <sub>Tyr</sub> ), 4.63 (t, J = 6.3 Hz, 1H, CH <sub>α</sub> <sub>His</sub> ), 4.53 (dd, J = 9.6 Hz, 5.1 Hz, 1H, CH <sub>α</sub> <sub>Tyr</sub> ), 3.90 (d, J = 16.6 Hz, 2H, CH <sub>2</sub> <sub>Gly</sub> ), 3.74 (d, J = 16.6 Hz, 2H, CH <sub>2</sub> <sub>Gly</sub> ), 3.24 (dd, J = 14.9 Hz, 6.1 Hz, 1H, CH <sub>2</sub> β <sub>His</sub> ), 3.11 (dd, J = 15.4 Hz, 6.6 Hz, 2H, CH <sub>2</sub> β <sub>His</sub> , CH <sub>2</sub> β <sub>Tyr</sub> ), 2.81 (dd, J = 14.2 Hz, 9.6 Hz, 1H, CH <sub>2</sub> β <sub>Tyr</sub> ), 1.98 (s, 3H, CH <sub>3</sub> <sub>Ac</sub> );	<sup>13</sup> C-NMR (100.6 MHz, CD <sub>3</sub> OD, 25°C): δ (ppm) = 178.3/173.5/171.9 (CO), 153.9 (CH <sub>Ar</sub> -OH), 135.0 (CH <sub>Imi</sub> ), 131.3 (C <sub>qImi</sub> ), 131.0 (C <sub>qTyr</sub> ), 130.8 (CH <sub>Ar</sub> <sub>Tyr</sub> ), 118.8 (CH <sub>Imi</sub> ), 116.3 (CH <sub>Ar</sub> <sub>Tyr</sub> ), 56.4 (CH <sub>α</sub> <sub>Tyr</sub> ), 53.7 (CH <sub>α</sub> <sub>His</sub> ), 45.6 (CH <sub>2</sub> <sub>Gly</sub> ), 38.7 (CH <sub>2</sub> β <sub>Tyr</sub> ), 28.0 (CH <sub>2</sub> β <sub>His</sub> ), 22.6 (CH <sub>3</sub> <sub>Ac</sub> );	calculated: 416.43; found: 417.2 [M+H] <sup>+</sup> .
Ac-D-His-L-Tyr-NH-TG/H 119a/b		C <sub>17</sub> H <sub>21</sub> N <sub>5</sub> O <sub>4</sub> 359.35	50.0 (quant.)	<sup>1</sup> H-NMR (400.0 MHz, CD <sub>3</sub> OD, 25°C): δ (ppm) = 8.71 (s, 1H, CH <sub>Imi</sub> ), 7.05 (d, J = 8.6 Hz, 3H, ArH <sub>Tyr</sub> , CH <sub>Imi</sub> ), 6.68 (d, J = 8.6 Hz, 2H, ArH <sub>Tyr</sub> ), 4.60 (t, J = 6.3 Hz, 1H, CH <sub>α</sub> <sub>His</sub> ), 4.54 (dd, J = 9.6 Hz, 4.8 Hz, 1H, CH <sub>α</sub> <sub>Tyr</sub> ), 3.10 (m, 2H, CH <sub>2</sub> β <sub>His</sub> ), 2.89 (dd, J = 15.6 Hz, 7.3 Hz, 2H, CH <sub>2</sub> β <sub>Tyr</sub> ), 2.76 (dd, J = 14.1 Hz, 9.8 Hz, 2H, CH <sub>2</sub> β <sub>Tyr</sub> ), 1.94 (s, 3H, CH <sub>3</sub> <sub>Ac</sub> );	<sup>13</sup> C-NMR (100.6 MHz, CD <sub>3</sub> OD, 25°C): δ (ppm) = 173.5/171.9 (CO), 157.4 (CH <sub>Ar</sub> -OH), 134.8 (CH <sub>Imi</sub> ), 131.3 (C <sub>qImi</sub> ), 129.3 (C <sub>qTyr</sub> ), 128.3 (CH <sub>Ar</sub> <sub>Tyr</sub> ), 118.3 (CH <sub>Imi</sub> ), 116.3 (CH <sub>Ar</sub> <sub>Tyr</sub> ), 56.0 (CH <sub>α</sub> <sub>Tyr</sub> ), 53.7 (CH <sub>α</sub> <sub>His</sub> ), 38.7 (CH <sub>2</sub> β <sub>Tyr</sub> ), 28.1 (CH <sub>2</sub> β <sub>His</sub> ), 22.5 (CH <sub>3</sub> <sub>Ac</sub> );	calculated: 359.35; found: 360.2 [M+H] <sup>+</sup> .

## 5 Experimental part

Peptide	Structure	MW (g/mol)	Yield (mg)	<sup>1</sup> H-NMR	<sup>13</sup> C-NMR	ESI-MS (m/z)
Ac-D-His-L-His-NH-TG/H 120a/b		C <sub>14</sub> H <sub>19</sub> N <sub>7</sub> O <sub>3</sub> 333.35	50.0 (quant.).	<sup>1</sup> H-NMR (400.0 MHz, CD <sub>3</sub> OD, 25°C): δ (ppm) = 8.80 (s, 2H, CH <sub>Imi</sub> ), 7.34 (d, J = 5.1 Hz, 2H, CH <sub>Imi</sub> ), 4.70 (dd, J = 8.8 Hz, 5.4 Hz, 1H, CHα <sub>His</sub> ), 4.59 (dd, J = 8.5 Hz, 5.4 Hz, 1H, CHα <sub>His</sub> ), 3.25 (m, 2H, CH <sub>2</sub> β <sub>His</sub> ), 3.10 (dq, J = 8.8 Hz, 6.3 Hz, 2H, CH <sub>2</sub> β <sub>His</sub> ), 1.96 (s, 3H, CH <sub>3</sub> Ac);	<sup>13</sup> C-NMR (100.6 MHz, CD <sub>3</sub> OD, 25°C): δ (ppm) = 174.4/173.9/172.5 (CO), 135.1/135.0 (Cq <sub>Imi</sub> ), 131.3/131.2 (CH <sub>Imi</sub> ), 118.4/118.3 (CH <sub>Imi</sub> ), 54.0 (CHα <sub>His</sub> ), 53.4 (CHα <sub>His</sub> ), 27.9 (CH <sub>2</sub> β <sub>His</sub> ), 27.5 (CH <sub>2</sub> β <sub>His</sub> ), 22.5 (CH <sub>3</sub> Ac);	calculated: 333.35; found: 334.2 [M+H] <sup>+</sup> .
Ac-L-Cys-Gly-L-Ala-NH-TG/H 121a/b		C <sub>10</sub> H <sub>18</sub> N <sub>4</sub> O <sub>4</sub> S 290.34	40.0 (quant.).	<sup>1</sup> H-NMR (400.0 MHz, d <sub>6</sub> -DMSO, 25°C): δ (ppm) = 4.32 (dd, J = 7.3 Hz, 5.6 Hz, 1H, CHα <sub>Cys</sub> ), 4.17 (q, J = 7.2 Hz, 1H, CHα <sub>Ala</sub> ), 3.71 (d, J = 4.1 Hz, 2H, CH <sub>2</sub> Gly), 2.77 (dd, J = 13.6 Hz, 5.4 Hz, 1H, CH <sub>2</sub> β <sub>Cys</sub> ), 2.66 (dd, J = 13.6 Hz, 7.6 Hz, 1H, CH <sub>2</sub> β <sub>Cys</sub> ), 1.88 (s, 3H, CH <sub>3</sub> Ac), 1.20 (2s, 3H, CH <sub>3</sub> Ala);	<sup>13</sup> C-NMR (100.6 MHz, d <sub>6</sub> -DMSO, 25°C): δ (ppm) = 174.0/170.3/169.7/168.1 (CO), 55.2 (CHα <sub>Cys</sub> ), 47.7 (CHα <sub>Ala</sub> ), 41.9 (CH <sub>2</sub> Gly), 25.7 (CH <sub>2</sub> β <sub>Cys</sub> ), 22.4 (CH <sub>3</sub> Ac), 18.1 (CH <sub>3</sub> Ala);	calculated: 290.34; found: 313.3 [M+Na] <sup>+</sup> .
Ac-L-Asp-rac-ACHC-L-Tyr-NH-TG/H 122a/b		C <sub>22</sub> H <sub>30</sub> N <sub>4</sub> O 462.50	47.3 (76%)	<sup>1</sup> H-NMR (400.0 MHz, d <sub>6</sub> -DMSO, 25°C): δ (ppm) = 6.97 (d, J = 6.3 Hz, 4H, ArHTyr), 6.61 (d, J = 7.9 Hz, 4H, ArHTyr), 4.50 (t, J = 6.6 Hz, 1H, CHα <sub>Tyr</sub> ), 4.44 (dd, J = 9.5 Hz, 3.8 Hz, 1H, CHα <sub>Tyr</sub> ), 4.32 (dd, J = 8.5 Hz, 4.7 Hz, 1H, CHα <sub>Asp</sub> ), 4.26 (t, J = 7.2 Hz, 1H, CHα <sub>Asp</sub> ), 3.72 (dt, J = 11.0 Hz, 3.8 Hz, 1H, CHβ <sub>ACHC</sub> ), 3.55 (dt, J = 11.0 Hz, 3.8 Hz, 1H, CHβ <sub>ACHC</sub> ), 2.92 (dd, J = 13.8 Hz, 4.7 Hz, 1H, CH <sub>2</sub> β <sub>Tyr</sub> ), 2.77 (dd, J = 13.2 Hz, 7.6 Hz, 1H, CH <sub>2</sub> β <sub>Tyr</sub> ), 2.64 (m, 4H, CH <sub>2</sub> β <sub>Tyr</sub> , CH <sub>2</sub> β <sub>Asp</sub> ), 2.36 (m, 2H, CH <sub>2</sub> β <sub>Asp</sub> ), 2.20 (m, 2H, CHα <sub>ACHC</sub> ), 1.75 (brs, 7H, CH <sub>2</sub> ACHC, CH <sub>3</sub> Ac), 1.55 (m, 6H, CH <sub>2</sub> ACHC), 1.37 (m, 1H, CH <sub>2</sub> ACHC), 1.13 (m, 8H, CH <sub>2</sub> ACHC);	<sup>13</sup> C-NMR (100.6 MHz, d <sub>6</sub> -DMSO, 25°C): δ (ppm) = 172.6/172.5/171.6/171.5/169.6/169.0 (CO), 155.5 (C <sub>Ar</sub> OH), 130.0 (CH <sub>Ar</sub> Tyr), 129.9 (CH <sub>Ar</sub> Tyr), 128.0 (Cq <sub>Tyr</sub> ), 127.9 (Cq <sub>Tyr</sub> ), 114.8 (CH <sub>Ar</sub> Tyr), 114.6 (CH <sub>Ar</sub> Tyr), 54.1 (CHα <sub>Tyr</sub> ), 54.0 (CHα <sub>Tyr</sub> ), 53.5 (CHα <sub>Asp</sub> ), 53.4 (CHα <sub>Asp</sub> ), 49.4 (CHα <sub>ACHC</sub> ), 48.9 (CHβ <sub>ACHC</sub> ), 36.9 (CH <sub>2</sub> β <sub>Tyr</sub> ), 36.7 (CH <sub>2</sub> β <sub>Tyr</sub> ), 36.6 (CH <sub>2</sub> β <sub>Asp</sub> ), 36.3 (CH <sub>2</sub> β <sub>Asp</sub> ), 32.1 (CH <sub>2</sub> β <sub>Asp</sub> ), 32.0 (CH <sub>2</sub> ACHC), 28.9 (CH <sub>2</sub> ACHC), 28.6 (CH <sub>2</sub> ACHC), 24.4 (CH <sub>2</sub> ACHC), 24.3 (CH <sub>2</sub> ACHC), 24.3 (CH <sub>2</sub> ACHC), 24.2 (CH <sub>2</sub> ACHC), 22.4 (CH <sub>2</sub> ACHC), 22.3 (CH <sub>3</sub> Ac);	calculated: 462.50; found: 575.7 [M+TFA]

## 5.3 Coatings

### 5.3.1 *Au(111) plates*

*The substrate:* The base material borosilicate glass: Borosilicate Glass thickness 0.7 +/- 0.1 mm. The special glass substrate is well suited for the flame annealing procedure that is used to obtain Au(111) terraces. As adhesive layer, a thin, Chromium layer is applied to the glass surface: Chromium layer 2.5 +/- 1.5 nm. This layer guarantees optimal adhesion to the glass as well as to the subsequently deposited gold layer. A final gold layer is presented on top of the thin Chromium layer: Gold layer 250 +/- 50 nm, size 11x11 mm (surface:121mm<sup>2</sup>)

Before the experiment, a flame annealing is necessary to obtain the Au(111) terraces. The flame annealing is made with a Bunsen burner. Caution: if the applied flame is too hot, the chromium layer can diffuse on a surface. As the flame annealing removes all impurities, there is no need for further cleaning.

#### 5.3.1.1 In situ crystallisation

*General sample preparation:* The plates are treated one by one in a separate closed glass vessel (15ml). The flame annealed plates are immediately immersed after cooling down into a disulfide solution for pre-treatment. 0.182g bis 2-((4-pyridinylcarbonyl)oxy)ethyl disulfide (M: 364 g/mol) is dissolved in 100ml CH<sub>2</sub>Cl<sub>2</sub>/EtOH 1/1 solvent (5mM solution). 10 ml of this solution is used for 1 plate. The time of pre-treatment is 5 days. Then, the plate is removed and washed with EtOH and immediately put into the Ag(L1)NO<sub>3</sub> (=AdI7) solution. The concentration and the treating time of the complex solution vary. In general, equal concentration of AgNO<sub>3</sub> and L1 solution are prepared separately. Then, 5 ml of each solution is measured into the glass vessel over the gold plate, closed and placed in the dark for the determined treating time (from 3h to 14 days). Finally, the plates are removed, washed with EtOH, placed in a light protected desiccator and dried under vacuum over P<sub>2</sub>O<sub>5</sub>. The prepared samples are kept in the dark, in a closed, clean container, to avoid the light reduction of the product and the contamination of the surface. The concentrations and the treating times are changed depending on the aim of the experience.

*Example of 5pcs 2mM/3days samples:* 91mg bis 2-((4-pyridinylcarbonyl)oxy)ethyl disulfide (M: 364 g/mol) are dissolved in 50ml CH<sub>2</sub>Cl<sub>2</sub>/EtOH 1/1 solvent (5mM solution). The flame annealed plates are placed one by one in a 15ml glass vessel and 10 ml of disulfide solution is measured. The vessels are closed and kept immobile for 5 days. Then the plates are removed, washed with EtOH and placed in a clean 15ml glass vessel. 16.67mg AgNO<sub>3</sub> is dissolved in 25ml EtOH/THF 1/1 solvent (4mM solution) and 26.6mg L1 is dissolved in 25ml EtOH/THF

1/1 solvent (4mM solution). 5 ml of each solution are measured into the glass vessel over the gold plate, mixed briefly, closed and placed in the dark for 3 days. Then the plates are removed from the solution, washed with EtOH and dried in a desiccator under vacuum over P<sub>2</sub>O<sub>5</sub>.

*Samples for AFM measurements:* 1<sup>st</sup> sample (**Fig.3.2-8**): the pre-treatment was carried out as described in a general sample preparation. The gold plate was fixed vertically and immersed by half into the solution (1mM for the AdI7 compound), in a closed vessel and kept in dark. The solution was continuously stirred for 5 days to avoid big crystal formation. After 5 days, the plate was removed and washed with EtOH and dried under vacuum. For the second measurements (**Fig.3.2-9-12**) the samples were prepared in a general way, using 0.5mM/3h, 0.25mM /7days treating conditions.

*Samples for XPS measurements:* the following samples were prepared: *sample2:* 0,25mM/3h; *sample3:* 1mM/3d; *sample 4:* 2mM/3h. The last two samples were used in the dissolution test described later. *sample5:* 1mM/3d, 24h incubation in MHB for 24h; *sample6:* 1mM/3d, 24h incubation in SM.

*Powder X-ray spectra:* The sample is prepared in a general way. After the disulfide pre-treatment, the plate is treated with a 2mM AdI7 solution for 14days. These conditions are identical to the ones used for the dental implant materials.

*Samples for dissolution studies and Silver determination on a surface by AAS:*

In order to study how the loading of the surface changes with the concentration and the treating time, total screening was made changing the treating time from 3h to 7days and the concentration of the complex solution from 0.5mM to 2mM. The prepared samples are listed in **Table 5-9**. After the pre-treatment, the plates, one by one, were put into the 10ml solution and removed after the defined time, then washed and dried as previously described. One plate of each condition was kept for the SEM measurements. The others were used to determine the loading and to incubate them in different biological media. For the dissolution experiment the prepared coated substrates were put into a crystallisation plate (Combo plate, USA) each hole has a determined 2ml volume), one plate in every hole, then 2ml of synthetic medium or Müller-Hinton medium was layered on each plate, then closed. The plates were kept immobile in the dark for 24h. After this 24h incubation time, the substrates were removed, washed with EtOH dried and kept for the further experiments. From each substrate, the solution was removed filtered through 0.40 µm Millipore disposable filter. AAS measurement was carried out to determine the silver concentration of the media after the incubation.

**Table 5-9:** Samples prepared for the test to study the time and concentration dependency of the loading and their dissolution in different media

Sample name	Starting conc Ad7 (mM)	Treating time (h)	incubated in medium	Ag ng on a surf.	Ag ng in the sol.	sum. ng surf+sol	Ag in sol (ppm)
I/1a	0.5	3	no	0.432	-	0.432	
I/1b	0.5	3	MHB	0.437	0.000	0.437	0.000
I/1c	0.5	3	SM	0.336	0.000	0.336	0.000
I/2a	0.5	24	no	0.985	-	0.985	
I/2b	0.5	24	MHB	0.884	0.000	0.884	0.000
I/2c	0.5	24	SM	0.730	0.000	0.730	0.000
I/3a	0.5	72	no	2.754	-	2.754	
I/3b	0.5	72	MHB	1.764	0.000	1.764	0.000
I/3c	0.5	72	SM	1.687	0.000	1.687	0.000
I/4a	0.5	168	no	3.778	-	3.778	
I/4b	0.5	168	MHB	3.345	0.000	3.345	0.000
I/4c	0.5	168	SM	2.663	1.139	3.802	0.5697
II/1a	1	3	no	2.176		2.176	
II/1b	1	3	MHB	0.364	0.000	0.364	0.000
II/1c	1	3	SM	0.412	0.000	0.412	0.000
II/2a	1	24	no	16.800	-	16.800	
II/2b	1	24	MHB	1.070	0.000	1.070	0.000
II/2c	1	24	SM	0.812	2.058	2.870	1.029132
II/3a	1	72	no	17.090	-	17.090	
II/3b	1	72	MHB	1.895	1.767	3.662	0.8835
II/3c	1	72	SM	9.682	2.125	11.807	1.062745
II/4a	1	168	no	37.400	-	37.400	
II/4b	1	168	MHB	3.588	2.282	5.870	1.1412
II/4c	1	168	SM	2.195	2.114	4.309	1.057143
III/1a	2	3	no	55.800		55.800	
III/1b	2	3	MHB	11.068	9.408	20.476	4.704202
III/1c	2	3	SM	19.138	3.627	22.764	1.813445
III/2a	2	24	no	135.150		135.150	
III/2b	2	24	MHB	64.000	6.182	70.182	3.090756
III/2c	2	24	SM	30.675	3.492	34.167	1.746218
III/3a	2	72	no	211.475		211.475	
III/3b	2	72	MHB	80.100	8.691	88.791	4.345658
III/3c	2	72	SM	39.275	6.316	45.591	3.157983
III/4a	2	168	no	234.175		234.175	
III/4b	2	168	MHB	80.575	6.047	86.622	3.023529
III/4c	2	168	SM	68.325	2.551	70.876	1.27563

For the AAS measurements, the external standard method is used. The following standard solutions are prepared: Stock solution 20ppm concentration: 1ml 1000ppm Fluka standard solution is diluted to 50ml with nanopure water. (**Table 5-10**)



**Table 5-10:** Standard solutions for the loading and dissolution experiments

	Conc. (ppm)	Stock solution (ml)	10% HNO <sub>3</sub> added (ml)	Solution volume (ml)
Blank	0	0	0,5	50
Standard1	0,1	0,5	1,0	100
Standard2	0,2	0,5	0,5	50
Standard3	0,4	1,0	0,5	50
Standard4	0,8	2,0	0,5	50
Standard5	1,6	4,0	0,5	50

**Figure 5-1:** One example of the standard line

	conc.real	Abs
stand1	0.1	0.0230
stand2	0.2	0.0457
stand3	0.40	0.0882
stand4	0.80	0.1722
stand5	1.60	0.3358

The silver concentration of the sample solution should be in the region determined by the standard solutions. Therefore, the dilution might change sample-by-sample keeping the concentration in this region.

AAS samples:

Ag concentration of the mediums after the incubation: to 1ml of filtered solution, 0,5ml 10% HNO<sub>3</sub> is added and diluted to 10 ml with water.

Ag loading on a surface I-II series: The Au plates were sonicated for 2 min with 1ml 20% HNO<sub>3</sub> then the whole amount of solution is filled up to 10ml with nanopure water.

Ag loading on a surface III series: The Au plates were sonicated for 2 min with 1ml 20% HNO<sub>3</sub> then the whole amount of solution was filled up to 25ml with nanopure water.

The complete removal of the coating from the surface was controlled by SEM.

After the measurements, the results are given in ppm. (The ppm for diluted aqueous solution can be converted to mg/l without making errors. Then the results, given in mg/l for Ag are calculated to mols.)

The detailed parameters of the machine are found later in the Chapter 5.4.1.

### 5.3.1.2 Layer-by-layer method

The alternating dip coating method is used. 20ml 2mM AgNO<sub>3</sub> solution and 20ml 2mM L1 solution in THF/EtOH were prepared in separate vessels. The pre-treated Au(111) plate was immersed into the AgNO<sub>3</sub> solution first for 1min, then removed and washed with EtOH and immersed into the ligand solution for 1min, then removed and washed with EtOH, and put into the silver solution. The cycle AgNO<sub>3</sub>-washing-L1-washing was repeated 15 times. After the last washing, the gold plate is dried and kept under vacuum until further experiments.

### *5.3.2 Ti and Au dental implant materials*

General sample preparation:

The numbered gold and titanium implant material plates (13x13mm sizes, suitable for the flow-chamber experiment) have been polished in the Institut für Präventivzahnmedizin und Orale Mikrobiologie. The plates are polished in average after every 3<sup>rd</sup> measurement. Since the substrates are used several times, a cleaning process is used to remove all the organic and inorganic contaminations from the surface. 30 ml freshly prepared piranha solution (21ml ccH<sub>2</sub>SO<sub>4</sub>+9 ml ccH<sub>2</sub>O<sub>2</sub>) is used for 6-8 samples. After the acid removal, the surface is cleaned for 10 min in sonicator once with EtOH and three times with distilled water, then dried under vacuum, over P<sub>2</sub>O<sub>5</sub>. For the treatment, one plate is placed in 10 ml solution, to keep the surface solution ratios similar as in the case of the gold plates. The pre-treatment time is 7 days. After the pre-treatment, the samples are washed one by one abundantly with EtOH and directly after are treated with the compound solution. The concentration of the (AgNO<sub>3</sub>+L1) solution is 2mM and treating time 14 days generally. In the **Table 5-11**, the different treatment methods are presented.

**Table 5-11:** Different treatment methods in order to optimize the surface coating for the dental implant materials

No.	Substrate	Name	Chem. Treatment	Notes
1	Au	Complete treatment	Disulfide+AgNO <sub>3</sub> +Lig (1 mM)	Spotted small cryst and inhomogeneous surface
2	Au	Crystals	AgNO <sub>3</sub> +Lig (2 mM)	Big crystals
3	Au	Crystals	AgNO <sub>3</sub> +Lig (2 mM)	Bigger cryst then 2 but less dense
4	Au	Heated crystals	AgNO <sub>3</sub> +Lig (2 mM)→ 50 min in 200 °C	Big crystals+small crystals
2	Ti	Less conc. Crystals	AgNO <sub>3</sub> +Lig (1 mM)	Inhomogeneous surface (similar then Au1)
3	Ti	Complete treatment II	Isonicotinic acid+AgNO <sub>3</sub> +Lig (1 mM)	Small spots, probably cryst, homogeneous surface
4	Ti	Crystals	AgNO <sub>3</sub> +Lig (2 mM)	Big crystals+small crystals

After the cleaning procedure, one gold plate is immersed into the mixture of 5ml 4mM AgNO<sub>3</sub> in EtOH/THF 1/1 solution and 5ml 4mM L1 in EtOH/THF 1/1 solution in a 15ml glass vessel. The closed vessel is kept in the dark for 14 days, then the plate is removed, washed with EtOH and dried under vacuum over P<sub>2</sub>O<sub>5</sub>. The ready plates are kept in the dark in a closed container until use.

After the cleaning procedure, one titanium plate is immersed in 10 ml 5mM isonicotinic acid solution in EtOH/CH<sub>2</sub>Cl<sub>2</sub>. After 5 days, the plate is removed and washed with EtOH. The pre-treated plate is put into a mixture of 5ml 4mM AgNO<sub>3</sub> in EtOH/THF 1/1 solution and 5ml 4mM L1 in EtOH/THF 1/1 solution in a 15ml glass vessel. The closed vessel is kept in the dark for 14 days, then the plate removed and washed with EtOH and dried under vacuum over P<sub>2</sub>O<sub>5</sub>. The ready plate is kept in the dark in a closed container until use. The plates were photographed under the microscope.

#### Silver determination by AAS

To determine the silver loading on a surface, the crystalline compound was removed from the surface with 2 ml 20% HNO<sub>3</sub> aq solution. The acidic solution was filled up to 25ml with nanopure water, then this solution is diluted 20 times (1ml to 20ml with nanopure water). The prepared solution was measured by AAS. The methods and standards are described in Chapter 5.3.1.1.

To determine the silver concentration of the flow chamber liquid, the following conditions have been chosen: a flow chamber experiment with 4 samples in the chamber, 2 gold substrates (one treated with Ag, the other not (reference Au)) and two titanium ones (a treated with Ag, the other not (reference Ti)),. The treated surface was 2 times (14x14=)196 mm<sup>2</sup>. The chamber contained exactly 16.8 ml of suspension: Saliva/Buffer/Bacteriae. 8 ml of this

suspension was received in 4 Eppendorf tubes (contained 2ml of each). One part of the suspension, 4 ml, was measured without any filtration and dilution. A second part, 4 ml, of solution was measured after filtration, through a sterile filter: MILLEX GS 0.22 $\mu$ m from Millipore (used by the dental lab generally). For the measurements the following standard solutions were used:

a., Standards

AgNO<sub>3</sub> stock solution: 100 ppm (5ml Standard certified solution AgNO<sub>3</sub> from FLUKA 1000 ppm to 50 ml Nanopure water), the 10% HNO<sub>3</sub> solution is prepared from 66% fuming HNO<sub>3</sub> and diluted 7.6 ml cc acid was diluted to 50ml with nanopure water.

**Table 5-12:** Standards for the silver concentration determination in the flow chamber liquid

Standard No	ml of AgNO <sub>3</sub> stock sol.	ml of 10% HNO <sub>3</sub>	True value (ppm)	Abs	Real conc. (ppm)
Blank	0	1			
stand1	1	1	1	0.1296	0.8648
stand2	2	1	2	0.2538	2.0185
stand3	4	1	4	0.4868	4.1829
stand4	6	1	6	0.688	6.0519
stand5	8	1	8	0.885	7.8819

All the standard solutions are filled up to 100 ml with nanopure water.

b., Samples & Results

The samples are measured concentrated, without dilution. The measurement of the *1<sup>st</sup> sample, without filtration* gives an absorption 0.1618, which means **1.5 ppm** concentration. During the measurement, the change of the abs. was high, meaning that the error of the measurement is higher than usual for this method. This variation comes probably from the inhomogeneity of the samples. The measurement of the *2<sup>nd</sup> sample, with filtration* gives an absorption 0.030, which means **0.17 ppm** concentration. The filtered sample was homogeneous and the variation of the absorbance was much lower. The flow-chamber contained exactly 16.8 ml of suspension, this amount of suspension contained **0.025 mg Ag**, and from this amount, only **0.003 mg Ag** was in the bacterial free solution. The loading of the gold and titanium dental implant substrates are determined in a same way described by the gold plates for the III series.

### 5.3.3 Titanium and steel implant materials

*General sample preparation:*

The samples are cleaned. First, the samples are sonicated for 10 min once in EtOH and three times in distilled water, then dried under vacuum, over P<sub>2</sub>O<sub>5</sub>. For the treatment, 5 disks or cylinders from the same material are treated together in 10 ml solution, to keep the surface/solution ratios similar as in the case of the gold plates. The pre-treatment time varies between 3 days and 8 days. After the pre-treatment, the samples are washed one by one abundantly with EtOH and treated directly with the Adl7 solution. The concentration of the (AgNO<sub>3</sub>+L1) solution varies between 0.5mM and 2mM depending on the experiment.

Samples with *different treating methods*:

To test the microbiological activity, samples were prepared with different treating methods (**Table 5-13**).

**Table 5-13:** Different treatment methods in order to optimize the coating on various substrates, 1a : Steel rough cylinder; 1b : Steel smooth cylinder; 2a : Steel rough disks; 2b : Steel smooth disks; 3a : Ti rough cylinder; 4a : Ti rough disks; 4b : Ti smooth disks; 5 : Gold plate

No.	Method description	1a	1b	2a	2b	3a	4a	4b	5
0	Cleaning	x	x	x	x	x	x	x	x
1	Isonic. acid 5mM, 3 days+ Ladl/AgNO <sub>3</sub> cryst, 2 mM, 10 days	x	x	x	x	x	x	x	
2	Isonic. acid 5mM, ~8 days+ Ladl/AgNO <sub>3</sub> cryst, 1 mM, 20 days	x	x	x	x	x	x	x	
3	Disulfide 5mM, ~8 days+ Ladl/AgNO <sub>3</sub> cryst, 1 mM, 20 days								x
4	Ladl/AgNO <sub>3</sub> cryst, 2 mM, 14 days	x	x	x	x	x	x	x	x
5	Pyridine-4-boronic acid, ~8 days+ Ladl/AgNO <sub>3</sub> cryst, 1 mM, 20 days	x	x	x	x	x	x	x	

Based on the microbiological results new sets of samples were prepared, this time only for one treating method with 2mM complex concentration, with a large timescale window from 3h to 10days of treatment, to optimize the treating time

**Table 5-14:** *Time dependence* measurements for the method 4: Ladl/AgNO<sub>3</sub> (Adl7) *in-situ* crystallization, 2 mM, 14 days

No.	Treating time	1a	1b	2a	2b	3a	4a	4b
0	Cleaning	x	x	x	x	x	x	x
1	3 hours	x	x	x	x	x	x	x
2	7 hours	x	x	x	x	x	x	x
3	1 days	x	x	x	x	x	x	x
4	5 days	x	x	x	x	x	x	x
5	10 days	x	x	x	x	x	x	x

5 samples per treating time, all of the materials were prepared and tested. For the dissolution tests and the silver determination on surface, new samples were prepared, listed in **Table 5-15**.

Sample	Treatment	Dissolution	
		MHB	SM
TiR	1mM/3days	x	x
	2mM/3days	x	x
TiS	1mM/3days	x	x
	2mM/3days	x	x
StR	1mM/3days	-	-
	2mM/3days	-	-
StPol	1mM/3days	-	-
	2mM/3days	-	-

**Table 5-15:** Samples prepared for the dissolution tests of the restorative implant materials

The loading is removed with 1ml 20% HNO<sub>3</sub> solution with 2min sonication. The whole amount of solution washed out in a 10ml vessel and filled up with nanopure water and the silver concentration of this solution is determined by AAS. The previously described (in the chapter 5.3.1.1) silver standards are used and the sample solutions are further diluted on demand. The primary results are used for further calculations. The dissolution tests were carried out as previously described. One ml of the medium was removed after a 24h incubation and the silver concentration was determined.

### 5.3.4 Coating on T-Gel resin

The isonicotinic acid coupled and the His-ACHC-Tyr-TG T-gel resin were used to build up the coating on a surface. 37.4mg isonicotinic acid and 40.3mg tripeptide coupled resin were used for the *in-situ* crystallisation. The resins were immersed in 10ml 0.2mM complex solution (10ml 0.4mM AgNO<sub>3</sub> and 10mm 0.4mM L1 solution in THF/EtOH were prepared and 5ml of each solutions were mixed in a 15 ml glass vessel) and kept closed in the dark for 14 days. Then the resins were washed 3 times with EtOH, dried and kept in the dark and cold for the further experiments. For the layer-by-layer experiments, 30mg isonicotinic acid coupled T-gel were used. 10ml 2mM AgNO<sub>3</sub> solution and 10ml 2mM L solution in THF/EtOH were prepared in separate vessels. The resin was transferred into a syringe closed with a PE filter, then the AgNO<sub>3</sub> solution was layered onto. The syringe was shaken and the solution flows slowly through. Then the resin was washed with EtOH three times and the L solution layered upon the resin. After the solution has flown through, the resin was washed three times with EtOH and AgNO<sub>3</sub> solution layered upon. This cycle AgNO<sub>3</sub>-washing-L was repeated twelve times and after the last washing, the resin was dried and kept in the dark and

cold for further experiments. The SEM measurements were carried out without any other treatment.

The silver loadings of the resins are determined by AAS. The standard solutions (described in the chapter 5.3.1.1) are used. Ca. 2,5-3.0 mg T-gel resin are weighed. 1ml 20% HNO<sub>3</sub> is added, sonicated for 2 min, then the total amount of solution is removed and filled up to 5ml with nanopure water. The 5ml solution is filtered, in order to remove the beads, and 1ml of the filtrate is diluted to 10ml with water. The silver concentration of the prepared solution is determined and the loading respectively calculated.

## 5.4 Molecular mechanism of Ag<sup>+</sup>

### 5.4.1 *General method descriptions*

#### *General description of the light reduction method:*

Around 30mg T-gel beads are weighed into a 3ml plastic vessel. Then, 2 ml 0.05M AgNO<sub>3</sub> solution (made with nanopure water) is measured and the closed vessel is sonicated for 15min in the dark. For some experiments, only 10mg T-gel beads are used. This quantity of beads is treated with 0.66ml 0.05M AgNO<sub>3</sub> solution, to keep the Ag<sup>+</sup>/peptide ratio fixed around ten. The incubated T-gel beads are washed 5 times with 2.5ml nanopure water to remove all free Ag<sup>+</sup>. The last washing solution is almost completely removed and the wet beads are placed under the 15W electrical lamp from a 10cm distance. After 8h, the beads are removed, a photo is taken with the optical microscope, and the sample is dried under vacuum for further experiments.

#### *General description of the chemical reduction method:*

Around 30mg T-gel beads are weighed into a 3ml plastic vessel. Then, 2 ml 0.05M AgNO<sub>3</sub> solution (made with nanopure water) is measured and the closed vessel is sonicated for 15min in the dark. For some experiments, only 10mg T-gel beads are used. This quantity of beads is treated with 0.66ml 0.05M AgNO<sub>3</sub> solution, to keep the Ag<sup>+</sup>/peptide ratio fixed around ten. The incubated T-gel beads are washed 5 times with 2.5ml nanopure water to remove all free Ag<sup>+</sup>. The last washing solution is almost completely removed and 3ml 0.05M sodium ascorbate solution (in nanopure water) is added to the wet beads. After 5-10min, the sodium ascorbate solution is removed and the reduced beads are washed 5 times with nanopure water. The wet beads are than photographed with the optical microscope and dried under vacuum for further experiments.

*General description of the uptake measurements:*

The AAS method is developed to determine the silver uptake of the tripeptide coupled T-gel beads.

a) Standards: The standard solutions are different than during the previous experiments were used. Since concentration of the samples solutions are much higher the standard concentrations should be adjusted. The following standard solutions are prepared (**Table 5-16**) from the AgNO<sub>3</sub> stock solution: 100 ppm. 5ml Standard certified solution AgNO<sub>3</sub> from FLUKA/ACROS 1000 ppm to 50 ml Nanopure water.

**Table 5-16:** Standard solutions for silver uptake measurements

Standard No.	ml of the stock AgNO <sub>3</sub> sol.	ml HNO <sub>3</sub> 10%	Theoretical conc. ppm
Blank	0	1	0
Stand1	1	1	1
Stand2	2	1	2
Stand3	4	1	4
Stand4	6	1	6
Stand5	8	1	8

All the standard solutions are filled up with Nanopure water to 100 ml.

b., Samples Sample solutions are prepared from the remaining AgNO<sub>3</sub> solution after the incubation of the T-gel beads. For the incubation, the same procedure is used as for the tripeptide treated for the light and chemical reduction methods. Exactly weighed ~ 10 mg tripeptide loaded T-Gel are measured into a plastic vessel and 0.66ml of the prepared ~0.05 M AgNO<sub>3</sub> solution is added. After 15 min of sonication (keep the samples away from the direct light and shake it from time to time to avoid that the T-Gels stick together), the beads are decanted and 0.50 ml of the AgNO<sub>3</sub> solution is removed above the beads and filled up to 50 ml with Nanopure water (1<sup>st</sup> dilution). Then, 5 ml of this solution is removed, added to 1.0 ml of HNO<sub>3</sub> 10% in nanopure water solution and filled up to 100 ml with Nanopure water. The sample solutions are then measured and the silver concentration is determined and the uptake is calculated. In order to control the processes reference solutions are prepared. These solutions represent the 0 % uptake. The 0.05M AgNO<sub>3</sub> solution, used for the incubation, is diluted in the same way as the sample solutions. The treating 0.05M AgNO<sub>3</sub> solution is prepared from 0.423 g AgNO<sub>3</sub> salt measured into 50 ml Nanopure water. It is important to prepare the silver nitrate solution freshly and use the same solution for the sample preparation and for the reference solutions.



AAS measurements parameters:

Ag(328.1nm) Comment: Flame

### Instrument Information

Device Name: AA-6300

Type	Model Name	ROM Version	S/N
AA	AA-6300	1.03	A30524300690
ASC			
GFA			

### Optics Parameters

Element:	Ag	Slit Width(nm):	0.7
Socket #:	6	Lamp Mode:	NON-BGC
Lamp Current Low(mA):	10	Peak(nm) :	327.94
Wavelength(nm):	328.1		

### Atomizer/Gas Flow Rate Setup

Fuel Gas Flow Rate(L/min):	2.2	Burner Height(mm):	12
Support Gas Flow Rate (L/min):	15.0	Burner Angle(degree):	0
Flame Type:	Air-C2H2		

### Measurement Parameters

Order:	1st	Pre-Spray Time (sec):	3
Zero Intercept:	Non-Pass	Integration Time (sec):	5
Conc. Unit:	ppm	Response Time:	1
Repetition Sequence:	SM-M-M-...		

	Num Repts.	Max Repts.	RSD Limit	SD Limit
Blank	2	3	0.00	0.1000
Standard	2	3	3.00	0.0000
Sample	2	4	3.00	0.0000
Reslope	2	3	3.00	0.0000

### Example

BLK Average

Abs.	%RSD
0.0001	282.84

Calibration Curve (C# : 02)

Abs=0.086310Conc+0.064320  
r=0.9970

Conc(ppm)	Abs
2.0000	0.2158
4.0000	0.4166
6.0000	0.6097
8.0000	0.7632
10.0000	0.9056

### ***5.4.2 Preliminary experiments with isonicotinate T-Gel beads***

The 1:1 mixture of the iso-TG – acet-TG and NH<sub>2</sub>-TG–acet-TG is treated in the same way as described in the general procedure for the light reduction method.

For the XPS measurements, iso-TG beads are prepared: light reduced, chemical reduced, silver nitrate treated and no treated iso-TG beads. The first two samples are prepared via general procedure. The AgNO<sub>3</sub> treated samples are prepared in a following way: 30mg iso-TG were incubated in 2ml 0.05M AgNO<sub>3</sub> aq. solution for 15min. The silver excess was removed from the beads by washing 5x with nanopure water. Then the beads were dried under vacuum and kept away from light until further utilisation. For the XPS measurements, silicium wafers were used as substrate. The prepared T-gel beads were watered with nanopure water and placed onto the silicium wafer. The samples were then dried under vacuum and kept in the dark. During the XPS measurements, the samples were protected against the light. The samples were measured, at room temperature, in high vacuum and on different spots.

### ***5.4.3 Peptide Ag<sup>+</sup> interactions***

#### **5.4.3.1 Combinatorial assay**

##### ***Library synthesis*** [176]

*Splitting and encoding:* Amino-functionalized Tentagel resin (2.1 g, 0.92 mmol, loading 0.44 mmol/g) was split into seven equal portions of 300 mg (0.13 mmol) each and placed into fifteen 25 mL Merrifield shaking vessels. Each portion was then suspended in dry CH<sub>2</sub>Cl<sub>2</sub> (5 mL). 2 mol% of each tag were dissolved in 1 mL DMF and added into the fifteen reaction vessels together with HOBt (20 mg, 0.13 mmol, 1 eq. per tag) dissolved in DMF (0.5 mL). The mixtures were shaken for at least 5 min to ensure an equal distribution of the tags. After the addition of DIC (20 µL, 0.20 mmol, 1.5 eq. per tag) to each reaction vessel, the mixture was shaken immediately and the reaction allowed to proceed overnight. The fifteen portions of resin were then washed with DMF (3x) and with CH<sub>2</sub>Cl<sub>2</sub> (3x).

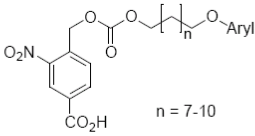
*Decoding of tags:* In order to check the success of the tag coupling, three beads from each of the fifteen vessels were isolated and placed into 25 µL micropipettes. The beads were washed with DMF (2x), then DMF (2.5 µL) was added and the micropipettes were sealed. The tag alcohols were released by photolysis using a UV lamp (366 nm, 15W) for 2 h and analyzed by

EC-GC. If EC-GC detection of the tags was successful, the resin was carried on to the amino acid coupling, if not, the tag coupling process was repeated.

*Coupling of the Amino Acids:* The amino acid couplings and the Fmoc-deprotections were performed as described in the general protocol of peptide synthesis (chapter 5.2.4.1.). After drying the resin for at least 2 hours; the processes of splitting, encoding of the resin and coupling of each amino acid cycles were repeated using the protocols described above until the tripeptides were assembled. Finally, the N-termini were acetylated following the general protocol for acetylation. [2,194]

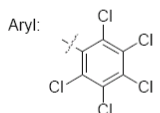
**Figure 5-2:** Tag molecules formula and amount used for each encoding step

*Tag molecules used for the synthesis:*

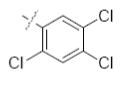


$n = 7-10$

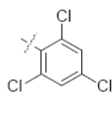
Aryl:



$\text{Cl}_5$



$2,4,5\text{-Cl}_3$



$2,4,6\text{-Cl}_3$

<b>Step 1:</b>	$(\text{CH}_2)_{10}\text{-Cl}_5$ (646.74 g/mol, 2.64 $\mu\text{mol}$ , 8.5 mg) = tag Nr. 1 ( $\text{T}_1$ ) $(\text{CH}_2)_{11}\text{-Cl}_5$ (660.77 g/mol, 2.64 $\mu\text{mol}$ , 8.7 mg) = tag Nr. 2 ( $\text{T}_2$ ) $(\text{CH}_2)_{12}\text{-Cl}_5$ (674.80 g/mol, 2.64 $\mu\text{mol}$ , 9.0 mg) = tag Nr. 3 ( $\text{T}_3$ )
<b>Step 2:</b>	$(\text{CH}_2)_{12}\text{-2,4,6-Cl}_3$ (604.90 g/mol, 2.64 $\mu\text{mol}$ , 8.0 mg) = tag Nr. 1 ( $\text{T}_4$ ) $(\text{CH}_2)_{12}\text{-2,4,5-Cl}_3$ (604.90 g/mol, 2.64 $\mu\text{mol}$ , 8.0 mg) = tag Nr. 2 ( $\text{T}_5$ ) $(\text{CH}_2)_9\text{-Cl}_5$ (632.72 g/mol, 2.64 $\mu\text{mol}$ , 8.4 mg) = tag Nr. 3 ( $\text{T}_6$ )
<b>Step 3:</b>	$(\text{CH}_2)_{10}\text{-2,4,5-Cl}_3$ (576.85 g/mol, 2.64 $\mu\text{mol}$ , 7.6 mg) = tag Nr. 1 ( $\text{T}_7$ ) $(\text{CH}_2)_{11}\text{-2,4,6-Cl}_3$ (590.88 g/mol, 2.64 $\mu\text{mol}$ , 7.8 mg) = tag Nr. 2 ( $\text{T}_8$ ) $(\text{CH}_2)_{11}\text{-2,4,5-Cl}_3$ (590.88 g/mol, 2.64 $\mu\text{mol}$ , 7.8 mg) = tag Nr. 3 ( $\text{T}_9$ )

**Figure 5-3:** Scheme of the encoding

Step 1	M [g mol <sup>-1</sup> ]	m [mg]	Tag	Code		
				T <sub>1</sub>	T <sub>2</sub>	T <sub>3</sub>
Fmoc-L-Asp(O <sup>t</sup> Bu)-OH	411.45	163	T <sub>3</sub>	0	0	1
Fmoc-D-Asp(O <sup>t</sup> Bu)-OH	411.45	163	T <sub>2</sub>	0	1	0
Fmoc-L-Ser(O <sup>t</sup> Bu)-OH	383.44	152	T <sub>2</sub> + T <sub>3</sub>	0	1	1
Fmoc-D-Ser(O <sup>t</sup> Bu)-OH	383.44	152	T <sub>1</sub>	1	0	0
Fmoc-L-His(Trt)-OH	619.72	245	T <sub>1</sub> + T <sub>3</sub>	1	0	1
Fmoc-D-His(Trt)-OH	619.72	245	T <sub>1</sub> + T <sub>2</sub>	1	1	0
Fmoc-L-Tyr(O <sup>t</sup> Bu)-OH	459.54	182	T <sub>1</sub> + T <sub>2</sub> + T <sub>3</sub>	1	1	1
Step 2	M [g mol <sup>-1</sup> ]	m [mg]	Tag	Code		
				T <sub>4</sub>	T <sub>5</sub>	T <sub>6</sub>
1) Fmoc-Aib-OH (Pro-Aib)	325.36	129	T <sub>6</sub>	0	0	1
2) Fmoc-L-Pro-OH (Pro-Aib)	337.37	134				
Fmoc-ε-Ahx-OH	353.40	140	T <sub>5</sub>	0	1	0
Fmoc-Cl (kein Motif)	258.70	102	T <sub>5</sub> + T <sub>6</sub>	0	1	1
Fmoc-Gly-OH	297.31	118	T <sub>4</sub>	1	0	0
1) Fmoc-Gly-OH	297.31	118	T <sub>4</sub> + T <sub>6</sub>	1	0	1
2) Fmoc-L-Pro-OH	337.37	134				
Fmoc-β-Alanin-OH	311.30	123	T <sub>4</sub> + T <sub>5</sub>	1	1	0
Fmoc-rac-Achc-OH	365.00	145	T <sub>4</sub> + T <sub>5</sub> + T <sub>6</sub>	1	1	1
Step 3	M [g mol <sup>-1</sup> ]	m [mg]	Tag	Code		
				T <sub>7</sub>	T <sub>8</sub>	T <sub>9</sub>
Fmoc-L-Asp(O <sup>t</sup> Bu)-OH	411.45	163	T <sub>9</sub>	0	0	1
Fmoc-D-Asp(O <sup>t</sup> Bu)-OH	411.45	163	T <sub>8</sub>	0	1	0
Fmoc-L-Ser(O <sup>t</sup> Bu)-OH	383.44	152	T <sub>8</sub> + T <sub>9</sub>	0	1	1
Fmoc-D-Ser(O <sup>t</sup> Bu)-OH	383.44	152	T <sub>7</sub>	1	0	0
Fmoc-L-His(Trt)-OH	619.72	245	T <sub>7</sub> + T <sub>9</sub>	1	0	1
Fmoc-D-His(Trt)-OH	619.72	245	T <sub>7</sub> + T <sub>8</sub>	1	1	0
Fmoc-L-Tyr(O <sup>t</sup> Bu)-OH	459.54	182	T <sub>7</sub> + T <sub>8</sub> + T <sub>9</sub>	1	1	1

*Combinatorial screening results:*

Approximately 10 mg of the library were suspended in a solution of AgNO<sub>3</sub> (0.05 M, 660 μL, ~6 equiv.), sonicated for 5 min and allowed to incubate for another 10 min. After washing 5x with deionized water (1 mL each), the beads were either irradiated with an electric lamp for 8 h (light reduction assay) or incubated with a solution of sodium ascorbate (0.05 M, 660 μL, ~6 eq.) for 5 min (chemical reduction assay) before washing with deionized water (5x). The combinatorial screening assays were evaluated using a light microscope, single beads were isolated and the peptide sequences analyzed.

**Table 5-17:** Consensus sequences of library **1** after light reduction

Colour	AA2	Linker	AA1	No. of analyzed beads bearing this sequence
Red	D-His	Achc	L-Tyr	7
	L-His	Achc	L-Tyr	3
	D-His	Pro-Aib	L-Tyr	4
	D-His	Pro-Gly	L-Tyr	1
	L-Ser	Achc	L-Tyr	3
	D-Ser	Achc	L-Tyr	4
	L-Tyr	Achc	L-Tyr	2
	D-Ser	Pro-Aib	L-Tyr	1
	L-Ser	Pro-Aib	L-Tyr	2
	D-Ser	Pro-Gly	L-Tyr	1
	L-Tyr	Achc	D-Ser	5
	D-Ser	Pro-Aib	L-Ser	1
	L-Ser	Pro-Aib	L-Ser	1
	D-Ser	Pro-Gly	D-Ser	2
	L-Tyr	Pro-Gly	D-Ser	1
	L-His	Pro-Gly	D-Ser	1
	D-His	Achc	L-Ser	1
	D-His	Achc	L-Ser	1
	L-His	Gly	D-Ser	1
	D-His	Ahx	L-Ser	1
	L-His	Gly	L-Ser	1
	D-His	Pro-Aib	L-Ser	1
	D-Ser	Pro-Aib	L-His	2
	D-Ser	Pro-Gly	L-His	1
	D-Ser	Pro-Gly	D-His	1
	L-Ser	$\beta$ -Ala	D-His	1
	L-Ser	Gly	L-His	1
	L-Tyr	Achc	L-His	1
	L-Tyr	Pro-Aib	D-His	2
	L-Tyr	Pro-Gly	D-His	1
	L-Tyr	Ahx	D-His	1
	L-His	Gly	L-His	1
	D-His	$\beta$ -Ala	L-His	1
L-His	Gly	D-His	1	
L-Ser	Pro-Aib	D-Asp	1	

**Table 5-18:** Consensus sequences of library **1** after chemical reduction

Colour	AA2	Linker	AA1	No. of analyzed beads bearing this sequence
Dark orange Red	D His	Pro-Aib	D Asp	1
	D His	Pro-Aib	L Asp	2
	L His	-	L Asp	1
	L His	Ahc	D Asp	1
	D Asp	Ahx	D His	1
	D Asp	Ahc	D His	1
	D Asp	-	L His	1
	D Asp	Pro-Gly	L His	1
	L Asp	Pro-Aib	L His	1
	L Asp	Ahc	L His	1
	L Asp	Ahx	D His	1
	D His	-	D Ser	1
	L His	Ahc	L Ser	1
	L Ser	Gly	L His	1
	L Ser	Ahx	D His	1
	L Ser	Ahc	L His	1
	D Ser	Ahx	D His	1
	L His	Ahx	L Tyr	1
	L His	Ahc	L Tyr	1
	L Tyr	Ahc	D His	1
	L Tyr	Gly	D His	1
	L Tyr	Ahx	L His	1
	L Tyr	Ahc	L Tyr	1
	D His	Pro-Gly	D His	1
	L His	-	D His	1
	D His	$\beta$ -Ala	L His	1
	D His	Gly	L His	1
	D His	Pro-Aib	L His	1
	L His	Gly	D His	1
	L His	Gly	D His	1
	L His	Ahc	D His	1
Light orange Yellow	L-Tyr	Ahc	D-Ser	1
	L-Tyr	Ahx	D-Ser	1
	D Asp	Pro-Aib	D Asp	1
	D Asp	Pro-Gly	L Asp	1
	L Asp	$\beta$ -Ala	D Asp	1
	L Asp	Pro-Gly	L Asp	1
	L Asp	$\beta$ -Ala	L Asp	1
	L Asp	Gly	L Asp	1
	D Asp	Pro-Gly	L Ser	1
	L Asp	Ahx	D Ser	1
	D Ser	Pro-Aib	D Asp	1
	D Asp	Pro-Gly	D His	1
	D Asp	-	D His	1
	D His	Ahx	D Asp	1
	D Ser	-	D His	1
	D Ser	-	L His	1
	D His	-	L His	1
	L Tyr	-	D His	1

## 5.4.3.2 Silver nanoparticle generation on a surface

The synthesised tripeptide sequences (the detailed parameters are presented in the Chapter 5.2.4) are reduced by the previously described two methods. The reduced beads are photographed via the optical microscope and SEM measurements are carried out. The characterisation of the last group of the tripeptides is presented in the supplementary information of the [2]. In **Table 5-19**, the results of other synthesized tripeptide sequences are listed.

**Table 5-19:** The results of the complementary tripeptide sequences (not shown in the Chapter 3)

Peptides-NHTG	Light reduction		Chemical reduction		Uptake mMAg/ mM pept
	Colour	NP size (nm)	Colour	NP size (nm)	
AcDHis-SSturn-LTyr	Red	~500nm aggr.	D.red	1-300nm aggr.	0.63
AcDHis-RRturn-LTyr	Red	3-500 cryst.	D.red	1-300nm aggr..	0.44
AcDSer-SSturn-LTyr	L.orange	500 cryst.few	Yellow	100nm few	0.30
AcDSer-RRturn-LTyr	L.orange	500 cryst.few	Yellow	100nm few	0.57
AcLTyr-SSturn-DSer	Orange	>1 $\mu$ m isol.cryst.	L.Yellow	<100nm aggr.	0.33
AcLTyr-RRturn-DSer	Orange	>1 $\mu$ m isol.cryst.	L.Yellow	<100nm aggr.	0.15
AcCys-Gly-Ala	Colourless	-	D.yellow	<30nm	0.36
AcLAsp-turn-LTyr	Colourless	-	Grey	~400nm aggr.	0.37
AcDHis-turn-LPhe	Violet	2-300nm	D.violet	200nm aggr	0.43
AcLHis-ProGly-DAsp	Colourless	2-300nm isol	Orange	1-400nm aggr	0.64
AcLAsp- $\beta$ Ala-DHis	Colourless	2-300nm isol.	D.yellow	1-200nm cov	0.59
AcLSer- $\beta$ Ala-LHis	Violet	1-200nm	Braun	1-200nm cov	0.70

Powder X-ray measurements were carried out on different chemically reduced beads. The light reduced beads did not contain enough crystalline particles to be detected with this method. The **Fig.5-4,5** present all the performed powder X-ray spectra.

**Figure 5-4:** Powder X-ray spectra of the chemically reduced silver incubated beads with tripeptides: LAsp-ProGly-LAsp-NHTG, LAsp- $\beta$ Ala-LAsp-NHTG, DHis-Gly-LHis-NHTG, DHis-LTyr-NHTG, LHis-Gly-LHis-NHTG, DHis-LHis-NHTG

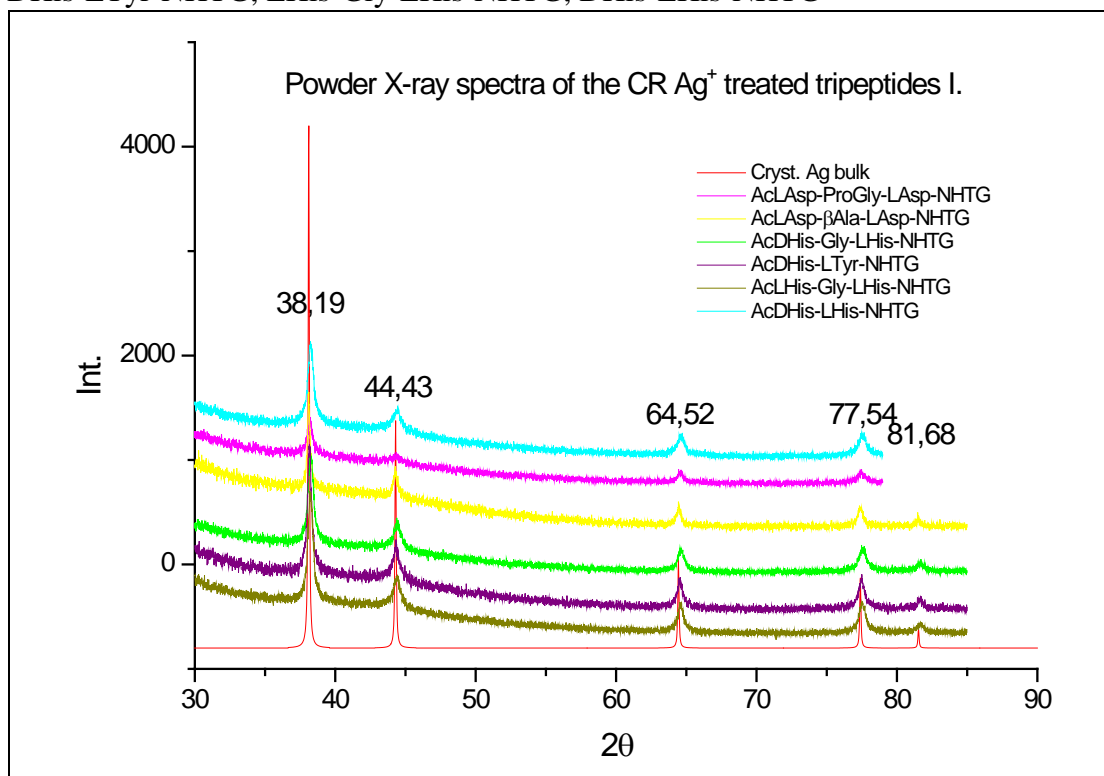
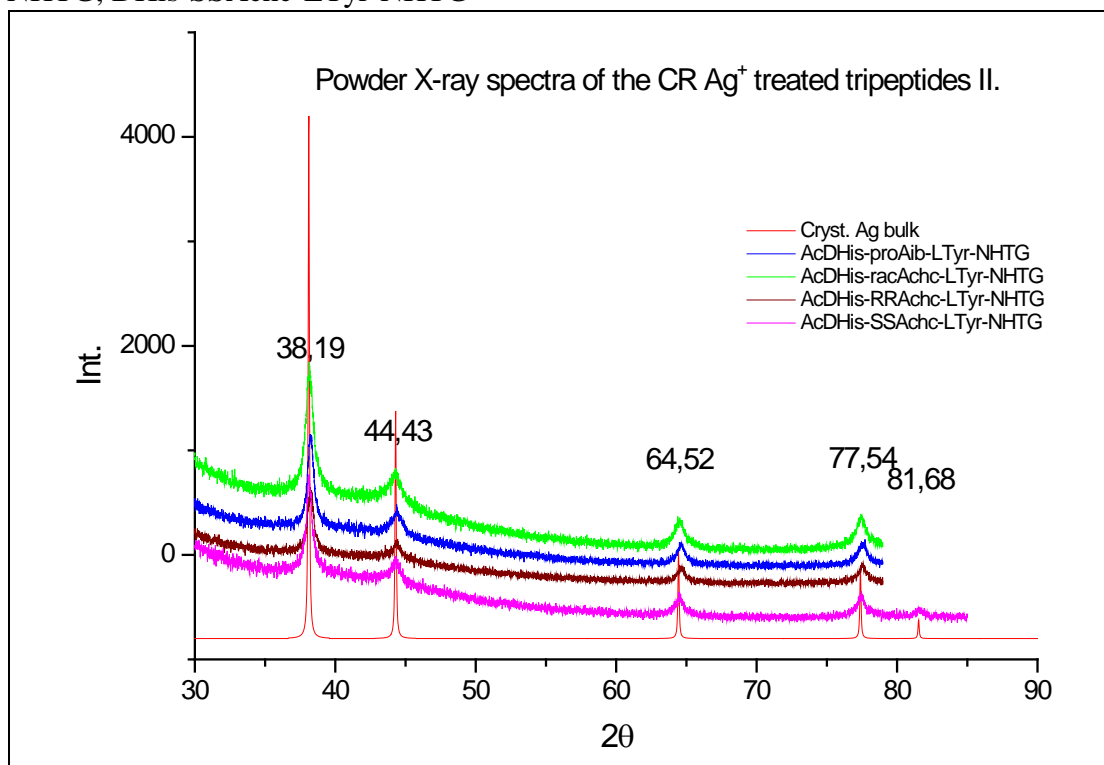


**Figure 5-5:** Powder X-ray spectra of the chemically reduced silver incubated beads with tripeptides: DHis-proAib-LTyr-NHTG, DHis-racAchc-LTyr-NHTG, DHis-RRAchc-LTyr-NHTG, DHis-SSAchc-LTyr-NHTG





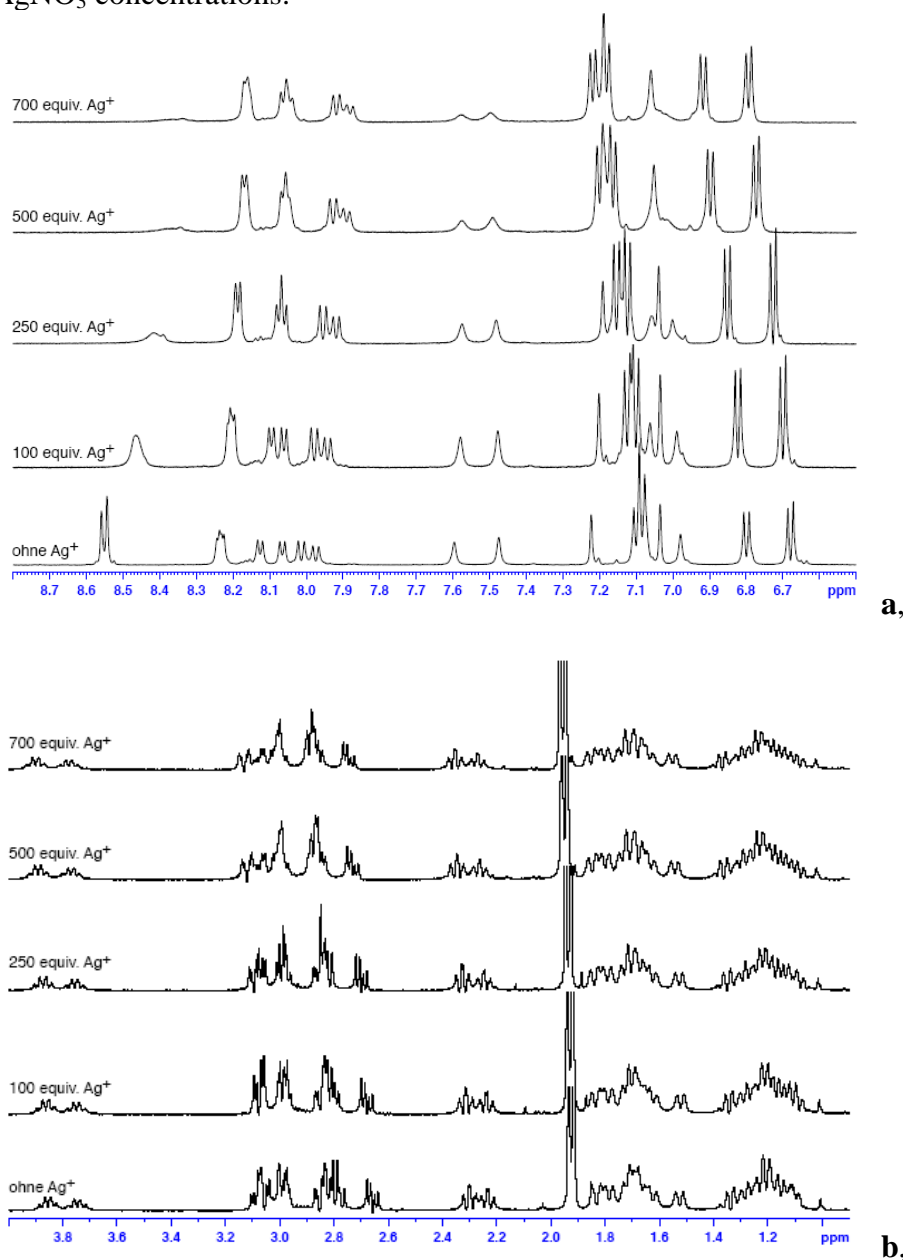
## 5.4.3.3 Complementary experiments of the solution phase tripeptides

*NMR titration* of the AcDHis-Achc-LTyrNH<sub>2</sub> TFA salt:

The chemical shifts of the tripeptide signals with 700eq Ag<sup>+</sup> excess:

H $\epsilon$ -His (180 ppb), NH-Tyr (67.4 ppb), NH-His (63.5 ppb), NH-Achc (97.2 ppb), NH<sub>2</sub>-Terminus (-21.2/35.2 ppb), H $\delta$ -His (-22.8 ppb), H $\epsilon$ -Tyr (-110 ppb), H $\alpha$ -His (-64.1), H $\alpha$ -Tyr (-9.7), H1-Achc (-41.4), H2-Aachc (-50.8), Acetyl (-30.7), H $\delta$ -Tyr (-131 ppb), H $\beta$ -Tyr (-24.0/ -77.1 ppb), H $\beta$ -His (-28.1/ -81.7 ppb).

**Figure 5-6a,b:** The NMR spectra of the AcDHis-Achc-LTyrNH<sub>2</sub> tripeptide with different AgNO<sub>3</sub> concentrations:



The binding constant of the TFA salt of the tripeptide was calculated from the chemical shifts represented as a function of the silver concentration. (**Fig.5-7**).

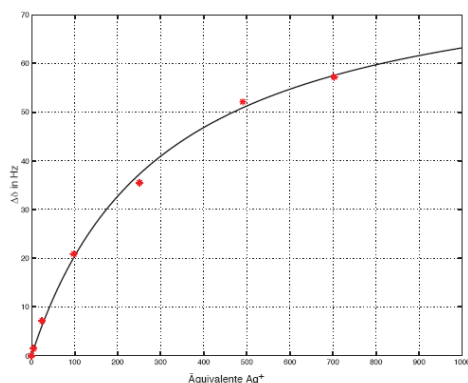


**Figure 5-7:** Chemical shift- silver concentration curve for the binding constant calculation

## 5.5 Biological assays

### 5.5.1 *Isothermal microcalorimetry experiments*

For the IMC measurements, the following samples were used:

*Free compounds:* Adl7, prepared in the previously described way (Chapter 5.2.3.) AgCl is filtered from the equimolar mixture of AgNO<sub>3</sub> and NaCl aq. solution.

*Adl7 compound on polymer surface:* the compounds are presented in the Chapter 5.3.4. All of the three compounds were tested.

*The peptide generated AgNPs* tested by IMC are the LR,CR AcHis-Achc-Tyr-NHTG, LR iso-TG, Ag<sup>+</sup> incubated AcHis-Achc-Tyr-NHTG, LR iso-TG, no treated iso-TG, acetylated-TG. The preparation of these samples is presented in Chapters 5.2.4.and 5.4.1. The Ag<sup>+</sup> incubated samples are prepared as the reduced beads, just the last redaction step is skipped.

*General sample preparation* for the IMC measurements. The dried materials are weighed very exact because the weight of the sample is important to normalize the heat flow values or to compare the heat flow of the different weighed samples. The samples are weighed directly into the 3ml volume glass vessels, then the bacterial suspension (*S.epidermidis*) in BHI is added. The vessels are sealed and placed into the calorimeter. The vessels are shaken before the experiment in order to avoid the aggregation of the substrate. The measurements begin after 40 min equilibration time. During this time, the vessel takes on the surrounding temperature assured by the thermostat. Except for the free compound measurements, 1ml bacterial suspension is added to the sample. The free compounds are measured with 3ml suspension. Heat flow is measured as a function of the time. The experiment time was varied between 36h-72h. In some cases, the normalized heat flow value is presented, during the calculations, because it facilitates the interpretation. The normalized heat flow means that the heat flow value is corrected by the weight of the sample.

### 5.5.2 Flow chamber experiments

The following samples were prepared to optimize the surface treatment method for the flow chamber experiments.

**Table 5-20:** Gold alloy plates surface treatment methods to optimize the coating

Treatment method	Observations
2,5 mM AgNO <sub>3</sub> :L <sub>adl</sub> complex sol. EtOH/THF; there was a precipitation, but I heated it to 60°C and cooled it down slowly after putting the sample in the glass, for 2 weeks	Nice crystals on the surface
Complex crystals (adl7) were deposited on the cleaned Au surface and heated in the oven at 200°C for 1 h.	Small black particles, can be removed easily.
Disulfide (5mM in CH <sub>2</sub> Cl <sub>2</sub> /EtOH for 5 days) +[(AgL1)NO <sub>3</sub> ] 1 mM in EtOH/THF for 2 weeks	Spotted small crystals and inhomogeneous surface
[(AgL1)NO <sub>3</sub> ] 2 mM in EtOH/THF for two weeks	Big crystals
2 mM [(AgL1)NO <sub>3</sub> ] complex sol. EtOH/THF for 2 weeks, solution mixed normally without heating; nice crystals on the surface; plates are removed from the solution, washed and dried, put into the oven for 50 min in 200°C	Big and small dark crystals.

**Table 5-21:** Titanium plates surface treatment methods to optimize the coating

Treatment method	Observations
1,5 mM disulfid solution in EtOH/CH <sub>2</sub> Cl <sub>2</sub> treated for 1.5 days	Nothing can be observed
1,5 mM AgNO <sub>3</sub> :L <sub>adl</sub> complex sol. EtOH/THF for 1.5 days	Crystals on the surface
2,5 mM AgNO <sub>3</sub> :L <sub>adl</sub> complex sol. EtOH/THF for 2 weeks, solution mixed normally without heating	Nice crystals on the surface
5 mM disulfide solution in EtOH/CH <sub>2</sub> Cl <sub>2</sub> treated for 5 days 08.-13.06.06 and put into a 1,5 mM AgNO <sub>3</sub> and leave it in for 7 days	Crystals on the surface
2,5 mM AgNO <sub>3</sub> :L <sub>adl</sub> complex sol. EtOH/THF for 2 weeks, solution mixed normally without heating, nice crystals on the surface, plates are removed from the solution, washed and dried, put in the oven for 40 min in 200°C	Small metallic crystals on the surface

**Table 5-21 continued:**

Treatment method	Observations
5 mM disulfide solution in EtOH/CH <sub>2</sub> Cl <sub>2</sub> treated for 7 days 02.-8.06.06 and 2,5 mM AgNO <sub>3</sub> :L <sub>adl</sub> complex sol. EtOH/THF for 10 days, solution mixed normally without any heating	Nice crystals on the surface
[(AgL1)NO <sub>3</sub> ] 1 mM in EtOH/THF for two weeks	Inhomogeneous surface
Isonicotinic acid solution (5mM in CH <sub>2</sub> Cl <sub>2</sub> /EtOH for 5 days) +[(AgL1)NO <sub>3</sub> ] 1 mM in EtOH/THF for 2 weeks	Small spots, probably cryst, homogeneous surface
Isonicotinic acid solution (5mM in CH <sub>2</sub> Cl <sub>2</sub> /EtOH for 5 days) +[(AgL1)NO <sub>3</sub> ] 2 mM in EtOH/THF for 2 weeks	Big crystals+small crystals

All of these samples were tested in the flow chamber and after discussion of the results, the best sample preparation method was chosen. The further experiments were done on gold plates treated by 2 mM [(AgL1)NO<sub>3</sub>] in EtOH/THF for two weeks. The titanium plates were treated with isonicotinic acid solution (5mM in CH<sub>2</sub>Cl<sub>2</sub>/EtOH) for 5 days, then the plates are removed, washed with EtOH and treated with 2 mM (AgL1)NO<sub>3</sub>] in EtOH/THF for 2 weeks.

The prepared samples were placed in the flow chamber and the result evaluations were done in a previously described way (Chapter 3.3.1.3). For the SEM measurements, the removed gold and titanium plates were prepared as follows: the plates are treated with 2-4 % Glutaraldehyd for 2h in 20°C. Then these are washed twice with PBS for 1 min, then washed twice with H<sub>2</sub>O for 2-5 s and dried with different concentrations ethanol: 30% 50% 70% 90% 2x100% per 10 min, to remove all of the water. Then the plates are dried and sputtered with gold, or platinum.

### 5.5.3 *In vitro* biological assays

#### 5.5.3.1 *In vitro* bacterial growth inhibition tests

##### *Au(111) plates*

General sample preparation is described in the previous chapter concerning the coatings. The following Au(111) plates were prepared, shown in **Table 5-22**.

**Table 5-22:** Different surface treatment methods to optimize the coating on Au(111) surface

Samples	Ag(L1)NO <sub>3</sub>	Treat.time	Method	Method description
Adl7+AgNO <sub>3</sub> and L1 control	2mM	1h, 3h, 5h, 1d, 3d, 7d, 14d	1	The plate is placed into the mixture of the Ag(L1)NO <sub>3</sub> for the determined time interval. Then removed, rinsed with EtOH and dried under vacuum.
Adl7+AgNO <sub>3</sub> and L1 control	1mM	1h, 3h, 5h, 1d, 3d, 7d, 14d	1	
Adl7+AgNO <sub>3</sub> and L1 control	0.5mM	1h, 3h, 5h, 1d, 3d, 7d, 14d	1	
Adl7+AgNO <sub>3</sub> and L1 control	2mM	1h, 3h, 5h, 1d, 3d, 7d, 14d	2	5mM disulfide solution in CH <sub>2</sub> Cl <sub>2</sub> /EtOH for 10 days, the plate is removed, rinsed and placed into the mixture of the Ag(L1)NO <sub>3</sub> for the determined time interval. Then removed, rinsed with EtOH and dried under vacuum.
Adl7+AgNO <sub>3</sub> and L1 control	1mM	1h, 3h, 5h, 1d, 3d, 7d, 14d	2	
Adl7+AgNO <sub>3</sub> and L1 control	0.5mM	1h, 3h, 5h, 1d, 3d, 7d, 14d	2	

Silver determination in the inhibition zone:

The inhibition zone is removed diluted with 1ml 10% HNO<sub>3</sub> and 1ml nanopure water, and the suspension is heated until the complete dissolution. From the cooled solution, 1,0 ml is removed and diluted to 10ml with nanopure water. The remained solution is filtered through 0,22 µm sterile single use filter (Millipore, Millex-GV, PVDF 0,22 µm) and 0,5ml filtered solution is diluted to 5ml with nanopure water. Parallel with the samples solution, control solutions were prepared in the same way than the samples using the agar, outside from the inhibition zone. These samples, all, without any exception, showed zero silver concentration. (It means that the silver never diffused further than the inhibition zone.) The prepared solutions, samples and controls, were then measured by AAS (described previously). The standard solutions are:

	conc.real	x ml stock to 100ml	stock solution: 40 ppm (2ml 1000ppm standard is diluted to 50ml)
Blank	0	0	
stand1	0.2	0.5	
stand2	0.40	1.0	
stand3	0.80	2.0	
stand4	1.60	4.0	
stand5	4.00	10.0	

The silver concentration in the inhibition zone is then calculated.

#### *Titanium and stainless steel substrates*

The general treatment method is described previously in Chapter 5.3.3

**Table 5-23:** 1<sup>st</sup> General method development for titanium and steel restorative implant materials

No.	Method description	1a	1b	2a	2b	3a	4a	4b	5
0	Cleaning	x	x	x	x	x	x	x	x
1	Isonic. acid 5mM, 3 days+ Ladi/AgNO <sub>3</sub> cryst, 2 mM, 10 days	x	x	x	x	x	x	x	
2	Isonic. acid 5mM, ~8 days+ Ladi/AgNO <sub>3</sub> cryst, 1 mM, 20 days	x	x	x	x	x	x	x	
3	Bisulfide 5mM, ~8 days+ Ladi/AgNO <sub>3</sub> cryst, 1 mM, 20 days								x
4	Ladi/AgNO <sub>3</sub> cryst, 2 mM, 14 days	x	x	x	x	x	x	x	x
5	Pyridine-4-boronic acid, ~8 days+ Ladi/AgNO <sub>3</sub> cryst, 1 mM, 20 days	x	x	x	x	x	x	x	

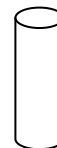
1a : Steel rough cylinder; 1b : Steel smooth cylinder; 2a : Steel rough disks; 2b : Steel smooth disks; 3a : Ti rough cylinder; 4a : Ti rough disks; 4b : Ti smooth disks; 5 : Gold plate

**Table 5-24:** Method development to optimize the crystallisation time for titanium and steel restorative implant materials

Samples	Ag(L1)NO <sub>3</sub>	Treat.time	Substrate	Material
Adl7+AgNO <sub>3</sub> and L1 control	2mM	3h, 7h, 1d, 5d, 10d	Ti rough disks	Titanium
Adl7+AgNO <sub>3</sub> and L1 control	2mM	3h, 7h, 1d, 5d, 10d	Ti rough cylinder	
Adl7+AgNO <sub>3</sub> and L1 control	2mM	3h, 7h, 1d, 5d, 10d	Ti smooth cylinder	
Adl7+AgNO <sub>3</sub> and L1 control	2mM	3h, 7h, 1d, 5d, 10d	Steel polished disk	Stainless steel
Adl7+AgNO <sub>3</sub> and L1 control	2mM	3h, 7h, 1d, 5d, 10d	Steel rough disk	
Adl7+AgNO <sub>3</sub> and L1 control	2mM	3h, 7h, 1d, 5d, 10d	Steel polished cylinder	
Adl7+AgNO <sub>3</sub> and L1 control	2mM	3h, 7h, 1d, 5d, 10d	Steel rough cylinder	

5.5.3.2 *In vivo* assaysCoating of the Ti cages for *in vivo* experiments

(Regine Landmann's group)

d: 10mm; l:30mm surface: 2041 mm<sup>2</sup>

The cages (13pcs) are cleaned: 1x15min sonication with EtOH, 3x15min sonication with nanopure water, then dried in desiccator over P<sub>2</sub>O<sub>5</sub> under vacuum. Half of the cages are used as control sample: these are used without any coating. The other cages (7pcs) are placed into a 24 ml solution (in a 25ml glass container) of a 1 to 1 mixture of 2mM AgNO<sub>3</sub> in THF/EtOH and 2mM Ladl in THF/EtOH for 3 days in the dark. The cages are removed and washed with EtOH and dried over P<sub>2</sub>O<sub>5</sub> under vacuum and delivered on the next day. (On the surface of the cages, there are only some small crystals.)

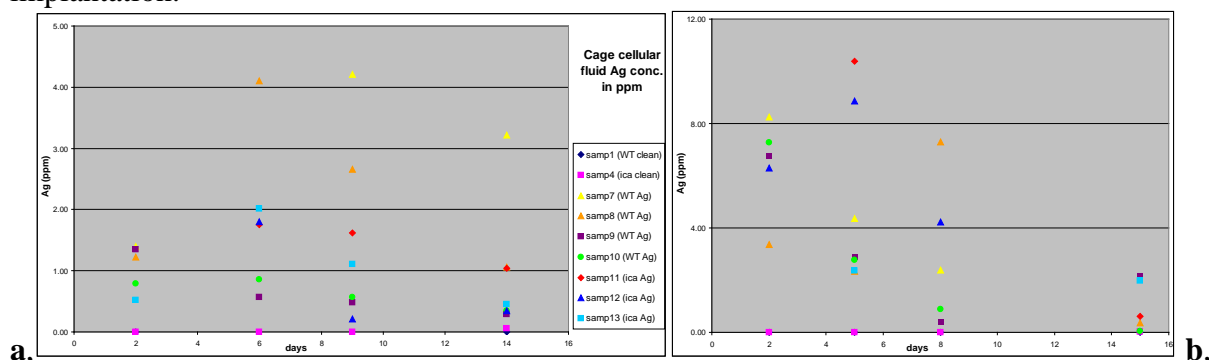
Silver loading determination by AAS

a, Silver concentration of the tissue cage fluid measured by AAS

b, On the surface of the cages before and after *in vivo* experiment

a, For the silver determination, the whole quantity of the removed tissue cage fluid has been diluted to 5ml using 100μl 10% HNO<sub>3</sub>. The acid is given to the almost completely diluted solution to avoid the precipitation of the peptides. The solution is then measured by AAS using standard solutions between 0,1-3,2 ppm (described previously). The silver concentration is then calculated. The results are shown on **Fig.5-7a,b**.

**Figure 5-7a,b:** Silver concentration of the tissue cage fluid, after 2,5,9 and 14 days the implantation.



b, To determine the silver concentration of the treated cages, after and before the *in vivo* experiments, the cages are placed in a thin glass tube and 4ml 20%HNO<sub>3</sub> is added. The glass tube is then sonicated for 15min to remove all the coating from the surface, and the whole

amount of acidic solution is transferred and diluted to 20ml. Further dilutions were made when needed. The silver concentration of the solutions was then measured and the loading calculated.



## 6 Bibliography

- [1]: T.Vig Slenters, I.Hauser-Gerspach, A.U. Daniels, K.M.Fromm; *J.Mater.Chem.*, **2008**, *18*, 5359
- [2]: K.Belser, T.Vig Slenters, C.Pfumbiadzai, G.Upert, L.Mirola, K.M.Fromm, H.Wennemers; *Angew.Chem.Int.Ed.* **2009**, *48* accepted
- [3]: J.South; *Mild silver protein against internal and topical infection*, www.smart-drugs.com/JamesSouth-silver.htm
- [4]: <http://www.jm.com/msds/EN2213.pdf>, *Safety Data Sheet*
- [5]: <http://www.lenntech.com/elements-and-water/silver-and-water.htm>
- [6]: M.J.Rosenblat; *J.Am.Osteopath.Assoc*; **1987**, *87*(7): 509
- [7]: Y.Ohbo, H.Fukuzako, K.Takeuchi, M.Takigawa; *Psychiatry Clin. Neurosci.*, **1996**, *50*(2), 89.
- [8]: S.M.Mirsattari, R.R.Hammond, M.D.Sharpe, F.Y.Leung, G.B.Young; *Neur.*, **2004**, *62*(8), 1408.
- [9]: K.I.Batarseh, *Leukemia*, **2008**, *22*, 448
- [10]: K.I.Batarseh, *J. Antimicrob. Chemother.*, **2004**, *54*, 546.
- [11]: I.Neamtu, A.P.Chiriac, L.E.Nita, M.Bercea; *J. Optoelectr. Adv. Mater.*, **2007**, *9*(11), 3459.
- [12]: Y.Kawaguchi; *Silver protein complexes as dispersants for oily compositions, oil-containing antibacterial antifungal compositions, and sterilization method*, **2002**, Jpn. Patent, JP 2002275011,
- [13]: M.Oda, H.Itoh, T.Sudo, S.Sakuma, K.Nomiya, Y.Suzuki, Y.Jyonoshita, A.Kikuchi, Y.Takabatake; *Preparation of thiol silver complexes as antibacterial, antifungal and antiviral agents*, **1995**, WO 9512602
- [14]: Y.Kani, M.Wakana; *Antibacterial and antifungal phosphate complex salts containing silver*, **1993**, JP 05294808
- [15]: A.A.Isab, M.I.M.Wazeer, M.Fettouhi, B.A.Al-Maythalony, A.R.Al-Arfaj, N.O.Al-Zamil; *Inorg. Chim. Acta*, **2007**, *360*(12), 3719.
- [16]: A.Melaiye, R.S.Simons, A.Milsted, F.Pingitore, C.Wesdemiotis, C.A.Tessier, W. J.Youngs; *J. Med. Chem.*, **2004**, *47*(4), 973.
- [17]: Y.Yokosawa; *Antibacterial polymer compositions and their films*, **2003**, JP 2003192916
- [18]: T.Yoshioka, A.Kawato, T.Ozaki, Y.Suwa, S.Hamada, A.Fujiwara; *Cosmetics containing silver chloro complex salts as antiseptics*, **2001**, JP 2001247425
- [19]: V.Sambhy, M.M.MacBride B.R.Peterson, A.Sen; *J. Am. Chem. Soc.*, **2006**, *128*(30), 9798.
- [20]: T.Tomioka, K.Tomita, H.Oka, K.Hoshino, A.Nishino; *National Technical Report (Matsushita Electric Industrial Company)*, **1994**, *40*(1), 39.
- [21]: V.Sambhy, M.M.MacBride B.R.Peterson, A.Sen; *J. Am. Chem. Soc.*, **2006**, *128*(30), 9798.
- [22]: R.Barbucci, G.Leone, A.Magnani, L.Montanaro, C.R.Arciola, G.Peluso, O.Petillo; *J. Mater. Chem.*, **2002**, *12*(10), 3084.
- [23]: F.Jinhong, J.Jian, F.Dezeng, S.Jiacong; *J. Biomed. Mater. Res.A*, **2006**, *79*(3), 665.
- [24]: U. Fluckiger, M. Ulrich, A. Steinhuber, *Infect Immun* **2005**; *73*: 1811.
- [25]: Y.Kawaguchi; *Silver protein complexes as dispersants for oily compositions, oil-containing antibacterial antifungal compositions, and sterilization method*. **2002**, JP 2002275011
- [26]: J.S. Kim, (S. Korea);; *Refrigerator coating containing antibacterial silver nanoparticles*. **2004**, U.S. Pat. Appl.,US 2004137213

- [27]: X.Ding; *Antibacterial shoe material and its production*, **2008**, CN 101116558
- [28]: C-Y.Chen, C-L.Chiang; *Mater.Lett.* , **2008**, 62(21-22), 3607.
- [29]: <http://orthopedics.about.com/od/hipkneereplacement/a/implants.htm>
- [30]: <http://www.fredphillips.co.nz/orthopaedic-wellington/knee-replacement.html>
- [31]: <http://www.uniteddentaldc.com/listings1.nxg>
- [32]: R. O. Darouiche; *New Engl. J. Med.*, **2004**, 350, 1422.
- [33]: P. Kingshott, J. Wei, D. Bagge-Ravn, N. Gadegaard and L. Gram; *Langmuir*, **2003**, 19, 6912.
- [34]: H. J. Kaper, H. J. Busscher and W. Norde; *J. Biomater. Sci., Polym. Ed.*, **2003**, 14, 313.
- [35]: J. A. Nagel, R. B. Dickinson and S. L. Cooper; *J. Biomater. Sci., Polym.Ed.*, **1996**, 7, 769.
- [36]: M.Stigter, J.Bezemer, K.de Groot, P.Layrolle, B. Chienna, V.Bilthoven; *Neth. J. Contr. Rel.*, **2004**, 99(1), 127.
- [37]: C.S.Adams, J.Parvizi, H.M.Davidson, R.J. Composto, T.A. Freeman, E.Wickstrom, P.Ducheyne, D.Jungkind, I.M.Shapiro, N.J. Hickok; *Biomater.*, **2008**, 29(35), 4684.
- [38]: B.Jose, V.Antoci, A.R.Zeiger E.Wickstrom, N. J. Hickok; *Chem. Biol.*, **2005**, 12, 1041
- [39]: P.Podsiadlo, S.Paternel, J-M.Rouillard, Z.Zhang, J.Lee, W-L.Jaebeom; E.Gulari, N.A.Kotov; *Langmuir*, **2005**, 21(25), 11915-11921
- [40]: J.S.Rudra, K.Dave, D.T. Haynie; *J. Biomater. Sci., Polym.Ed.*, **2006**, 17(11), 1301.
- [41]: M.Bertau, D.Scharnweber, K.Leppchen, R. Beutner, M.Schloemann, S. Kaschabek, L.Messner; *Antimicrobial and biocompatible coating for metal surfaces*. **2006**, DE 102006020728
- [42]: K.Hilpert, M. Elliott, H.Jenssen, J. Kindrachuk, C.D.Fjell, J. Koerner, D.F.H. Winkler, L.L.Weaver, P. Henklein, A.S.Ulrich, S.H.Y.Chiang, S.W.Farmer, N. Pante, R.Volkmer, R.E.W.Hancock; *Chem. Biol.*, **2009**, 16(1), 58.
- [43]: N.Managoli; *Implantable medical devices comprising flavonoids' coating for prevention of restenosis.* , **2007**, WO 2007010342
- [44]: X.Pang, I.Zhitomirsky; *ECS Trans. Bioelectr. Biointerf. Biomed. Appl.2*, **2007**, 3(26), 15.
- [45]: Q. L.Feng, F. Z.Cui, T. N.Kim, J. W.Kim; *J. Mater. Sci. Lett.* **1999**, 18(7), 559-561.
- [46]: K.Das, S.Bose, A.Bandyopadhyay, B.Karandikar, B.L. Gibbins; *J.Biomed. Mater. Res., B:Appl.Biomater.*, **2008**, 87B(2), 455.
- [47]: D.Vyacheslav, N.Yakeemovich, V.DiTizio, F.DiCosmo; *Antimicrobial photo-stable coating composition and medical device coated thereby* PCT Int. Appl. **2009**, WO 2009015476
- [48]: Z. Shi; K.G.Neoh; S.P.Zhong, L.Y.L.Yung, E.T.Kang, W.Wang; *J.Biomed. Mater. Res. A.*, **2006**, 76(4), 826.
- [49]: E. Sheehan, J. McKenna, K. J. Mulhall, P. Marks and D. McCormack; *J. Orthop. Res.*, **2004**, 22, 39.
- [50]: Evan M. Hetrick and Mark H. Schoenfisch; *Chem. Soc. Rev.*, **2006**, 35, 780.
- [51]: R. Kumar and H. Munstedt; *Biomater.*, **2005**, 26, 2081
- [52]: R. Kumar and H. Munstedt, *Polym. Int.*, **2005**, 54, 1180.
- [53]: F. Furno, K. S. Morley, B. Wong, B. L. Sharp, P. L. Arnold, S. M. Howdle, R. Bayston, P. D. Brown, P. D. Winship and H. J. Reid; *J. Antimicrob. Chemother.*, **2004**, 54, 1019.
- [54]: C.von Eiff, G.Peters, C.Heilmann; *Lanc. Infect. Diseas.*, **2002**, 2(11), 677.
- [55]: J.W.Gray, S.J. Pedler; *J. Hosp.Infect.*, **1992**, 21(1), 1.
- [56]: I.G.Duguid, E.Evans, M.R.Brown, P.Gilbert; *J. Antimicrob. Chemother.*, **1992**, 30(6), 791
- [57]: J.O.Anglen, S.Apostoles S; G.Christensen, B.Gainor; *J. Orthop. Tr.*, **1994**, 8(5), 390.
- [58]: M Katsikogianni, Y. F.Missirlis; *Eur. Cell. Mater.*, **2004**, 8, 37

- [59]: R.R.Isberg, P. Barnes; *Cell*, **2002**, 110(1), 1.
- [60]: I.Klapper, C.J.Rupp, R.Cargo, B.Purvedorj, P.Stoodley; *Biotech. Bioeng.*, **2002**, 80(3), 289
- [61]: Y.Liu, J-H.Tay; *Wat. Res.*, **2002**, 36(7), 1653.
- [62]: J.Hubble; *Chem. Eng. Sci.*, **2003**, 58(19), 4465.
- [63]: M.J.McWhirter, J.A.McQuillan, P.J.Bremer ; *Coll.Sur. B.*, **2002**, 26(4), 365
- [64]: J.M.Schierholz, C.Fleck, J. Beuth, G. Pulverer; *J. Antimicrob. Chemother.*, **2000**, 46(1), 45.
- [65]: C.R.Arciola, L.Baldassarri, L.Montanaro; *J. Biomed. Mater. Res.*, **2002**, 59(3), 557
- [66]: M.Kiremitci-Gumusderelioglu, A.Pesmen; *Biomater.*, **1996**, 17(4), 443.
- [67]: T.R.Scheuerman, A.K.Camper, M.A.Hamilton; *J. Coll. Interf. Sci.*, **1998**, 208(1), 23.
- [68] R. L.Taylor, J.Verran, G. C.Lees, A. J. P. Ward; *J. Mater. Sci.: Mater. Med.*, **1998**, 9(1), 17.
- [69]: C.Diaz, M.C.Cortizo, P.L.Shilardi, S.G.Gomez de Savaria, M.A.F.Lorenzo de Mele; *Mater. Res.*, **2007**, 10, 11
- [70]: K. A. Poelstra, N. A. Barekzi, A. M. Rediske, A. G. Felts, J. B. Slunt and D. W. Grainger; *J. Biomed. Mater. Res.*, **2002**, 60, 206.
- [71]: R. A. Bologna, L. M. Tu, M. Polansky, H. D. Fraimow, D. A. Gordon and K. E. Whitmore; *Urology*, **1999**, 54, 982.
- [72]: N.George, J.Faoagali, M.Muller; *Burns*, **1997**, 23, 493
- [73]: U.Tattawasart, J.Maillard, J.R.Furr, A.D.Russel; *Int. J. Antimicrob. Agents*, **2000**,16, 233
- [74]: AD.Russel, I.Chopra; *Understanding antibacterial action and resistance*, 2<sup>nd</sup> edn, **1996**, Chinchester:Ellis Horwood
- [75]: D. Lee, R. E. Cohen and M. F. Rubner; *Langmuir*, **2005**, 21, 9651.
- [76]: S.L.Percival, P.G.Bowler, D.Russel; *J. Hosp. Infection*, **2005**,60,1
- [77]: S.Silver, L.T.Phung; *J. Ind. Microbiol. Biotechnol.*, **2005**,32,587
- [78]: S.Silver, L.T.Phung,G.Silver; *J. Ind. Microbiol. Biotechnol.*, **2006**, 33, 627
- [79]: S.Silver; *FEMS Microbiol. Rev.*, **2003**, 27, 341
- [80]: P.D.Bragg, D.J.Rannie; *Can. J. Microbiol.*, **1974**, 20, 883.
- [81]: A.D. Russel, W.B.Hugo; *Prog. Med. Chem.*, **1994**, 31, 351.
- [82]: R.B.Thurman, C.P. Gerba; *CRC Crit. Rev. Environm. Cont.*, **1989**, 18, 295.
- [83]: J.R.Furr, A.D. Russel, T.D.Turner, A.Andrews; *J. Hosp. Infect.*, **1994**, 27, 201.
- [84]: S.Y.Liau, D.C.Read, W.J.Pugh, J.R.Furr, A.D.Russel; *Lett. Appl. Microbiol.*, **1997**, 25, 279.
- [85]: Q.L. Feng, J.Wu, G.Q.Chen, F.Z.Cui, T.N.Kim, J.O.Kim; *J. Biomed. Mater. Res*, **2000**, 52, 662.
- [86]: K.B Holt, A.J Bard, *Biochemistry*, **2005**, 44, 13214.
- [87]: I.Zeiri, B. V.Bronk, Y. Shabtai, J.Eichler, S.Efrima; *Appl. Spectrosc.*, **2004**, 58, 33-40.
- [88]: M.W.G.de Bolster; *Int. Union of Pure and Appl. Chem.*, **1997**.  
<http://www.chem.qmul.ac.uk/iupac/bioinorg/CD.html#8>. Retrieved on: 2009-03-26.
- [89]: RegisFrey; <http://commons.wikimedia.org/wiki/File:CellRespiration.svg>
- [90]: Salsb; <http://en.wikipedia.org/wiki/File:7ACN.jpg#file>
- [91]: X.J. Chen et al. ; *Science*, **2005**, 307, 714
- [92]: T. Friedrich; *Biochim. Biophys. Acta* **1998**, 1364, 134-146
- [93]: Adeline Robin; *Doctoral thesis, Structural diversity of Cu(I), Ag(I) and Cu(II) coordination polymers with the ligand ethanediyl bis(isonicotinate)*, **2005**, Basel
- [94]: A.Y.Robin, M.Meuwly, K.M.Fromm, H.Goesmann, G.Bernardelli; *Cryst. Eng. Comm.*, **2004**, 6, 336
- [95]: J.C.Bailar, Jr.; *Prep. Inorg. React*, **1964**, 1, 1.
- [96]: C.Janiak; *Dalton. Trans.*, **2003**, (14), 2781

- [97]: X.-H. Bu, W. Chen, W.-F. Hou, M. Du, R.-H. Zhang, F. Briss; *Inorg. Chem.*, **2002**, 41(13), 3477
- [98]: L. Yang, X. Shan, Q. Chen, Z. Wang, J.S. M.; *Eur. J. Inorg. Chem.*, **2004**, (7), 1474
- [99]: G. Zhang, G. Yang, Q. Chen, J.S. Ma; *Cryst. Grow. Des.*, **2005**, 5(2), 661
- [100]: Q.L.Feng, J.Wu, G.Q.Chen, F.Z.Cui, T.N.Kim, J.O. Kim; *J. of Biomed.Mater. Res*, **2000**, 52, 662
- [101]: H. Liu, H.Yamamoto, J. Wei, D.H. Waldeck; *Langmuir* (**2003**), 19(6), 2378
- [102]: P.Persson, S.Lunel, P.A.Bruhwyler, J.Schnadt, S.Sodergren, J.N.O'Shea, O.Karis, H.Siegbahn, N. Martensson, M.Bassler, L.Patthey; *J. Chem. Phys.*, **2000**, 112(9), 3945.
- [103]: W. Ostwald; *Lehrbuch der Allgemeinen Chemie*, vol. 2, part 1., **1896**, Leipzig, Germany
- [104]: Priscilla Brunetto unpublished data
- [105]: H. Hoffmann, personal communication
- [106]: H.Chen, S.Kuranari, M.Matsuoka,J.Zhang, M.Anpo; *Catal lett.* **2008**, 126(3-4), 218
- [107]: H.Li; *J.Phys.Chem.*, **2007**,111, 2102.
- [108]: D. Hudetz. S. Ursic, Hudetz, L. G. Harris, R. Luginbühl, N. F. Friederich, R. Landmann; *Clin Microbiol Infect*, **2008**, 14(12),1135-45
- [109]: E.M. Hetrick and M. H. Schoenfisch; *Chem. Soc. Rev.*, **2006**, 35, 780
- [110]: Y. H. An and J. R. Friedman; *J. Biomed. Mater. Res.*, **1998**, 43, 338
- [111]: J.E.Ladbury, B.Z. Chowdhry; *Biocalorimetry, Applications of Calorimetry in the Biological Sciences.* **1998**,Wiley
- [112]: A.E.Beezer; *Thermochim. Acta*, **2001**,380, 205
- [113]: U.von Stockar, I.W.Marrison; *Adv. Biochem. Eng.* **1986**. 40, 92
- [114]: R.Hölzel, C.Motzkus, I.Lamprecht; *Thermochim. Acta* **1994**. 239, 17
- [115]: T.Maskow , W.Babel; *J. Biotech.*, **2003**, 101, 267
- [116]: Y.Nakagawa, R.Schäfer, H.-J.Güntherodt, *Appl. Phys. Lett.* **1998.**, 73, 2296 [117]:
- [118]: I.Lamprecht, E.Schmolz, *Thermochim. Acta* **2000.**, 355, 95
- [119]: I.Wadsö; *ISBC XII Calorimetry: a tool in health and environmental studies*, **2001**, Santiago de Compostella, Spain
- [120]: T. Maskow, W. Babel; *Thermochim. Acta*, **2002**, 382, 229–237
- [121]: S.J.Charlebois, A.U.Daniels, R.A.Smith *J. Biomed. Mater. Res.* **2002**, 59: 166
- [122]: <http://www.stk-online.ch/lausa07/abstract%20daniels.pdf>.
- [123]: A.Trampuz, S.Salzmann, J.Antheaume; A.U.Daniels, *Transfusion*, **2007**, 47(9), 1643
- [124]: I.Hauser-Gerspach, P.Scandiucci de Freitas, A.U. Dan Daniels, J.Meyer; *J Biomed Mater Res Part B: Appl Biomater*, **2008**, 85,: 42,
- [125]: Ueli von Ah; *Unpublished data*, **2008**
- [126]: M. Madigan, J. Martinko; *Brock Biology of Microorganisms* (11th ed. ed.), **2005**, Prentice Hall
- [127]: R.M. Atlas; *Handbook of Microbiological Media*, **2004**, London: CRC Press. p. 1226.
- [128]: J.G.Holt, *Bergey's Manual of Determinative Bacteriology* (9th ed.). **1994**, Williams & Wilkins
- [129]: G,Hedin, *Scan. J. Infect. Disea.*, **1993**
- [130]: F. Gotz, *Mol. Microbiol* **2002**; 43: 1367
- [131]: M.E.Rupp, J.S.Ulphani, P.D.Fey, K.Bartscht, D.Mack, *Infect. Immun.* **1999**; 67: 2627.
- [132]: P.D. Marsh; *Caries. Res.*, **2004**, 38, 204
- [133]: B.Rosan, R.J.Lamont; *Microbes Infection*, **2000**, 2, 1599
- [134]: P.E.Kolenbrander; *Annu. Rev. Microbiol.* **2000**;54: 413.
- [135]: J.Li, E.J.Helmerhorst, C.W.Leone, R.F.Troxler, T.Yaskell, A.D.Haffajee, S.S.Socransky, F.G.Oppenheim; *J. Appl. Microbiol*, **2004**, 97, 1311.
- [136]: I. Hauser-Gerspach, E. M. Kulik, R. Weiger, E. M. Decker, C. Von Ohle and J. Meyer, *Dent. Mater. J.*, **2007**, 26, 361

- [137]: I.Hauser-Gerspach, P.Scandiucci de Freitas,A.U. Dan Daniels, J.Meyer; *J Biomed Mater Res Part B: Appl Biomater*, **2008**, 85B: 42
- [138]: G.Müller, A.Kramer; *J. Antimicrob. Chemother.*, **2008**, 61, 1281
- [139]: M.Y.H.Chin, H.J.Busscher, R.Evans, J.Noar, J.Pratten; *The European Journal of Orthodontics*, **2006** 28(1),1.
- [140]: M. Katsikogianni and Y. F. Missirlis; *Eur. Cells Mater.*, **2004**, 8, 37
- [141]: J.M.Schierholz, L.J.Lucas, A.Rump, G.Pulverer; *Journal of Hospital Infection*, **1998**, 40, 257
- [142]: R. Weiger, E. M. Decker, G. Krastl and M. Brex; *Arch. Oral Biol.*,**1999**, 44, 621.
- [143]: C. Dawes, S. Watanabe, P. Biglow-Lecomte and G. H. Dibdin; *J. Dent. Res.*, **1989**, 68, 1479.
- [144]: R. Weiger, E. M. Decker, G. Krastl and M. Brex; *Arch. Oral Biol.*, **1999**, 44, 621.
- [145]: E. M. Decker, R. Weiger, C. von Ohle, I. Wiech and M. Brex; *Clin. Oral Invest.*, **2003**, 7, 98–102;
- [146]: E. M. Decker; *Lett. Appl. Microbiol*, **2001**, 33, 188.
- [147]: N.L.Rosi, D.A.Giljohann, C.S.Thaxton, A.K.R.Lytton-Jean,M.S.Han, C.A.Mirkin; *Science*, **2006**, 312, 1027
- [148]: C.Xue, C.A. Mirkin; *Angew.Chem.Int.Ed.* **2007**, 46,
- [149]: W. L. Barnes, A. Dereux, T. W. Ebbesen ; *Nature* **2003**, 424, 824
- [150]: S. Eustis, M. A. El-Sayed; *Chem. Soc. Rev.* **2006**, 35, 209.
- [151]: Z.S. Pillai, P.V. Kamat; *J.Phys.Chem. B* **2004**, 108, 945
- [152]: K.M.Sheker, H.J.Black, J.L.Lach; *Am.J.Hosp.Pharm.*, **1972**, 29, 852
- [153]: J.M. Slocik, M.O. Stone, R.R. Naik; *Small* **2005**, 1, 1048
- [154]: A. Pal, T. Pal ; *J.Raman.Spectrosc.* **1999**, 30, 199
- [155]: N. Vigneshwaran et al; *Mater. Lett.*, **2007**, 61, 1413
- [156]: N. Durán et al. ; *J.Nanobiotech.* **2005**, 3-8;
- [157]: A.R. Shahverdi et al ; *Proc.Biochem.* **2007**, 42, 919
- [158]: T. Klaus et al. ; *PNAS* **1999**, vol.96, no.24, 13611
- [159]: MSDS, Silver nitrate, Acros, Belgium
- [160]: S.A. Kumar et al; *Biotechnol Lett.* **2007**, 29, 439
- [161]: R.M. Kramer et al; *J.Am.Chem.Soc.* **2004**, 126, 13282
- [162]: R.R. Naik et al; *Nature Mat.* **2002**, nov., 169
- [163]: J.Yu, S.A.Patel, R.M.Dickson, *Angew. Chem. Int. Ed.* **2007**, 46,
- [164]: Ray, A.K.Das, A.Banerjee ; *Chem.Commun.* **2006**, 2816
- [165]: Si et al; *Chem.Eur.J.* , **2006**, 12, 1256
- [166]: Selvakannan et al; *Langmuir* **2004**, 20, 7825
- [167]: D. Campoccia, L. Montanaro, C. R. Arciola; *Biomaterials*, **2006**, 27, 2331
- [168]: Y. Ono, K. Nakashima, M. Sano, Y. Kanekiyo, K. Inoue, J. Hojo and S. Shinkai, *Chem. Commun.*, **1998**, 1477
- [169]: J. H. Jung, Y. Ono and S. Shinkai; *Angew. Chem., Int. Ed.*, **2000**, 39, 1862
- [170]: K. Sugiyasu, S. Tamura, M. Takeuchi, D. Berthier, I. Huc, R. Oda, S. Shinkai; *Chem. Commun.*, **2002**, 1212
- [171]: S. Kobayashi, K. Hanabusa, N. Hamasaki, M. Kimura, H. Shirai and S. Shinkai; *Chem. Mater.*, **2000**, 12, 1523
- [172]: S. Kobayashi, N. Hamasaki, M. Suzuki, M. Kimura, H. Shirai and K. Hanabusa; *J. Am. Chem. Soc.*, **2002**, 124, 6550
- [173]: D. Sone, E. R. Zubarev and S. I. Stupp; *Angew. Chem., Int. Ed.*, **2002**, 41, 1705
- [174]: Yu, S.A.Patel, R.M.Dickson; *Angew. Chem., Int. Ed.* **2007**, 46,
- [175]: J.J.Mock, M.Barbic, D.R.Smith, D.A.Schultz, S.Schultz; *J. Chem. Phys.*, **2002**, 116(15), 6755

- [176]: M. H. J. Ohlmeyer, R. N. Swanson, L. W. Dillard, J. C. Reader, G. Asouline, R. Kobayashi, M. Wigler, W. C. Still; *Proc. Natl. Acad. Sci. USA* **1993**, *90*, 10922
- [177]: H. P. Nestler, P. A. Bartlett, W. C. Still; *J. Org. Chem.* **1994**, *59*, 4723.
- [178]: A. Furka, F. Sebestyén, M. Asgedom, G. Dibo; *Int. J. Pept. Protein Res.* **1991**, *37*, 487
- [179]: K. S. Lam, S. E. Salmon, E. M. Hersh, V. J. Hruby, W. M. Kazmierski, R. J. Knapp; *Nature* **1991**, *354*, 82
- [180]: S. Brenner, R. A. Lerner; *Proc. Natl. Acad. Sci. USA* **1993**, *89*, 5381
- [181]: I. Pastoriza-Santos, L. M. Liz-Marzán; *J. Mater. Chem.* **2008**, *18*, 1724
- [182]: C. J. Murphy, A. M. Gole, S. E. Hunyadi, J. W. Stone, P. N. Sisco, A. Alkilany, B. E. Kinard, P. Hankins; *Chem. Commun.* **2008**, 544
- [183]: N. L. Rosi, C. A. Mirkin, A. Chad; *Chem. Rev.*, **2005**, *105*, 1547
- [184]: K. Aslan, J. Zhang, J. R. Lakowicz, C. D. Geddes; *J. Fluoresc.*, **2004**, *14*, 391
- [185]: A. Roucoux, J. Schulz, H. Patin ; *Chem. Rev.*, **2002**, *102*, 3757
- [186]: R. C. N. Rao, G. U. Kulkarni, P. J. Thomas, P. P. Edwards; *Chem. Soc. Rev.* **2000**, *29*, 27
- [187]: A. Henglein, *Chem. Rev.* **1989**, *89*, 1861
- [188]: MSDS, Silver Oxide, Columbus Chem. Indust. Columbus, Canada
- [189]: J.Xie, J.Y.Lee, D.I.C.Wang, Y.P.Ting; *Nano* **2007**, *1*, 429
- [190]: S.Si, R.R.Bhattacharjee, A.Banerjee, T.K.Mandal; *Chem. Eur. J.* **2006**, *12*, 1256
- [191]: S.Ray, A.K.Das, A.Banerjee; *Chem. Comm.* **2006**, *12*, 2816
- [192]: M. B. Francis, N. S. Finney, E. N. Jacobsen; *J. Am. Chem. Soc.* **1996**, *118*, 8983
- [193]: S.D.Evans, A.Urankar, A.Ulman, N.Ferris; *J. Am. Chem. Soc.*, **1991**, *113*, 4121
- [194]: Kirsten Belser, PhD dissertation: *Peptid-Metall Wechselwirkungen-Anwendung selektiver Bindung zur Esterhydrolyse und Bildung von Silber-Nanopartikeln*, **2008**, Basel
- [195]: K. Nomiya, S.Takahashi, R.Noguchi, S.Nemoto, T.Takayama, M.Oda; *Inorganic Chemistry*, **2000**, *39*(15), 3301
- [196]: Laurent Mirolo, *Doctoral thesis*, **2009**, Fribourg
- [197]: P.Patai, Z.Rappaport; *The chemistry of organic derivatives of gold and silver*, **1999**, Wiley
- [198]: G.Faúndez, M.Troncoso, P.Navarrete, G.Figueroa; *BMC Microbiology* **2004**, *4*:19
- [199]: J. Cosier, A.M. Glazer; *J. App. Cryst.*, **1986**, *19*(2), 105
- [200]: E. Blanc, D. Schwarzenbach, H.D. Flack; *J. App. Cryst.*, **1991**, *24*(6), 1035.
- [201]: G.M. Sheldrick. *SHELX-99, Program for Crystal Ctructure Refinement*, **1999**, University of Göttingen, Göttingen
- [202]: T.Dorn, K.M.Fromm, C.Janiak; *Aust.J.Chem.*, **2006**, *59*, 22.
- [203]: Q-H.Wei, L-Y.Zhang, L-X.Shi, Z-N.Chen; *Inorg. Chem. Comm.*, **2007**, *7*, 286
- [204]: E. Kaiser, R. L. Colescott, C. D. Bossinger, P. I. Cook, *Anal. Biochem.* 1970, *34*, 595
- [205]: W. S. Hancock, J. E. Battersby, *Anal. Biochem.* 1976, *71*, 261
- [206]: Silver chloride MSDS, Sciencelab.com, Inc., Texas, USA
- [207]: Jorge Luis Sague Doimeadios, Doctoral thesis, *Silver Coordination Compounds with a Family of Ditopic Ligands of Varying Flexibility: about Chains, Rings, Helices and Polycatenanes*, **2006**, Basel
- [208]: W.Levason, M.D.Spicer; *Coord.Chem.Rev.*, **1987**, *76*, 17
- [209]: M.A.Eltayeb, Y.Sulfab; *Polyhedron*, **2007**, *26*, 39
- [210]: W.Bi, D.Sun, R.Cao, M.Hong; *Acta Cryst. E*, **2002**, *58*(7), 324
- [211]: J.H.Liao, P.L.Chen, C.C.Hsu; *J. Phys. Chem. Solids*, **2001**, *62*, 1629
- [212]: S.A. Kumar et al, *Biotechnol Lett.* **2007**, *29*, 439

## Curriculum Vitae

Full name: Tünde VIG SLENTERS  
Nationality: Swiss, Hungarian  
Marital status: Married, one child  
Date and place of birth: 2 April 1973, Eger

---

### Professional experience:

June 2005-: University of Basel, Dept. of Chemistry

Doctoral student in chemistry for the project: Functionalized Surfaces, Prof. K. Fromm's group. Assistant for „Übungen: Einführung in die Chemie(I) für Studierende der Naturwissenschaften“ and for „Praktikum: Anorganische Chemie“

2003-2004: EPFL (Lausanne), FSB-ISIC-LPI:

Doctorant-assistant for the project: Surface treatment of Ti implants–Dept. of molecular chemistry.

1998-2000: BIOGAL-TEVA Pharmaceutical Works Ltd. (Debrecen, Hungary)

Analytical engineering in the R&D department.

1996-1997: University of Debrecen Dept. of Inorg. and Anal. Chem. (Debrecen, Hungary)

### Formal education:

2003-2004: • Doctoral School of EPFLausanne : Passed the doctoral school admission exams with success.

2000-2003: • French teacher diploma of Université de Lausanne (UNIL)

1996-1997: • Chemistry teacher diploma (University of Debrecen, Hungary)

1991-1996: • M.Sc. in Chemistry (University of Debrecen, Hungary)

### Publications & conferences:

K.Belser, T.Vig Slenters, C.Pfumbiadzai, G.Upert, L.Mirollo, K.M.Fromm, H.Wennemers; *Angew. Chem. Int Ed.*, 2009, 48, accepted

T.Vig Slenters, I.Hauser-Gerspach, A.U. Daniels, K.M.Fromm: *J.Mater.Chem.*, 2008, 18, 5359

A.Y.Robin, J.L.Sague Doimeadios, A.Neels, T.Vig Slenters, K. M Fromm; *Inorg. Chim. Acta*, 2007, 360(1), 212

W.Maudez, T.Vig Slenters, L.Mirollo, A.Fleury, K.M.Fromm; *Main Gr. Chem.*, 2006, 5(1), 41.

T.Vig Slenters; Antimicrobial Ag-compounds as coatings for implant materials, Presentation, Meet the expert: Material- und Oberflächentechnologie für Implantate, 19-20 März 2009, Interlaken

K.Koch, T.Vig Slenters, K.M.Fromm, H.Wennemers: Selective Interactions of Silver Ions with Peptides, Poster, SCS, Fall meeting, 2007, Lausanne

T. Vig Slenters, A.Y. Robin, K.M. Fromm; New Application of Silver Coordination Polymer Networks, Poster, 37th International Conference of Coordination Chemistry, 2006, Cape Town, South Africa

T.Vig Slenters, AY.Robin, KM.Fromm; New Application of Silver Coordination Polymer Networks, Poster, International Conference on Nanoscience and Technology (ICN&T 2006), 2006, Basel, Switzerland

An meiner Hochschulausbildung waren folgende Dozenten beteiligt:

University of Debrecen:

Prof. Ernő Brücher, Prof. Dr. Ferenc Joó, Prof. Dr. Sándor Antus, Prof. Dr. Etelka Farkas

EPFL, Lausanne:

Prof. Dr. Michael Grätzel, Prof. Dr. H. Jörg Mathieu, Prof. Dr. Lothar Helm

University of Basel:

Prof. Dr. Katharina M. Fromm, Prof. Dr. Catherine Hauscroft, Prof. Dr. Marcel Mayor